TRIBOLOGICAL BEHAVIOUR OF DLC AND SI-DLC FILMS DEPOSITED ON NITRILE RUBBER FOR HANDPUMP PISTON SEALS

Michael Lubwama

M.Sc., B.Sc.

PhD   **2013**

TRIBOLOGICAL BEHAVIOUR OF DLC AND SI-DLC FILMS DEPOSITED ON NITRILE RUBBER FOR HANDPUMP PISTON SEALS

by

Michael Lubwama

(M.Sc., B.Sc.)

Thesis presented to Dublin City University in fulfilment of the requirement for the degree of Doctor of Philosophy

School of Mechanical and Manufacturing Engineering

Dublin City University

Ireland

June 2013

Main Supervisor: Dr. Brian Corcoran

Co-supervisors: Mr. Kimmitt Sayers
                          Dr. John Baptist Kirabira
                          Dr. Adam Sebbit

Declaration

I hereby declare that this material, which I now submit for assessment on the programme of study leading to the award of Doctor of Philosophy is entirely my own work, that I have exercised reasonable care to ensure that the work is original, and does not to the best of my knowledge breach any law of copyright, and has not been taken from the work of others save and to the extent that such work has been cited and acknowledged within the text of my work.

Name: Michael Lubwama

Signature:

Student Number: 10100148

Date: June 2013

Acknowledgements

Rita, Edel, Evelyn, Martina, Lorraine, Cillian, Paul, Quande, Allan, Nina, Louise, Marguerite, Luna, Jess, Rex and Ben for many special moments in Dublin.

Finally, a special thank you goes to Harriet, my dear wife. Thanks for being patient and understanding as I embarked upon this research. Thanks are also due to mummy and Maggie. The motivation and encouragement that you constantly gave to me during this research are one of the main reasons it has come to a successful conclusion. You believed in me, when no one else did!

Finally, and most importantly, I give all the glory to God for enabling me to complete this research project.

Thank You.

Dedication

This thesis is dedicated to my lovely wife, Harriet. It is also dedicated to my mum, dad and sisters.

Table of Contents

List of Figures

List of Tables

List of Abbreviations

a-C:H	Hydrogenated amorphous carbon
ACM	Acrylate
Ar	Argon
C	Carbon
Ca	Calcium
CA	Contact angle
CFUBMS	Closed field unbalanced magnetron sputtering
CFUBMSIP	Closed field unbalanced magnetron sputtering ion plating
CoF	Coefficient of friction
CTE	Coefficient of thermal expansion
Cr	Chromium
CVD	Chemical vapour deposition
CH_4	Methane
C_2H_2	Acetylene
C_4H_{10}	Butane
DC	Direct current
DCU	Dublin City University
DkIT	Dundalk Institute of Technology
Disp(G)	G peak dispersion
DLC	Diamond like carbon
DLCH	Hydrogenated diamond like carbon
EDX	Energy Dispersive X-ray
eV	Electron volts
EPDM	Ethylene propylene diene monomer
FKM	Flouro-carbon
FWHM(G)	Full width at half maximum of G peak
GLCH	Graphite like hydrogenated amorphous carbon
H	Hydrogen
HNBR	Hydrogenated nitrile rubber
I_D	Intensity of the D peak
I_G	Intensity of the G peak
IDWSSD	International drinking water supply and sanitation decade
Mak	Makerere University
MDG	Millennium Development Goal
MMM	Medical Missionaries of Mary
Mo	Molybdenum
NGO	Non-Government Organisation
NBR	Acrylonitrile butadiene rubber / nitrile rubber
O	Oxygen
PECVD	Plasma enhanced chemical vapour deposition
PEEK	Poly ether ether ketone
PL	Photoluminescence
PLCH	Polymer like hydrogenated amorphous carbon
Pos(G)	G peak position
Pos(D)	D peak position
PTFE	Poly tetra fluoro ethylene
PVD	Physical vapour deposition

RF	Radio frequency
RT	Room Temperature
RCSI	Royal College of Surgeons Ireland
S	Sulphur
SEM	Scanning electron microscope/microscopy
Si	Silicon
Si-C	Silicon-carbon
Si-DLC	Silicon doped diamond like carbon
SiO$_2$	Silicon oxide
SZM	Structure zone model
ta-C:H	Hydrogenated tetrahedral amorphous carbon
Ti	Titanium
TCD	Trinity College Dublin
UNCST	Uganda National Council of Science and Technology
UV	Ultraviolet
UV-VIS	Ultraviolet-visible
UWASNET	Uganda Water and Sanitation Network
VLOM	Village led/level operation and maintenance
W	Tungsten
WC-Co	Tungsten carbide-Cobalt
XPS	X-ray Photoelectron Spectroscopy
Zn	Zinc
Zr	Zirconium

Publications

This work has been disseminated through the following publications.

Selected Peer Reviewed Journals

[1] **M. Lubwama**, K. A. McDonnell, J. B. Kirabira, A. M. Sebbit, K. Sayers, D. Dowling, B. Corcoran, Characteristics and Tribological Performance of DLC and Si-DLC Films Deposited on Nitrile Rubber, Surf. Coat. Technol. 206 (2012) 4585-4593

[2] **M. Lubwama**, B. Corcoran, K. Sayers, J.B. Kirabira, A. Sebbit, K.A. McDonnell, D. Dowling, Adhesion and Composite Micro-Hardness of DLC and Si-DLC Films Deposited on Nitrile Rubber, Surf. Coat. Technol. 206 (2012) 4881-4886

[3] **M. Lubwama**, B. Corcoran, K.V. Rajani, C.S. Wong, J. B. Kirabira, A. Sebbit, K. A. McDonnell, D. Dowling, K. Sayers, Raman analysis of DLC and Si-DLC films deposited on nitrile rubber, In Press, Surf. Coat. Technol. (2013) http://dx.doi.org/10.1016/j.surfcoat.2013.06.013

[4] **M. Lubwama**, B. Corcoran, J.B. Kirabira, A. Sebbit, K.A. McDonnell, D. Dowling, K. Sayers, Flexibility and frictional characteristics of DLC and Si-DLC films deposited on nitrile rubber, Under Review in Surface and Coatings Technology Journal (2013), Reviewers' comments addressed.

[5] **M. Lubwama**, B. Corcoran, J.B. Kirabira, A. Sebbit, K.A. McDonnell, D. Dowling, K. Sayers, XPS analysis and nano-mechanical properties of hybrid DLC and Si-DLC films, Under Review in Surface and Coatings Technology Journal (2013).

[6] **M. Lubwama,** F. Abdelalkhimi, B. Corcoran, J.B. Kirabira, A. Sebbit, K. Sayers, Wear mechanisms of piston seals coated with DLC and Si-DLC films, Under Review in Wear Journal (2013)

[7] **M. Lubwama**, B. Corcoran, J.B.Kirabira, A. Sebbit, K.A. McDonnell, D. Dowling, K. Sayers, Interaction of frictional coefficients and Raman parameters with dry and

wet sliding for DLC and Si-DLC films deposited on nitrile rubber, Manuscript under preparation for submission to Appl. Surf. Science Journal (2013)

Conference Proceedings/Presentations:

[1] **M. Lubwama**, K. Sayers, J. B. Kirabira, B. Corcoran, Wear Mechanisms of Piston Seals for reciprocating handpumps for rural water supply, Proceedings of the 2nd International Conference on Advances in Engineering and Technology, Macmillan Africa, pp. 612 – 618 (2011), Kampala, Uganda.

[2] **M. Lubwama**, J. B. Kirabira, A. M. Sebbit, K. Sayers, B. Corcoran, Closed Field Unbalanced Magnetron Sputtering Ion Plating of DLC and Si-DLC Films on NBR Rubber, Proceedings of the 29th International Manufacturing Conference (IMC29), August 29th – 30th (2012), University of Ulster, Belfast, UK.

[3] **M. Lubwama**, K. A. McDonnell, J. B. Kirabira, A. M. Sebbit, K. Sayers, D. Dowling, B. Corcoran, Role of Si-C Interlayer on the Properties of DLC and Si-DLC Films Deposited on Nitrile Rubber, Proceedings of the 15th International Conference on Advances in Materials and Processing Technologies (AMPT 2012), September 23rd – 25th (2012), Wollongong, Australia.

Poster Presentations:

[1] **M. Lubwama**, A. M. Sebbit, J. B. Kirabira, K. Sayers, B. Corcoran, Wear Mechanisms of Nitrile Rubber Piston Seals for reciprocating handpumps for rural water supply, Poster presentation, Faculty Research Day, Faculty of Engineering and Computing, 12th May (2011), Dublin City University, Ireland.

[2] **M. Lubwama**, Wear Mechanisms of Piston Seals for reciprocating handpumps for rural water supply, Poster Presentation, Proceedings, 35th International WEDC Conference, July 6th -8th (2012), Loughborough, UK.

[3] **M. Lubwama**, B. Corcoran, K. Sayers, Characteristics and tribological performance of DLC and Si-DLC films deposited on NBR rubber, Poster presentation, Faculty

Research Day, Faculty of Computing, 12th September (2012), Dublin City University, Ireland.

[4] **M. Lubwama**, B. Corcoran, K. Sayers, Deposition and characterization of hybrid DLC and Si-DLC films deposited on nitrile rubber, Abstract accepted for poster presentation during the Symposium on Frontiers in Polymer Science in conjunction with journal Polymer, 21st – 23rd May (2013), Sitges, Spain.

Abstract

Large numbers of rural populations in the developing world rely on the handpump for access to drinking water from ground sources. The functional sustainability of handpumps is affected by the low availability of handpumps at any given period of time. The wear of the nitrile rubber piston seals contribute significantly towards this low availability accounting for a significant percentage of maintenance interventions.

In this study a novel approach is used to improve the wear resistance of the nitrile rubber piston seals. Hybrid coatings of diamond-like carbon (DLC) and silicon doped diamond-like carbon (Si-DLC), with and without Si-C interlayers, were deposited onto both sample nitrile rubber substrates and actual piston seals. The deposition was done using a combination of closed field unbalanced magnetron sputtering ion plating (CFUBMSIP) and plasma enhanced chemical vapour deposition (PECVD) in Ar/C_4H_{10} plasma.

Film characterisation was carried out using visible (488 nm) and UV (325 nm) Raman spectroscopy , X-ray Photoelectron Spectroscopy (XPS), Energy Dispersive X-ray (EDX) analysis, Scanning electron microscopy (SEM), surface profilometry, hardness measurements, hydrophobicity and surface energy analysis, adhesion and flexibility analysis, and tribological investigations under dry and wet conditions for normal loads of 1N and 5N. A piston seal wear test rig was used to test the wear resistance of the coated piston seals.

Experimental results show a dense, non-columnar microstructure with a dendritic morphology. This dendritic crack-like structure promotes film flexibility. The G peak position for the coatings was centred approximately around 1580 cm^{-1}. The intensity ratio (I_D/I_G) generally tended to increase for coatings with Si-C interlayer. Full width at half maximum, FWHM(G), was observed to reduce for coatings with Si-C interlayers. Calculated hydrogen values for all of the films were between 24% and 31%. The internal compressive residual stress in the coatings was reduced. The contact angle of water droplets showed that the coatings were hydrophobic. The deposited coatings showed excellent adherence with an adhesion rating of 4A for films with a Si-C interlayer. The composite micro-hardness was highest for DLC coatings at 15.5 GPa for indentation load of 147.1 mN using a Vickers micro-hardness tester. Nano-indentation results show that all of the coatings tested had the same order of nano-mechanical properties with hardness values of approximately 3.6GPa and

Elastic modulus values of 35GPa. XPS survey scans showed the contributions from C 1s (~285 eV), O 1s (~531 eV), Si 2p (~100 eV) and Si 2s (~151 eV). C-Si (C 1s) and Si-C (Si 2p) configurations corresponding to bonding between carbon and silicon atoms in SiC were observed. The sp^3/sp^2 ratio increased for the Si-DLC and DLC with Si-C interlayer coating compared to the DLC coating. All of the coatings showed excellent tribological results with an over 50% reduction in the coefficient of friction compared to uncoated nitrile rubber. There was no penetration of the coatings for normal loads of 1N and 5N under wet sliding and 1 N normal load under dry sliding, which is important for potential application onto piston seals.

These results were attributed to reduction of defects in the sp^2 amorphous carbon networks indicating a more graphitic organization and a decrease of sp^3 C-C hybridisation percentage. Raman analysis of the wear tracks indicated a possibility of increased graphitization during pin-on-disc experiments. After over 100,000 strokes of operation of the piston seal wear test rig, extremely small changes in weight for the coated piston seals were observed with increased crack density of the coatings. The main wear mechanisms taking place on the coated piston seals were identified as a combination of fatigue and abrasive wear. The results and discussion indicate the potential of applying DLC and Si-DLC with and without Si-C interlayers onto nitrile rubber piston seals.

Chapter One

Introduction

1.1. Background

According to Millennium Development Goal (MDG) number 7, halving by 2015 the proportion of people without access to safe drinking water and sanitation is one of the specific targets under the aim to ensure environmental sustainability [1]. Figure 1.1 shows that over 800 million people worldwide do not have access to improved water sources. Sub-Saharan Africa accounts for 330 million people, which implies that sub-Saharan Africa is not on target to meet MDG number 7.
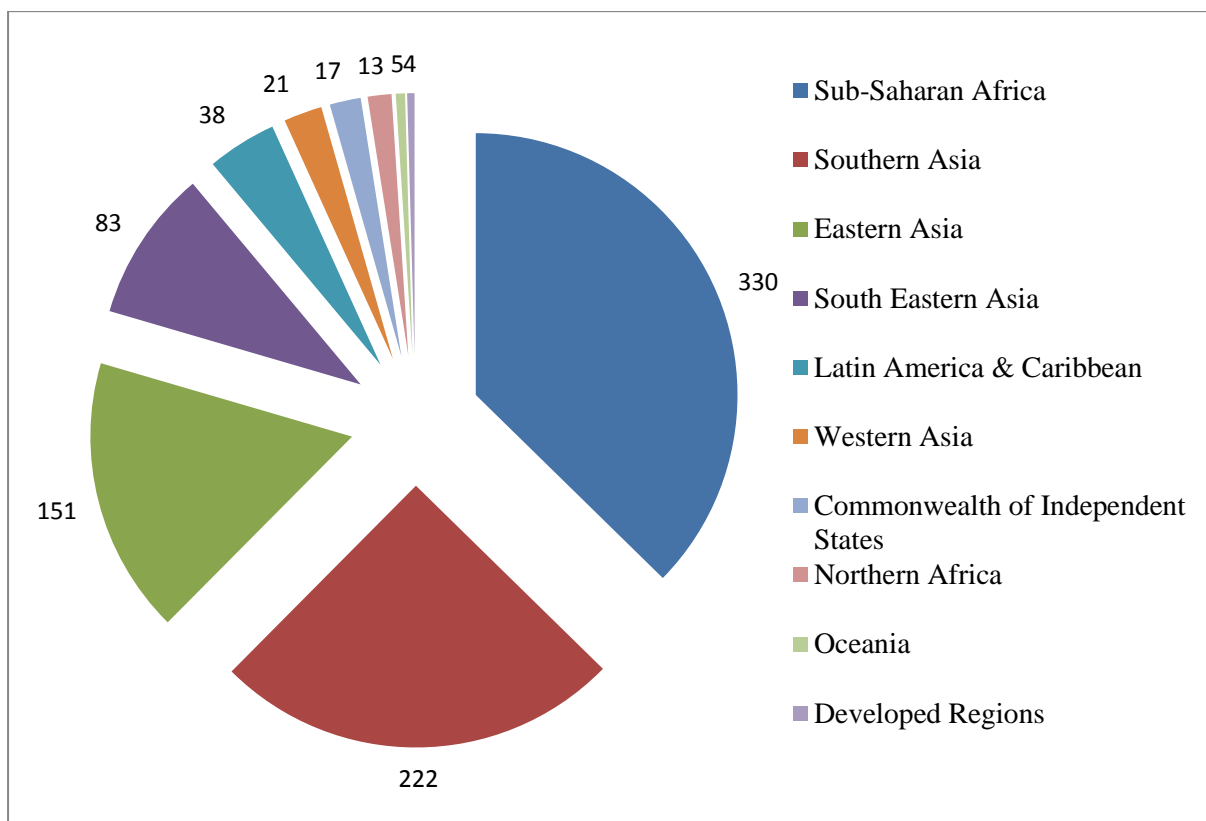
Figure 1.1. Regional distribution of people (millions) whom do not have access to improved drinking water sources [1].

Access to drinking water is defined as the availability of at least 20 litres of drinking water per person per day within 1 km of that person's dwelling. Improved water sources are assumed to be safe water sources. Safe drinking water is defined as water that meets accepted quality standards and poses no significant health risk. As such groundwater is recognized as safe drinking water [2]. Recently, quantitative maps of groundwater resources in Africa have indicated that groundwater is the largest and most widely distributed store of fresh water in Africa [3]. Groundwater is the major source of safe water and its use for irrigation is forecast to increase substantially to combat food insecurity as a result of climate change effects [4]. The most common cost effective means of accessing and delivery of groundwater for rural water supply are by the use of handpumps [5].

During the International Drinking Water Supply and Sanitation Decade (IDWSSD) from 1981 to 1990 significant effort was made towards the development of handpumps for groundwater extraction. In India alone, 1.3 million India Mark II handpumps were serving 360 million people by 1989. The India Mark II quickly established itself as the standard handpump design. The India Mark II design was made in the 1970s predating the Village Led/Level Operation and Maintenance (VLOM) concept and it relied heavily on centralized maintenance. India Mark II handpumps required a minimum of four semi-skilled workers with a mobile van and special tools to repair below ground components. Centralized maintenance of India Mark II was possible in India because of the dense populations in rural areas and developed bicycle manufacturing industry which meant that personnel and spare parts for handpump maintenance were readily available. [5, 6]

In 1983 modifications were made to the India Mark II design including using nitrile rubber for piston seals instead of leather seals in the India Mark III design during the Coimbatore project. The India Mark III is a VLOM derivative of the India Mark II. This model uses an open topped cylinder and 2.5 inch galvanised pipe for the rising main to enable the piston seal to be withdrawn for maintenance without extracting the rising main [5-7]. Figure 1.2 shows the below ground components of an India Mark III handpump [7]. Repairs to India Mark III pumps took just one third of the time needed to carry out similar repairs on below ground components to India Mark II pumps. A mechanic carrying all of the necessary tools on a motorbike could extract the nitrile rubber piston seal with the assistance of a pump caretaker or any other member of the user community [5, 6]. In the U3M handpump a

polyvinyl chloride (PVC) rising main replaces the typical galvanised steel rising mains used in the India Mark II and India Mark III handpumps [7].

As a result, priority in handpump design, manufacture and selection has focused more towards ensuring Village Level Operation and Maintenance (VLOM) rather than centralized maintenance [5, 6, 8]. VLOM was successfully applied in India, but its transfer to sub-Saharan Africa was not as successful due to social, cultural and hydro-geological differences [9]. Establishment of a supply chain for standardized spare parts was problematic in sub-Saharan Africa due to different types of handpumps introduced haphazardly by different Non-Governmental Organisations (NGO's) [10]. Also, by the end of the IDWSSD there was a shift towards 'software' issues that eclipsed handpump 'hardware' or handpump design issues, irrespective of the fact that pertinent design issues regarding handpumps remained [11]. These reasons, explain, in part, the frequent tendency towards inadequate performance and/or breakdown shortly after installation.
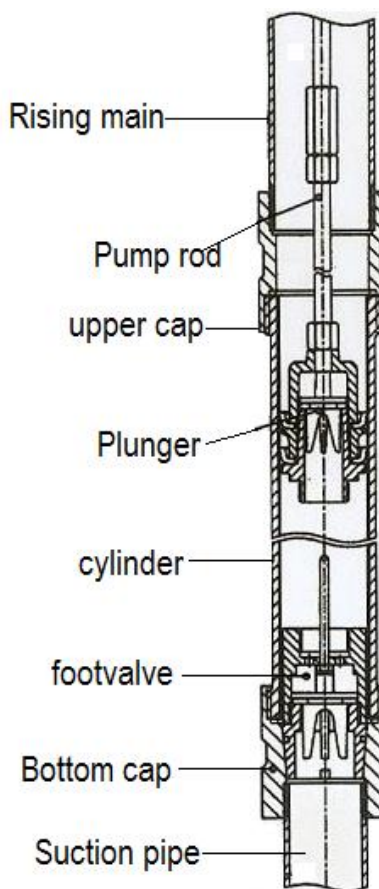
Figure 1.2. Below ground components of an India Mark III handpump [7]

3

In the water sector in developing countries, NGO's play a crucial role in shaping government water policy. Presently, NGO's continue to focus on rigidly attempting to satisfy the VLOM concept. This has encouraged the production and design of new handpumps, with each design claiming to satisfy the VLOM concept more precisely than previous designs. As a result, the handpump market is saturated with different kinds of handpumps, with very little standardization including India Mark II, India Mark III, Tara, and U3M handpumps. This has resulted in supply chain issues once maintenance interventions, either preventive or breakdown, are required. Therefore when the NGO that installed the handpump hands it over to be managed by the community its functional sustainability is low [6, 10].

A re-think to the handpump problem in Africa is required so that handpump functional sustainability can be ensured. Sustainability is the long term duration without external support for the project implemented with a clear understanding that support for development should bring with it autonomy for the beneficiaries [9]. Therefore, functional sustainability of a handpump technology can be defined as the availability and reliable operation of a handpump over a longer period without any maintenance interventions. Previous definitions of sustainability with regards to handpumps in developing countries have focussed more on the VLOM concepts. This approach has failed because the handpump as a technology still has pertinent design issues with the piston seals, rising mains, foot valves and bearings [6]. However, for the reciprocating handpump very few attempts have been made to improve on its problematic components, to understand common failure modes and to systematically refine common designs to improve their performance.

Reliability is an important parameter in handpump technology. A reliable handpump is one that supplies 30 litres per head per day for 95% of the year. Handpump reliability is the probability that the handpump is in operating condition on any one day calculated as the sum of operating time before failure divided by the total time. This definition has been adopted to account for the period of time of which many handpumps stand idle while waiting to be repaired [5]. Handpump reliability, R, is defined as shown in eq. (1.1) [5, 6]:

$$R = \frac{\sum T_F}{\sum T_T} \qquad (1.1)$$

where $\sum T_F$ is the sum of the total operating time before failure and $\sum T_T$ is the total time. This definition of handpump reliability is the same as mechanical availability. Typically

availability is low. This results in low reliability. The unreliability of handpumps is a common reason given by users in rural communities in Africa for not paying access fees to use the handpumps; along with the fact that most people view water as a free resource of nature [12]. It can therefore be implied that any endeavour that seeks to maximise the availability of the handpump also promotes handpump reliability.

By the end of the IDWSSD it was reported that 75% of repairs and maintenance interventions carried out on handpumps were because of below ground components [6]. Figure 1.3 shows that failure of piston seals is singly responsible for most handpump failures at about 24% [8]. Since the modification of the India Mark II to the India Mark III which is a more VLOM compatible design, and after extensive testing during IDWSSD, acrylonitrile butadiene rubber/nitrile rubber (NBR) has been the material of choice for piston seals [5, 6, 13]. The main reason for the choice of nitrile rubber was due to its low cost.
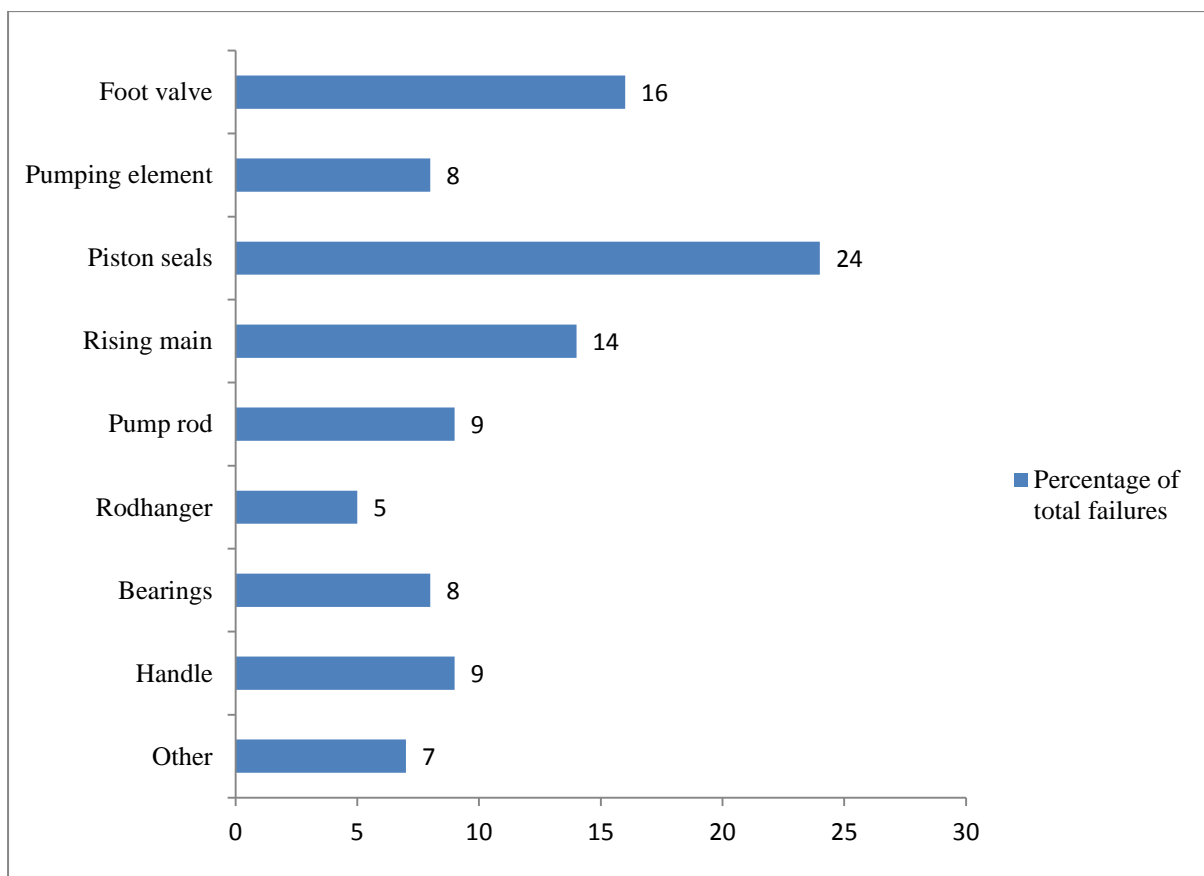
Figure 1.3. Percentage of total handpump failures by each handpump component [7]

The low cost of nitrile rubber piston seals is very important as the piston seal is a high wearing component responsible for most handpump failures [14]. The piston seals endure frequent reciprocating motion during operation. Constant adhesion and abrasion with the metallic cylinder wall that encloses it results in high rates of wear. The entrapment of solid particles within the pumping element also enhances abrasive wear [14]. Therefore, in order to maintain normal handpump performance it is recommended that nitrile rubber piston seal replacements be carried out at an interval of 2.5 years at the least with more frequent replacements once the water flow from the spout is reduced [6]. For a multitude of reasons, many of which are non-technical these replacements simply do not take place. Nitrile rubber also exhibits excellent visco-elastic and deformation properties that allow proper sealing of the pumping element during both upstroke and downstroke motion during water pumping with minimal leakage levels. However, the wear of elastomeric seals is seldom discussed in the literature [15].

Piston seals are responsible for maintaining pressure levels during both upstroke and downstroke operation of the piston assembly in the handpump, and directly affect the water output at the sprout. Therefore, a worn piston seal is a significant problem for handpump users. A worn piston seal implies that leakage rates will increase resulting in lower water flow rates at the spout. This may lead to a perception of handpump unreliability by the handpump users [12]. The long duration it takes to acquire replacements and personnel to carry out these replacements [10], means that people in rural communities are faced with the realisation that their only source of safe water, groundwater is unreachable. As a result handpump users in these rural communities seek alternative water sources. Frequently, women and children would be required to walk miles to working handpumps in other villages which implies more demand and use on these handpumps thus accelerating the wear of the seals. However, due to the long queues at the handpump point, many users turn to unsafe water sources such as open wells whose health implications including diarrhoea and worm infestation are well documented [1].

From Figure 1.3 it can be easily ascertained that most failure interventions are related to failure of the nitrile rubber piston seal [6]. The failure of the piston seal is due to the wear of the seal [5, 6, 14]. However, simple seal replacements seldom occur implying that handpump availability and hence reliability is low. In order to achieve functional sustainability of

handpumps this research considered a novel approach. A surface engineering approach was used to improve the wear resistance of nitrile rubber piston seals, which are the most problematic components responsible for most maintenance interventions. The novel approach that was considered in this research involved the deposition of diamond-like carbon (DLC) and silicon doped DLC (Si-DLC) films onto nitrile rubber substrates and onto actual nitrile rubber piston seals. This approach recognises that the wear of the piston seal is the most significant problem due to its responsibility for most of the handpump repairs. Therefore, any improvement on the wear resistance of the seal would be significant in that the maintenance interventions required on the handpump would be reduced, thus enhancing the functional sustainability of the handpump. This approach also recognizes the fact that the piston seal is expected to perform under both dry and wet sliding conditions. Figure 1.4 shows a schematic of dry and wet sliding in the cylinder assembly of a reciprocating handpump.
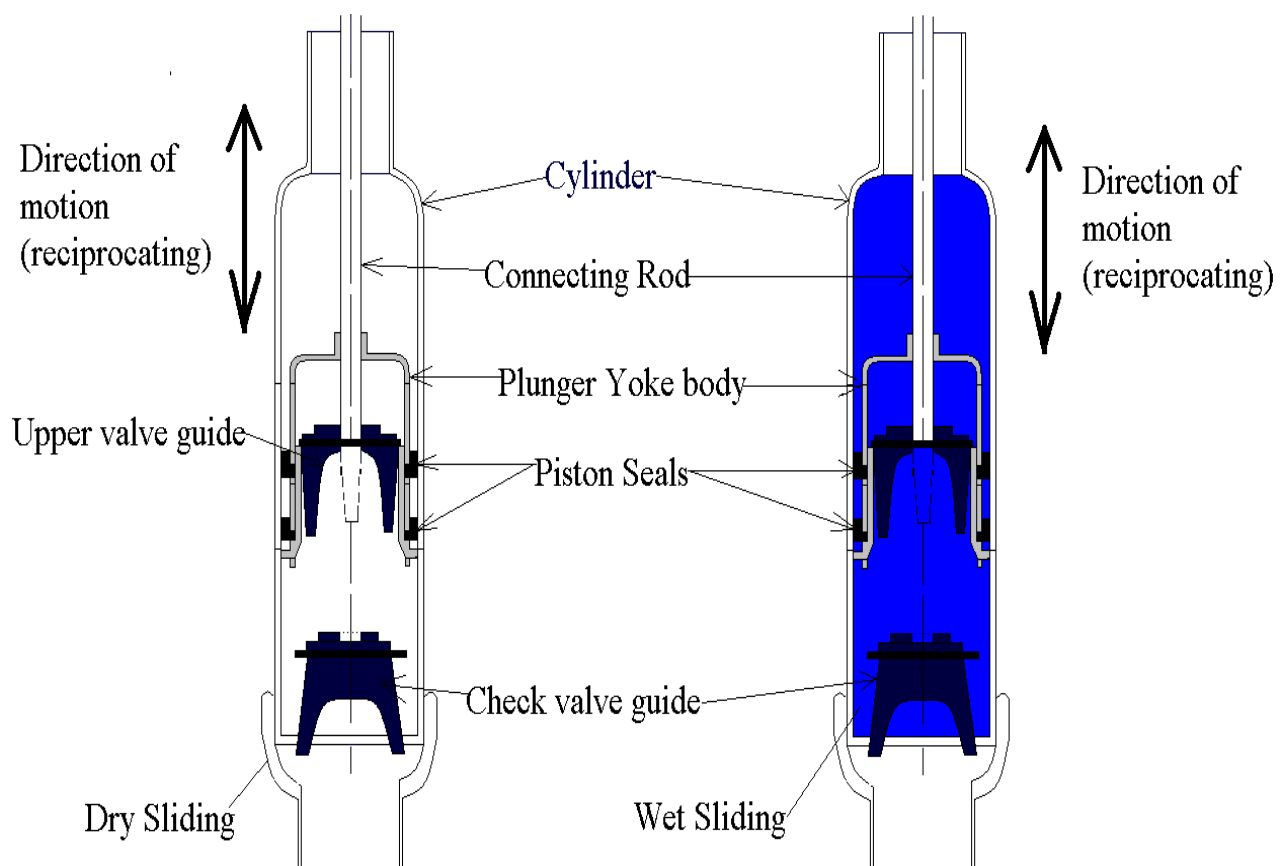
Figure 1.4. Schematic of dry and wet sliding in the cylinder assembly

Furthermore, the design and production of a new handpump would not suffice, but actually compound the problem even more. A new handpump would require its own maintenance

training of personnel and additional supply chain and logistical demands. This is in addition to the systems in place for the numerous designs and millions of handpumps available. A number of different designs of the piston/cylinder assembly e.g. the India Mark II, India Mark III, Afridev, U3M handpump were considered in the IDWSSD [5, 8]. The aim of many of the projects during the IDWSSD was to reduce the frequency of piston seal replacements [5]. Seal-less pistons were also considered in the IDWSSD e.g. the Volanta pump, but were not widely adopted due to inherently high leakage rates and high pressures required for operation [6]. The blue pump design from the Netherlands uses seal-less piston design [16], however, maintenance of this pump is very difficult. Aspegren et al. advocated for increased handpump availability through longer operation time of the piston seals [13]. Therefore, in this research, a surface engineering approach was considered as an approach to increase piston seal life by increasing on its wear resistance. A surface engineering approach was chosen because it would not affect the already established front end processes involved in handpump manufacturing. It also presents the advantage of retaining the same supply chain systems, maintenance systems and personnel that are already in place for ordinary seals.

1.2. Motivation for the study

Since the nitrile rubber piston seal is the most frequently worn part of the handpump, one possible effective way to increase its service life is to apply a thin coating of amorphous diamond-like carbon (DLC). DLC films provide an optimal combination of relatively high hardness, chemical inertness, low friction coefficients and low wear rates [17]. However, DLC and DLC related coatings were previously deposited exclusively onto metals and ceramics, initially. The idea of applying DLC film on rubber was considered at first with reluctance because the concept of applying a hard thin hard film like DLC onto a deformable substrate like rubber without interfacial delamination was untested [18].

However, researchers in Japan successfully showed that DLC could be deposited onto rubber [19-21]. The explicit application of DLC coatings onto various rubber substrates was demonstrated by Nakahigashi et al. [19]. Flexible DLC was deposited onto various rubber substrates including nitrile rubber. Investigations into DLC coating frictional and wear behaviour, water repellence and adhesion properties for potential application of DLC films onto rubber O-ring seals for zoom lens systems of 35 mm compact cameras were undertaken

[19]. More recently, Martinez et al. [18] applied DLC to nitrile butyl rubber like materials in order to modify surface and tribological properties. A significant decrease in the coefficient of friction (CoF) after coating with DLC was observed, with the DLC coated nitrile rubber exhibiting hydrophobic characteristics [18]. Significant progress has subsequently been made in the field of DLC and DLC related films deposited on rubber. The microstructure, chemical bonding, influences of substrate bias, use of doped DLC films and tribological behaviour was discussed by the De Hosson group [22-24].

However, in comparison to DLC films deposited on other materials including metals and ceramics, the deposition and characterization of DLC films deposited on rubber still lags behind. More specifically, with regards to the suitability of DLC deposited on nitrile rubber significant knowledge gaps exist. Firstly, previous tribological studies of DLC films deposited on rubber have ignored analysis under wet sliding conditions. Such an analysis is important because it is expected that a water handpump piston seal should operate in both dry and wet conditions (see Figure 1.4). This is due to the variations in groundwater table levels in the wet and dry seasons [5]. Results for DLC films deposited on rubbers under wet sliding have never been presented and as such would present a significant contribution to the field.

Secondly, doping DLC with Silicon, Si (Si-DLC) is known to improve on coating characteristics and tribological performance in water [25, 26]. Si-DLC has been deposited on fluoro-carbon rubber and shown to reduce the coefficient of friction and wear rate against steel counterpart material [27]. However, studies involving Si-DLC on other rubbers remain few in the literature. Si-DLC has also been reported as being responsible for reducing the residual stress felt by the films [28]. However, a qualitative assessment of the residual stress of films deposited on rubbers has not been reported for DLC films deposited on nitrile rubber. This presents another gap this research attempts to fill.

Thirdly, the influence of a Si-C interlayer between the DLC or Si-DLC film and the nitrile rubber substrate has never been considered before with regard to the characteristics and tribological behaviour of DLC based films. Drees et al. noted that using alternating layered coatings of Si-DLC/DLC enhanced the wear resistance of the film [29]. Previous studies of the tribological behaviour of DLC films under water lubrication conditions investigated a film category with a Si-C interlayer which was included for adhesion promotion between the DLC and Si substrate [26, 30].

In previous tribological and characterisation studies carried out on DLC and DLC related films deposited on rubbers, no attempt has been made to relate the tribological characteristics to the structural bonding of the film. Previous studies have indicated that the wear mechanism involved in DLC and DLC related films under sliding tests can change as a result of the gradual destabilization of the carbon-hydrogen bond in the sp^3 tetrahedral structure due to the removal of hydrogen at elevated temperatures [31, 32]. This study presents a comprehensive Raman analysis of DLC and Si-DLC films, with and without Si-C interlayer, deposited on nitrile rubber substrates.

Finally, this study employs the original approach of depositing DLC, Si-DLC, DLC with Si-C interlayer and Si-DLC with Si-C interlayer on both flat substrates and actual nitrile rubber piston seals. This is the first time such an approach is being used for DLC and DLC related films deposited on rubber. An automatic piston seal wear test rig was used for studying the wear of coated piston seals. This rig automatically imposes a duty cycle on the seal that would be similar to that experienced in service.

1.3. Research Problem

For rural communities in Uganda access to safe potable water is still a challenge. The handpump is a robust technology that can provide safe water from groundwater resources. However, the large number of non-functioning handpumps indicates that a new approach that aims at improving availability and reliability may be required to successfully tackle this problem and ensure functional sustainability. Most hand pump technical failures are due to wearing of the nitrile rubber piston seals, which results in low delivery rates of pumped water and more pumping cycles per unit of output, which are indicators of low pumping efficiency. The wear mechanisms involved include adhesive wear, abrasive wear and fatigue wear. A surface engineering intervention using diamond like carbon (DLC) surface coatings initially, then doping with silicon (Si-DLC) and the inclusion of Si-C interlayers, presents a generational progression of possible functional surface coatings that could be utilized for this intervention. The research field with regards to DLC coatings on rubber substrates is still in its infancy stage and various gaps have been identified including:

- The tribological influence of DLC, Si-DLC, with and without Si-C interlayers on nitrile rubber under dry and wet sliding.
- The understanding of the wear mechanisms involved in DLC and Si-DLC films, with and without Si-C interlayers deposited on nitrile rubber as a result of tribological behaviour evaluation.
- The role of the Si-C interlayer on the structural and mechanical properties of DLC and Si-DLC films.
- Study of the wear mechanisms involved on actually coated piston seals using a purposefully built test rig for this purpose.

1.4. Aim and objectives of the study

The overall aim of this study was to improve handpump availability and reliability through improving the tribological performance of nitrile rubber substrates and actual piston seals by the deposition of DLC and Si-DLC, with and without Si-C interlayers. As such the objectives of this study were:

- To quantify field and user operating conditions related directly and indirectly to piston seal failure
- To develop a method of improving the surface technology of nitrile rubber substrates. This was done by depositing DLC and Si-DLC films, with and without Si-C interlayers onto nitrile rubber substrates and actual piston seals using an industrial closed field unbalanced magnetron sputtering ion plating (CFUBMSIP) rig.
- To determine the performance characteristics of the coatings. This was done by characterising the structural, mechanical and tribological properties of DLC and Si-DLC films, with and without Si-C interlayers deposited on nitrile rubber substrates
- To determine the wear mechanisms of actual piston seals coated with DLC and Si-DLC films, with and without Si-C interlayers, using a piston seal wear test rig.

1.5. Hypotheses of the study

The underlying hypothesis was that handpump availability and performance can be tremendously improved by improving the surface wear resistance of the nitrile rubber. The specific hypotheses were:

1.5.1. Development of DLC and Si-DLC films for tribological applications

It was hypothesised that the deposition of thin DLC and Si-DLC films onto nitrile rubber using a CFUBMSIP process would allow the formation of a dense film with increased wear resistance and reduced coefficient of friction compared to uncoated nitrile rubber [22, 27, 33, 34]. Figure 1.5 shows the combinations of DLC and Si-DLC, with and without Si-C interlayers, deposited on nitrile rubber that was hypothesised in this study.
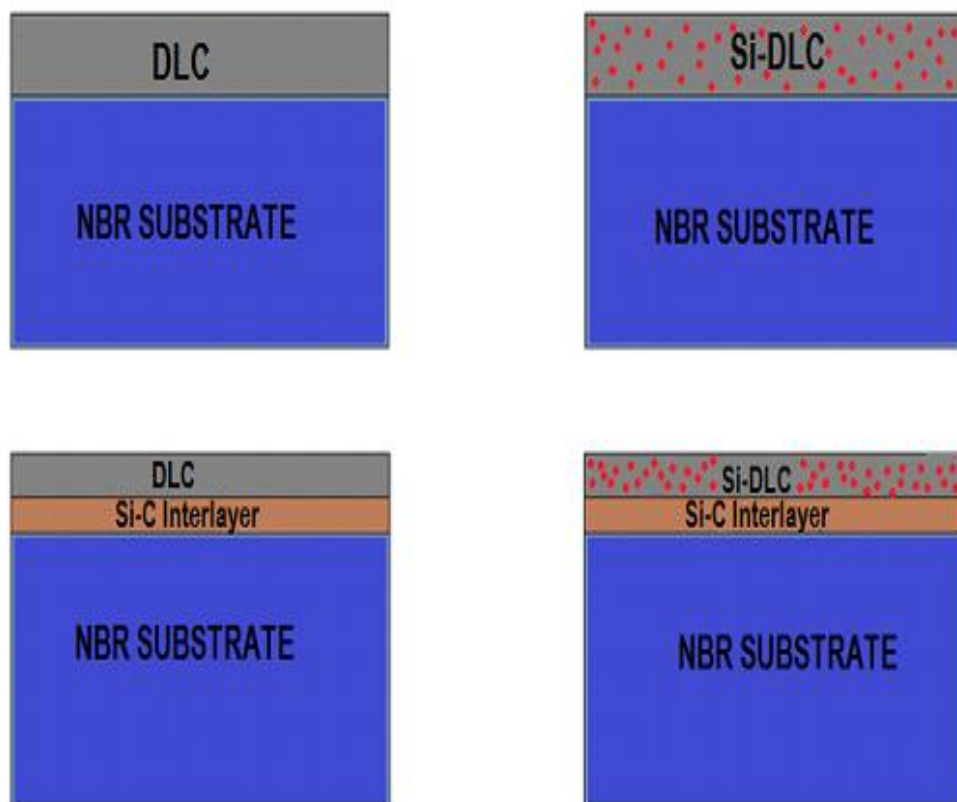
Figure 1.5. Combinations of DLC and Si-DLC films, with and without Si-C interlayer deposited on nitrile rubber

The production of dense films was hypothesised to result in good adhesion of the DLC and Si-DLC films onto nitrile rubber substrates. Also, the sputtering process would allow deposition of DLC films with moderate amounts of hydrogen which would in turn allow the films to retain the properties of DLC, but have a greater proportion of carbon (C) sp^2 hybridisations in the structure of the films than C sp^3 content. This is very important in promoting the adhesion of the film onto the nitrile rubber substrate. Also the Si-DLC films would reduce the residual stress in the films as well as improve on the tribological performance in wet sliding conditions [28].

1.5.2. Role of Si-C interlayer on the properties of DLC and Si-DLC films

It was hypothesised that the Si-C interlayer would influence the properties of DLC and Si-DLC films deposited on nitrile rubber. This was hypothesised to arise from the re-orientation of the structural bonding as a result of the inclusion of the Si-C interlayer. The Si-C interlayer was also hypothesised to promote the adhesion of the films and reduce the internal stress in the films [30].

1.5.3. Evolution of wear mechanisms of DLC and Si-DLC films deposited on nitrile rubber

It was further hypothesised that possible structural changes may occur on the wear surfaces as a result of frictional evolution during tribo-testing [31]. Analysis of wear tracks before and after wear testing of DLC and Si-DLC films, with and without Si-C interlayers, was used to attempt to understand the wear mechanisms involved for the films deposited on nitrile rubber.

1.5.4. Application of DLC and Si-DLC films onto actual piston seals

Following the hypotheses identified in Sections 1.5.1 − 1.5.3 suggesting that a reduction of wear rate and coefficient of frictions arising from the application of DLC and Si-DLC films, with and without Si-C interlayers, a study with coated piston seals was hypothesised as being of value. Simulation of coated piston seals in a piston seal wear test rig was determined as essential to further understanding the wear mechanisms involved in actual operation of coated piston seals.

1.6. Water is Life Project

1.6.1. Introduction

The Water is Life research project was originally conceived from the close relationship between Dundalk Institute of Technology (DkIT) and the Medical Missionaries of Mary (MMM) in Ireland. The MMM charity runs a number of projects, including water and health projects, in Makondo Parish, Lwengo District (formerly part of Masaka District), Uganda. As a result of this partnership between DkIT and MMM, a project centred on water was commenced. Justification of the project is to work under MDG number 7 that aims to ensure environmental sustainability as an enabler to progress towards other MDGs.

The Water is Life project focuses on the social, economic, and technological issues surrounding water in Makondo parish. This project brings together NGOs (UWASNET, MMMs), researchers from Universities in Ireland (DCU, TCD, DkIT, RCSI) and Uganda (Mak) and various other stakeholders in the water sector. The project is in line with the vision and goals of Irish Aid in its Programme for Strategic Cooperation between Irish Aid and higher Education and Research Institutes 2007 – 2011 [35]. Irish Aid Country Strategy Paper for Uganda 2010 – 2014 has as its overall goal the reduction of chronic poverty and vulnerability in Uganda in line with the National Development Plan [36].

1.6.2. Survey location and brief background

Uganda has a total area of 241,138 km^2 with about 43, 942 km^2 of wetlands and open water area [2]. Figure 1.6 shows a map of Uganda within the continent of Africa [37]. The Joint Monitoring Programme report (2010) estimated Uganda's current population to be about 31.6 million of which 88% live in rural communities [1]. This implies current and future demand for groundwater resources and the use for handpumps is expected to increase [3]. In rural populations in Uganda, 63% of the population depend on improved water sources, mainly boreholes with handpumps. 36% depend on unimproved water sources such as open wells, and 1 per cent depends on piped water. Figure 1.7 shows a map of Makondo Parish [37].
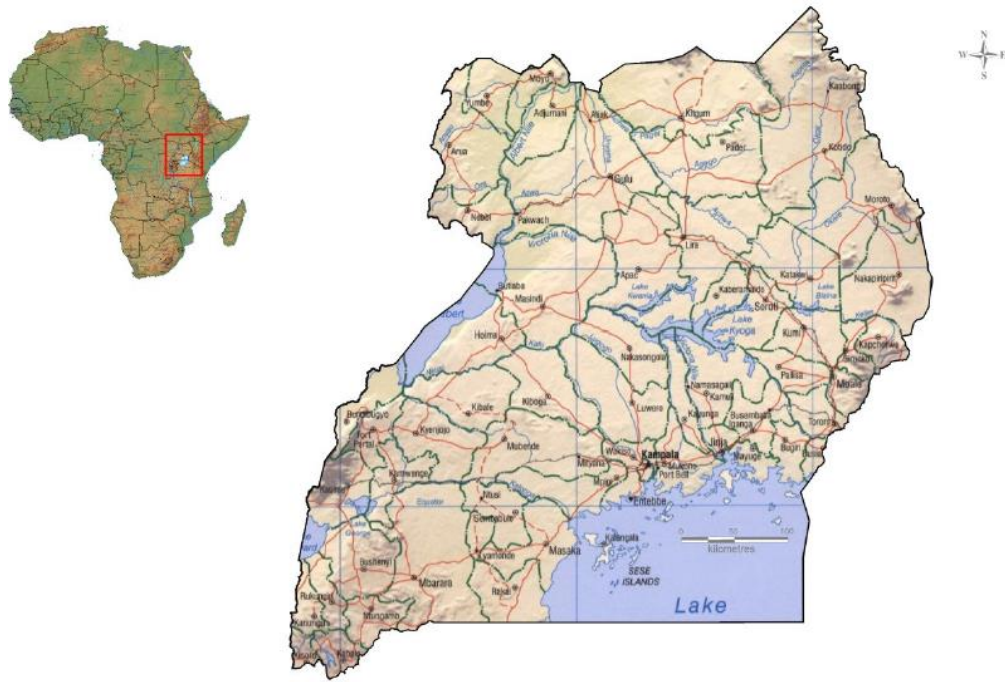
Figure 1.6. Map of Uganda located within the African continent [37]
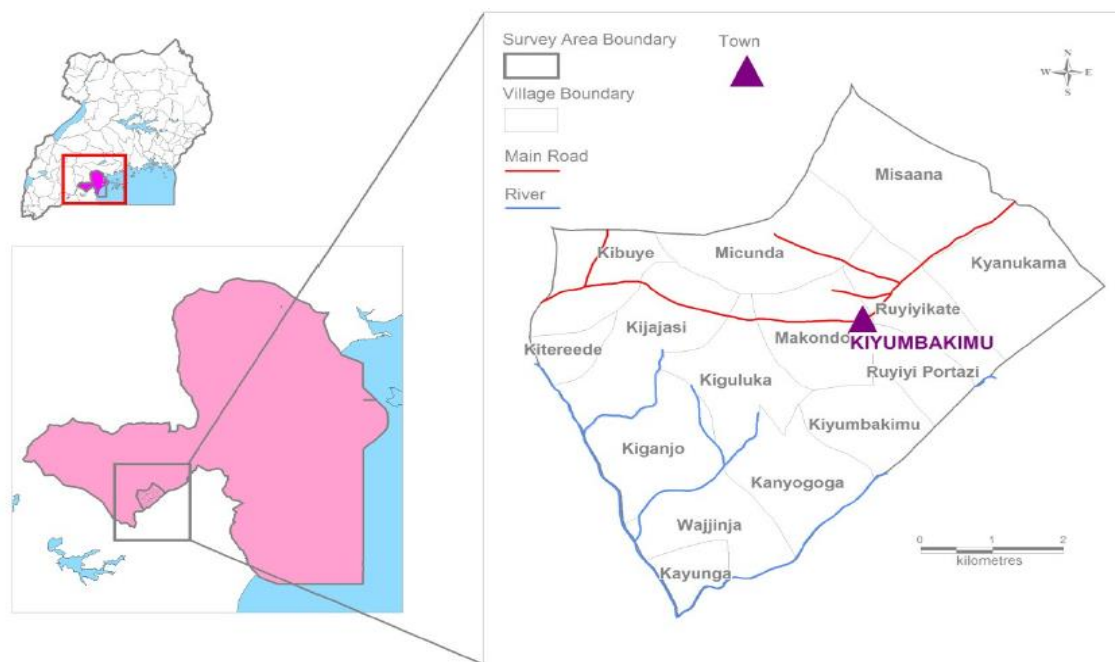
Figure 1.7. Map of survey area within Lwengo District in formerly Masaka District [37]

1.7. Structure of the thesis

This thesis has been divided into five chapters as shown in Figure 1.8. In Chapter One the overall background to the problem is introduced. The story of the handpump and its vital

importance as a primary technology for drawing safe water from groundwater resources in rural communities in sub-Saharan Africa is presented. In this chapter the reasons for focussing on the wear of piston seals are highlighted. The approach used which entails use of surface engineering techniques through the generational application of functional surface coatings, in particular DLC and Si-DLC films, with and without Si-C interlayers, is briefly highlighted. The aims and objectives of the study are also presented, as well as the hypotheses being investigated. The chapter ends by highlighting a brief background to the Water is Life Project.

In Chapter Two, a review of DLC, Si-DLC films and multi-layered DLC coatings deposited on rubber substrates is given. This state of the art review for DLC based films deposited on rubber substrates has not been presented before in the literature. The review also discusses the deposition technologies, in particular CFUBMSIP deposition technology. The tribological characteristics of DLC coatings are discussed.

Chapter Three discusses the methodology that was employed in this research. The methods used in data collection during field visits are highlighted. Social opinions, service and operational data from women, children and men regarding handpumps in their communities were obtained. The deposition method and process parameters used during the deposition of DLC and Si-DLC films, with and without Si-C interlayers, on nitrile rubber are discussed. The coating characterization techniques which were applied are detailed. The methods and procedures used during physical, mechanical, chemical and tribological characterization of the coatings are discussed. The piston seal wear test rig and testing regime is briefly described.

The presentation of results and discussion of field visits and characterisation techniques is detailed in Chapter Four. Field visit results are related to the wear of the nitrile rubber piston seal. First level surface analysis was used to identify the possible wear mechanisms involved in piston seals. The field visit results were used to quantify the testing regime for the coated nitrile rubber piston seals during simulation with the piston seal wear test rig. The preliminary results of testing of coated nitrile rubber piston seals are presented. The wear mechanisms of coated piston seals are detailed. The wear mechanisms of the coated piston seals are detailed. The conclusions, contributions to the field, and recommendations for future work are discussed in Chapter Five.

Chapter One: Introduction
- Background
- Motivation of the study
- Research Problem
- Aim and objectives of the study
- Hypotheses of the study
- Water is LifeProject

Chapter Two: Literature Review
- DLC and Si-DLC films
- Multilayer films
- DLC and Si-DLC films deposited on rubber
- Characteristics of DLC films deposited on rubber
- Closed field unbalanced magnetron sputtering

Chapter Three: Field Visit, Experimental and Characterisation Methods
- Field visit objectives, scope and methodology
- Experimental and coating characterisation techniques
- Piston seal wear test rig set up

Chapter Four: Results and Discussion
- Characteristics of DLC and Si-DLC films deposited on NBR
- Tribological behaviour of DLC and Si-DLC films deposited on NBR
- Role of Si-C interlayer on mechanical and structual properties of DLC and Si-DLC deposited on NBR
- Evolution of wear mechanisms after tribo-testing and rig testing

Chapter Five: Conclusions and Recommendations
- Conclusions
- Contributions to the field
- Recommendations for future work

References

Appendices
- Questionnaires used during field visit

Figure 1.8. Structure of thesis flow chart

Chapter Two

Literature Review

2.1. Introduction

This chapter gives a thorough review of DLC and DLC related films deposited on rubber substrates. Such a review of the state of the art of DLC, doped DLC and DLC multi-layer films deposited on rubber substrates is yet to be seen in the literature. Fundamental characterization and tribological properties of DLC films deposited on rubber substrates are reviewed. Also, a short review is given of closed field unbalanced magnetron sputtering ion plating as a deposition technology of choice. A brief description of nitrile rubber as a substrate concludes the chapter.

2.2. Diamond-like Carbon (DLC) Films

2.2.1. Introduction

Diamond-like Carbon (DLC) films have been studied extensively for over four decades since the pioneering work of Aisenberg and Chabot [38]. However, Schmellenmeier has been credited for their discovery [39]. DLC films were reviewed extensively previously [17, 39, 40].

DLC is a metastable form of amorphous carbon containing a significant fraction of C-C sp^3 hybridisations [17]. DLC has also been defined as composites of nano-crystalline diamond and/or amorphous carbon with or without hydrogen (required to passivize the dangling bonds of carbon) [41].

Generally, the "DLC" term is commonly used to designate the hydrogenated form of diamond-like carbon (a-C:H), while the "ta-C" (tetrahedral carbon) term is used to designate the non-hydrogenated carbon (a-C), containing high fractions of sp^3 hybridized carbon. Figure 2.1 shows a proposed ternary diagram that illustrates the specific domains of carbon

based films with respect to their carbon sp^2 and sp^3 hybridisation characteristics and hydrogen content [17].
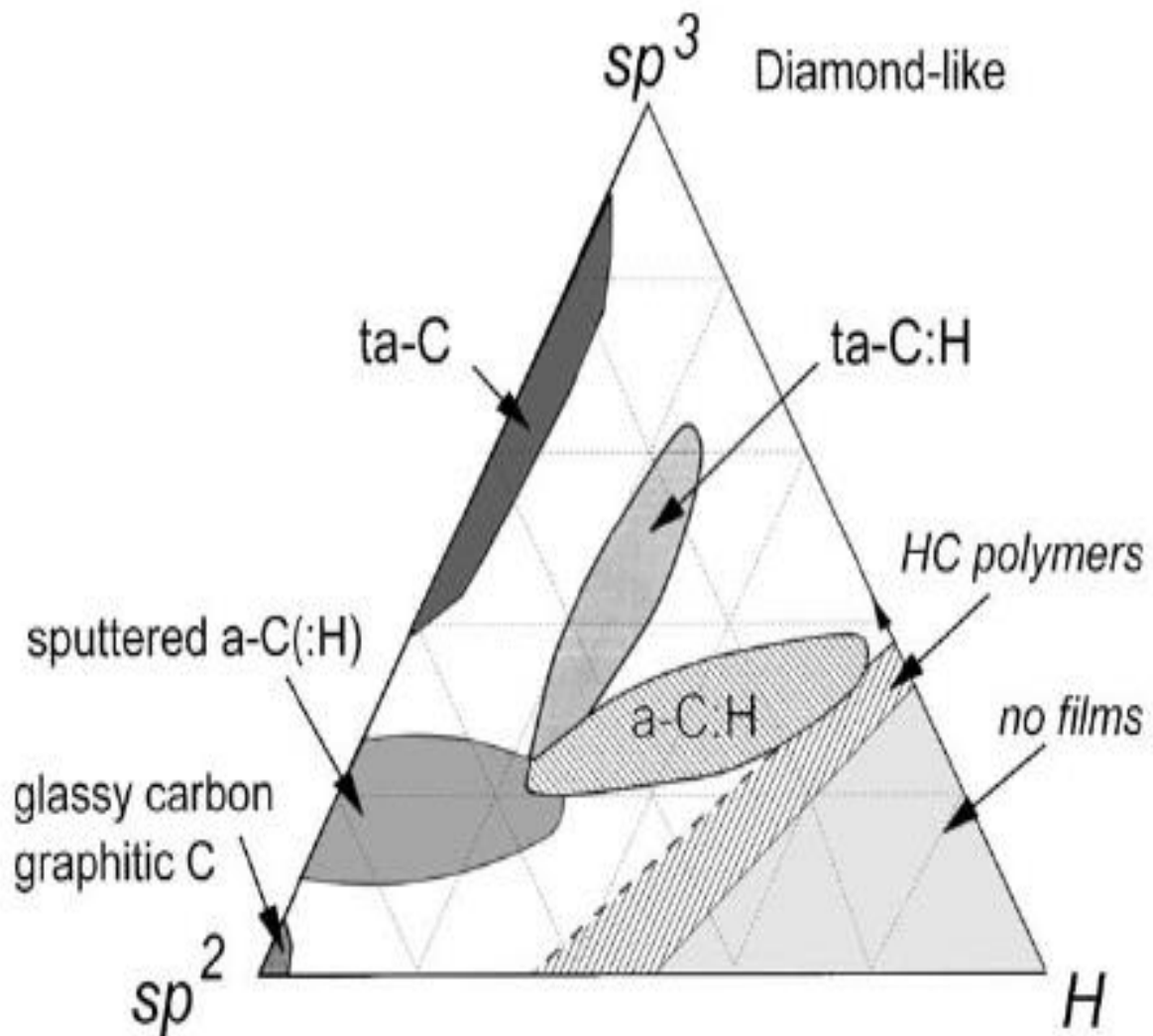
Figure 2.1. Ternary phase diagram of bonding in amorphous carbon-hydrogen alloys [17]

As indicated from Figure 2.1 hydrogenated amorphous carbons can be classified into four types [42], namely:

a) Polymer-like a-C:H (PLCH)

- a-C:H films with the highest H content (40 – 60 at. %).
- PLCH films can have up to 70% sp^3
- Most of the carbon sp^3 hybridisations are hydrogen terminated
- This material is soft and has low density
- Optical band gap ranges from 2 eV to 4 eV

b) Diamond-like a-C:H (DLCH)

- a-C:H films with intermediate H content (20 – 40 at. % H)
- DLCH films have lower overall sp^3 content, but have more sp^3 content in C-C bonds than PLCH films; resulting in better mechanical properties
- Optical gap is between 1 and 2 eV

c) Hydrogenated tetrahedral amorphous carbon films (ta-C:H)

- Class of DLCH films in which the C-C sp^3 content can be increased while keeping hydrogen content fixed (25 – 30 at. % H).
- Higher density (up to 2.4 g/cm^3) and Young's modulus (up to 300 GPa) compared to DLCH
- Optical gap can reach 2.4 eV.

d) Graphite-like a-C:H (GLCH)

- a-C:H films with the lowest H content (less than 20 at. % H).
- GLCH films have a high sp^2 content
- Optical band gap is less than 1 eV

The ability of carbon to exist in three hybridisations, sp^3, sp^2 and sp^1, has resulted in carbon forming a great variety of crystalline and disordered structures [17, 43]. The character of DLC is between diamond and graphite. Figure 2.2 shows these structures, constitutive elements, and typical processing parameters [19]. In the sp^3 configuration, as in diamond, a carbon atom's four valence electrons are each assigned to a tetrahedrally directed sp^3 orbital, which makes a strong σ bond to an adjacent atom. In the three-fold co-ordinated sp^2 coordination as in graphite, three of the four valence electrons enter trigonally directed sp^2 orbitals, which form σ bonds in a plane. The fourth electron of the weaker sp^2 atom lies in pπ orbitals, which lies normal to the σ bonding plane. This π orbital forms a weaker π bond with a π orbital on one or more neighbouring atoms. In the sp^1 configuration, two of the four valence electrons enter σ orbitals, each forming an σ bond directed along the ± x-axis, and the other two enter pπ orbitals in the y and z direction (see Figure 2.3) [17, 43].
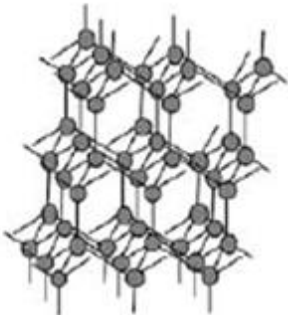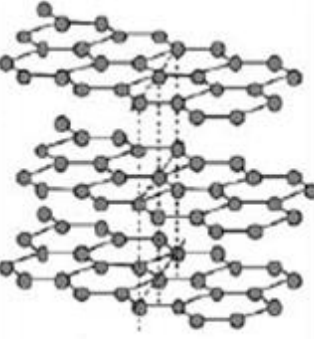
	DIAMOND	DLC (DiamondLikeCarbon)	GRAPHITE
STRUCTURE	crystalline (sp3 bondings)	amorphous sp3 and sp2 bondings	crystalline (sp2 bondings)
CONSTITUTIVE ELEMENT	C	C-H	C
PROCESS	Plasma Asisted Chemical Vapour Deposition (PACVD) (Non-equilibrium Plasma)	PACVD Ion Plating (Non-equilibrium Plasma)	CVD Equilibrium Plasma
REACTIVE GAS	C_nH_m and H_2 $CH_4:H_2 = 1:100$	C_nH_m or C Vapour CH_4, C_2H_2, C_6H_6, etc	C_nH_m
PROCESSING TEMPERATURE	~ 700 °C	RT - ~300 °C	> 1500 °C

Figure 2.2. Comparison of carbon-containing materials structure and typical deposition parameters [19]

The carbon sp^3 hybridisation of DLC confers on it many of the beneficial properties of diamond itself, such as its mechanical hardness, chemical and electrical inertness, and wide band gap. This ability and unique characteristic to exist in three hybridisations renders DLC as an optimal protective coating due to the combination of relatively high hardness, chemical inertness, low friction coefficients and low wear rates [17]. As such, research into DLC continues to generate significant interest with ever more innovation and application in micro-electronics, optics, manufacturing, transportation and biomedical fields [44]. More recently, significant efforts are being made to extend the application of DLC films onto rubber substrates [19-21].
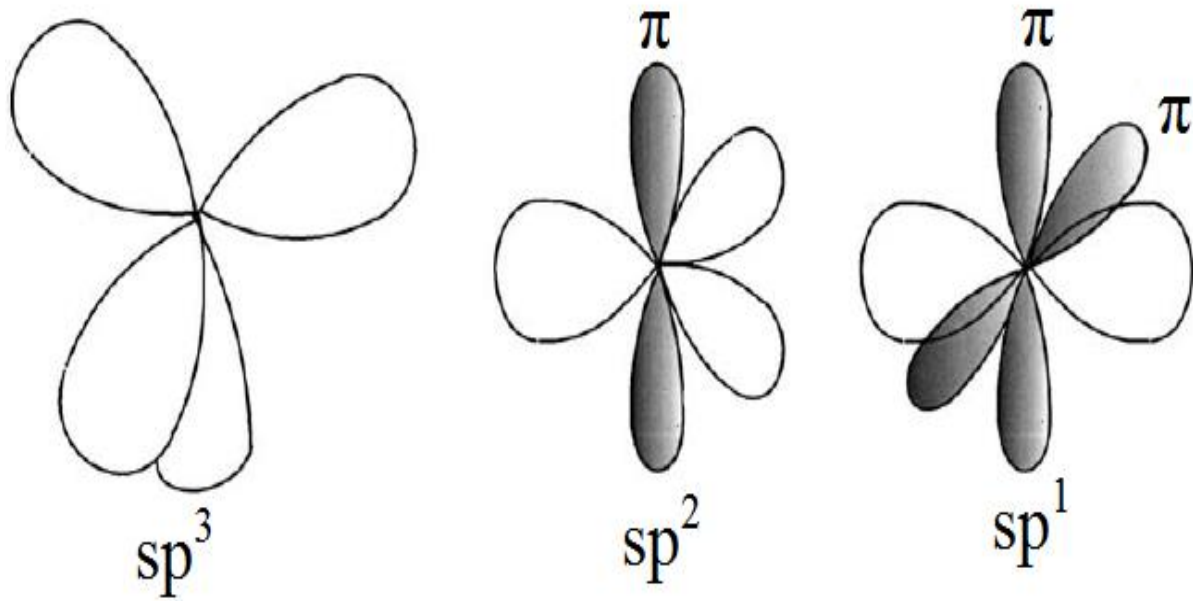
Figure 2.3. The sp^3, sp^2 and sp^1 hybridised bonding [17]

2.3. DLC films deposited on rubber substrates

2.3.1. Introduction

Rubbers are widely used in various engineering applications. Nonetheless, rubbers exhibit very high friction when sliding against other materials. For example, rubber seals are known to be a major source of friction of lubrication systems or bearings, which may take 50-70% of the total friction loss. The high friction of rubbers is due to the adhesion of rubber to the counterpart, the ploughing of asperities of harder counterpart on the rubber and the so-called "hysteresis" effect that relates to the viscoelastic nature of rubber [45]. Besides the high friction, wear of rubbers is usually severe and mostly relates to adhesive and abrasive wear [46-48]. So far, there are three solutions that can be used to reduce the friction and enhance the wear resistance of rubber components: lubrication, incorporation of micronized powders and coatings. The application of a lubricant such as oil and grease to improve the surface lubricity of rubbers is prohibitive in some applications due to the degradation of lubricants and environmental pollution problems. It was recently shown that the incorporation of micronized powders of poly (ether ether ketone) (PEEK) and poly (tetra fluoro ethylene) (PTFE) did not improve the resistance to wear of rubbers due to lack of adhesion to the rubber matrix [49]. For the third solution, a layer of appropriate wear-resistant material, such

as DLC, is coated on the working surfaces of rubber components in order to protect the rubbers from wear and to reduce friction. The development of advanced deposition methods, such as reactive magnetron sputtering and its easy scale-up for industrial production, makes the coating solution very promising [24].

The application of DLC films on rubber substrates is still at an infancy stage. Previously, efforts on the application of DLC films were focussed on DLC deposition on materials such as metals and ceramics with high hardness [50]. The idea of applying DLC film on rubber (elastomer) materials was considered illogical due to the fact that it was expected that the application of a thin hard film on a deformable substrate would promote the occurrence of interfacial delamination [18].

DLC and DLC based films have been applied in industry for decades due to their excellent properties such as very low friction when sliding against most engineering materials and low wear (for both coating and counterpart) [17, 50]. As such there is now significant effort in literature to characterize the properties of DLC and doped DLC films deposited on rubber substrates. Discussions of recent possible applications of DLC and DLC based films deposited on rubber substrates for application in O-rings for zoom cameras, rubber seals and ball bearings for aerospace and automotive industries have brought to bear the fact that DLC films can be applied onto rubber substrates and may provide useful advantages including low friction coefficients and low wear rates [19, 34].

Figure 2.4 shows a reduction in the coefficient of friction (CoF) for DLC films deposited on rubber compared to various uncoated substrates [19]. In all of cases investigated a distinct reduction in CoF was noted. This reduction in CoF has been attributed to various reasons including possible graphitization of DLC film where DLC is transformed to generate a thin graphitic layer at the sliding interface [31, 51]. Also, other studies have indicated that hydrogen plays an important role in CoF reduction during friction tests [52]; with evidence of a hydro-carbon transfer layer formed [53].

23
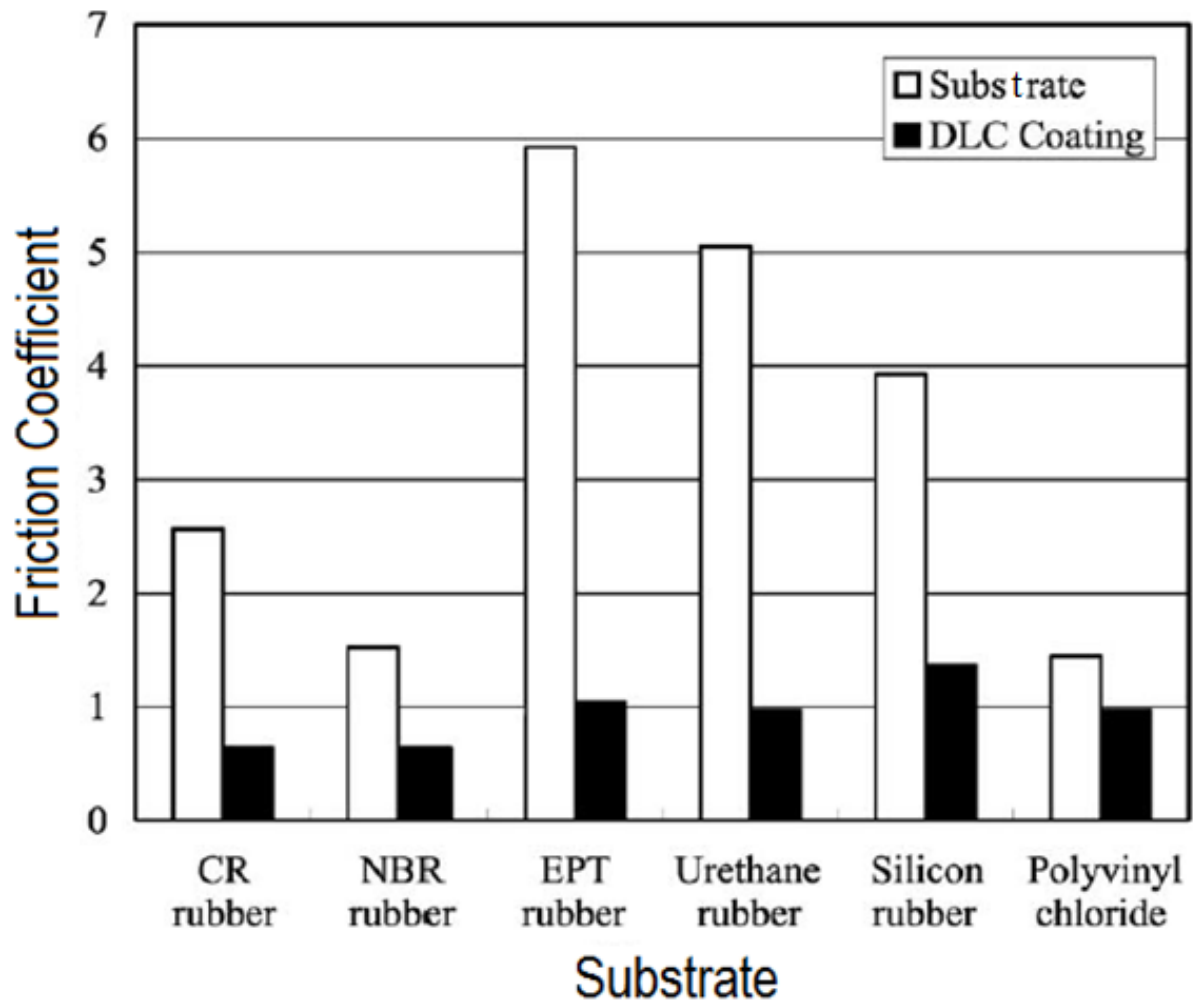
Figure 2.4. Friction coefficient of flexible DLC on polymer materials [19]

2.3.2. Doped DLC and multilayer coatings

Recent developments in advanced coating deposition techniques have resulted in the development of multifunctional DLC coatings with multi-layered or nano-structured/nanocomposite architecture that can provide excellent hardness, adhesion, frictional and wear rates [44, 54]. Doped or alloyed DLC coatings are an important category of DLC films characterized by the incorporation of different elements in their structure to achieve improved properties with respect to pure DLC films [22, 23, 44]. The addition of dopants to DLC is done mainly to reduce its typically high internal compressive stress, to reduce it surface energy (or increase its hydrophobicity) and to enable further lowering of its friction coefficients [54, 55].

DLC based multi-component films may also be combined to obtain property controlled multilayer coatings, including: interface layers to improve adhesion; large number of repeated layers with different intrinsic mechanical properties; diverse property layers to combine several protective functionalities such wear resistance and adhesion; and elimination or minimization of compressive stresses. [44, 56, 57]

More specifically, with regards to DLC films deposited on rubber substrates, few efforts have been made in investigating the effects of doped DLC and the inclusion of multilayers on the rubber substrates [22, 23, 58]. Metallic coatings such as Ti, Cr, Mo, W and Zr were deposited on rubbers via self-ion-assisted deposition in order to modify their surface [59, 60]. A slight increase in the hydrophobicity, less than expected reduction in CoF, poor adhesion of coatings to rubber were reported [58-60].

Various works on W-DLC and one on Ti-DLC films deposited via reactive magnetron sputtering on FKM (fluorocarbon), ACM (acrylate), and HNBR (hydrogenated nitrile butadiene) followed [22, 23, 58]. Masami et al. justified Si incorporation in DLC films deposited on rubbers from studies of Si incorporation in DLC films deposited on stainless steel which showed Si-DLC contributing to the reduction of CoF and wear [27].

Figure 2.5 shows a reduction in coefficients of friction for W-DLC films [23], and Si-DLC films [27] deposited on HNBR and FKM rubbers respectively compared to uncoated HNBR and FKM rubbers. The Cr interlayer inclusion also reduced the friction coefficients when compared to uncoated HNBR and FKM rubbers. A detailed review of characterization results of DLC and DLC related films deposited on rubbers in the literature is given in Section 2.3.4 of this review.

These very few studies present the current state of the art regarding doped DLC films deposited on rubber substrates and further justify the need for more such studies so that our understanding of doped DLC films can be enhanced. One particular gap is the role of Si-DLC deposited on rubbers and its role in wet sliding for possible application onto piston seals for reciprocating hand pumps.

Si incorporation has been widely studied for DLC films deposited on metals and is reported as being effective in reducing friction coefficients in wet conditions [25, 54, 61] with limited

deterioration of the wear resistance [62]. The tribological behaviour is attributed to the formation of SiO_2 wear particles and their interaction with the humid environment through tribo-chemical effects. The SiO_2 nano domains promote the absorption of water with the formation of Si-O-OH groups. The formation of this hydrated silica phase at the frictional interface is responsible for the low friction coefficient measured [63]. A systematic analysis of DLC, Si-DLC and DLC films with interlayers deposited on rubber substrates for both dry and wet sliding has never been presented before in literature.
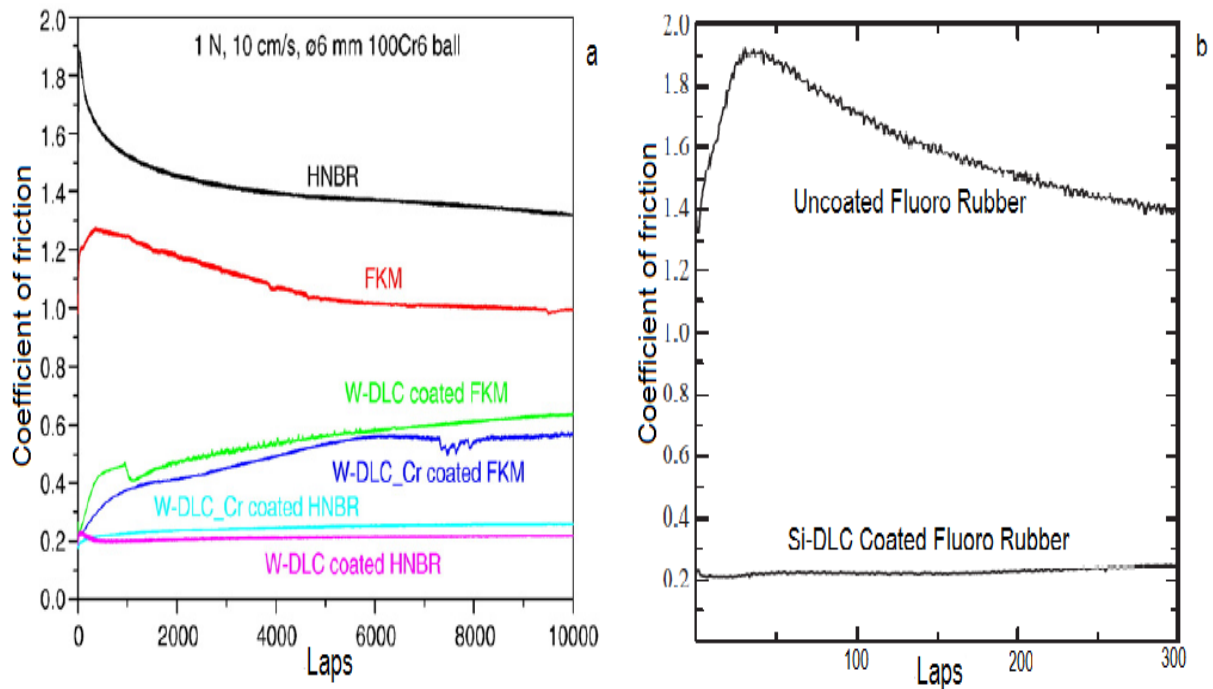
Figure 2.5. Coefficient of friction of uncoated HNBR and FKM and W-DLC coated HNBR and W-DLC coated FKM (a) [23]; and Coefficient of friction of uncoated and Si-DLC coated fluoro rubbers (b) [27].

2.3.3. Closed field unbalanced magnetron sputtering (CFUBMS) deposition technology

2.3.3.1. Introduction

DLC can be deposited via physical vapour deposition (PVD) for hydrogen free DLC, or chemical vapour deposition (CVD) for hydrogenated DLC or a-C:H [17]. Formation of a film deposit under both PVD and CVD can be generally realised in three steps as illustrated in

Figure 2.6 including; Firstly, creation of vapour phase species (deposition species) by evaporation, sputtering or chemical vapours and gases; Secondly, transport of vapour species from source to substrate which can occur under line-of-sight, thermal scattering, or molecular flow conditions (i.e. without collisions between atoms and molecules), or alternatively, if the partial pressure of the gas species in the vapour state is high enough for some of these species to be ionized (by creating a plasma), there will be a large number of collisions in the vapour phase during transport to the substrate; and, thirdly, coating film growth on the substrate once the atoms or molecules are deposited and film nucleation and growth occurs on the substrate. Microstructure and composition of the film can be modified by bombardment of the growing film by ions from the vapour phase, resulting in sputtering and re-condensation of the film atoms and enhanced surface mobility of the atoms in the near surface and surface of the films [64, 65]. The role of plasma for surface treatment of elastomers has been mentioned in the literature with varying effects including reduction of initial frictional coefficients [66]; reduction in the hydrophobicity [67]; and surface cleaning [18, 65].
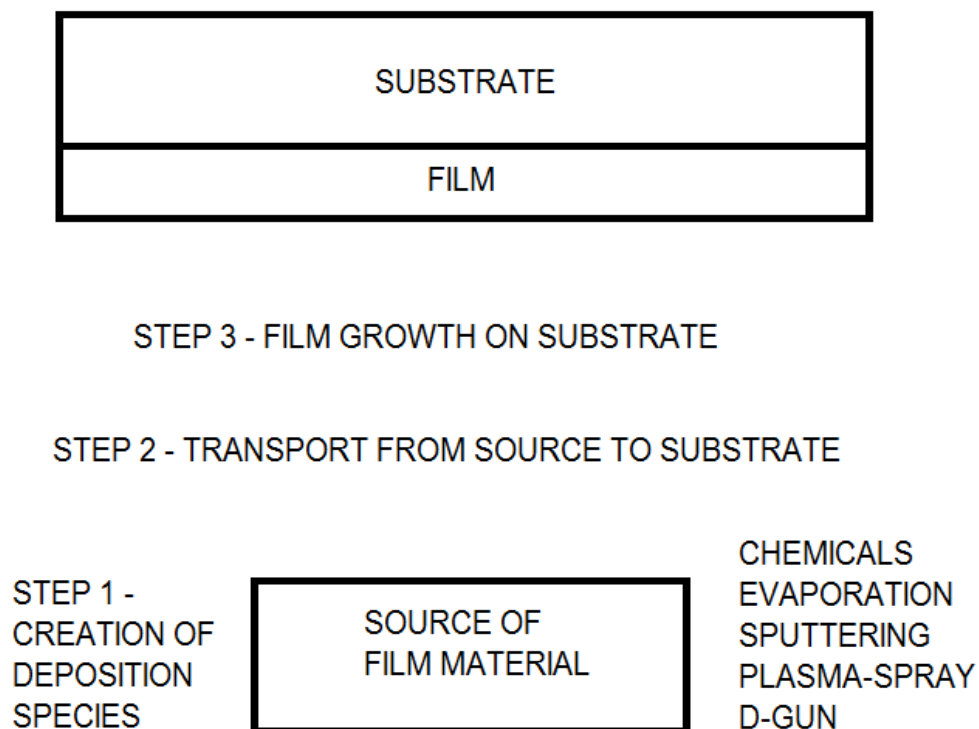
Figure 2.6. Schematic of typical three steps in deposition process [64]

More specifically, the most consistent deposition technology mentioned in the literature for the deposition of DLC and DLC based films onto rubber substrates was pioneered by the De Hosson research group in the Netherlands. In their work DLC films were deposited onto

various rubber substrates including HNBR, FKM and ACM by using a Plasma enhanced chemical vapour deposition (PECVD) process with an Ar and C_2H_2 plasma environment in a closed field unbalanced magnetron sputtering (CFUBMS) rig [24, 33, 34, 68-70]. Reactive magnetron sputtering has been used to deposit Ti-DLC and W-DLC films onto HNBR rubber in a CFUBMS system [22, 24, 58]. The scalability, reproducibility and known advantages of CFUBMS [71], combined with the breakthrough results presented including low frictional coefficients and low wear rates seem to give credence to this approach as the deposition method of choice for DLC and DLC based films deposited on rubber substrates.

2.3.3.2. Magnetron Sputtering

Sputtering as a technique to deposit thin coatings has been known for centuries, with one of the first published reports in 1852 [72]. Sputtering is the ejection of atoms by the bombardment of a solid or liquid target by energetic particles, mostly ions, and results from collisions between the incident energetic particles and/or resultant recoil atoms, with surface atoms as shown in Figure 2.7 [73]. After long periods of stagnation particularly due to limited understanding of the processes that occur during ion bombardment onto solid surfaces, sputtering as a deposition technique is on the increase in many research and industrial plants due to its ability to deposit a wide variety of materials, including DLC [73-75].
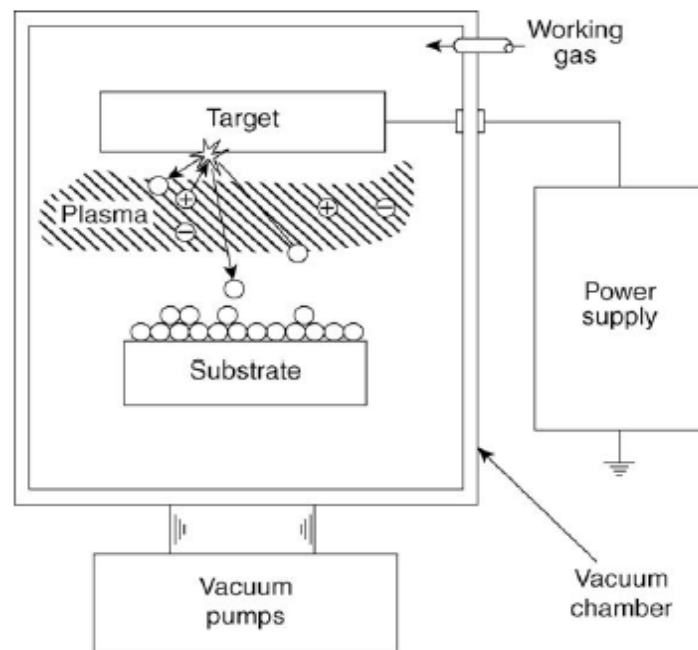
Figure 2.7. Basic sputtering process [73]

28

Two approaches used to produce ions and sputter the target materials include using an ion source aimed toward the target (ion beam sputtering) and plasma based sputter deposition. A typical plasma based deposition system includes a cathode and an anode positioned opposite each other in a vacuum chamber. The DLC deposition sputtering is either DC or RF biased of a graphite electrode in Ar plasma. In the sputtering process, positive gas ions (usually argon gas) produced in a glow discharge (gas pressure 20 – 150 mtorr) bombard the target material (also called the cathode), dislodging groups of atoms which then pass into the vapour phase and deposit onto the substrate. [73]

However, because of the low sputter yield (defined as the ratio between the number of sputter-ejected atoms and number of incident projectiles [73]) of graphite, low deposition rates, and low ionisation efficiencies in the plasma, magnetron sputtering is often used to increase the deposition rate [74]. The placement of magnets behind the targets enables the electrons to spiral and increase their path length, hence increasing the degree of ionisation of the plasma. The magnetrons are arranged in such a way that one pole is positioned at the central axis of the target and the second pole is formed by a ring of magnets around the outer edge of the target [71].

The application of a magnetic field during sputter deposition enhances the entrapment of electrons in the discharge longer and, hence, production of more ions for the same electron density by increasing the probability of an ionising electron-atom collision occurring [71, 73]. These magnetrons can be powered by various methods including; RF, DC, pulsed DC and high power impulse magnetron sputtering [71].

Magnetrons make use of the fact that a magnetic field configured parallel to the target surface can constrain secondary electron motion to the vicinity of the target, resulting in increased ionisation efficiency, dense plasma in the target region, increased ion bombardment of the target, higher sputtering rates, lower operating pressures (typically, 10^{-3} mbar, compared to 10^{-2} mbar), lower operating voltages (typically, -500V compared to -2 to -3 kV) and therefore, higher deposition rates at the substrate than is possible in basic sputtering mode [71]. As ion bombardment helps the formation of carbon sp^3 hybridisations, the magnetic field can be configured to pass across the substrate, causing Ar ions to also bombard the substrate, in an 'unbalanced magnetron' configuration [76].

2.3.3.3. Closed Field Unbalanced Magnetron Sputtering (CFUBMS)

In a conventional magnetron the plasma is strongly confined to the target region, which implies that films grown on substrates positioned in this region will be subjected to concurrent ion bombardment, however, substrates placed outside this region will lie in an area of low plasma density with ion current drawn at the substrate being insufficient to modify the film structure [71]. Unbalanced magnetrons provide the conditions necessary to deposit dense films without introducing excessive intrinsic stresses.

Kelly and Arnell [71], in their excellent review of magnetron sputtering, have classified unbalanced magnetrons into two types, Type 1 and Type 2. In Type 1 the central pole is strengthened relative to the outer pole and has limited applicability. In Type 2 systems the outer ring of magnets is strengthened relative to the central pole, which implies that not all of the field lines are closed between the central and outer poles in the magnetron, but some are directed towards the substrate with some secondary electrons being able to follow these field lines as first discussed by Window and Savvides [76, 77]. Consequently, the plasma is no longer confined to the target region, but is also allowed to flow out towards the substrate; hence, high ion currents providing a high flux of coating atoms (compared to basic sputtering) can be extracted from the plasma without the need to bias the substrate [71].

Figure 2.8 shows a schematic representation of the plasma confinement observed in conventional and unbalanced magnetrons. The adoption of multiple magnetron systems for commercial and research based CFUBMS systems was pioneered in the 1990s through the work of Teer Coatings Ltd, Hauzer Techno Coating and others [78-80]. In these systems an even number of vertically opposed magnetrons surround the rotating substrate holder with adjacent magnetrons having opposite magnetic polarities and closed field lines. This has resulted in CFUBMS systems being used extensively for the deposition of advanced coatings such as multi-layered, doped or alloyed films including DLC and DLC based films, as each of the magnetron targets can, in principle, be of a different material. By sputtering the targets at different rates any desired alloy composition can be attained. CFUBMS has been successfully used to deposit DLC films onto rubber substrates [22, 24, 33].
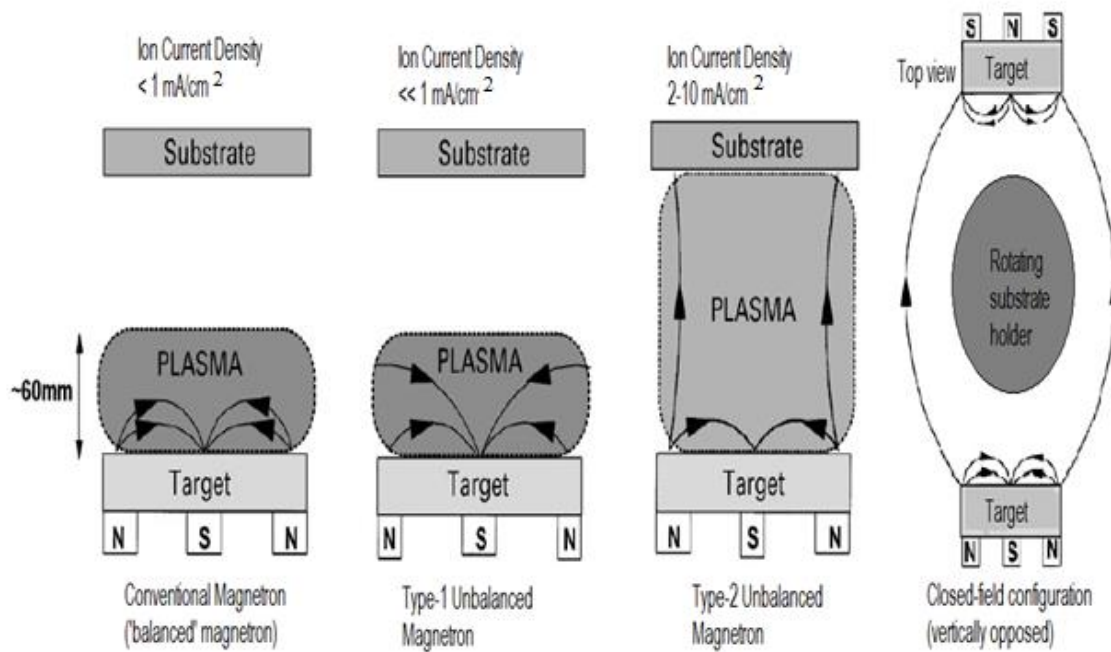
Figure 2.8. Schematic representation of the plasma confinement observed in conventional and unbalanced magnetrons [71]

2.3.3.4. Reactive Magnetron Sputtering

Reactive sputtering can be defined as the sputtering of elemental targets in the presence of chemically reactive gases that mass react with both the ejected target material and target surface [81, 82]. Usually a metal target is sputtered in a mixture of argon (Ar) and one or more reactive gases [81, 83]. Reactive magnetron sputtering has been used to deposit Ti-DLC and W-DLC films onto HNBR rubber in a CFUBMS system [22, 23, 58].

The popularity of DC reactive sputtering from elemental targets can be attributed to several factors including: capability of producing thin compound films of controllable stoichiometry and composition at high deposition rates and on an industrial scale [81-83]; higher purity of elemental targets usually implies high-purity films can be produced; avoidance of the complexity and expense of RF systems since metallic targets are generally electrically conductive, and hence, DC power can be applied; ease to machine and bond elemental targets; thermal conductivity of metallic targets allows for more efficient cooling these targets, thus, the range of the applied power can be extended without the fear of being cracked; and, film deposition at temperatures less than 300°C [81].

Although reactive sputtering is conceptually simple and advantageous compared to compound sputtering, reactive sputtering is in fact a complex non-linear process and in most cases suffers from hysteresis effects due to target poisoning emanating from the interaction of the target with the reactive gases [73, 81, 83, 84]. Consequently, the sputtering yield and the sputtering rate decrease as a result of the build-up on an electrically less conductive compound layer on the cathode surface which could lead to charge accumulation and arcing [83].

2.3.3.5. Structure zone models

Structure zone models (SZMs) are attempts by several authors to summarize the influence of deposition parameters on film morphology and microstructure in a single diagram where relationships between process parameters and the structure and properties of the films are displayed [71, 73]. For CFUBMS systems, Kelly and Arnell [71] compared, in terms of homologous temperature of the positions of the zonal boundaries given in published SZMs of Thornton [85] and Messier [86] relating to other sputtering systems (see Figure 2.9).
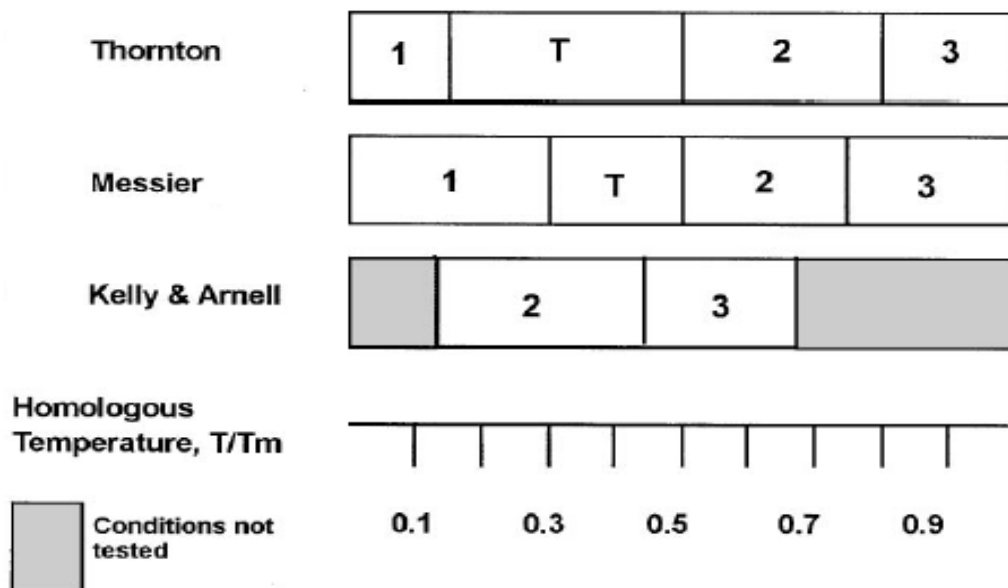
Figure 2.9. A comparison, in terms of homologous temperature, of the positions of the zonal boundaries given in published structure zone models relating to other sputtering systems with the boundaries observed for CFUBMS systems [87]

Clear evidence showed that operating in the closed field unbalanced magnetron sputtering mode suppressed the formation of porous columnar zone 1-type structures and promoted the formation of fully dense structures at low substrate temperatures. They consequently proceeded to develop a novel SZM adequate for CFUBMS systems that describes the film structure in terms of homologous temperature, ion-to-atom ratio and bias voltage [87].

2.3.3.6. Other Deposition technologies for DLC on rubber substrates

DLC can be deposited via physical vapour deposition (PVD) for hydrogen free DLC, or chemical vapour deposition (CVD) for hydrogenated DLC or a-C:H [17]. More specifically, various deposition technologies abound in literature for the application of DLC and DLC based thin films onto rubber substrates.

Martinez et al. deposited DLC on nitrile-butyl rubber like materials using a plasma enhanced CVD (PECVD) process with RF biasing, utilising an organosilicon precursor and afterwards C_2H_2 gas. CoF values of 0.5 were reported [18]. Takikawa et al. prepared DLC films on rubber substrates using T-shape filtered arc deposition with Ar, H_2, acetylene (C_2H_2), ethylene (C_2H_4), and methane (CH_4) introduction gases [20]. The DLC films were reported to contain hydrogen when hydrocarbon gases were used. With C_2H_2 gas, the highest deposition rate with lower surface roughness values was achieved. Miyakawa et al. also used a T-shape filtered-arc-deposition with C_2H_2 gas to deposit a stretchable and bendable DLC [21]. Nakahigashi et al. used radio frequency (RF) plasma assisted CVD with methane (CH_4) plasma to deposit DLC films onto various rubber substrates, including NBR [19]. The coefficient of friction when sliding against stainless steel counterparts for NBR was approximately 0.7 compared to 1.5 for uncoated NBR. Aoki and Ohtake also deposited DLC films onto rubber and aluminium substrates by RF-plasma CVD with methane gas [88]. Masami et al. deposited Si-DLC coatings on fluoro – rubber by a bipolar pulse type plasma based ion implantation system [27]. Yoshida et al. deposited DLC on silicone rubber by femtosecond-pulsed laser ablation of frozen $C_5H_{11}OH$ target [89]. However, the coefficient of friction of the coated rubber was inadequately determined and instead a 30 per cent reduction in friction angle was reported for DLC coated rubber compared to uncoated one.

2.3.4. Film Characteristics

2.3.4.1. Introduction

A significant aspect of the research into DLC films deposited on rubbers is dedicated to determination of the film characteristics and quantification of specific film properties. Whereas DLC films have been discussed extensively and their characteristics and film properties amply elaborated previously for DLC films deposited on metals, ceramics, and specific polymers [17], studies focused on characteristics of DLC films deposited on rubber continue to lag far behind due to the fact that actual deposition of DLC onto rubbers was realized much later [18, 19]. Also different characteristics can be expected for the various types of rubber each of which can have unique properties and grades including NBR, HNBR, ACM, FKM, to name a few [18, 19, 27, 33, 68]. The DLC films deposited on rubbers are fabricated in a variety of compositional, morphological and microstructural configurations with monolithic (DLC films only [19]), alloyed (Ti-DLC [22], W-DLC [23, 58], Si-DLC [27], etc.), and graded structures (W-DLC deposited on HNBR with Cr interlayer [23]). These various unique processing conditions including: substrate influence on properties, presence of interlayers, and alloyed compositions affect the characteristics of the films and necessitate a continuous characterisation effort [90].

2.3.4.2. Raman Analysis

All carbons show common features in their Raman spectra in the $800 - 2000$ cm^{-1} region, the so-called G and D peaks, which lie at around 1560 cm^{-1} and 1360 cm^{-1}, respectively, for visible excitation, and the T peak at around 1060 cm^{-1}, for UV excitation [91-94]. The G peak is due to the bond stretching of all pairs of sp^2 atoms in both rings and chains. The D peak is due to the breathing modes of sp^2 atoms in rings [42, 95]. The T peak is due to the C-C sp^3 vibrations [94]. These common features imply that Raman spectroscopy, which is a fast and non-destructive characterization method, provides an effective way of studying the chemical bonding and structure of DLC and DLC based films [42, 92].

For DLC films deposited on rubber few studies have investigated the chemical and structural bonding of these films [20, 21, 68, 88, 89]. Takikawa et al. [20] analysed the DLC film prepared on EPDM rubber with a laser micro Raman spectrophotometer (under various

excitation wavelengths) and found that for all of the films typical DLC spectra such as the broadened hybrid spectra of G-band (at approximately 1580 cm^{-1}) and D-band (at approximately 1380 cm^{-1}) were observed. Also a weak shoulder at approximately 1150 – 1200 cm^{-1} appeared only for the film prepared under C_2H_2. Similar results were displayed by Miyakawa et al. [21]. The origin of this shoulder is still inconclusive in the literature with some arguments for assignment of these peaks to nano-crystalline diamond or other sp^3-bonded phases or as an indicator of C-C bonds in the films [96-98] and other arguments for assignment to transpolyacetylene segments at grain boundaries and surfaces [41, 99]. An increase in the photoluminescence background was observed for films prepared under H_2 and hydrocarbon gases an indicator of H_2 in the films [20, 42, 68]. Furthermore, for deposition of DLC films onto rubber with C_2H_2 gas, a broad C-H stretching band, around 2800 – 2900 cm^{-1} was clearly observed, further categorising the film as hydrogenated amorphous carbon (a-C:H) [21].

Yoshida et al. used Raman spectroscopy (Jasco, NR-1800 using a 514.5 nm excitation wavelength) analysis to identify DLC films deposited on silicone rubber [89]. A broad Raman peak centred at 1530 cm^{-1} was measured for the film deposited on silicone rubber, showing a DLC. A double Gaussian peak analysis was used to quantify the ratio of intensity of the D peak to that of the G peak, I_D/I_G. It was found that the ratio of I_D/I_G for DLC deposited on Si wafer were higher than for DLC film deposited on silicone rubber. Yoshida et al. [89] concluded that the sp^3 content in the films deposited on silicone rubber was therefore higher based on the work of Ferrari and Robertson [95]. In addition it was also suggested that sp^3 content and I_D/I_G ratios do not depend on film thickness [89], which is contrary to the work of Jaoul et al. who determined that the intensity of the G peak (I_G) reduced as the DLC thickness reduced [100].

Martinez-Martinez et al. studied the chemical bonding of DLC films deposited on ACM rubber by means of Raman spectroscopy (see Figure 2.10) using a 532 nm excitation wavelength for DLC films prepared at different voltages (300, 400 and 600 V) [68]. They obtained qualitative information about the bonding structure in DLC coatings by performing a fitting analysis using a combination of Lorentzian and Breit-Wigner-Fano functions for D and G peaks. The G position and intensity ratios (I_D/I_G) in the range of 1528 – 1539 cm^{-1} and 0.4 – 0.5 were reported [68]. The low I_D/I_G ratio and G position arise from low sp^2 clustering and high structural disorder of the carbon network as it is generally observed in many

amorphous hydrogenated and free-H carbon films [42]. Martinez-Martinez et al. concluded by noting that the change of bias voltage does not have a significant influence on the sp^2 content, but rather on the structural and topological disorder [68].
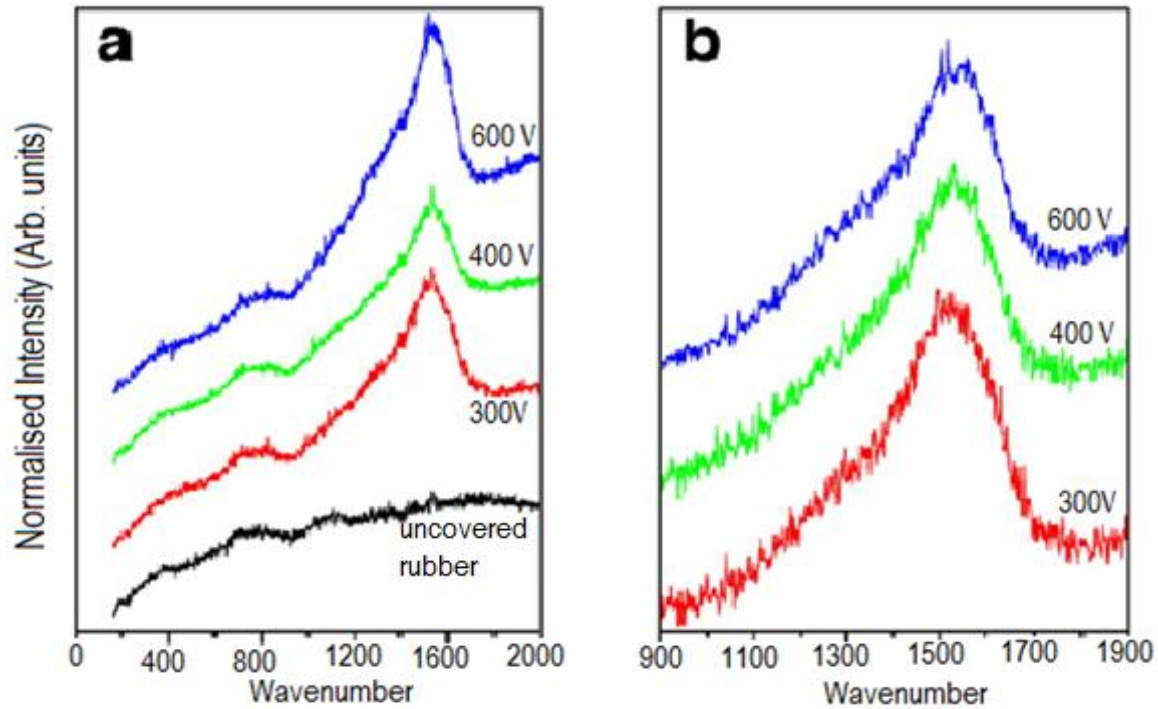
Figure 2.10. Raman spectra of films prepared at different voltages of 300, 400 and 600 V including the ACM substrate a); and detail of the region from 900 to 1900 cm^{-1} b) [68]

Based on the review of the literature regarding Raman analysis as a characterisation technique for determining the chemical and bonding structure for DLC films deposited on rubber, certain gaps become quite apparent. Firstly, no Raman analysis has been carried out on doped DLC films and DLC films with interlayers deposited on rubber. Therefore, the influence of the dopant on the bonding structure of such films deposited on rubber substrates remains unknown. Secondly, most of the Raman analyses were performed at visible excitation energies. Few Raman spectroscopy analyses have been carried out for DLC and DLC related films deposited on rubber substrates [20, 21]. Such a multi-wavelength analysis was recommended by Casiraghi et al for DLC and DLC related films as a means of determining the dispersion of the G peak (Disp(G)) [42]. Finally, Raman spectroscopy analysis has been used to successfully determine the wear mechanisms involved during tribo-tests for DLC films sliding against metals by analysing the wear track before and after tribo-

testing [31, 32, 51]. Such an analysis has never been carried out for DLC films deposited on rubber substrates.

2.3.4.3. Surface morphology and microstructure

The surface morphology of DLC films deposited on rubber substrates is characterised by a dendritic regular crack-like network [18-20, 34], which has been recognised as contributing positively to the performance of the DLC coatings on rubber due to the improvement in flexibility of the coatings when the substrate deforms without interfacial delamination [23]. As shown in Figure 2.11, these crack networks separate the coatings into micrometre-scale domains (patches). The patches were observed to reduce from 70 µm to 10 µm with increasing bias voltage from 50 V to 300 V [22].
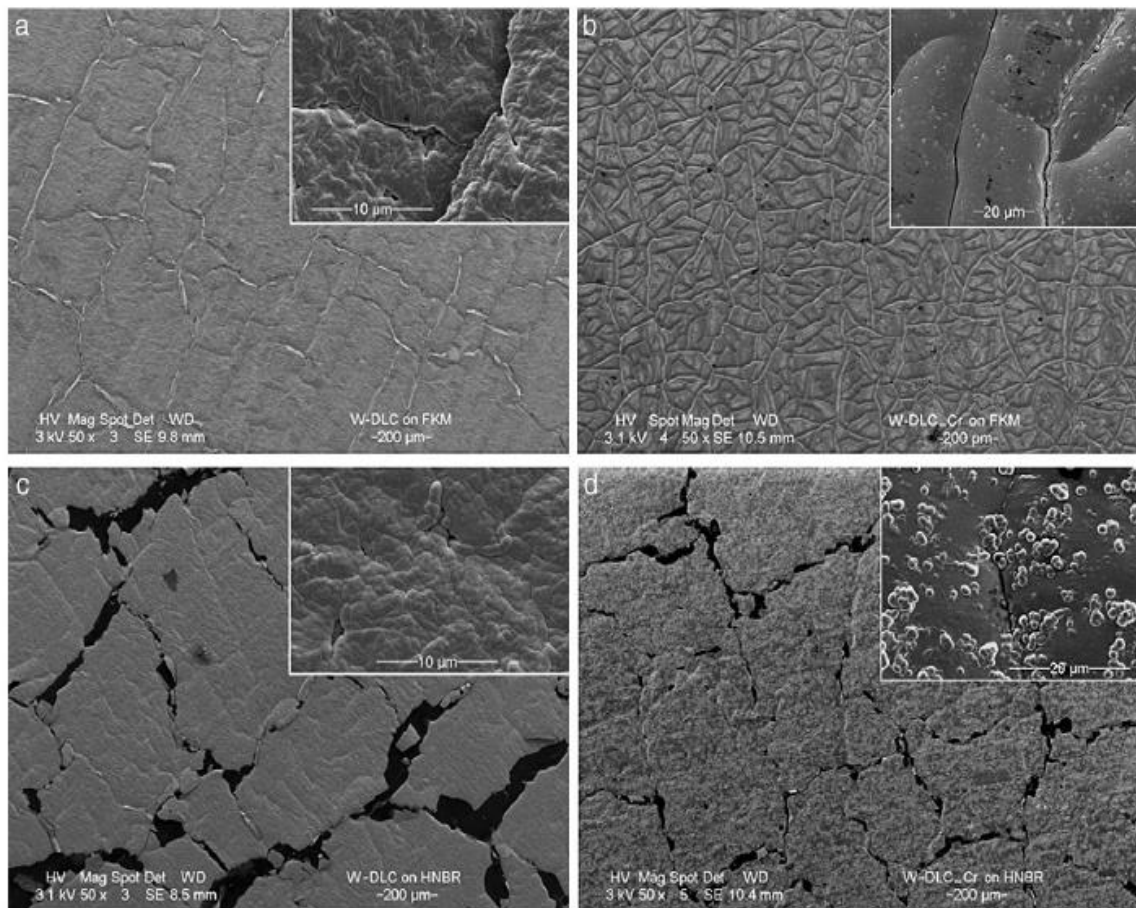
Figure 2.11. Surface morphology of W-DLC coatings deposited on FKM rubber (a - without Cr interlayer; b - with Cr interlayer) and HNBR rubber (c - without Cr interlayer; d - with Cr interlayer) [23]

This evolution of surface morphology has been related to the maximum deposition temperature and the temperature variation per revolution of the sample carrousel. Due to the huge difference in coefficient of thermal expansion (CTE) between DLC (6×10^{-6} K^{-1}) when compared to rubber (CTE for HNBR is 180×10^{-6} K^{-1}) [58], the amount of expansion or shrinkage of the rubber substrate during each revolution of the sample carrousel is high enough to break up the coatings when the adhesion between the coating and the rubber is strong enough (at 100, -200 and -300 V bias). Delamination bands may form in the case of poor adhesion (-50 V bias), due to large size patches and the release of thermal strain of rubber substrate during the cooling phase after deposition [22].

These cracks originate at the first atomic layer of DLC on rubber due to thermal stress mismatch and continuously grow upwards together with the film itself resulting in a patch size of the DLC films in the micrometre scale range [24]. A much smoother morphology was observed when a Cr interlayer was employed on FKM rubber. For W-DLC doped on HNBR rubber with a Cr interlayer a large amount of micrometre sized patches were observed. This was correlated to the powdery surface of HNBR rubber, which leads to enhanced instability of the growing interface during the deposition of the Cr interlayer [23]. DLC films deposited on rubber substrates have been characterised as having a columnar microstructure [22, 23, 68] from fracture cross-section analyses for films deposited using CFUBMS systems. The columnar growth is related to the interface structure of the growing coating, which is controlled by the intensity of the concurrent ion impingement [101]. This assertion is contradictory to the work by Kelly and Arnell [87] who showed that for CFUBMS systems the formation of columnar structures is suppressed and instead fully dense structures are formed at low substrate temperatures.

Despite considerable effort made towards understanding the surface morphology and microstructure of DLC and DLC films deposited on rubber substrates some gaps still persist. Few studies have investigated the role of dopants in the DLC films [22, 23]; and the role of an interlayer on the structure of DLC and DLC based films deposited on rubber substrates [24, 58]. Also the impact of deposition at lower substrate bias voltages (< 50 V bias) on the surface morphology and microstructure has also not been discussed.

2.3.4.4. Hydrophobicity studies and surface free energy calculation

Studies investigating the hydrophobicity and surface free energy of DLC films deposited on rubber substrates are very few in the literature [18-20]. Information about the hydrophobicity of the surface is important in determining possible industrial application as contact angle (CA) is typically the property measured for estimation of surface energy of non-stick coatings [18]. A hydrophobic surface is one whose contact angle is over 90° [102].

Martinez et al. carried out measurements of CA by sessile drop method on NBR substrates coated with amorphous hydrogenated DLC coatings [18]. The CA measurement results are shown in Figure 2.12. The DLC coated NBR samples were more hydrophobic with water contact angles of up to 116°. An increase in the hydrophobic properties of DLC coated elastomers was explained by the presence of a mixture of sp^2 and sp^3 hybridized carbon bonds in the DLC coatings, which is also related to a lower reactivity of the DLC coated surface [103]. The variation in the CA for DLC coated HNBR compared to uncoated HNBR was insignificant. It is suggested that the hydrogenation of unsaturated bonds to form HNBR results in different reactivity of the elastomer towards the DLC coatings [18].
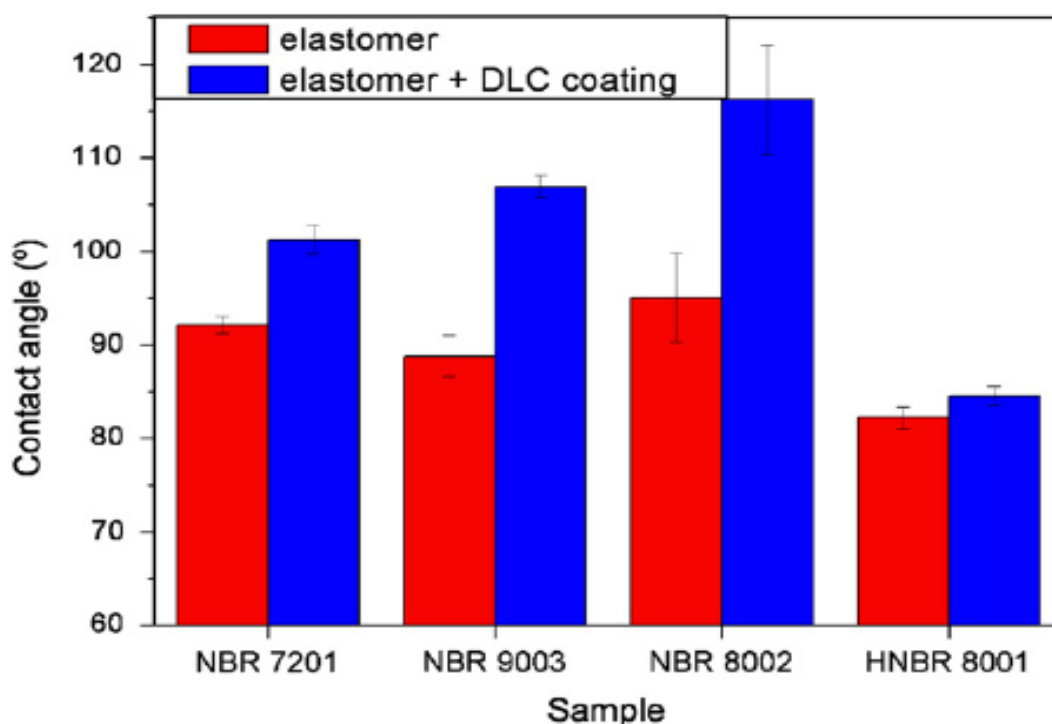
Figure 2.12. Water CA measurements before and after coating with DLC [12]

Takikawa et al. [20] investigated the water contact angle for DLC films prepared under various gas species deposited on EPDM rubber substrates. The water contact angle was measured by a face contact angle meter with a water droplet volume of approximately 10 μl. The water contact angle of the DLC film surface was higher than the EPDM surface for all deposition conditions investigated, indicating a slight modification of hydrophobic property [20]. Using the same method, Nakahigashi et al. [19] carried out water repellence measurements on polyurethane rubber substrates, one unprocessed and the other coated with DLC. The contact angle for pure water for the unprocessed substrate was approximately 80°, while it was 90° for the DLC film coated sample indicating high water repellence of the DLC coated sample.

Surface energy is usually obtained by measuring the CA for more than one liquid and distributing the tension between the dispersive and polar components [17]. Water, glycerol, ethylene glycol, diiodomethane and formamide would be typical liquids used for such an analysis [18]. Calculated surface free energy values were between 33 and 43 mJ/m^2 for DLC films deposited on nitrile-butyl rubber substrates using the acid-base regression method [18]. For the NBR elastomers the total surface free energy decreased after DLC coating, whereas for the HNBR elastomer coated with DLC coating, the total surface free energy increased. Lower CAs and higher surface free energies are expected for surfaces containing more polar oxygen functional groups [18].

The following gaps can be identified from the literature of DLC films deposited on nitrile rubber in connection to hydrophobicity and surface free energy studies: The impact of doped DLC and multilayer DLC based coatings deposited on rubbers on the water CA measurements has not been presented. An investigation into the mechanical properties of amorphous carbons as a bio-mechanical coatings showed that the addition of Si or F resulted in a decrease in the surface energy to between 19 and 24 mN m^{-1} [104]. The influence of doped DLC and multilayer DLC based films deposited onto rubber substrates on the surface free energy has also not been presented.

2.3.4.5. Adhesion and flexibility

Good adhesion between the DLC film and the substrate is essential in order to optimise the functionality of the film [17]. Adhesion of DLC films deposited on rubber substrates has been investigated by relating the adhesion of the DLC films to simple flexibility analysis [20, 21, 24, 33]. The peel tape test [105] was used successfully for the determination of the adhesion of DLC films to polymer substrates [106, 107].

By making use of the substantial thermal mismatch between DLC film and rubber substrate, a dense network of cracks forms in the DLC films and contributes to flexibility of DLC film [70, 108, 109]. DLC films deposited on EPDM substrate adhered well and did not peel off when the substrate was bent and stretched by hand. The flexibility of the DLC film coated on the rubber was observed also when the substrate was folded and clipped [20]. Films prepared under no gas were found to contain smaller and round DLC islands on the rubber separated from each other, while the films prepared under C_2H_2 gas were found to contain larger and rectangular DLC islands separated. The island textured structure allowed the flexibility of the coating to follow the stretch of the rubber [20]. Miyakawa et al. performed their flexibility tests by bending at 180° the DLC film deposited on rubber 10 times and observing the surface (see Figure 2.13) [21]. The DLC film on the rubber was observed not to peel off and this has been attributed to the many cracks which open when the substrate is stretched [21].
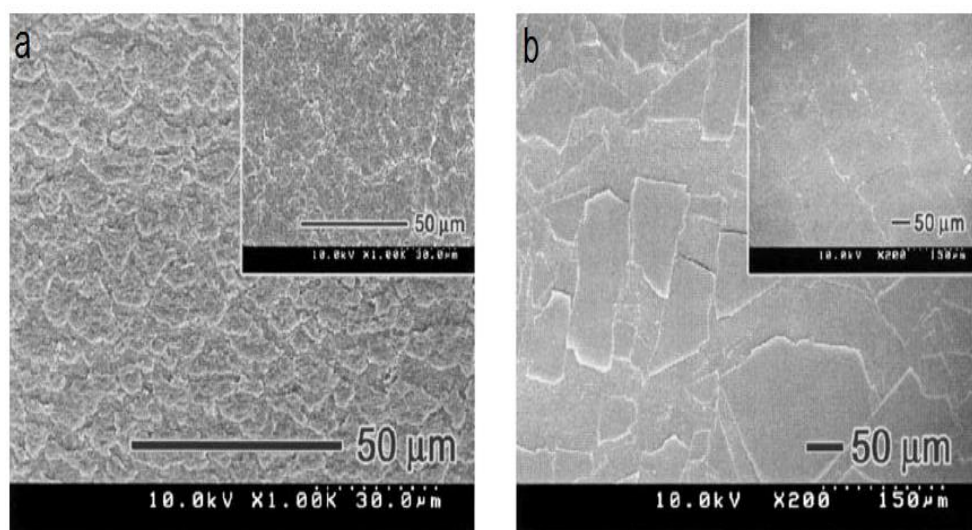
Figure 2.13. FE-SEM micrographs of DLC film surfaces prepared on EPDM when the substrate was bent approximately 10 times. Insets show the surface after releasing the bending force; a - without C_2H_2; b - with C_2H_2 gas flow [21]

Various strategies have been proposed in the literature in order to improve the adhesion of DLC films deposited on rubber substrates. One strategy focusses on plasma pre-treatment prior to deposition of DLC films with the purpose of surface cleaning and activating the substrate surface [24, 33, 69]. Following different plasma pre-treatments the interfacial adhesion strength and flexibility of DLC films on HNBR substrates were examined by tensile stretch tests and in situ SEM observation. At high strain rate (50 per cent), new generations of cracks form and split the segments further [24]. If the adhesion strength between the DLC film and rubber substrate is good, generation and opening of cracks are the only mechanism responsible for releasing the stress applied on the whole system resulting in a higher crack density as illustrated in Figure 2.14a. However, if the adhesion is poor, de-bonding at the crack banks occur in order to release stress resulting in fewer cracks but with larger openings (lower crack density) as illustrated in Figure 2.14b [24, 110]
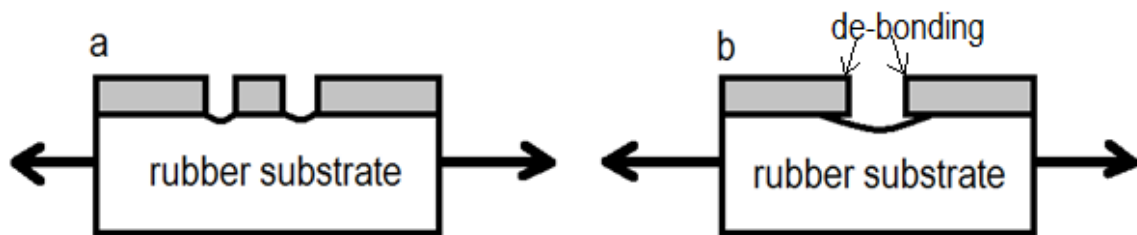
Figure 2.14. Schematic of the response of DLC thin film coated HNBR with, a - strong adhesion, b - weak adhesion [24]

The second approach involves the use of an interlayer. The idea is that the intermediate layer should yield locally below the film, and thereby absorb the effect of the compressive stress [17]. Pei et al. [23] used this approach for W-DLC coated on FKM and HNBR rubbers. A chromium (Cr) interlayer of 120 nm thickness was deposited before the W-DLC film. SEM micrographs showing the wear tracks on W-DLC coated HNBR rubbers with Cr interlayer were almost undetectable. The Cr interlayer did not enhance the adhesion of the coatings on FKM rubber and, the interfacial delamination of the films was attributed to the Cr interlayer [23]. The enhancement of adhesion for HNBR rubber and the dis-enhancement for FKM rubber implies that more work is required to understand the role an interlayer can play in promoting adhesion of DLC and DLC based films onto rubber substrates.

2.3.4.6. Hardness

Measurement of DLC film hardness on rubber materials is very difficult as the rubber itself undergoes deformation [19, 22]. Using a super-minute hardness meter pushed into 20 places at the centre part of the grain of DLC, Nakahigashi et al. estimated a hardness value of 0.1 GPa [19]. This value is much lower than the value of 10 – 20 GPa reported for both hard and soft hydrogenated amorphous carbons [17]. The Meyer hardness, which represents the ratio of indentation load to contact area, was obtained for fluoro rubber and DLC coated rubber using an optical indentation microscope system. A Berkovich shape diamond tip was used as indenter tip with a maximum indentation load of about 1 mN. The Meyer hardness for Si-DLC coated rubber was 2.38 MPa and is about 1.4 times larger than that for uncoated rubber [27]

In order to circumvent the problem of rubber substrate deformation, Bui et al. [22] deposited Ti-DLC films simultaneously on both HNBR rubber substrates and Si wafer under similar deposition conditions. Hardness measurements were carried out on the Si wafer coated with the Ti-DLC film as a reference using a nano-indenter (XP) with a Berkovich diamond indenter. Coating hardness was observed to increase from approximately 9 to 16 GPa with a bias from -50 to -300V as shown in Figure 2.15 [22].
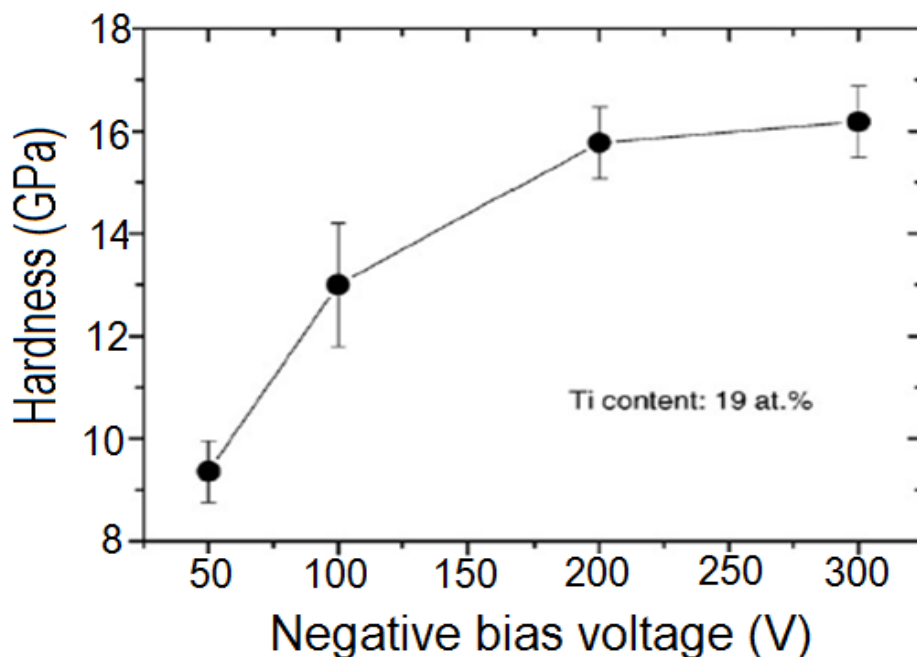
Figure 2.15. Hardness as a function of the bias voltage of Ti-DLC coatings deposited on Si wafer [22]

The coating hardness increase with increasing bias voltage is due to the adsorption of species at the growing interface and the implantation at the subsurface which depend on the ion energy and bias voltage [111]. Under low voltages the ion energy is not high enough to knock adatoms to penetrate through the interface and most of the ions are only trapped on the growing interface. This results in the formation of loose cross-linking bonds with low density and low sp^3 fraction, hence low hardness. However, under high bias voltages, the ion species have sufficient energy to penetrate into the subsurface. This ion implantation is associated with higher compressive strength, film densification, increase in sp^3 fraction and higher hardness. The hardness values for DLC coatings deposited on rubber substrates are expected to be lower, but to follow a similar trend. [22]

2.3.4.7. Coefficient of friction

Most publications dealing with DLC and DLC based films deposited on rubber substrates discuss their tribological behaviour [18, 19, 22-24, 27, 34, 58, 69, 70, 88]. Friction is the resistance to relative motion between two bodies when relative motion occurs between them [112]. Friction is the dissipation of energy as two surfaces move over each other [113].

The coefficient of friction μ is given as the ratio of the lateral (tangential) friction force, F, to the normal force, W, as shown in eq. (2.1) [17, 113].

$$\boldsymbol{\mu = \frac{F}{W}} \qquad (2.1)$$

Low friction coefficients are characteristic of the frictional behaviour of DLC [17]. This low frictional behaviour can be explained by the phase transformation that takes place as the contact region becomes elastic [114], graphitization of the contact area [31, 51] and the formation to a transfer layer [52] implying that the contact is between similar hydrophobic DLC surfaces.

More specifically for DLC films deposited on rubber substrates, Nakahigashi et al. using RF CVD deposition with CH_4 gas obtained frictional coefficients ranging from 0.6 to 1.3 for DLC films deposited on various rubbers compared to frictional coefficients ranging from 1 to

6 depending on the substrate material (See Figure 2.4) [19]. The application of DLC onto rubber substrates significantly reduced the frictional coefficients. The friction coefficients were measured with a load of 0.1 N and ball speed of 10 mm/s. An aluminium ball of diameter of 8 mm was used as the counterpart.

Aoki and Ohtake [88] deposited DLC onto rubber substrates using a similar method to Nakahigashi et al. [19]. The frictional characteristics were evaluated using a rotational ball on disc apparatus. A sliding speed of 0.1 m/s and a normal load range of $0.5 - 5$ N were used. Stainless steel balls of diameter of 6 mm were used as counterpart material. The frictional coefficients of the DLC film were approximately constant between 0.1 and 0.2 during 9000 cycles at loads of 0.98 to 1.96 N. However, at higher loads of 2.94 and 4.9 N, a higher friction coefficient was observed at around 200 cycles because the rubber substrate was fatally damaged due to the high load rather than due to the DLC film peeling off. Frictional coefficients were less than 0.4 even during tests where the film was damaged [88]

Yoshida et al. deposited DLC on silicone rubber by femtosecond-pulsed laser ablation of frozen $C_5H_{11}OH$ target [89]. The friction of coated rubber was evaluated via the angle of friction. A 30 % reduction in friction angle was reported with DLC film deposited on silicone rubber compared to uncoated silicone rubber.

The De Hosson group performed their tribo-tests on a CSM high temperature tribometer with ball on disc configuration. The counterpart material was 100Cr6 steel ball of diameter of 6 mm and hardness HRC 60-62. Tribo-tests were carried out at sliding velocities of ranging from 5 cm/s to 40 cm/s and normal loads of 1, 3 and 5 N [22-24, 33, 34, 58]. Table 2.1 gives a summary of the state of the art for coefficient of friction results for DLC films prepared on various rubber substrates. All of the coefficient of friction results discussed above and shown in Table 3.1 were obtained for tests carried out in dry conditions. There is no study that looks at the influence of wet sliding on the coefficient of friction for DLC coated rubber substrates.

Literature suggests that higher coefficients of friction are expected for DLC films during wet sliding [26, 115, 116]. Studies have also shown that Si-DLC films have lower friction coefficients during wet sliding [25]. However, such an analysis for DLC and Si-DLC films coated on rubber substrates has never been reported. Such an investigation is necessary so that the possible applications of coated DLC films deposited on rubber substrates can be

extended to wet sliding applications. One such application is DLC films coated on nitrile rubber piston seals used in reciprocating handpumps as discussed in Chapter One.

Table 2.1. Coefficient of friction results for DLC films deposited on rubber substrates

Substrate	Preparation		Tribo-test condition		Best CoF	Reference
	Method	Precursor	Load (N)	Speed (cm/s)		
Butyl rubber	PACVD (RF)	CH_4	0.98, 1.96	10	0.1-0.2	Aoki et al. [88]
			2.94, 4.90	10	Failure	
Several rubbers	PACVD (RF)	CH_4	0.1	10	~0.7	Nakahigashi et al. [19]
NBR, HNBR	PACVD (RF)	C_2H_2	10	10	0.49	Martinez et al. [18]
			40	1		
FKM, ACM, HNBR	PACVD* (DC)	C_2H_2	1, 3, 5	10	0.2-0.22	Pei et al. [58]
FKM, HNBR HNBR	PACVD* (DC)	C_2H_2	1	10	0.2-0.25	Pei et al. [23]
HNBR	PACVD* (DC)	C_2H_2	1, 3	10	0.19-0.2	Bui et al. [22]
HNBR	PACVD* (DC)	C_2H_2	1, 3	10	0.175-0.2	Bui et al. [33]
HNBR	PACVD* (DC)	C_2H_2	1, 3	10	0.167-0.18	Pei et al. [24]
Fluoro rubber	PACVD**	TMS, $Si(CH_3)_4$	0.49	1	0.2-0.25	Masami et al. [27]
ACM	PACVD* (DC)	C_2H_2	1	20	~0.22	Martinez-Martinez et al. [34]
ACM	PACVD* (DC)	C_2H_2	1, 3	5, 10, 20, 40	0.18-0.2	Schenkel. et al. [69]

* The deposition was done using CFUBMS with a pulsed DC power unit as substrate bias source
** The deposition was done by a bipolar plasma based ion implantation system

Finally, dependence of coefficient of friction on the precursor used during DLC deposition has been reported. The lower friction coefficient of DLC made from CH_4 compared to C_2H_2 is due to few dangling C bonds to form residual carbon [117]. Where precursor gases have been used in CVD and PECVD deposition of DLC films onto rubber substrates CH_4 and C_2H_2 gases have been used. Relations in terms of friction coefficients as a result of other precursor gases such as butane, C_4H_{10}, have never been made for DLC and DLC based films deposited on rubber substrates.

2.3.4.8. Wear

Wear involves the physical removal of material from a solid object as a result of one contact moving over another [57, 112, 113]. Wear is not a material property. Wear is a system response that varies depending on contact conditions including counterpart material, contact pressure, sliding velocity, contact shape, suspension stiffness, environment and lubrication

[57, 112]. As a result wear can proceed via various mechanisms such as abrasive wear, adhesive wear, fatigue wear, erosive wear, fretting wear and chemical wear [118].

Wear is the volume of material removed from a surface by relative contact. The volume of wear per unit track length, Q, is given by eq. (2.2) [17]:

$$Q = KA \qquad (2.2)$$

where K is the wear coefficient (a dimensionless number) and A is the real contact area. The real contact area A is given as the ratio of load, W, to the pressure or Hardness, H, of the softer surface. This result in the Archard equation as shown in eq. (2.3) [119]:

$$Q = K \times \frac{W}{H} = kW \qquad (2.3)$$

A dimensional coefficient k (with units of $mm^3N^{-1}m^{-1}$) is introduced. According to the Archard equation, the wear coefficient is inversely proportional to the hardness of the surface, which implies that harder surfaces wear less.

Quantitative analysis of wear of DLC films deposited on rubber substrates have not been performed because of the high deformation of rubber [69]. Since the deformation of rubber is high, the evaluation of wear by measuring the worn volume with profilometry is discouraged [69]. Due to the high deformation of rubber, Nakahigashi et al. in determining the wear rate of flexible DLC deposited on rubber substrates performed a comparative study by determining the wear volume for flexible DLC deposited on a Teflon sheet [19].

Wear analysis of DLC films deposited on rubber substrates usually proceeds qualitatively [22-24, 27, 33, 58, 69]. Qualitative comparisons of the same point of the film before and after the tribo-test are performed using scanning electron microscopy (SEM) analysis to examine the evolution of the wear track as shown in Figure 2.16 [22, 24]. The partial exposure of rubber substrate due to coating failure naturally increases the friction. However, the presence of some coating-steel counterparts resulted in coefficients to remain low at 0.46 for DLC films deposited on HNBR compared to > 1.3 for uncoated HNBR [22]. Optical microscopy (OM) is frequently used as well to analyse the wear track on the films as well as to discuss the wear of the counterpart balls after the tribo-tests [23, 27].
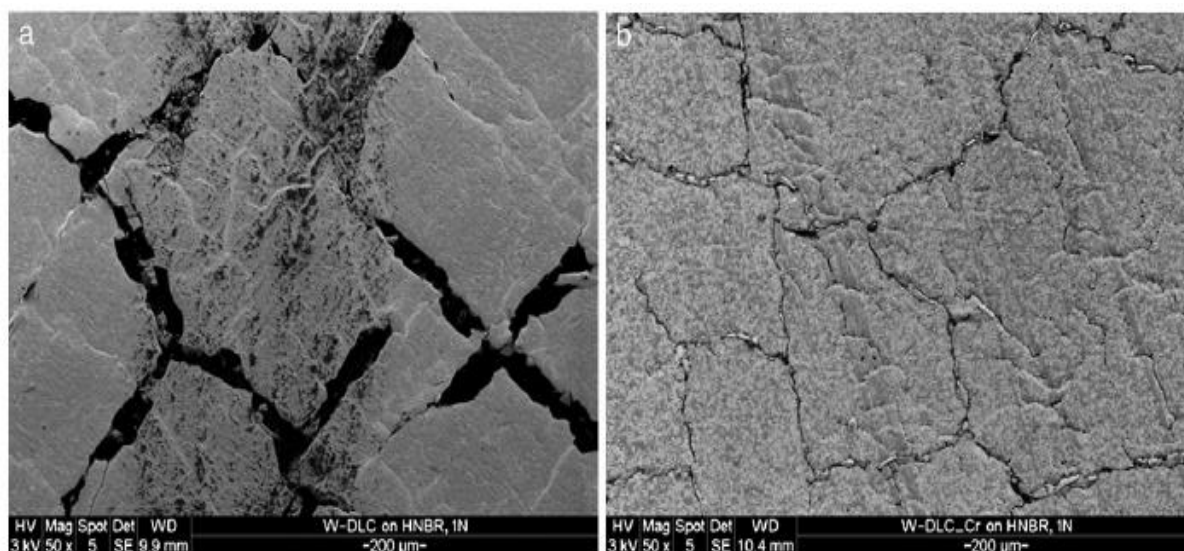
Figure 2.16. SEM micrographs showing the wear tracks on W-DLC coated HNBR rubbers: (a) without Cr interlayer and (b) with Cr interlayer [23]

Generally, for DLC films, doped DLC films and DLC films with interlayers deposited on rubber substrates very little attempts have been made to quantify the wear rate for these films. Also, the specific wear mechanisms involved in the wear of DLC and DLC based films deposited on nitrile rubber substrates have not been discussed in the literature.

2.4. Nitrile rubber as a substrate

Nitrile butadiene rubbers (NBR; also termed nitrile rubber), in the solid or latex state, are one of the most widely used, commercialized polymer materials [120]. Nitrile rubbers are manufactured mostly by emulsion polymerization. Nitrile rubbers belong to a group of materials known as elastomers. Elastomers (natural and synthetic rubber) are amorphous polymers to which various ingredients are added to form a compound. After heating and reaction, these materials become "rubber" which essentially is rubbery and elastic. However, rubber also dissipates energy because of their viscoelastic nature [121].

NBR are emulsion copolymers of acrylonitrile and butadiene (see Figure 2.17) [121-124]. The monomer ratio is varied within a wide range, reflecting the specific application of the product. A high acrylonitrile-to-butadiene monomer ratio increases polarity and thus

resistance to swelling, but renders the polymer mechanically inflexible at low temperatures [124].
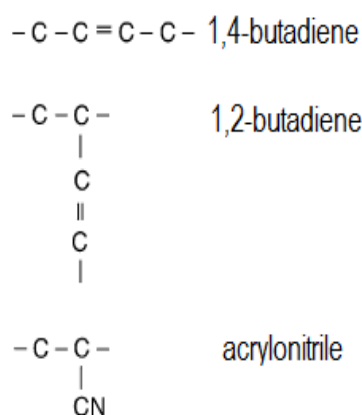
Figure 2.17. Monomers used in the synthesis of nitrile rubbers [122]

The acrylonitrile content in NBR can vary between 18 and 50%. An increase in acrylonitrile content is associated with an increase in strength, heat resistance and glass transition temperature; a decrease in resilience, die swell, and gas permeability is also associated [125]. The low-temperature flexibility of ordinary NBR varies in inverse proportion to its acrylonitrile content. Therefore, low-acrylonitrile NBR has better low-temperature flexibility than high-acrylonitrile NBR [126]. Because of unsaturation in the butadiene portion, NBR is susceptible to attack by oxygen and ozone. Nitrile rubber is widely used for seals [125].

2.5. Summary

A thorough review of DLC and DLC based films deposited on rubber substrates has been presented. This review is the first of its kind for DLC and DLC based films coated on rubber and is therefore a significant contribution to academia in this area. A review of the results of current characterization studies was presented. Gaps in the literature concerning DLC films deposited on rubber substrates have been highlighted. The development of closed field unbalanced magnetron sputtering as a deposition technology of choice for DLC and DLC based films onto rubber substrates was explained. The chapter ended with a brief description of NBR as a substrate material.

Chapter Three

Field Visits, Experimental and Characterization Methods

3.1. Introduction

The methods used in collecting data from field visits to Makondo Parish are described in this chapter. The deposition procedure of DLC and Si-DLC films onto nitrile rubber substrates and handpump piston seals is presented. The experimental methods and characterisation techniques that were used in this research study are detailed. The wear piston test rig and coated piston seal testing regime is also presented.

3.2. Field Visits to Makondo Parish

One of the main project objectives under the Water is Life Irish Aid sponsored project was that the social aspect of each research project be examined. As such field visits to Makondo Parish were necessary so that the hand pump as a developmental technology could be grounded in a specific rural community.

3.2.1. Objectives of the field visits

The objectives of the field visits were:

- To identify the actual hand pump users and to thus determine the problems that these hand pump users face as they use the handpumps
- To determine the availability of the handpumps in Makondo Parish as measured by the number of handpumps that are functional and those that are not functional
- To identify the handpump component that is replaced most frequently.
- To ascertain the extent of wear of piston seals and thus determine the characteristics in hand pump operation and the environment that are factors contributing to the wear of the piston seals.

In order to achieve the field visit objectives the following guiding questions were employed:

- Who are the actual handpump users?
- At what rate do handpump users fill water collecting containers?
- What problems do the users experience when using handpumps?
- What is the status of functionality of handpumps?
- Who is responsible for maintenance and repair of the handpumps?
- What component of the handpump is the most frequently replaced?
- To what extent can the wear of piston seals be categorized as a crucial factor affecting the life time of handpumps?
- What characteristics in handpump operation and the environment are determining factors contributing to the wear of the piston seals?

The responses to each of these questions were aimed at understanding the social and technical aspects related to piston seal wear. This information was necessary in determining the experimental variables during simulation of piston seal wear using the piston seal test rig. Emphasis on the piston seal was determined by the analysis of Reynolds who attributed 24% of handpump failures to failure of piston seals [6].

3.2.2. Sample Size

The sample size for respondents was determined using eq. 3.1.

$$n = \frac{Z^2\, p(1-p)}{c^2} \qquad\qquad 3.1$$

where n is the required sample size, which is the number of people accessing the functional handpumps; z is the confidence level at 95% (standard value of 1.96); p is the estimated prevalence of functional handpumps (handpump functionality was determined as 0.3) (See Section 4.2.1); and c the confidence interval at 5%. Handpump functionality of 0.3 is directly related to availability of safe water for these communities. This is guided by the fact that

handpump users access functioning handpumps. The calculated sample size was 322.64 respondents, which can be approximated to a minimum of 323 respondents.

3.2.3. Scope

From Figure 1.7 the geographical boundaries of Makondo Parish were identified. These boundaries provided the geographical location within which the field visit was carried out. In total fifteen villages were visited namely: Luyiiyi Kate, Misaana, Micunda, Makondo, Luyiiyi Protaz, Kiyumbakimu, Kijjajasi, Kiganju, Kibuye, Kiteredde, Kiguluka, Kanyogoga, Kayunga, Kyamukama and Wajjinja.

Women and children were the main target group for the structured and semi-structured interviews. Women and children are acknowledged in literature as the bearers of the water collecting burden. Men were also targeted. Hand pump mechanics in Makondo Parish were also a target group.

3.2.4. Methodology

The methods used during the field visit were complementary to each other. Both qualitative and quantitative methods were used. The data collection methods used in the field had to be flexible and ethically driven so that minimal intrusion to the daily schedule of the participants was achieved. The field visit lasted about 40 days.

3.2.4.1. Field Observation

Observation was used to physically locate the hand pumps and to determine their functionality. Field observation was used to observe the handpump users who operate the handpumps. Information on the number of strokes it takes to fill a water container (jerry can) was obtained in a non-intrusive manner. Before beginning any observational activity at a hand pump, the hand pump users were informed of the purpose of my visit so that a camaraderie atmosphere was developed at the functional hand pumps. Photographs were taken of the non-functional handpumps.

3.2.4.2. First Level of Surface Analysis

First level of surface examination as described by Ludema [127] was used to diagnose the tribological problem and identify the possible wear mechanisms and modes involved as follows:

- The hand pump was dismantled and worn piston seal surfaces cleaned.
- Sensory judgment (using visual inspection, touch, smell, etc.) to make a first judgment of the environment in which the surfaces are operating
- Observation of particular patterns using a 10X eyepiece magnifying glass was used.
- Determination of surface physical characteristics and the processes that produce them based on the observation of pits, ploughed ridges, and cracks on the surface.
- Observation was also used to identify worn piston seals during the maintenance of hand pumps by the hand pump mechanics.

3.2.4.3. Structured and semi-structured interviews

Semi-structured interviews were carried out with primary school children, women and men. All the participants were randomly chosen. Participatory approaches were used with the respondents given a set of cards to identify the hand pumps in their areas as well as locate problem areas. Different categories of respondents identified different types of hand pumps. In order to stimulate the identification process, the respondents were given A4 size photographs of different hand pump types. The respondents were also shown the internal components of the hand pump from which they were able to understand the components of the hand pump that actually fail including the chain, the rising main, the cylinder, the valves and the piston seals. The primary school children were aged between 9 to 14 years and the secondary school children had ages ranging from 15 to 18 years. There were at least two women representatives from each of the 15 villages that constitute Makondo Parish. The interviews were conducted in a relaxed atmosphere by the handpumps as users were queuing and during home visits. The respondents were encouraged to ask questions and cite examples related to their particular villages. These interviews each lasted between 30 and 45 minutes. As a prerequisite to participation, all participants were required to be regular handpump users.

Structured interviews were used with the two hand pump mechanics in Makondo Parish. The hand pump mechanics were informed of the purpose and the general structure of the interview. An appointment was made and a venue selected for these interviews. The duration of each interview was approximately 1 hour. The questionnaires used during the field visit are appended (See Appendix A).

3.2.4.4. Administration of questionnaires

Secondary school children (15 – 18 years) filled in questionnaires. There were 50 voluntary respondents. Prior to filling in these questionnaires, the students were informed about the purpose of the study.

3.2.4.5. Ethical Considerations

As the field visit required participation and interaction with human participants, ethical approval was obtained from the Research Ethics Committee, DCU, prior to commencement of the visits. The ethics review committee sought information on investigator details, participant details, risk management, project outline and proposed methods to be used in the field. An informed consent form, plain language statement and evidence of external approvals related to the field visit from UNCST were included in the ethics review application.

3.3. Experimental and Characterisation Methods

Hybrid DLC and Si-DLC were deposited onto nitrile rubber substrates. The DLC and Si-DLC films were deposited with and without a Si-C interlayer. The role of the Si-C interlayer on the film properties was also investigated. This discussion has not been presented elsewhere for DLC and Si-DLC films deposited on rubber substrates. This chapter discusses the experimental work and characterisation techniques carried out to determine the coating structure and properties. Figure 3.1 shows a summary of the processes involved in the deposition and characterization of DLC and Si-DLC thin films used in this study.

Substrates
- Nitrile rubber
- Si wafer
- Quartz glass wafer

Sample Preparation
- Ultrasonically cleaned (for Si and glass substrates
- Slight cleaning with methanol for nitrile rubber substrate

Ion Cleaning
- Substrates are bombarded with Ar plasma for 10 minutes

Coating Deposition
- Voltage and current control
- Pressure evacuation
- Substrate bias
- Deposition time

Characterisation
- Film composition: EDX for NBR substrates
- Film bonding structure: XPS for Si wafer; UV-VIS for glass substrate; Raman spectroscopy for NBR substrates
- Film thickness: Surface profilometry on Si wafer; fracture cross-sections on NBR substrate
- Film hardness: Vickers/Nano-hardness using Si wafer
- Film adhesion: X-cut method for NBR substrate
- Film flexibility on NBR substrates
- Tribological investigations: Pin on disc, SEM on NBR substrates
- Coated piston seals:Piston seal wear test rig

Figure 3.1. Processes involved in deposition and characterisation of DLC and Si-DLC thin films

The coatings deposited on Si crystal Si (1 0 0) substrates were used for nano-hardness, micro-hardness and X-ray Photoelectron spectroscopy (XPS) characterisation. The Tauc gap was estimated from UV-VIS (ultra violet–visible) spectrometer measurements for the films deposited on standard glass microscopic slides (manufactured according to BS 7011). All of the other characterisation techniques used in this study were carried out on the nitrile rubber substrates including adhesion and flexibility testing, scanning electron microscopy (SEM), Energy Dispersive X-ray (EDX) analysis, digital microscopy, optical microscopy, Raman spectroscopy and tribological investigations. A comprehensive overview of the physical, structural, chemical, mechanical and tribological characteristics of DLC films deposited on rubber substrates were presented and discussed in section 2.3.4 of this thesis.

3.4. Substrate preparation for coating deposition

3.4.1. Methanol cleaning

The substrate used in this research was a commercial nitrile rubber provided by James Walker, Ireland, Ltd (Unit 3, Richfield Business Park, Ballycurren, Kinsale Road, Cork, Ireland). The material specifications for the substrate are given in Table 3.1.

Table 3.1. Specification of nitrile rubber substrate used in DLC deposition

Property	Specification
Quality	High Grade
Hardness [Shore A]	60±5
Density [g/cm^3]	1.5±0.05
Tensile Strength [MPa]	3
Elongation [%]	250
Compression set [%]	35
Operating Temperature [°C]	-20/+70

In determining the cleaning method the aim was to avoid as much as possible the distortion of the rubber from its as received state. Firstly, the rubber samples were cut to dimensions of 100mm by 100mm by 3 mm. Then, a simple methanol cleaning method was used. An adsorbent cotton cloth was dipped in methanol slightly and then this was wiped lightly over the surface of the rubber substrates immediately before coating deposition. The purpose of this was to remove grease, oil, fingerprint marks and any other contaminant that may have

been on the surface of the substrate. No discolouring of the white cotton cloth was observed after cleaning with methanol.

3.4.2. Ultrasonic cleaning

The Si wafer and quartz substrates were cleaned using ultrasonic cleaning in acetone for 10 minutes. These samples were then washed in de-ionised water and air dried before being loaded into the sputtering chamber.

Ultrasonic sonic cleaning was not used for cleaning of the rubber substrates because of the chemical reactions taking place at the rubber surface between the rubber and acetone liquid. The rubber was observed to discolour immediately when the ultrasonic cleaning procedure was commenced indicating a modification of the rubber surface, hence, only methanol cleaning was used as described in section 3.4.1. The discolouring of the nitrile rubber substrates was attributed to the ejection of oils and fats which are essential in mixing carbon black in the rubber [19].

3.5. Coating deposition system and procedure

3.5.1. Introduction

The coating deposition of DLC and Si-DLC films, with and without Si-C interlayers, was conducted at Teer Coatings Ltd (Miba Coating Group), UK. This approach was chosen due to the functionality concerns of the closed field magnetron sputtering rig available in DCU. This, therefore, ensured that the state of the art regarding the deposition of DLC and Si-DLC films was used to optimize deposition and process settings. As a result the DLC and Si-DLC films deposited in this research were a hybrid produced by a combination of CFUBMSIP and PECVD in a Teer Coating UDP 450 sputtering rig. The deposition of DLC and Si-DLC films onto rubber substrates was also of interest to Teer Coatings Ltd for other possible commercial applications as the deposition of DLC and Si-DLC films onto rubber substrates was a first for them.

3.5.2. CFUBMSIP system components

Figure 3.2 is a photograph of the closed field unbalanced magnetron sputtering rig that was used for the deposition of DLC and Si-DLC films with and without Si-C interlayers onto the substrates. A control panel was used to regulate voltage, current, pressure levels and mass flow.
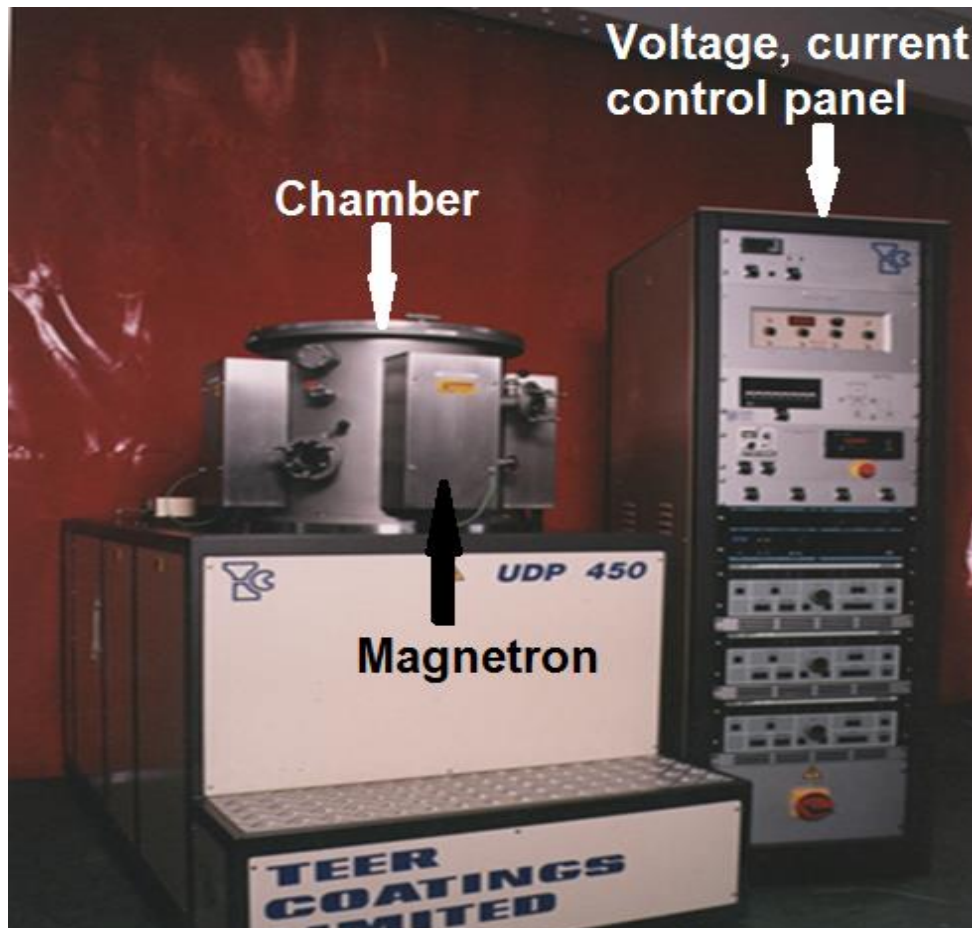
Figure 3.2. Closed field unbalanced magnetron sputtering system

The CFUBMSIP system was composed of the following components:

- Vacuum chamber
- Magnetrons with power supply
- Substrate rotary table
- Gas mass flow controllers
- Water cooling system

The vacuum chamber was made of AISI 304 stainless steel. It consists of a top plate, bottom plate and cylindrical wall upon which targets can be attached to obtain graded and composite films. Permanent magnets were placed directly behind the target plates. Planar magnetrons were used. Pure graphite (99.995%) was used as target material for carbon species. Pure silicon element (99.999%) was used as a source of Si species. Both targets were screwed onto the backing plates with the permanent magnets placed behind the targets. Prior to DLC and Si-DLC films deposition, the target surfaces were cleaned to minimize contamination and ensure good adhesion. Figure 3.3 shows a schematic of a CFUBMS system. Mechanical shutters (see Figure 3.3) were used to block the view in front of the target and also to prevent the sputtered species from reaching the substrate table and sample surfaces.
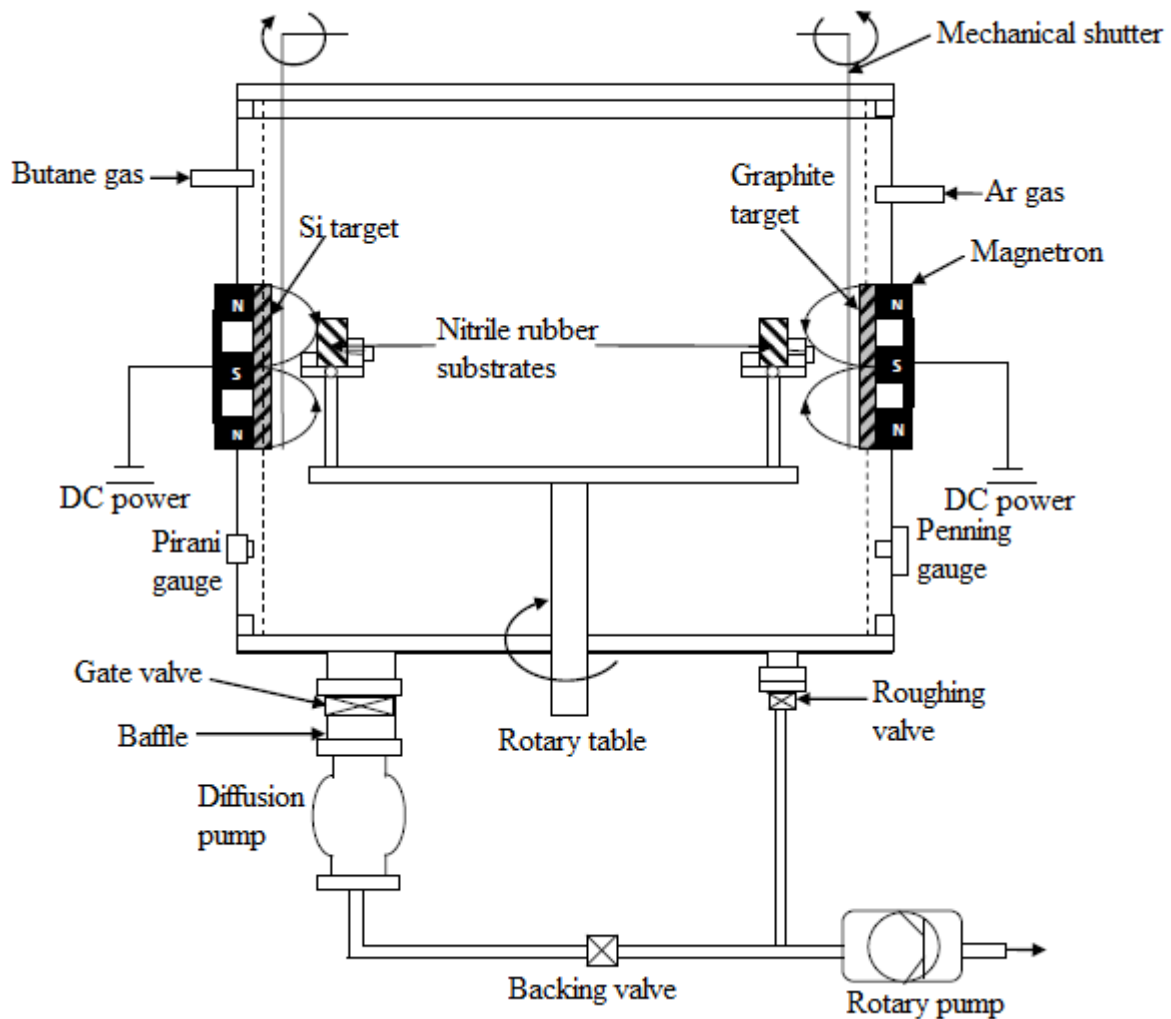
Figure 3.3. Schematic diagram of the CFUBMS system (Adapted from T. Abu Baker [128]).

The cylindrical plate itself had four equidistant magnetrons in the closed field unbalanced configuration. The shutter was located on the top plate. The shutter prevented unwanted sputtering of magnetrons that were not in use. The high vacuum port, water supply port (for cooling the substrate table), backing port and substrate table port were attached to the bottom plate. The vacuum chamber was double layered for the purposes of water cooling.

Figure 3.4 shows the inlet and outlet manifolds of the water cooling system. Water cooling was done to prevent targets from melting which arises due to temperature increases when power is supplied to the magnetrons. Certain components including the magnetrons, diffusion pump, chamber wall and shaft and feed through of rotary substrate table in the rig were cooled.
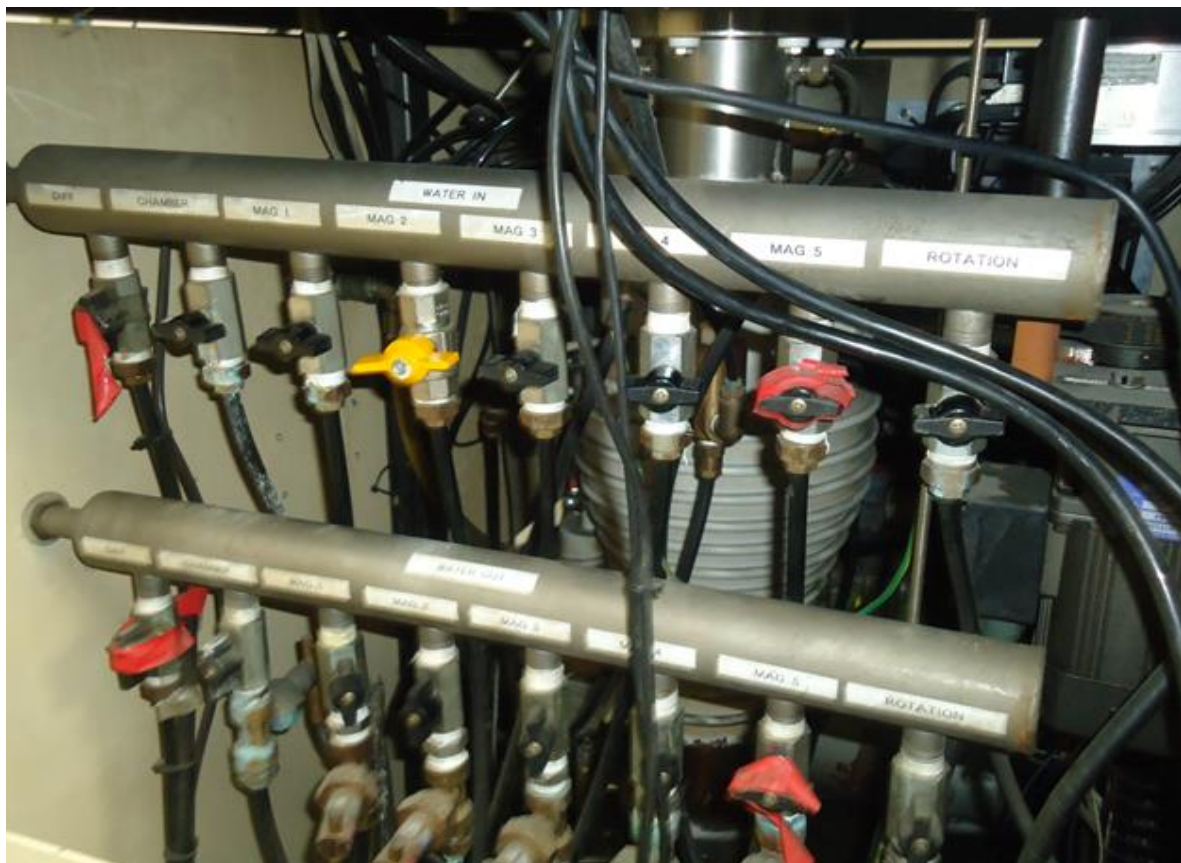
Figure 3.4. Water cooling system showing the inlet and outlet manifolds

The rotary table enabled the deposition of multilayer and composite coatings on the rubber substrates. Figure 3.5a shows the substrate rotary table with the plate on which the nitrile rubber samples were attached. Figure 3.5b shows the substrate rotary table with a fixture for

mounting the piston seals for coating deposition. The substrate rotary table was biased for both plasma cleaning and substrate biasing processes.
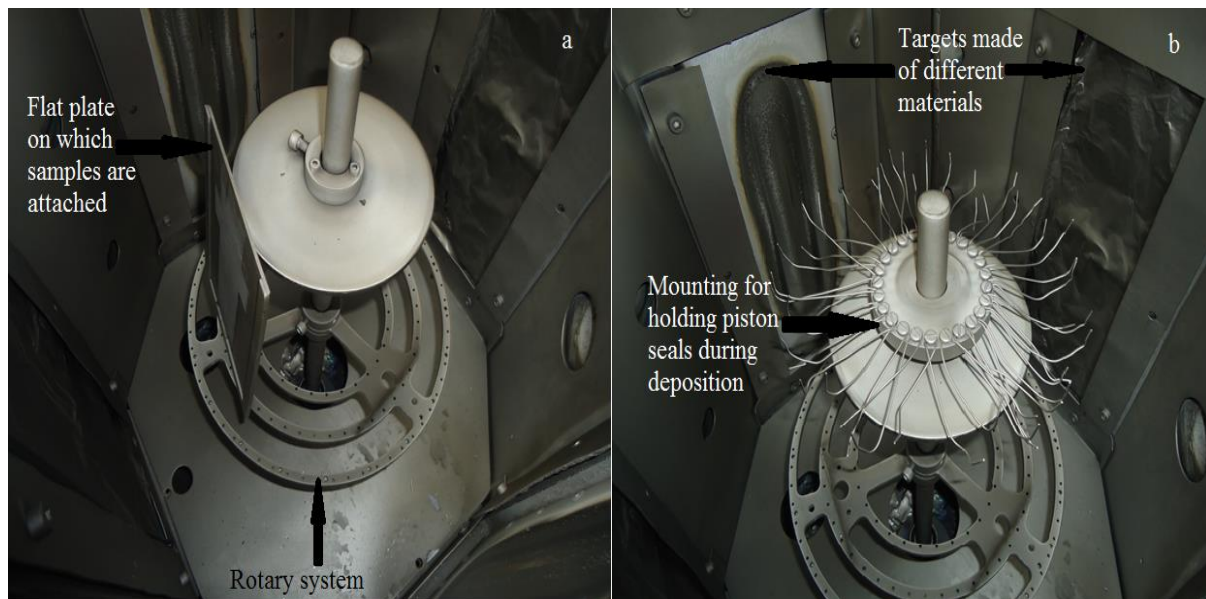
Figure 3.5. Substrate rotary table with plate on which the nitrile rubber samples were attached (a); and special mounting for holding piston seals (b) during film deposition

Figure 3.6 shows the rotary and diffusion pumps used in film deposition. The rotary pump evacuated the chamber to 10^{-3} torr. The diffusion pump evacuated the chamber to high vacuum conditions at 3.0×10^{-5} mbar and lower with vacuum chamber temperature $< 120°C$. During this step the vacuum chamber and the substrate table with the samples is degassed. This ensured that a system less prone to contamination was reached. The degassed species mainly consist of water vapour and were pumped away by the pumping system. A pirani gauge measured the low vacuum pressure and a penning gauge was used to measure the high vacuum pressure. The base pressure after pumping down before backfilling the chamber with Ar gas was 1.0×10^{-1} torr. This was the typical pressure at which the magnetron system was operated in Ar plasma.

The gases used in this study were argon (Ar) gas and butane (C_4H_{10}) gas. Ar was mainly supplied for generating the plasma. C_4H_{10} was used for reactive chemical vapour deposition of DLC. A mass flow controller was used to control the gas flow rate (see Figure 3.7). A regulator was attached to both Ar and C_4H_{10} cylinders. The purity of the Ar and C_4H_{10} gases was 99.9995%.
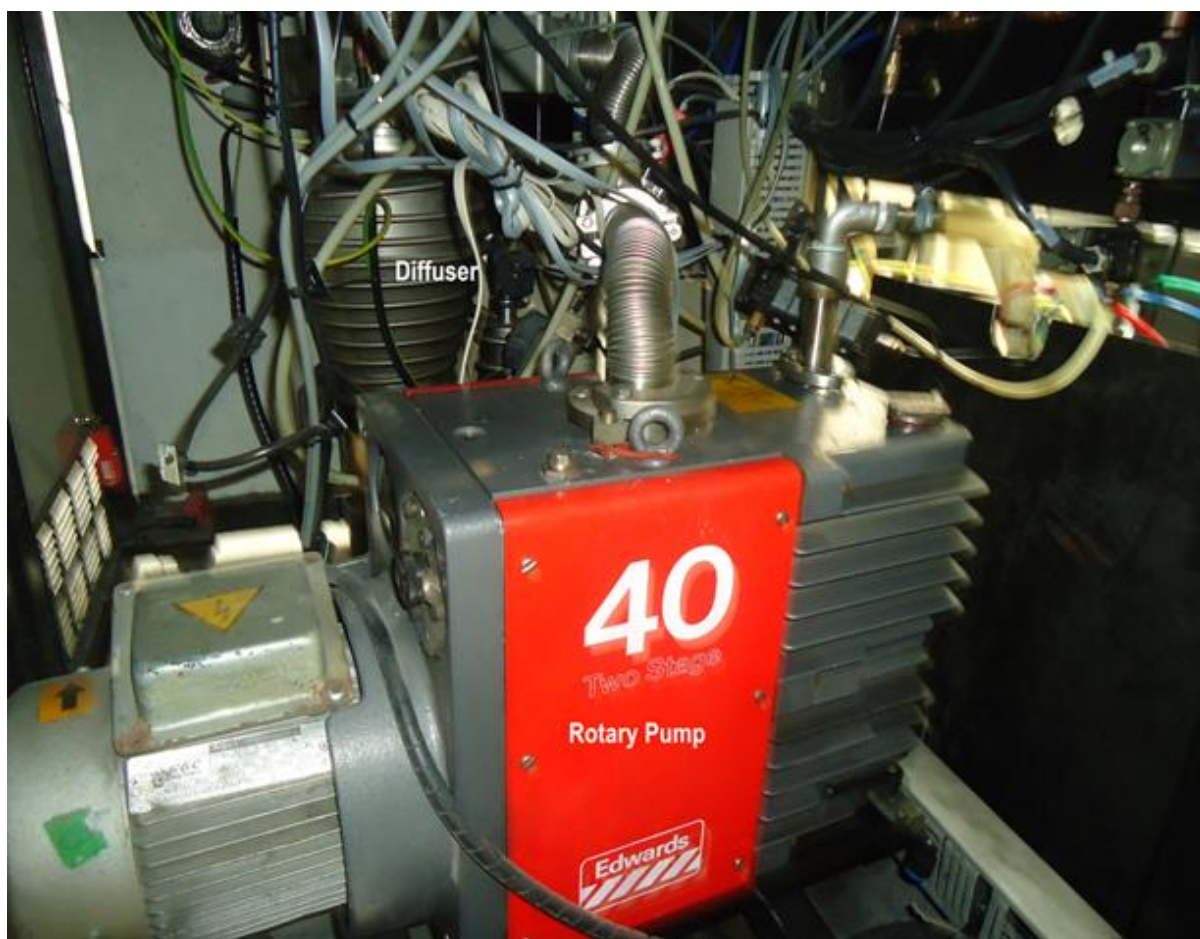
Figure 3.6. Diffuser and rotary pumps used in film deposition

Figure 3.7. Mass flow controllers (a) for regulating mass flow rates for argon gas (b) and butane gas (c)

3.5.3. Deposition procedure of DLC and Si-DLC films

Black acrylonitrile butadiene rubber/ nitrile rubber (NBR) sheet of 3 mm thickness was used as the substrate in this study. Plasma etching pre-treatment of rubber substrates and deposition of DLC films were carried out using a closed field unbalanced magnetron sputtering ion plating system, which consisted of four magnetrons evenly distributed around the chamber. A cross-section of a closed field unbalanced magnetron sputtering chamber is shown in Figure 3.8.
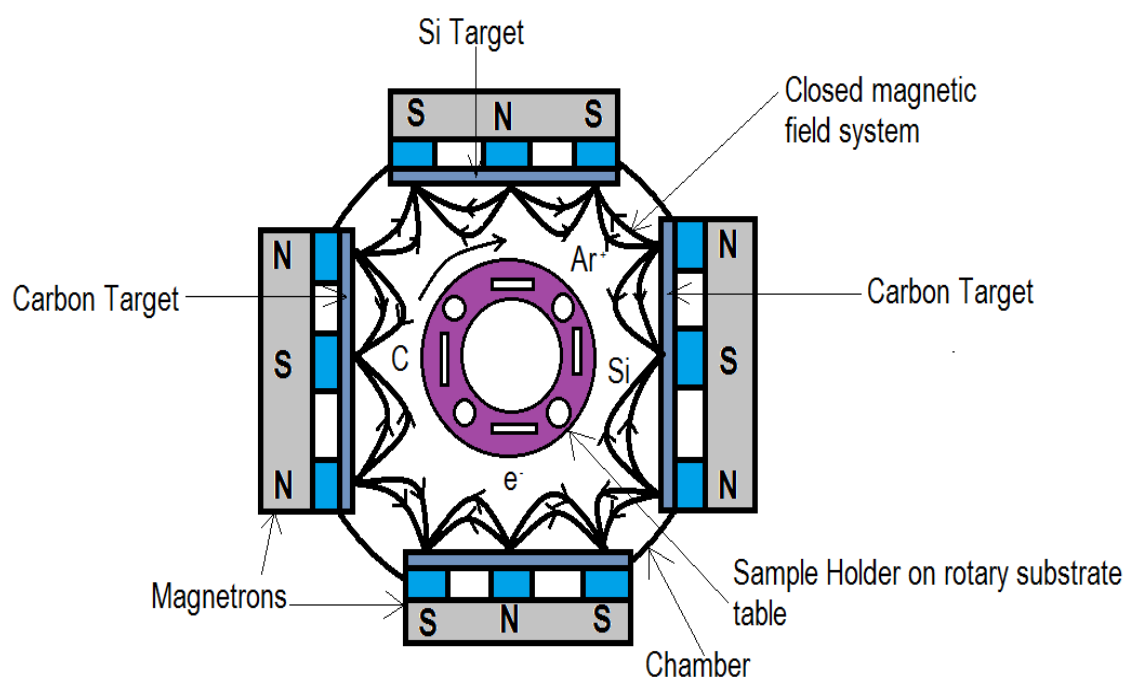
Figure 3.8. Cross-section of closed field unbalanced magnetron sputtering chamber

Two opposite magnetrons were used as carbon targets and one magnetron was used as the Si target. The fourth magnetron in the system was not used during the deposition process. Three pieces of nitrile rubber with dimensions 100 mm by 100 mm by 3mm thickness were mounted onto a holder in the centre of the system facing outwards towards the target. The sample holder was rotated at a speed of 5 rpm

Nitrile rubber substrates were etched in 150 kHz pulsed – dc Ar plasma for 10 min at a bias voltage of -200 V. The deposition process followed immediately after the plasma etching pre-treatment so as to reduce the likelihood of re-contamination between the cleaning and deposition process [33, 65]. The gas flow rate was set at Ar/C_4H_{10} = 12 sccm/8 sccm and the

nitrile rubber substrates were then biased with pulsed DC (150 kHz with a pulse off time of 150 ns) at a substrate bias of -30 V all of which were held constant during the deposition process. The total deposition time for DLC was 60 min This process was repeated for all samples including the Silicon (Si) doped DLC (Si-DLC) samples. In order to achieve the dopant of Si in Si-DLC, a current of 0.5 A was supplied to the Si target during the deposition. The Si-C interlayer was obtained by supplying a current of 1 A to the Si target and 1 A to the pure C target. The Si-C interlayer deposition time was 35 min and the subsequent time for DLC deposition was 40 min Figure 3.9 shows the process design for DLC and Si-DLC films deposited on nitrile rubber substrates. Table 3.2 summarizes the optimized process parameters used during the deposition of DLC and Si-DLC films onto nitrile rubber substrates.
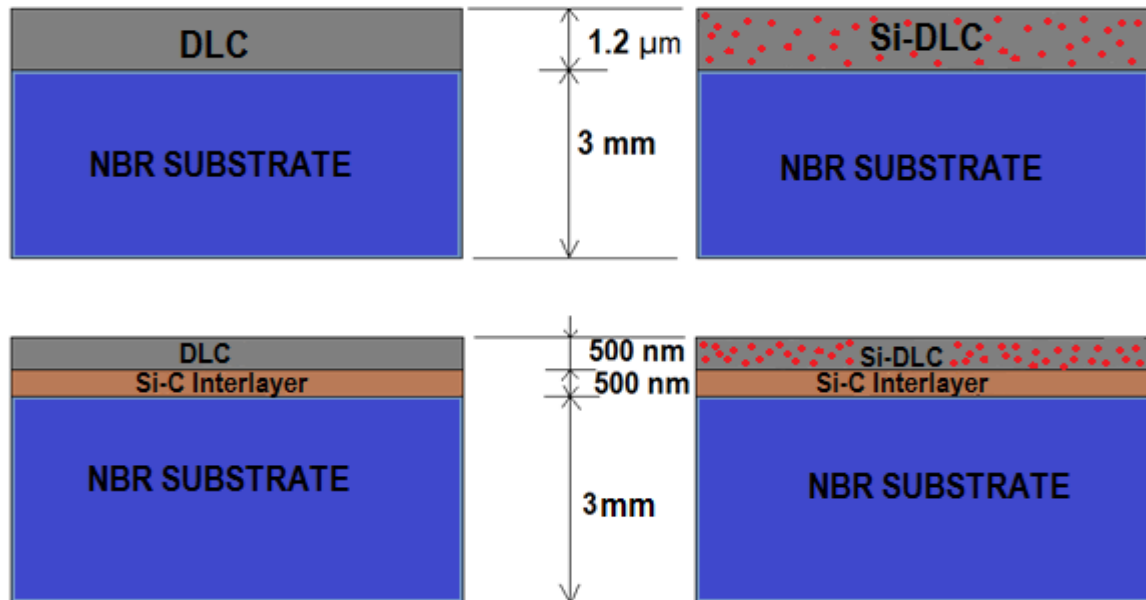
Figure 3.9. Process design of DLC and Si-DLC films deposited on nitrile rubber

Table 3.2. Summary of the deposition parameters used during the deposition of DLC and Si-DLC films

		Mass flow rate (sccm)		Coating deposition current (A)		Interlayer deposition current (min)		Total deposition time (min)	
Coating	Interlayer	Ar	C_4H_{10}	C	Si	C	Si	Interlayer	Coating
DLC	-	12	8	2	0	-	-	-	60
Si-DLC	-	12	8	2	0.5	-	-	-	60
DLC	Si-C	12	8	2	0	2	1	35	40
Si-DLC	Si-C	12	8	2	0.5	2	1	35	40

3.6. Coating Characterization Techniques

There are many reasons to characterize a film or coating, including [90]:

- Investigating the effect of processing variables on properties of the material
- Determining degradation modes and assisting in failure analysis
- Determining functionality and establishing performance limits for a specific application
- Establishing product acceptance specifications
- Establishing a baseline for satisfactory composition, structure, or performance so that subsequent materials may be compared to this 'standard'
- Monitoring reproducibility of processing
- Determining the stability of the material under service and degradation conditions

The following section describes the characterisation techniques that were used. The films were characterised in terms of their physical properties, structural and chemical characteristics, mechanical characteristics and tribological properties.

3.6.1. Physical properties

The physical properties of the film characterised in this study were coating thickness, coating surface roughness, contact angle and surface free energy.

3.6.1.1. Coating thickness

Coating thickness can be characterized using contact and non-contact methods. The choice of different methods depends on the thickness range, properties, desired accuracy and the application of the coating. Stylus step profilometry, ball cratering and scanning electron microscopy (SEM) give thickness values with satisfactory accuracy, while weighing underestimates the thickness [90]. Stylus step profilometry and fracture cross-section analysis using scanning electron microscopy were used to determine the coating thickness.

(a) Stylus Profilometry

Stylus profilometers have the advantage of offering long-scan profiling, ability to accommodate large-sized surfaces and pattern recognition. Stylus profilometers can give a horizontal resolution of about 100 Å and a vertical resolution as fine as 0.5 Å. Data acquisition, levelling and measurement functions are controlled by computers in modern instruments [90]. For coating thickness measurement using stylus profilometry, the films deposited on Si wafers were used. A step was made by masking a portion of the substrate and removing that after deposition. Coating thickness was directly measured as the height of the resulting step contour trace as shown in Figure 3.10.
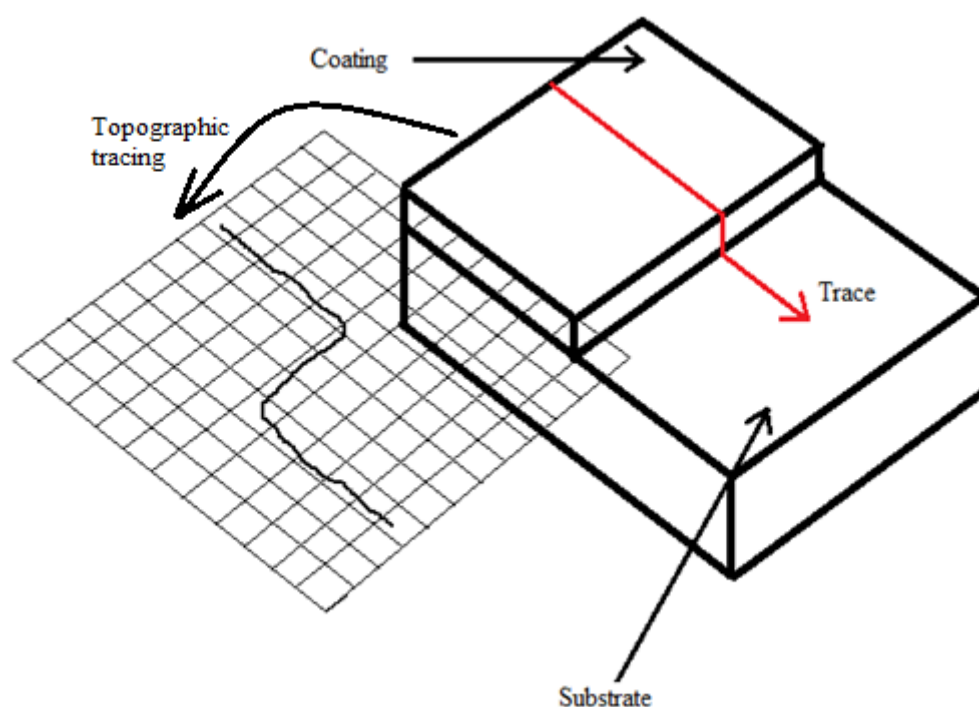
Figure 3.10. Schematic diagram of topography tracing of a coating-substrate system

A Dektak 150 surface profiler shown in Figure 3.11 with a low-inertia sensor (LIS 3) at a stylus force of 1 mg and 3 mg was used to determine coating thickness. The Dektak 150 surface profiler had a vertical range of 1 mm, vertical resolution of 1 Å and a lateral accuracy of < 0.1%. The stylus instrument amplifies and records the surface topography from the vertical motion of a stylus over the surface at a constant velocity. The stylus method

measures the thickness of a coating by the mechanical movement of a stylus by tracing the topography of a coating – substrate step.

Figure 3.11. Photo of a Dektak 150 surface profiler

(b) Fracture Cross-sections

Fracture cross-section method was used to determine the thickness measurements of the films deposited on nitrile rubber substrates. The approach that was used is similar to the approach described by Pei et al. [23]. The film/substrate samples (30 mm by 20 mm by 3mm) were placed in liquid nitrogen for 10 min. After removing the samples, they were fractured centrally and allowed to air dry for 30 min. After air drying the samples were placed in an SEM where images of the fracture cross-section were obtained. An EVO LS SEM was used to acquire and determine film and/or interlayer thickness. In order to view the fracture cross-section the sample was rotated at 90° on the SEM stage.

3.6.1.2. Surface Roughness

The surface roughness was determined for DLC and Si-DLC films deposited onto nitrile rubber. In this study, surface roughness was determined using both Dektak 150 surface profiler and a manual surface roughness tester.

The Dektak 150 surface profiler with a 1 mg stylus force over a sampling range of 2 mm was used to determine surface roughness parameters including average roughness. The roughness values were determined for 10 samples for each coating category. The probe pin of the manual surface roughness tester (TR-200) was made of diamond with a radius of 5μm and dynamo measurement of 4 mN. Measurement range for these tests was ± 20 μm with a resolution of 0.01μm. A total probe length of 1.6 mm was used due to loss of sensitivity as a result of step changes arising from dendritic crack-like surface morphology of the samples.

3.6.1.3. Contact Angle and Surface Free Energy

Measurements of film contact angle and determination of surface energy are important indicators of the water repellence character of the film surface [19]. Static water contact angle (CA) measurements were carried out at room temperature by the sessile drop method [18] using an optical contact angle measuring device (DataPhysics OCA) shown in Figure 3.12.
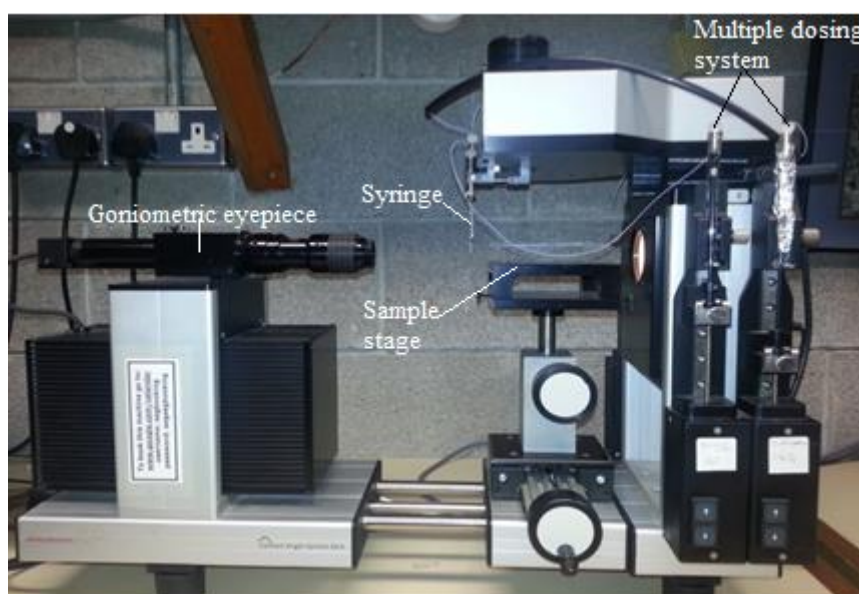
Figure 3.12. OCA 5 with multiple dosing system and manual syringe units

The OCA 5 system was used for the acquisition of the drop images of 1 µl. The contact angle measurements were repeated at least 10 times on each sample and the obtained results were averaged in order to minimize the measurement uncertainty. The surface free energy was calculated by the Owens-Wendt-Rabel and Keable method from which disperse, polar, acid and base parts of the surface free energy were easily determined [129]. The Owens Wendt-Rabel and Keable method was recommended for coatings applied to polymer substrates from which the dispersive and polar components of the surface energy were easily determined [130].

Table 3.3 shows the components of the surface free energy for the three liquids; water, diiodomethane and ethylene glycol, which were used in this study. The total free surface energy (γ) was determined as the sum of non-polar Lifshitz-Van der Waals (γ^{LW}) and polar acid (γ^{AB}) components. The last γ^{AB} component includes electron-acceptor (γ^+) and electron-donor (γ^-) components which are not additive as described in eq. 3.2 [131]:

$$\gamma^{AB} = 2\sqrt{\gamma^- \gamma^+} \qquad\qquad (3.2)$$

Table 3.3. Components of surface free energy (in mJ/m^2) of reference fluids [18, 129]

Liquid	γ_{tot}	γ^{LW}	γ^{AB}	γ^-	γ^+
Water	72.8	21.8	51.0	25.5	25.5
Diiodomethane	50.8	50.8	0.0	0.0	0.0
Ethylene glycol	48.0	29.0	19.0	39.6	2.28

3.6.2. Structural and Chemical Characterisation

Structural and chemical characteristics of the films were determined by scanning electron microscopy with energy dispersive X-ray (SEM with EDX) analysis, Raman spectroscopy, UV-VIS spectroscopy, X-ray photoelectron spectroscopy (XPS) and optical microscopy.

3.6.2.1. Scanning Electron Microscopy (SEM)

Scanning electron microscopy (SEM) is one of the most widely used analytical surface characterization techniques [132]. In an SEM instrument, a voltage is applied to an electron

emitting filament made of tungsten to produce an electron beam. The electron beam is focused by a system of magnetic lenses (condenser and objective lenses) to a small spot of interest. The beam then scans the surface by means of deflecting coils. If the energy of the primary electrons entering the surface is high enough, secondary low energy electrons are produced, which have short mean free paths. It is these secondary electrons that are detected, amplified, processed, displayed and stored. [132]

Figure 3.13 shows a photograph of the EVO LS 15 SEM that was used in this study. SEM was used to:

- Determine the surface morphology and microstructure of the films
- Observe fracture cross-sections to examine growth mechanisms and coating thicknesses
- Analyse wear tracks and debris after tribological investigations and flexibility tests.

Figure 3.13. Photo of EVO LS 15 SEM and EDX machine

The working distance during SEM analysis varied from 6 to 15 mm. The acceleration voltage used in the SEM analysis was 3 kV under normal pressure mode and at 20 kV acceleration voltage under variable pressure (VP) mode. The VP mode was used in order to image the films deposited on nitrile rubber substrates. Nitrile rubber substrates are non-conducting surfaces and as such were prone to charging from the sides and any areas that were not covered with the coating.

3.6.2.2. Energy Dispersive X-ray (EDX)

Energy Dispersive X-ray (EDX) analysis can analyse all elements in the periodic table, provided a suitable light X-ray is used. In EDX, electrons emitted from the filament (cathode) are accelerated with high energy to strike the specimen (anode) to be analysed. Electrons of the inner shells of the specimen atoms are excited by interaction with the electron beam, and X-rays are emitted from the irradiated area due to electron transitions between different shells. K_α X-rays are emitted if the electron transition occurs between L and K shells. K_β X-rays are emitted if the electron transition occurs between M and K shells. L_α X-rays are emitted if the electron transition occurs between M and L shells. The difference in energy between the levels involved in the electron transitions determines the energy of the emitted X-rays. Each atom has a unique set of X-ray spectral lines that serve to identify an element. [133]

This research made use of the EDX system that interfaced with the SEM system. EDX analysis was carried out using a Princeton Gamma-tech spectrometer attached to the EVO LS 15 SEM. Qualitative and quantitative analysis of elements present was analysed using Oxford Inca software. The peak areas were probed for Carbon (C), Silicon (Si), Oxygen (O) elements. Other elements were categorised as trace elements. The elemental composition of the coatings was determined.

3.6.2.3. Raman Spectroscopy

When a light quantum hits a surface, a mainly elastic scattering process (Rayleigh scattering) and inelastic scattering process (Raman scattering) occurs [132, 134]. This inelastic scattering carries information about energetic levels of the sample. In Raman scattering process, the

scattered photon has lost (Stokes scattering) or gained (anti-Stokes scattering) energy of elementary excitation. As the intensities of the anti-Stokes lines are lower, only Stoke lines are usually recorded in the Raman spectrum [134].

Raman spectroscopy is a popular non-destructive, ambient probing tool to characterise the structure of thin films. Raman spectroscopy is a very effective way to investigate the detailed bonding structure of DLC and DLC based films [42, 92, 132]. DLC coatings consist of amorphous carbon with short and medium range order of sp^2 and sp^3 sites. Their mechanical and optical properties depend on the sp^3 content as well as on the number and size of clusters with short range and medium range ordered sp^2 co-ordinated carbon atoms. Raman scattering of DLC coatings is a sensitive probe of sp^2 and sp^3 hybridisation configurations of the carbon atoms [134].

The Raman peak composed of the D and G components is one of the most widely investigated attributes in amorphous carbon films. For all kinds of amorphous carbon films, the Raman spectrum typically shows a G peak centred around 1560 cm^{-1} and a D peak centred at 1360 cm^{-1}. The success of conventional visible Raman spectroscopy to differentiate between different types of amorphous carbon films [135, 136] has led to the development of Raman excitation using ultraviolet light. This technique is a powerful method to characterise the carbon film structures and is considered to be the future method to characterise carbon films especially with respect to sp^3 C atoms [94, 99]. The advantage of UV Raman is its higher excitation energy than visible Raman. The Raman intensity from sp^3 C can be increased while previous dominant resonance Raman scattering from sp^2 C atoms is suppressed. Hence UV excitation is advantageous for obtaining Raman spectra from thin DLC films which have weak Raman signals e.g. films with high photoluminescence (PL) intensity [42].

In this study, Raman spectra were used to distinguish the bonding type, domain size, and sensitivity to internal stress in the DLC and Si-DLC films with and without Si-C interlayers deposited on the nitrile rubber substrates. Raman spectroscopy analysis was also performed on the wear tracks after tribological investigations. The Raman parameters that were analysed in the Raman spectroscopy analysis were:

- G and D peak positions

- Full width at half maximum (FWHM)
- Intensity ratio (I_D/I_G)
- G peak dispersion (Disp(G))

The most common Raman spectra fitting method is to employ two Gaussian peaks with linear background or non-linear background subtraction [137-139] with the D peak centred around 1360 cm^{-1} and the G peak at around 1580 cm^{-1}. The use of a double fit was recommended by Tamor et al [140]. The presence of the D peak in DLC and DLC based films prohibits the use of a single Breit-Wigner-Fano (BWF) line shape to quantify the sp^2/sp^3 ratio. BWF fitting method is not appropriate for a-C:H films due to the highly symmetrical G peak shape [141]. In this study, the individual G and D peak positions from the spectra were fitted with Gaussian line shapes to determine I_D/I_G and FWHM for the films. The curve fitting was done using Origin 6 (Professional). (R^2 for all fits was 0.9997 which means that the Gaussian line almost fits the data set).

The I_D/I_G ratio is known to vary in DLC films synthesized by different methods and parameters and sometimes even for films fabricated by the same method. I_D/I_G is related to size of the graphitic planes in DLC films [139]. For a-C:H films, Ferrari and Robertson assume that the intensity ratio, I_D/I_G, corresponds to the number of sp^2 bonded sites according to the relation between I_D/I_G and the graphitic cluster size, L_a, as shown in eq. (3.3) [95]:

$$\frac{I_D}{I_G} = C_\lambda . L_a{}^2 \qquad\qquad (3.3)$$

where C$_{488}$ nm is ~35Å. C$_\lambda$ is a variable scaling coefficient whose determination is explained by Matthews et al. [142]

The combination of UV and visible Raman spectra can be used to define Disp(G). Disp(G) is defined as the rate of change of G peak position with excitation wavelength [42, 143]. Disp(G) of DLC and Si-DLC films has been studied by means of a multi-wavelength Raman analysis using a 325 nm (UV) and 488 nm (visible) excitation wavelengths. Disp(G) of the films was determined from eq. (3.4) [143] as follows:

$$Disp(G) = \left| \frac{Pos(G)@\lambda_2 - Pos(G)@\lambda_1}{\lambda_2 - \lambda_1} \right| \qquad (3.4)$$

where $Pos(G)@\lambda_{1,2}$ is the G peak position at 488 and 325 nm respectively.

The photoluminescence (PL) background of DLC films has been related to the bonded hydrogen in the films [41, 42]. The PL background is defined as the ratio between the slope of the Raman spectra (m) between 800 and 1900 cm^{-1} as depicted in Figure 3.14. The PL background was measured from 488 nm Raman spectra. The bonded hydrogen in the DLC and Si-DLC films was estimated using eq. (3.5) valid for H > 20 at. % [42].

$$H[at.\%] = 21.7 + 16.6 \left\{ log \left(\frac{m}{I_G} \right) [\mu m] \right\} \qquad (3.5)$$

where m is the slope (dy/dx) of the fitted linear photoluminescence (PL) background from G peak position 800 cm^{-1} to 1900 cm^{-1}, and I_G is the intensity of the G peak.
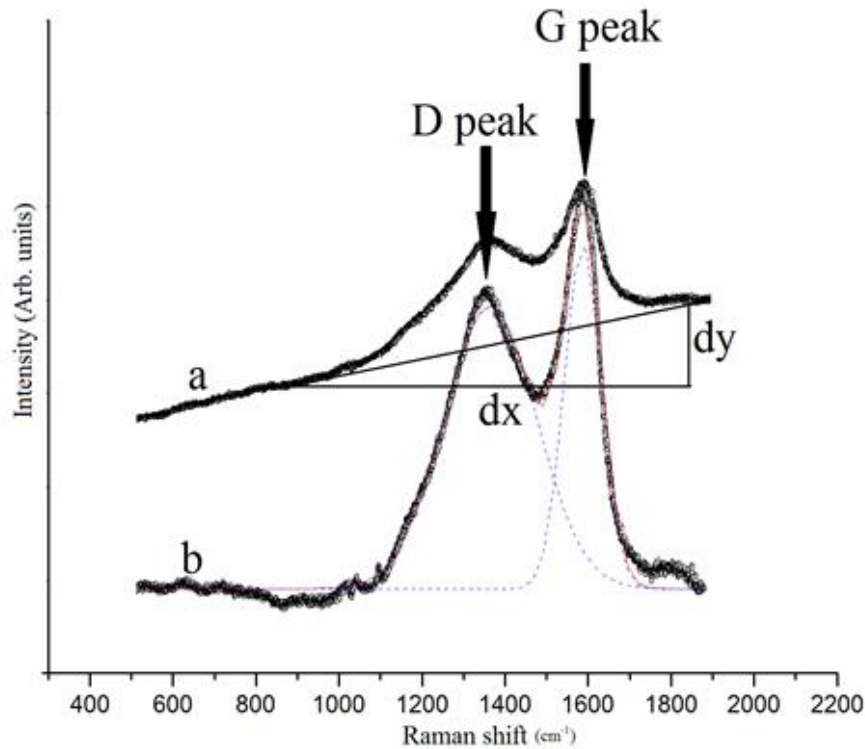
Figure 3.14. Schematic representation for hydrogen estimation in the films (a); and a typical Gaussian fit to determine the Raman parameter. The hollow circles are experimental data points. The deconvoluted components are shown by dashed lines. The resultant fitted curve is shown by the solid line (b).

74

The scale of the Raman shift is related to the sensitivity of the residual stress σ by eq. (3.6) as follows [144]:

$$\sigma = 2G \left\{\frac{1+v}{1-v}\right\} \left\{\frac{\Delta w}{w_o}\right\} \qquad (3.6)$$

where Δw is the shift in Raman wavenumber of the G peak, w_o is the Raman wavenumber of reference, G is the shear modulus (G = 70 GPa [145]) and v is Poisson's ratio (v = 0.3 [145]).

A LabRAM Horiba Jobin Yvon spectrometer was used in this study to acquire Raman spectra. The LabRAM Horiba Jobin Yvon spectrometer was equipped with a CCD detector using a UV laser at 325 nm for UV Raman spectra and an Ar laser at 488 nm for visible Raman spectra at 8mW. All measurements were recorded for the wavelength range of 500 – 3000 cm^{-1} for the same conditions (5 s of integration time and 5 accumulations) using a 100x magnification objective and a 200 μm pinhole. De Wolf showed that the penetration depth of Raman spectra is inversely related to the absorption coefficient [146]. For all of these films the penetration depth was estimated as being below 500 nm for a wavelength of 488 nm (2.541 eV) and an absorption coefficient range between 22000 and 30000 cm^{-1}.

3.6.2.4. UV-VIS spectroscopy

For an amorphous material the Tauc gap can be estimated using the relation between absorption coefficients (α) and incident photon energy (hv) as shown in eq. (3.7). (A is a constant and E_T is the Tauc gap of the material) [147]. Extrapolating the linear portion of the $(\alpha hv)^{1/2}$ vs. hv axis at α = 0, the Tauc gap can easily be determined. The E_{04} gap is determined from a plot of the absorption coefficient, α, vs. photon energy, indicating the typical Urbach-like tail, at the point where the absorption coefficient $\alpha = 10^4$ cm^{-1} [148].

$$\alpha hv = A(hv - E_T)^2 \qquad (3.7)$$

The bonded hydrogen (H > 20 at. %) for these films was estimated using eq. (3.8) that relates Tauc gap (E_T) and hydrogen content [42].

$$H[at.\%] = \frac{E_T[eV]+0.9}{0.09} \qquad (3.8)$$

The Tauc gap, E_T, was derived by UV-VIS spectrophotometry (Perkin Elmer Lambda 40 UV-VIS spectrometer) shown in Figure 3.15 for DLC and Si-DLC films with and without Si-C interlayer deposited on standard glass microscope slides. The film deposition was conducted under the same processing conditions as for the films deposited on nitrile rubber (see Table 3.2).

Figure 3.15. Photo of the Perkin Elmer Lambda 40 UV-VIS spectrometer

3.6.2.5. X-ray Photoelectron Spectroscopy (XPS)

Photoelectric effects cause electron emissions when a surface is irradiated with X-rays. Figure 3.16 shows a schematic of the emission process of photoelectrons by X-rays. XPS can be used to identify and determine the concentration of the electrons in the near surface region because each element has a unique set of binding energies. Variations in the elemental binding energies (chemical shifts) arise from the differences in the chemical potential of the compounds.[132]
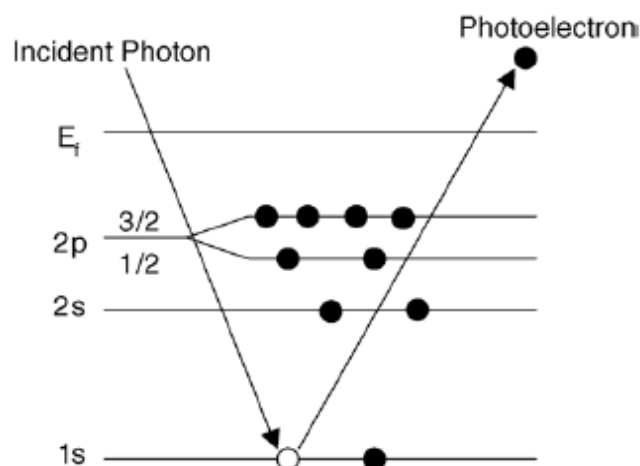
Figure 3.16. Schematic of the emission process of photoelectrons by X-rays [132]

Compared with optical analysis methods including Raman spectroscopy and UV-VIS spectroscopy, XPS is not as frequently used in the analysis of carbon films since it cannot detect hydrogen. However, because it can reveal the binding energy of the carbon atoms and discern the sp^3 and sp^2 hybridisations, XPS is a very powerful method to evaluate the structure of DLC films without causing significant damage to the materials [141, 147, 149-155]. Optical characterisation methods lack information concerning direct binding energy, and as such, XPS is usually used as a complementary characterisation technique [141, 147, 150, 152, 153, 155]. XPS is highly sensitive to chemical shifts or the chemical environment of the probed atom, which is particularly useful to characterise the structure of doped DLC film [147, 153, 155].

Carbon and silicon bonding configuration of the films deposited on Si wafers were determined by XPS. The analysis was performed on the samples using a VG Microlab 310F system with a hemispherical energy analyser. A non-monochromatic Mg K_α x-ray (1253.6 eV) was used as excitation source operated at 15 kV. The pressure in the system was 2×10^{-8} mbar.

The deconvolution of the C 1s of the XPS spectra was done using Origin 6 (Professional) software with a Gaussian distribution function with $R^2 = 0.9996$ for all of the curve fittings. The use of multiple Gaussian curve fittings for the C 1s peaks of XPS spectra of DLC films is typical [147, 155].

3.6.2.6. Optical microscopy and digital microscopy

Figure 3.17a and Figure 3.17b show the optical and digital microscopes that were used in this study. The surface of the ball before and after pin-on-disc tribo-tests was observed by an optical microscope (Olympus GX51 and EMZ-5TR Meiji microscope with capture software and camera). The digital microscope (Keyence 3D VHX-2000) was used to observe the film surfaces before and after flexibility testing, wear track analysis, and coated piston seal wear analysis after testing on the piston seal wear test rig.
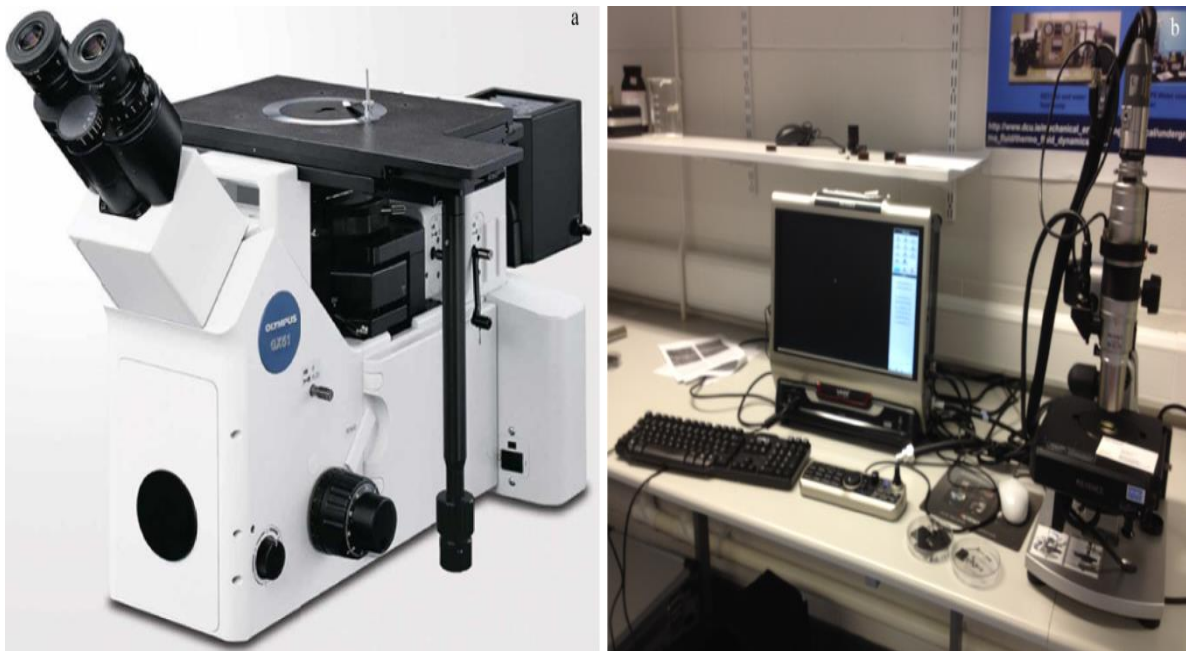
Figure 3.17. Olympus GX51 optical microscope (a); and Keyence 3D VHX 2000 digital microscope (b).

3.6.3. Mechanical Characterization

The mechanical properties and characteristics of the DLC and Si-DLC films were analysed by adhesion and flexibility tests, micro-hardness tests, nano-indentation tests and tribological investigations.

3.6.3.1. Adhesion

The practical ability of the coating to remain attached to a substrate under required operating conditions (adhesion) will be dependent on application or test method. The term effective

adhesion has been suggested to take into account the fact that coatings with similar bond strengths may in practice exhibit different adhesion behaviour [57]. Standard methods used to determine the adhesion performance of films to various substrates include peel test, scratch test, pin-pull test and Rockwell-C adhesion test [156]. The adhesion of DLC on polymer substrates has been researched by other groups and evaluated by the scratch test [157], adhesive tape test [158] and thermal cycling resistance [159]. Bui et al. performed stretch tests with a tensile stage inside a SEM [33].

The peel test was used to determine a qualitative measure of adhesion of DLC and Si-DLC films with and without Si-C interlayer onto nitrile rubber substrates. Table 3.4 shows the ratings of the film adhesion levels used during peel test analysis based of ASTM D3359-97 [105].

Table 3.4. Adhesion level film rating [105]

Adhesion Level	Comment
5A	no peeling or removal occurs at all (absence of peeling)
4A	trace peeling or removal occurs along incisions (no peeling occurs at the intersect and little peeling observed at the X-cut
3A	jagged removal along incisions occurs within 1.5 mm in either direction from the intersect of the X-cut
2A	jagged removal along incisions occurs up to 3.0 mm in either direction from the intersect of the X-cut
1A	most of the X-cut area peeled off with the adhesive tape
0A	removal beyond the X-cut area occurs

In the peel test a narrow strip of the film was gripped and pulled away from the substrate. The peel strength is defined as the force per unit strip width needed to detach the strip. In the determination of the adhesion of DLC films to polymer substrate, an X-cut was made in the films with the angle between the cuts equal to 30° (X-cut method). Cellophane adhesive tape (Scotch ® Pressure Sensitive Tape with adhesion to steel of 49 N/100 mm width) was attached to the film at room temperature. After adhesion for 1-2 min, the tape was pulled off rapidly (not jerked) back upon itself at as close to an angle of 180° as possible. The peeling of the film at the X-cut area was then examined by optical microscopy (EMZ-5TR Meiji microscope with capture software and camera) and its rating determined from Table 4.4 [105-107].

3.6.3.2. Film Flexibility

Flexibility tests similar to Miyakawa et al. [21] were carried out on DLC and Si-DLC films deposited on nitrile rubber. All of the coated samples were repeatedly loaded and unloaded 20 times by bending at approximately 180°. After final loading, the film on the coating was observed at the point of interest on the coating as shown in Figure 3.18. Digital microscopy observations of the point of interest were obtained before and after performing flexibility tests. Flexibility testing was carried out with the film on the exterior (Fig. 3.18a) and interior (Fig. 3.18b).
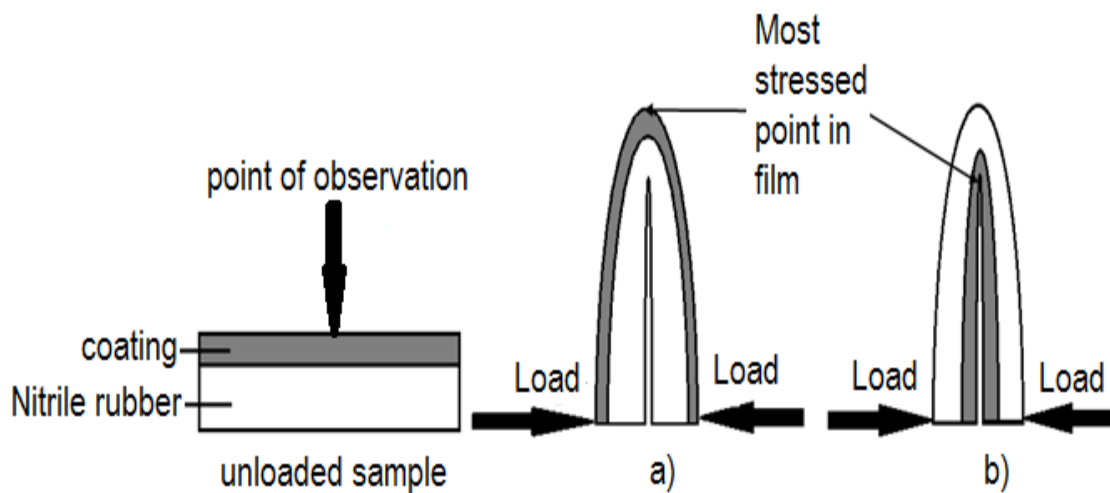
Figure 3.18. Schematic representation of flexibility tests: a) film on exterior; and, b) film on interior

3.6.3.3. Micro-hardness

For micro-hardness measurements the DLC and Si-DLC films were deposited on Si wafers under similar process conditions as for the deposition of nitrile rubber as shown in Table 3.2. Such an approach was used by Bui et al. [22] for determining the hardness of Ti-DLC deposited on Si wafer instead of HNBR rubber, despite the fact that the structure of the coatings deposited on rubber is rather different from that on Si wafer. This approach is used as reference, due to the difficulty in precise measurements of coatings deposited on rubber. Under the same deposition conditions, the hardness of the coating on rubber might be lower than on Si due to release of residual stresses, but the trend of hardness results is expected to be the same [22].

Figure 3.19 shows the Leitz mini-load hardness tester (Serial No. 88134) that was used to evaluate the Vickers micro-hardness of these films. After calibrating the system using a standard block, Vickers micro-hardness tests were performed with applied loads of 147.1 mN, 490.3 mN and 980 mN onto DLC and Si-DLC films deposited on Si wafers. Vickers micro-hardness (Hv) was determined by measuring the lengths of the diagonals of each indent at a magnification of 50× using an optical microscope system within the micro-hardness tester. At least 10 indentations were performed on each sample.
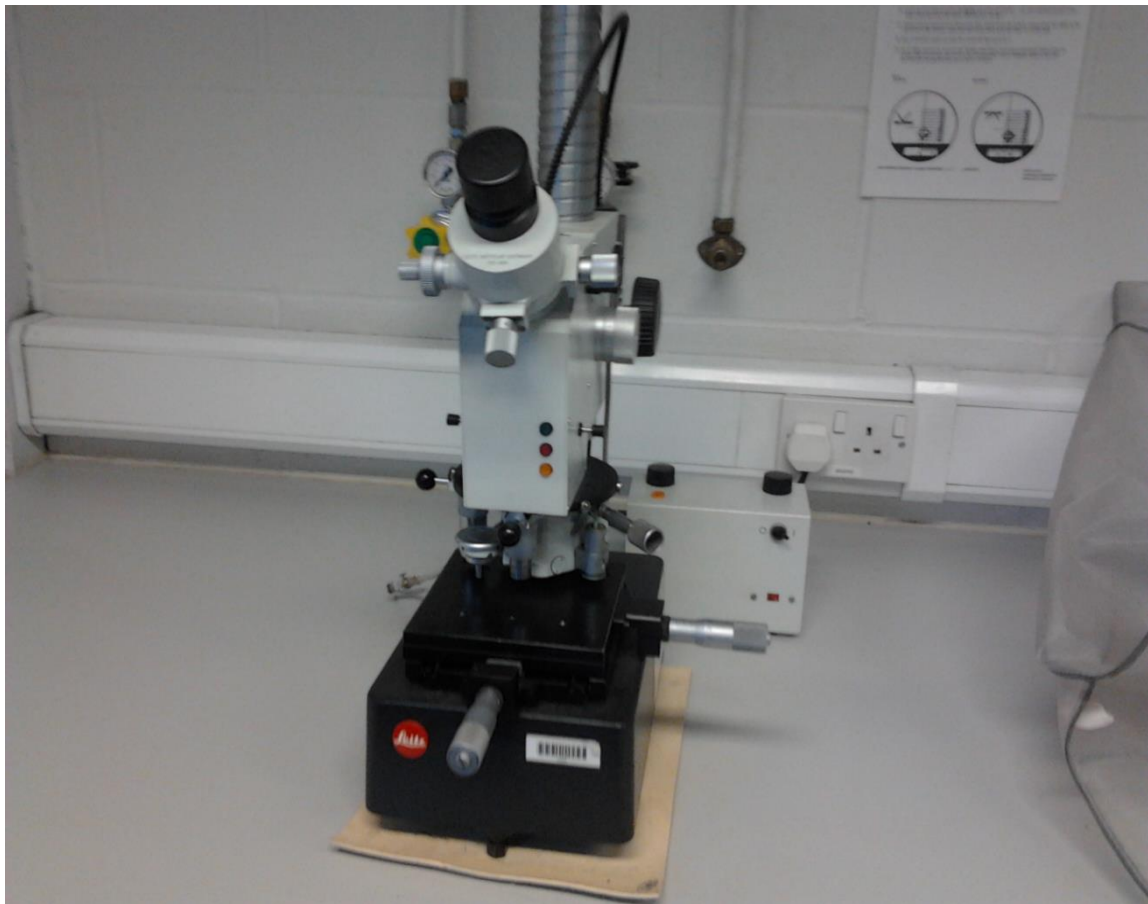
Figure 3.19. Leitz mini-load hardness tester (Serial No. 88134)

3.6.3.4. Nano-indentation

Nano-indentation tests were used to determine nano-hardness and elastic modulus values for DLC, Si-DLC and DLC film with Si-C interlayer deposited on Si wafer were performed using a Nano-indenter tester (NHT[2]) (CSM Instruments, Switzerland). A Berkovich diamond

indenter was used at an approach speed of 1000nm/min. The loading type was linear at a rate of 1.6 mN/min. The unloading rate was 1.6 mN/min. The maximum load was 0.8 mN. A pause of 5 s was held before unloading. All of the samples were tested at least five times.

In order to determine Nano-hardness and elastic modulus of the films, the Power Law method developed by Oliver and Pharr was used [160]. This method describes the upper portion of the unloading curve (see Figure 3.20) by a power law relationship as follows [17]:

$$F = F_{max} \left(\frac{h - h_p}{h_{max} - h_p} \right)^m \qquad (3.9)$$

where F is the test force; F_{max} is the maximum applied force; h is the indentation depth under applied test force; h_p is the permanent indentation depth after the removal of the test force; h_{max} is the maximum indentation depth at F_{max}; and, m is a power law constant exponent.
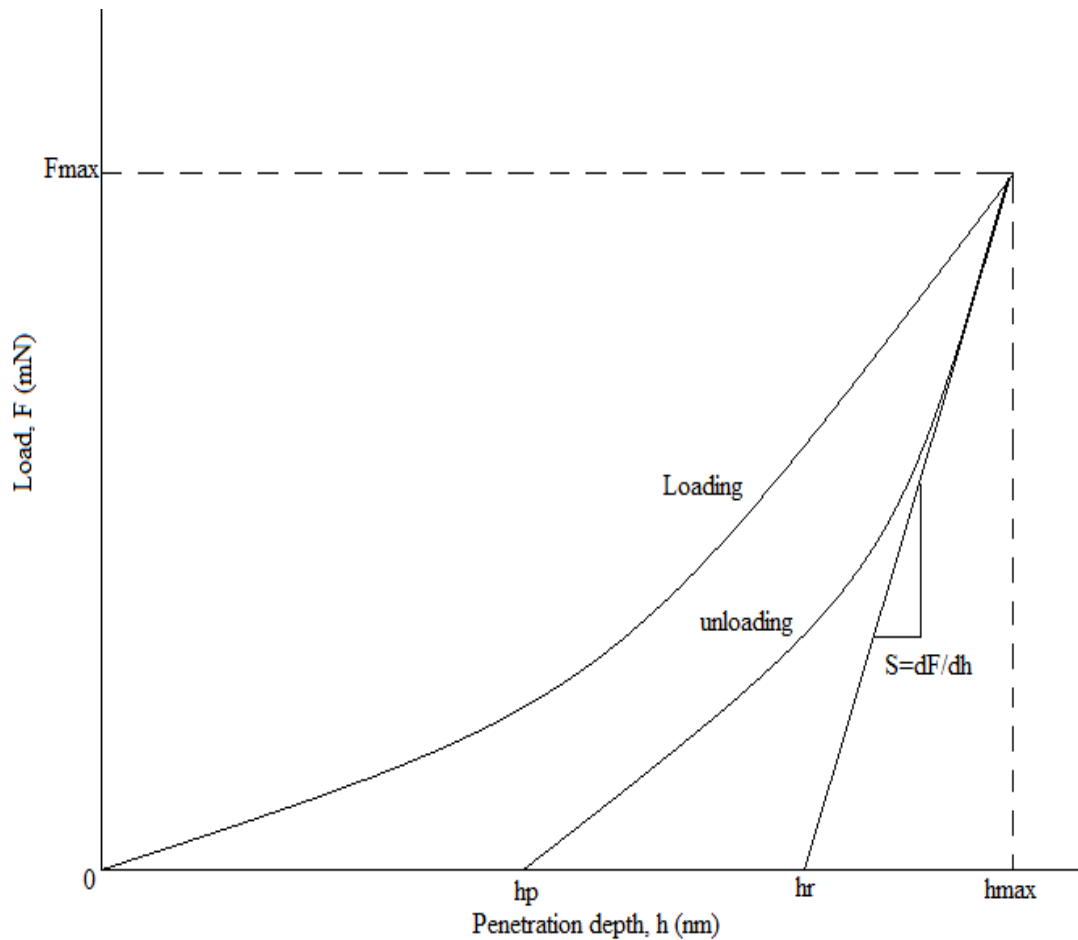
Figure 3.20. A typical load/displacement curve

The power law exponent m is determined by a least squares fitting procedure and is a function of the indenter geometry. The contact stiffness is given by the derivative at peak load as shown in eq. (3.10).

$$S = \left(\frac{dF}{dh}\right)_{max} = m.F_{max}\left(h_{max} - h_p\right)^{-1} \tag{3.10}$$

The tangent depth, h_r, is the point of intersection of the tangent to the unloading curve at Fmax with the penetration depth axis. This is given from eq. (3.11) as:

$$h_r = h_{max} - \frac{F_{max}}{S} \tag{3.11}$$

The contact depth, h_c, which is the depth of the contact of the indenter with the test piece at Fmax) is then calculated from eq. (3.12) as:

$$h_c = h_{max} - \varepsilon(h_{max} - h_r) \tag{3.12}$$

The indentation testing hardness, H_{IT}, is then determined from eq. (3.13) as:

$$H_{IT} = \frac{F_{max}}{A_p.h_c} \tag{3.13}$$

where $A_p.h_c$ is the projected area of contact of the indenter at distance h_c from the tip.

The reduced modulus of the indentation contact, E_r, is given by eq. (3.14):

$$E_r = \frac{\sqrt{\pi}.S}{2.\beta.\sqrt{A_p.h_c}} \tag{3.14}$$

where β is a geometric factor depending on the diamond shape (circular, $\beta = 1$; triangular, $\beta=1.034$; square, $\beta=1.012$)

The Young's modulus of the samples, E_{IT}, can then be obtained from eq. (3.15):

83

$$\frac{1}{E_r} = \frac{1-v_s^2}{E_{IT}} + \frac{1-v_i^2}{E_i} \qquad (3.15)$$

where v_i and v_s are the Poisson's ratio of the indenter and sample respectively; and E_i is the modulus of the indenter.

If the change of the indentation depth is measured with a test force kept constant during a pause time, a relative change of the indentation depth can be calculated. This is the value of the indentation creep, C_{IT}, of the material given by eq. (3.16).

$$C_{IT} = \frac{h_2 - h_1}{h_1} \qquad (3.16)$$

3.6.3.5. Tribological Properties

The tribological behaviour of the DLC and Si-DLC films deposited on nitrile rubber was evaluated at room temperature using a pin-on-disc (POD 2) tribometer shown in Figure 3.21. Standard Ø5 mm commercial stainless steel (DIN 5401) and WC-Co balls were used as counterpart material. A minimum of two different sliding tests were performed on each sample at a linear sliding speed of 10 cm/s at correlative test track diameters of 6 and 10 mm corresponding to a rotational speed of approximately 318 rpm and 191 rpm respectively. Three repetitions at 5000 revolutions were carried out for each film. In addition two different normal loads were studied, namely, 1 N and 5 N.

Figure 3.21. Photograph of the pin-on-disc tribometer used for tribological tests

Tribological investigations were carried out under both dry and wet sliding. Wet sliding conditions were achieved by attaching a pipette filled with water adjacent to the pin such that a continuous flow of water was dispensed. Prior to commencement of wet sliding tests, water was dispensed onto the coated samples so that an initial boundary lubrication contact was achieved. From the tribological investigations the coefficient of friction and the wear of the DLC and Si-DLC films were determined.

In order to study the possible effect of frictional heating on the tribological behaviour of DLC and Si-DLC films deposited on nitrile rubber under different tribo-testing conditions, the induced temperature rise is determined in this study by eq. (3.17) [31, 161]:

$$\Delta T = \frac{1}{4} \cdot \frac{\mu P v}{(K_1 + K_2)a} \qquad (3.17)$$

where ΔT is the induced temperature rise during the tribo-test; μ is the coefficient of friction; P is the applied load; v is the sliding speed; K_1 is the thermal conductivity of the stainless steel (17 W m^{-1} K^{-1} [31]) or WC-Co (97.5 W m^{-1} K^{-1} [162]) balls; K_2 is the thermal conductivity of the coating (3 W m^{-1} K^{-1} [31]); a is the contact radius of the real contact area determined by eq. (3.18) [31, 161]. H is the hardness of the DLC based material.

$$a = \left(\frac{P}{\pi H}\right)^{1/2} \qquad (3.18)$$

The contact radius for the films at normal loads of 1 N and 5 N were calculated as 9.4×10^{-6} m and 21.0×10^{-6} m, respectively.

3.7. Preliminary Testing of Coated Piston Seals

3.7.1. Introduction

One of the objectives of this study was to apply DLC based coatings onto actual piston seals. In this study DLC, Si-DLC and DLC with Si-C interlayer were applied onto piston seals. The piston seals were coated with DLC, Si-DLC and DLC with Si-C interlayer using the deposition procedure and parameters described in Section 3.3.3 and presented in Table 3.2.

The piston seal wear test rig used to characterise the wear mechanisms taking place on coated piston seals is also described in this section.

3.7.2. Components of the Piston Seal Wear Test Rig

Figure 3.22 shows the components from which the test rig was assembled. The rig was comprised of the following components:

- India Mark II cast iron cylinder with brass lining of inner diameter 63 mm. The upper and lower caps on the cylinder are made of cast iron and were of inner diameter 39.68 mm.

- Brass piston assembly that includes the upper and lower piston seal housing as well as piston valve. The pump rod was connected to the piston. The reciprocating motion of the piston seal is responsible for operation of the handpump. The piston valve is a unidirectional valve that allows water to fill the cylinder during upstroke.

- Nitrile rubber piston seal were placed in the upper and lower housing. The sealing action is achieved when the lip and side of the piston seal make contact with the inner part of the cylinder. The pressure difference across the piston seals is responsible for water flow across the cylinder of the handpump during upstroke and downstroke. The piston seals prevent leakage across the piston assembly. A detailed drawing of the piston seal is shown in Figure 3.23. The points of microscopy analysis including the piston seal base, side and lip are also shown.

- A unidirectional foot valve made from brass is located at the bottom cap of the cylinder assembly in this test rig.

- A steel pump rod of diameter 12 mm and length of 41 cm connects the piston assembly to the pneumatic system that provides the power for reciprocating motion.
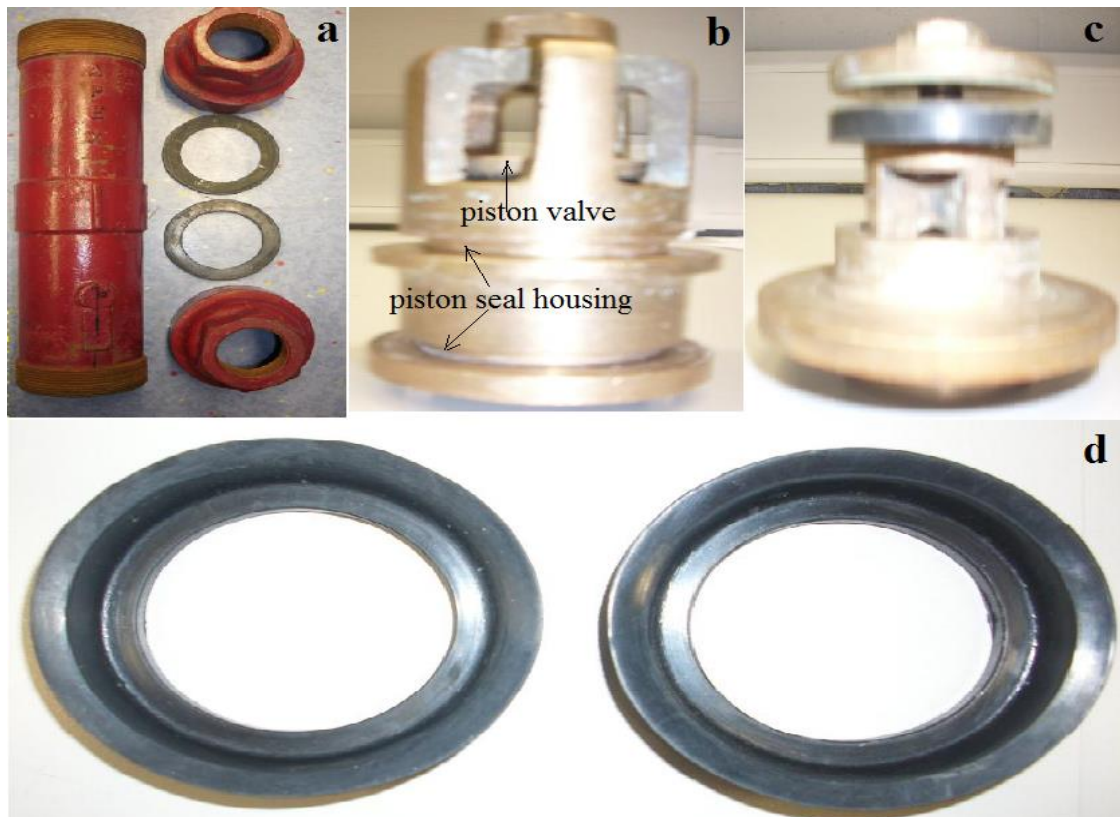
Figure 3.22. Components of the cylinder assembly of the piston seal wear test rig: a) cylinder and caps; b) piston; c) foot valve; d) piston seals
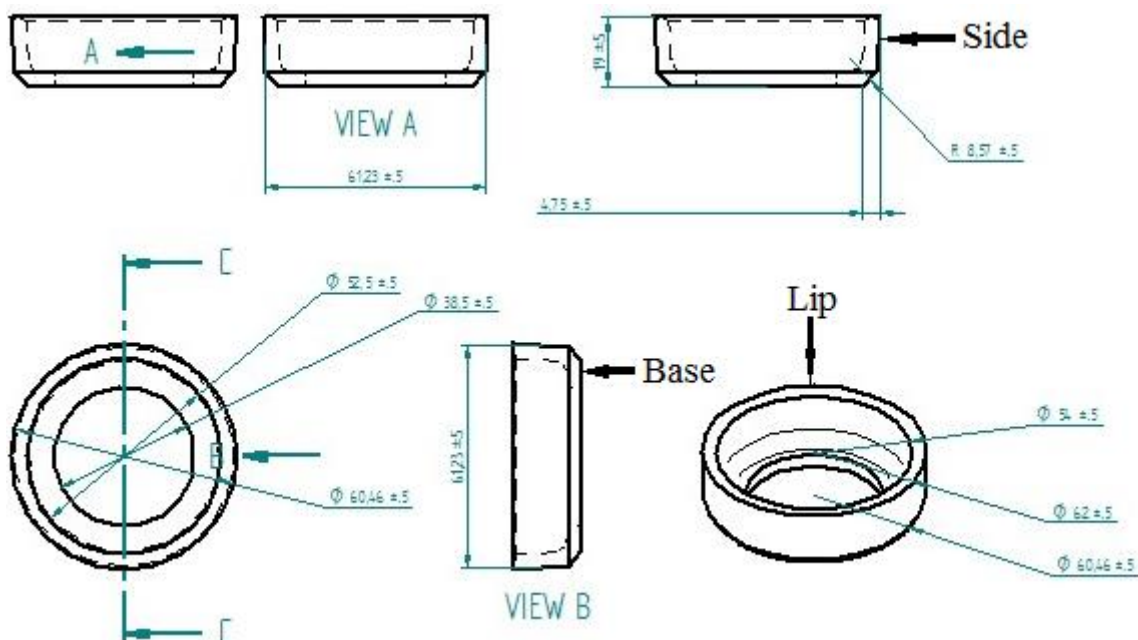
Figure 3.23. Detailed drawing of a typical piston seal. Microscopy analysis was done along the seal base, lip and side

87

3.7.3. Pneumatic system

Figure 3.24 shows the assembled piston seal wear test rig. In order to facilitate the reciprocating motion of the piston, the pump rod which connects to the piston was connected to a pneumatic actuator. The piston rod of the pump rig was connected to the pneumatic system through a screwed fixture component which allowed the pump rod to reciprocate as the pneumatic actuator does. The pneumatic actuator has a stroke length of 80 mm and was supplied with compressed air of maximum pressure of 10 bar.

Pressure gauges were attached to the air supply lines to monitor pressure drops across the actuator during upstroke and downstroke. Pressure regulators were attached to the air supply line to control and maintain pressure in the system so that circuit stroke speed could be varied. An air supply line was used to uniformly mix the water in the container particularly when sand particles were placed in the container. Air supply through the system was controlled by using a 5/2 valve and two lever operated 3/2 valves. The two lever operated 3/2 valves were located at the limits and end of the pneumatic cylinder travel to signal change of direction.
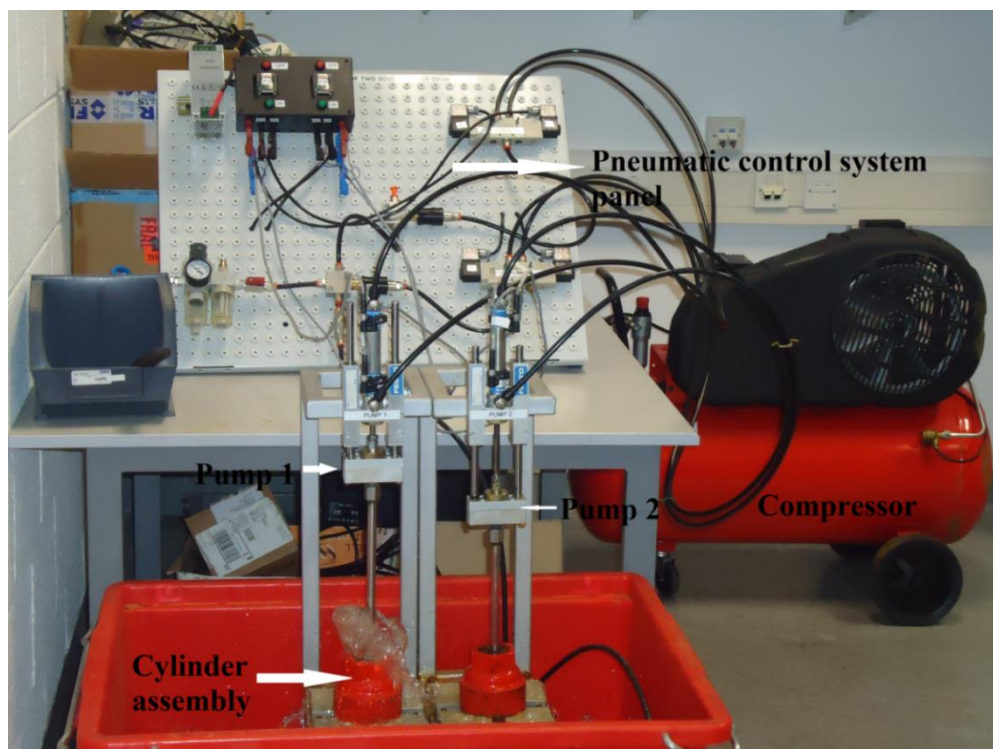
Figure 3.24. Piston seal wear test rig showing the pneumatic control system

3.7.4. Piston seal wear testing

Two seals each for DLC, Si-DLC and DLC with Si-C interlayer were tested. One of the seals acted as the top seal and the other as the bottom seal corresponding to their respective locations in the upper and lower housings in the piston assembly (see Figure 3.22b). Two testing condition were considered:

(a) Operation of the piston seals in normal water
(b) Operation of the piston seals in water with solid particles. The solid particles used were sand of particle size 0.05 mm.

The average number of strokes to fill a 20 litre container in two villages varied significantly from 80 to 150 strokes (See Section 4.2.1). For piston seal wear testing the test rig was set up to produce 115 strokes to fill a 20 litre container as an average between the numbers of strokes recorded in the villages. The stroke length for the piston in the cylinder assembly is 114 mm, but water is delivered during one half of a stroke (57 mm) and the other stroke was for suction of water into the cylinder. The total number of cumulative strokes that each seal was tested for was 100,000 strokes. This was equivalent to delivery of 17,768 litres of water. This testing regime was significant in that it represented an equivalent of filling about 890 containers of capacity of 20 litres. The tests were carried out at room temperature.

After testing the coated piston seals were analysed using the mass difference and digital microscopy techniques. A digital weighing scale (Mettler analytical balance with reproducibility of 0.1 mg and linearity of ±0.2 mg) was used to measure the weights of the piston seals before and after testing. A digital microscope was used to evaluate the surface evolution of the piston seals before and after testing for 100,000 strokes. The surface evaluation was done at the piston seal lip, base and side.

3.8. Summary

This chapter presented the methods used for data collection during field visits to Makondo Parish. The processes involved in deposition and characterisation of DLC and Si-DLC films deposited on nitrile rubber were also detailed. Due to the inherent visco-elastic nature of the

nitrile rubber substrate some characterisation was done on Si wafers and glass substrates deposited with DLC and Si-DLC under the same deposition conditions in order to determine the chemical bonding and structure of the films. A detailed description of the CFUBMSIP and PECVD deposition system used in this study has been given. The set up for tribological investigations under dry and wet sliding conditions for normal loads of 1 N and 5 N were explained. This chapter ended by describing the piston seal wear test rig that was used to characterise the coated piston seals. The wear testing was carried out in an automatic pneumatic driven piston seal wear test rig. The components of the wear test rig were described. The wear testing regime consisted of normal water conditions and conditions when sand particles were placed in the water.

Chapter Four

Results and Discussion

4.1. Introduction

In this chapter the results of the handpump survey, experimental and characterization techniques are discussed. The results and discussion begin with the analysis of handpump functionality and types in Makondo Parish. The handpump survey results determined the problems handpump users face. These problems were related to the wear of the nitrile rubber piston seals. The surface, structural and chemical properties of DLC and Si-DLC films are also discussed. The inherent chemical and structural characteristics of the films were analysed through surface morphology studies, Raman spectroscopy analysis, UV-VIS analysis and XPS analysis. The structural and chemical characteristics results were used to discuss the physical and mechanical characteristics of the films.

4.2. Results of Field Visits

4.2.1. Handpump functionality and types

A survey of all of the handpumps in Makondo Parish was made. This was done to determine the functional and non-functional handpumps, as well as to determine the sample size for respondents to be used in the handpump user survey. Out of a total of 34 hand pumps, only 10 hand pumps were functional. This represents less than one-third of all hand pumps in the parish. Figure 4.1 shows the functionality of handpumps at that given instance in each of the villages. A mapping of the functionality of handpumps in Makondo Parish is shown in Figure 4.2.

During the handpump survey it was determined that there are mainly three types of handpumps in Makondo Parish. These are the India Mark II, India Mark III and the U3M pump. These pumps mainly differ in their internal components (See Section 1.1). Figure 4.3 shows a typical India Mark II (a) and India Mark III (b) handpumps in Makondo Parish.
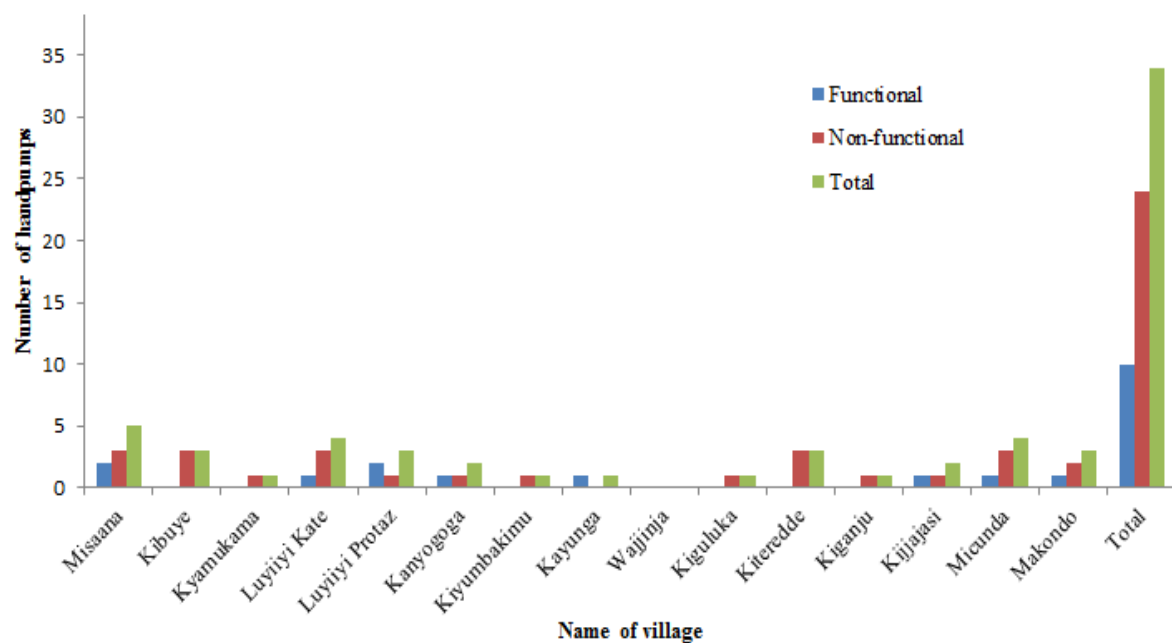
Figure 4.1. Functionality of handpumps in Makondo Parish
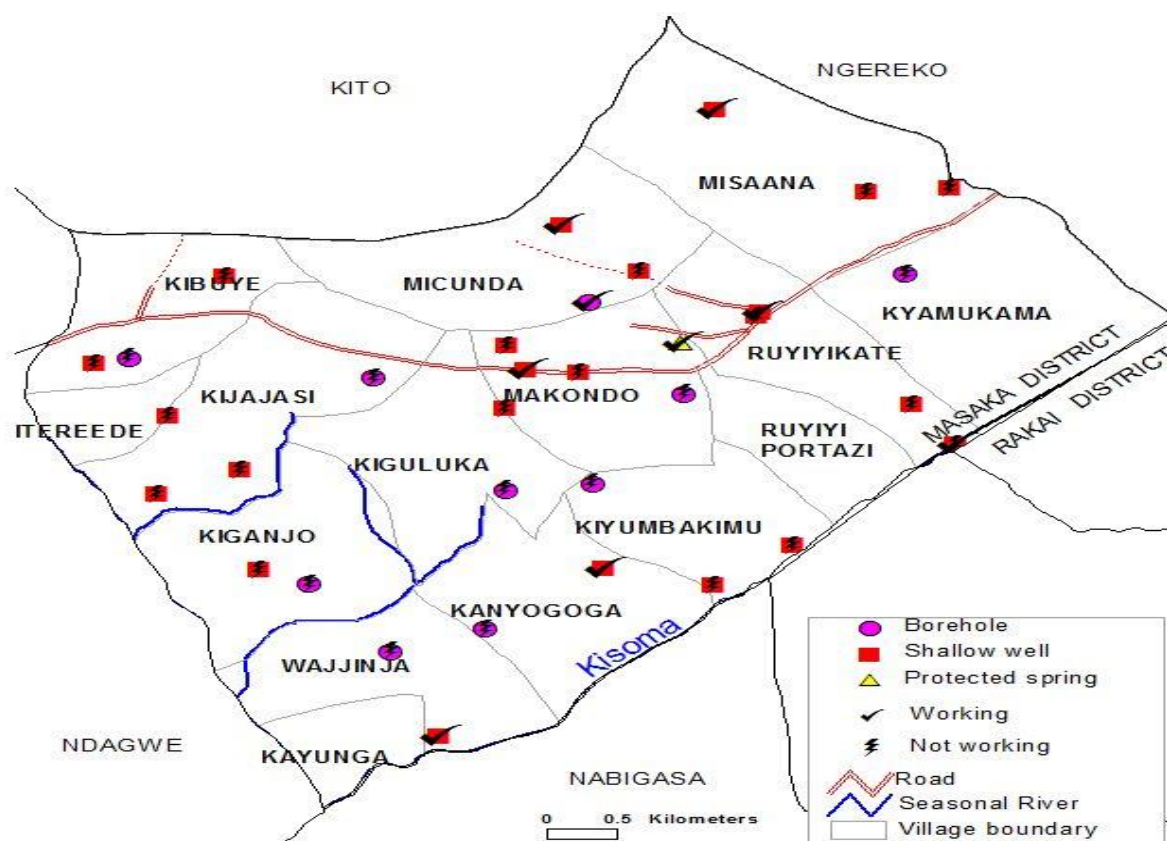
Figure 4.2. Mapping of the functional and non-functional handpumps in Makondo Parish [Water is Life Project Maps, www.dkit.ie/waterislife, accessed on 27th February, 2013]

92

Figure 4.3. Typical India Mark II (a) and India Mark III (b) handpumps in Makondo Parish

Two handpumps at different villages (Luyiiyi Kate and Misaana) were used to determine the number of strokes required to fill a 20 litre container. The average number of strokes required to fill a handpump in Luyiiyi Kate was 80 and for a handpump in Misaana it was 150 strokes. The differences in the number of strokes were attributed to the variation in the hydrogeological factors in these two villages. These average values were made from 40 observations at each handpump point. It was also observed that the number of strokes did not vary significantly between men, women and children.

4.2.2. Handpump user survey results

A total of 328 respondents participated in the handpump user survey. The number, percentage and distribution of respondents are shown in Figure 4.4. After field observations for one week, it was easily determined that primary school children were the most frequent users of

handpumps, followed by women, secondary school children and men. This order determined the number and category of respondents.
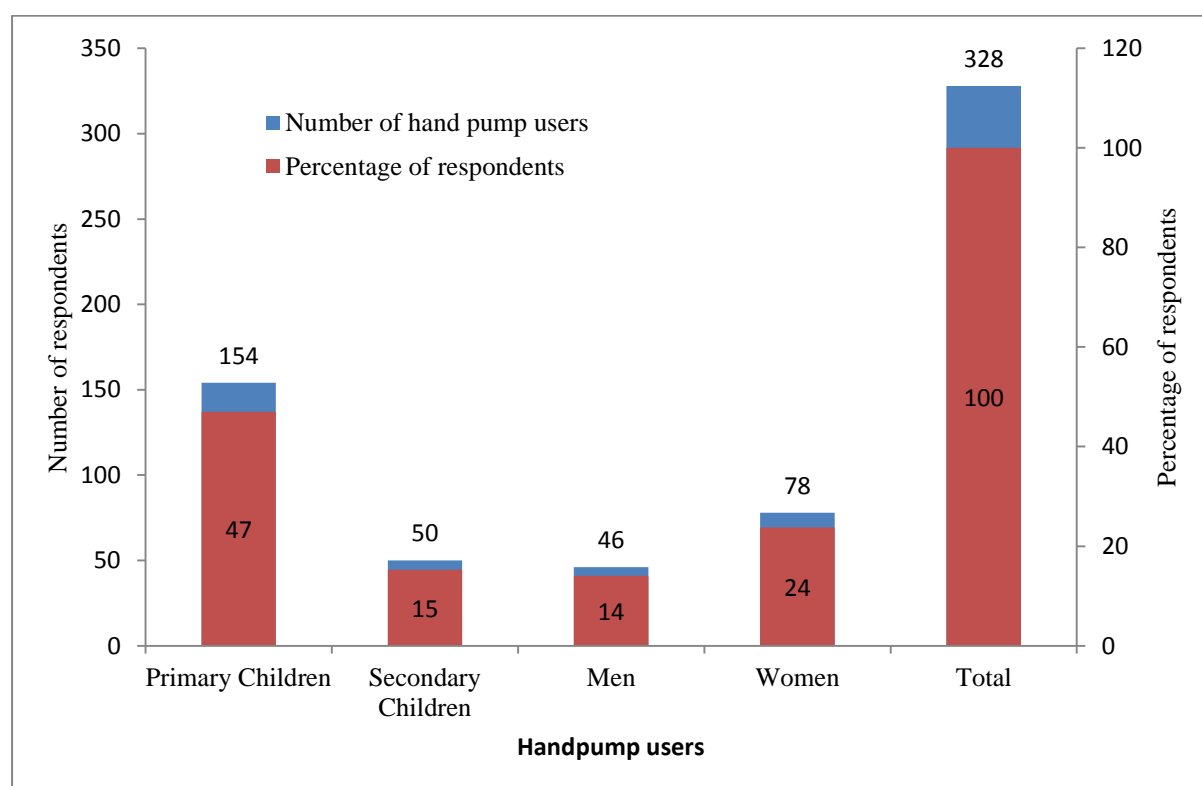
Figure 4.4. Categorisation, number and percentage of respondents

4.2.2.1. Problems users face when using hand pumps

Figure 4.5 shows the problems handpump users mentioned relating to handpumps in their villages as a percentage of user categories namely primary children, secondary children, women and men. Figure 4.6 shows a handpump with a broken handle (Figure 4.6a) and the rising mains of a non-functional handpump (Figure 4.6b).

For the primary children, long queues at the hand pump and blockages were the main problem. The hand pumps being a distance away from home were not such a big problem for them. However for the secondary school children the major problems were different. For them low output in terms of flow rate and the reddish brown colour early in the morning were their main concerns. For the women, frequent pump breakdowns and the long time it takes to repair them were of major concern.
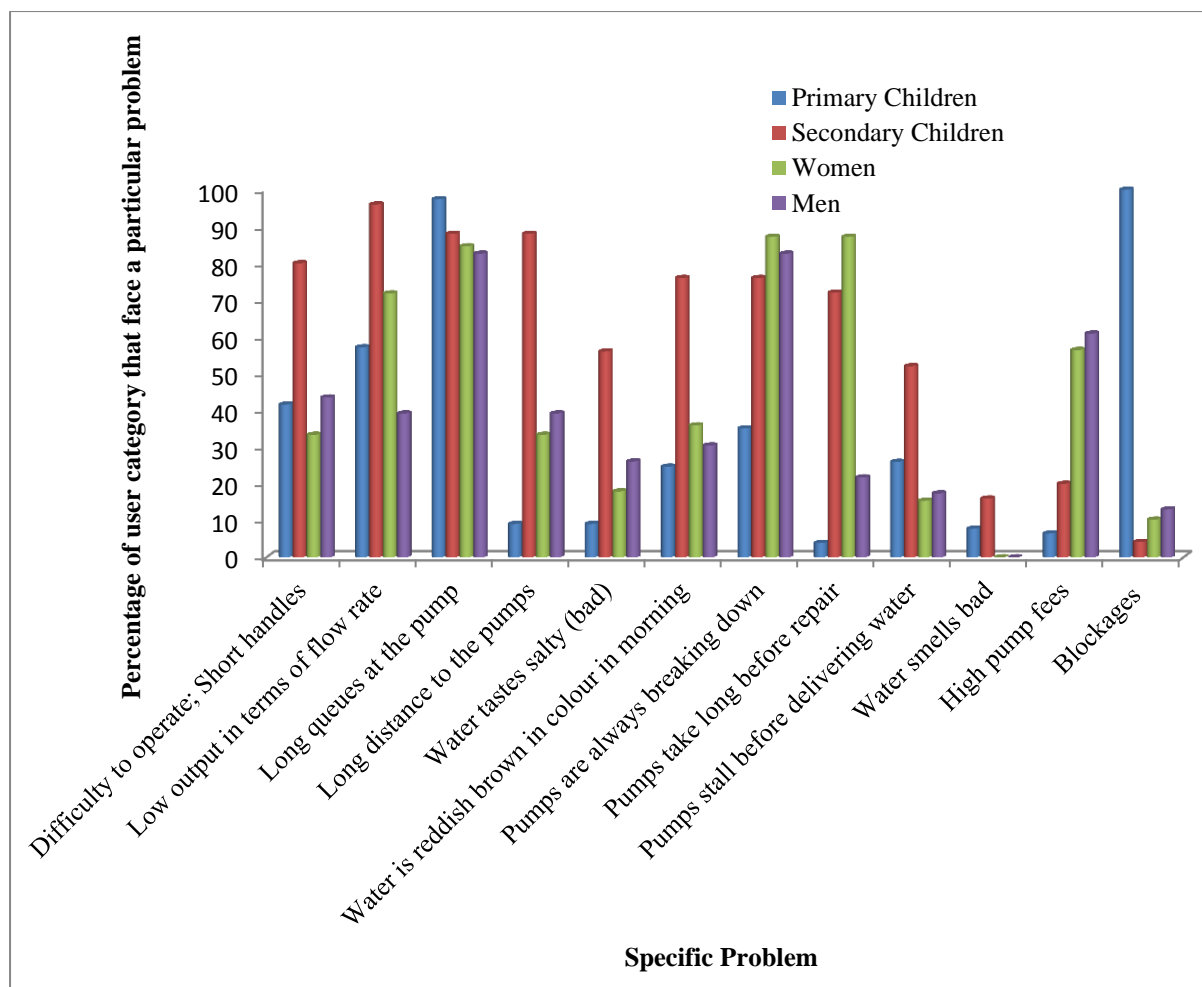
Figure 4.5. Problems faced by handpump users

Figure 4.6. A handpump with a broken handle (a); and rust accumulation along the rising mains (b).

From the field visit to Makondo Parish, the complexity of the wear problem was understood. According to the handpump mechanics, the piston seal is the component that is most frequently replaced during breakdown maintenance interventions. According to them these seals become worn out before the recommended 2.5 years, with replacements after 1 year being commonplace. Also, many of the problems highlighted by handpump users (see Figure 4.5) are related directly or indirectly to the functionality of the piston seal. For example, long queues at the pump can be due to low output in terms of flow rate or frequent breakdowns of other pumps in other localities resulting in people converging at a functional pump. This overarching problem is usually worn out piston seals, such that the sealing function is inadequate. During the delivery stroke, leakages along the cylinder wall and piston seal increase as the wear rate of the seal increases.

4.2.3. Wear of piston seals

The first level of surface analysis method was used to identify the possible wear mechanisms occurring in a piston seal as shown in Figure 4.7.

Figure 4.7. First level of surface analysis showing the possible wear mechanisms on a worn piston seal

From Figure 4.7, following the first level of surface analysis, wave patterns typical of rubber abrasion were observed. These wave patterns were also observed by Schallamach [47]. The direction of the wave formations parallel to the sliding direction of the piston seals is evidence of roll formation stemming from adhesive frictional behaviour. Differences in the surface roughness between the seal and cylinder promote adhesive wear. These wave formations arise as a result of the significant difference in hardness between the cylinder wall and nitrile rubber piston seal. This suggests that abrasive wear was a possible wear mode. A deep plough was also observed in Figure 4.7. This indicates that a third-body must have interacted between the piston seal and the cylinder wall. Possible sources of this third-body are rust particles (see Figure 4.6b) from the rising mains that break off. The rising main of most handpumps (India Mark II and India Mark III) in Makondo are made of galvanized iron. This oxidation of the iron in moist environments forms rust. These rust particles are responsible for the reddish-brown colour that the users complained about in Figure 4.5. Soil particle ingression is common for handpumps and may also be a source of third-body particles. These third body particles promote micro-cutting and third body abrasion between the piston seal and cylinder wall. Points of crack initiation were identified. A deep crack indicative of fatigue wear was observed. The embedment of particles in the piston seal presents a point of stress concentration that leads to points for crack initiation, propagation and fracture. This leads to fatigue wear of the piston seal. These results are in line with the wear mechanisms highlighted by Mofidi [163] who classified, based on the work of Moore [164], the wear mechanisms in elastomers as roll formation, which is related to waves of detachment and scratches parallel to the sliding direction [47], abrasion and fatigue. Wear is elastomers are therefore a mixed mode phenomenon. From the discussion above the following qualitative model (see eq. 4.1) describing the wear of piston seals can be postulated:

$$Volume_{wear\ total} = Volume_{abrasive\ wear} + Volume_{adhesive\ wear} + Volume_{fatigue\ wear} \qquad (4.1)$$

4.2.4. Implications for immediate research work

The implications of the field visits to Makondo on the research work were threefold. Firstly, any intervention had to focus on increasing the wear resistance of the nitrile rubber piston seals. DLC has excellent mechanical properties including high wear resistance. However, the

application and testing of DLC films deposited onto rubber substrates has only recently gained some attention in the literature. The deposition of DLC coatings onto actual piston seals has never been demonstrated before. The characterisation of DLC and DLC based films deposited on nitrile rubber substrates were deemed necessary to determine the tribological behaviour of such films and their potential application onto actual piston seals.

The second implication was that the piston seal wear test rig had to be based on the India Mark II or India Mark III model of handpump which were the most common handpumps in Makondo Parish. As such the piston seal wear test rig in DCU was based on the cylinder/piston arrangement of the India Mark II handpump as described in Section 3.7.2 of this thesis.

Thirdly, from the field visit it was determined that the number of strokes to fill a 20 litre container could vary from 80 to 150 strokes. The piston wear test rig was set to an average stroke value of the two at approximately 113 strokes. Simulations with the piston seal wear test rig were to be done in ordinary water and water with solid particles added into it and continuously mixed during the testing. Solid particles would simulate the impact of third bodies.

4.3. Surface Morphology, chemical composition and film microstructure

4.3.1. Surface Morphology

An overview of the surface morphology of the DLC and Si-DLC films coated on nitrile rubber is shown in Figure 4.8a and Figure 4.8b. The evolution of the microstructure as a result of the inclusion of the Si-C interlayer is also shown in Figure 4.8c and Figure 4.8d. The surface morphology of DLC deposited on rubber substrates is characterized by a dendritic crack-like network [18, 69]. These cracks originate at the first atomic layer of DLC on rubber due to thermal stress mismatch and continuously grow upwards together with the film itself resulting in a patch size of the DLC films in the micrometre scale range [24]. Nitrile rubber substrates exhibit a powdery morphology with a rough surface [23]. The presence of a dendritic micro-crack like network has been recognized as contributing positively to the performance of the DLC coatings on rubber due to the improvement in flexibility of the

coating when the substrate deforms without interfacial delamination [23]. The enhancement of flexibility is important for potential application of these coatings onto nitrile rubber piston seals as the seal deform extensively during the sealing function in handpumps.
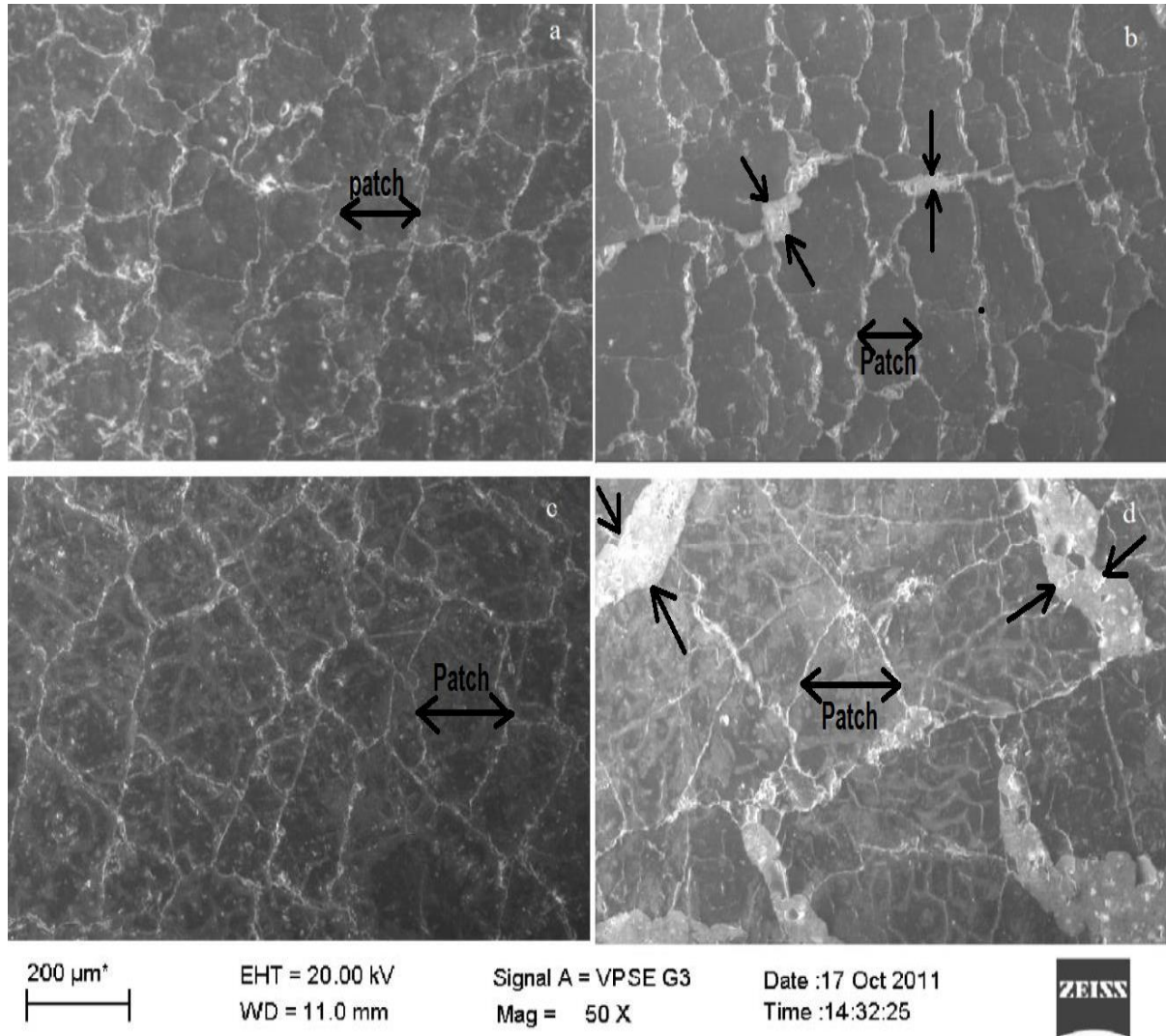
Figure 4.8. SEM Overview of the surface morphology for: a-DLC; b - Si-DLC; c - DLC with Si-C interlayer; d - Si-DLC with Si-C interlayer. Two arrows indicate partially delaminated bands in Figures 4.8b and 4.8d

However, from Figure 4.8b and Figure 4.8d, which show the surface morphology of Si-DLC and Si-DLC coating with a Si-C interlayer, more areas for potential delamination were observed. This may be attributed to the effect of Si dopant in the Si-DLC film, which causes an increase in contributions from sp^3 sites due to vibration in C-C bonds in sp^3 hybridisations of the Si-DLC films [94, 147, 155, 165]. The enhancement of sp^3 fraction is related to the Si valence structure which forms four-fold co-ordinated networks (Si-C) [165]. In the Si-DLC

higher values of the full width at half maximum (FWHM) of the Si-DLC films were observed. From Raman studies discussed later on, the higher values of FWHM indicate that the graphitic clusters were more strained for the films with Si-DLC [166].

4.3.2. Chemical composition

Figure 4.9 shows a typical EDX analysis for Si-DLC films deposited on nitrile rubber. The point of analysis is shown (Figure 4.9a) and its corresponding elemental chemical analysis (Figure 4.9b). For each sample six points were analysed and the average chemical composition in each film was determined. Table 4.1 shows the results of the elemental chemical composition of the coatings applied to nitrile rubber. The films mainly constituted C, O and Si. Trace elements of Sulphur (S), Calcium (Ca), Zinc (Zn), Argon (Ar) and Magnesium (Mg) were observed.
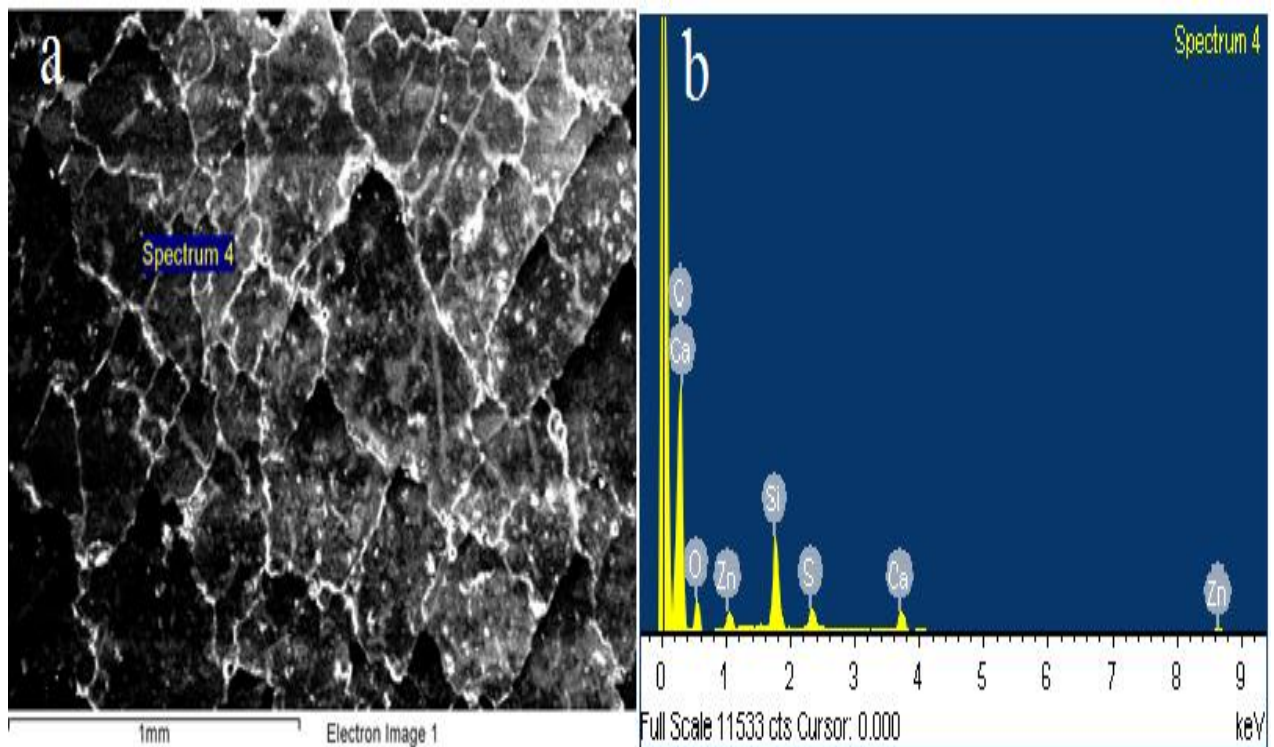
Figure 4.9. EDX analysis for Si-DLC films showing the chemical elements in the film: a) Location of analysis; b) EDX chemical spectrum

The results in Table 4.1 have been compared to the results obtained by Martinez et al. [18]. The differences in the results between the two studies were attributed to the differences in the deposition technologies used. Martinez et al. deposited DLC onto different types of nitrile

rubber substrate using a PECVD process using a combination of Ar, organosilicon precursor and C_2H_2 gas. In this study however the films were deposited using a CFUBMSIP system and a combination of Ar and C_4H_{10} gases.

Consideration of the H:C ratio of the films would imply that the films deposited in this study would be considerably more hydrogenated than the films deposited by Martinez et al. with lesser contributions from carbon. The high levels of oxygen in the films deposited in this study were attributed to air contamination during film deposition. This most probably arises as a result of surface contamination of the C and Si targets during storage to form compounds as a result of oxidation. The target condition strongly affects the properties of the resultant films [65, 167].

Table 4.1. Elemental composition of coatings applied to nitrile rubber by Energy Dispersive X-ray spectroscopy. The composition is compared to compositional results for DLC on NBR 7201, NBR 9003 and NBR 8002 from the work of Martinez et al [18].

	C (at. %)	O (at. %)	Si (at. %)	N (at. %)	Other (at. %)
DLC	85.08±3.64	14.03±2.58	0.19±0.06	-	Trace
Si-DLC	79.79±3.38	16.14±2.69	2.60±0.50	-	Trace
DLC with Si-C interlayer	82.88±3.75	10.07±3.90	5.25±0.35	-	Trace
Si-DLC with Si-C interlayer	82.45±2.45	10.87±0.47	5.47±1.43	-	Trace
DLC on NBR 7201	87.7	7.9	1.6	2.7	Trace
DLC on NBR 9003	88.6	7.9	1.3	1.3	Trace
DLC on NBR 8002	98.3	1.3	0.3	-	-

4.3.3. Film thickness and microstructure

Figure 4.10 shows the coating thickness for both DLC and Si-DLC coatings deposited on Si wafer substrates. The thickness of these coatings was approximately 1.2 μm. The coating thickness determined by this approach produced similar results to coating thickness on rubber with the minor differences observed being within the error of observation due to the rough interface of rubber substrates [22].

Figure 4.11 shows the coating thickness after fracturing of DLC and/or Si-DLC with Si-C interlayer. The coating thickness estimated using scanning electron microscopy was

101

approximately 500 nm for Si-C interlayer and approximately 500 nm for the top DLC or Si-DLC film.
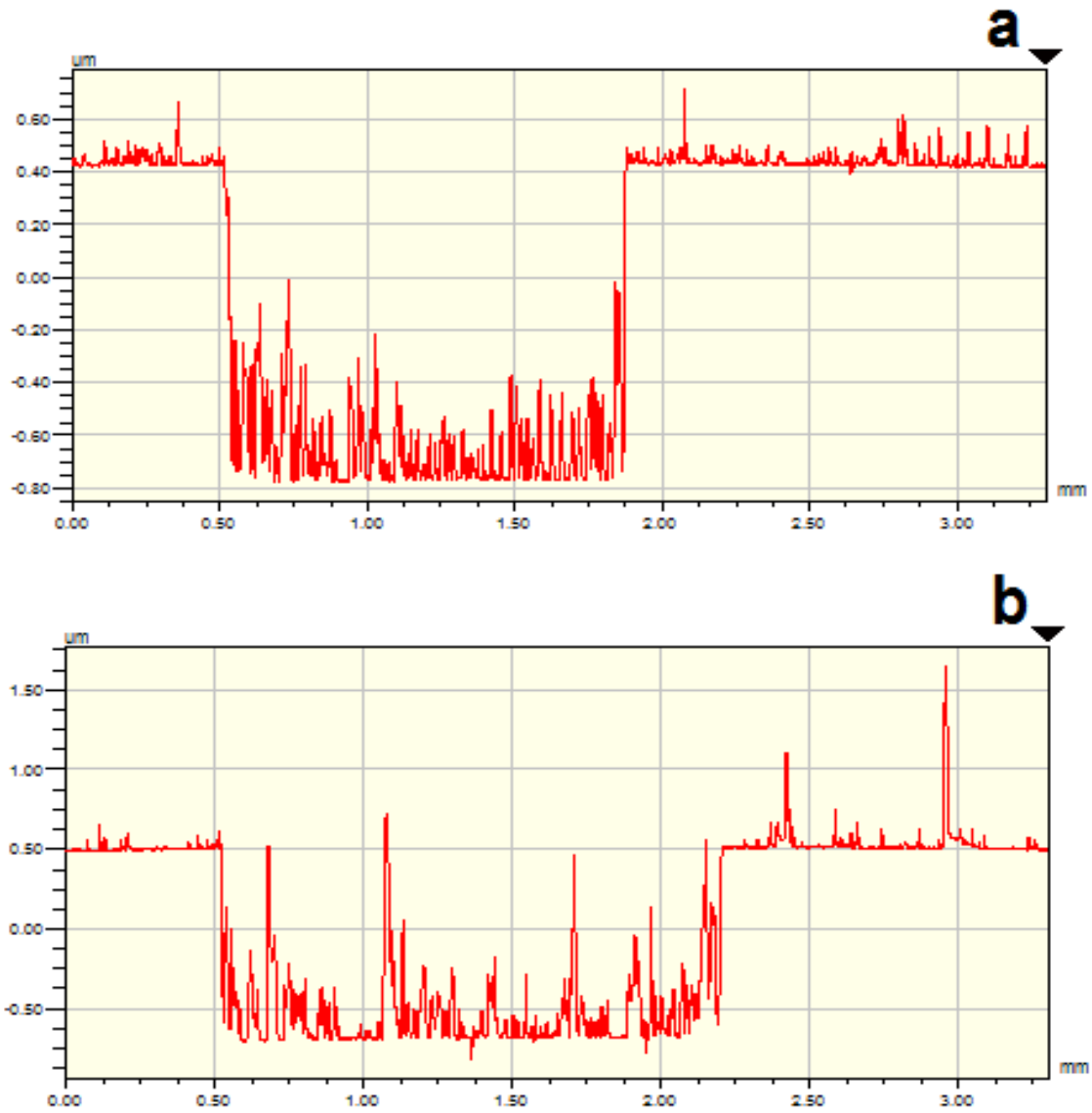
Figure 4.10. Step profile of the surface topography tracing after unmasking the coating for DLC (a) and Si-DLC coatings on Si wafer substrates
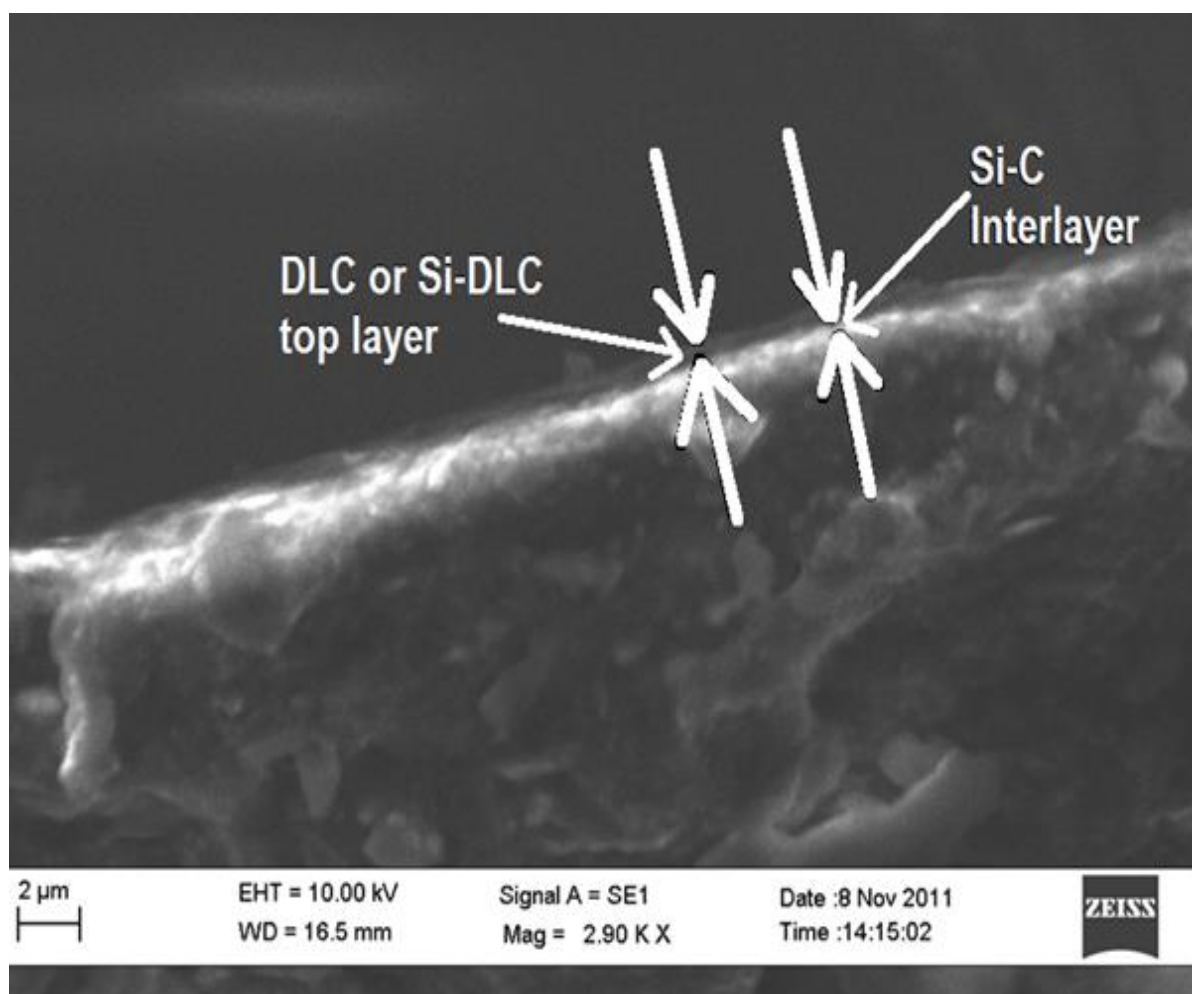
Figure 4.11. SEM micrograph of the fracture cross-section of DLC and/or Si-DLC with Si-C interlayers

In previous studies on DLC films deposited on rubber substrates, the fracture cross-sections showed a typical columnar structure [22]. In this study the fracture cross-sections did not show the typical columnar structure for the coatings deposited on nitrile rubber. Bui et al. showed that for DLC coatings on Si wafer, a bias voltage of -100 V was enough to prevent column formation leading to a dense, columnar free and featureless structure. They attributed the differences in the results between the DLC films deposited on rubber substrates and Si wafer to the differences in the surface morphology and roughness between rubber and Si wafer substrates [22].

Columnar growth has been related to interface structure of the growing coating, which is controlled by the intensity of concurrent ion impingement [101]. A closed field unbalanced magnetron sputtering ion plating system was used where the coating deposition is carried out

using a high density of low energy bombarding ions (-30 V bias voltage in this case), resulting in very dense, non-columnar coating structures. In this deposition configuration, the plasma that is present in vacuum chamber between the source and the nitrile rubber substrate is ideal for ion plating since the plasma allows energetic ion bombardment of the substrate which enhances ionization of vapour species even at low energies [168]. The substrate bias voltage used (-30 V) is even lower than the bias voltage of -50 V (in magnitude terms) described in the paper by Bui et al. who investigated the influence of different voltage biases on the surface morphology [22].

The non-columnar film dense micro-structures obtained for films deposited on nitrile rubber in this study are supported by the structural zone model developed by Kelly and Arnell [71, 87]. According to Kelly and Arnell [87], CFUBMS systems inherently suppressed the formation of porous structures and promoted the formation of fully dense structures at relatively low temperatures.

4.3.4. Surface Roughness

Figure 4.12 shows the typical surface profile for DLC coated on nitrile rubber and uncoated nitrile rubber. The average roughness values were obtained over a scan length of 2 mm. The average roughness value for uncoated nitrile rubber was 1.1 μm and for DLC coated on nitrile rubber it was 2.1 μm. Generally, for the DLC and Si-DLC films with and without Si-C interlayer, the average roughness values varied from 1.5 μm to 2.2 μm. The relatively high surface roughness was due to the film surface dendritic crack like network that forms as a result of thermal mismatch during film deposition [24]. The measurement scale of the resulting patches on the film surface (see Figure 4.8) is microns. As such the scan length of 2 mm inevitably traversed across a number of patches, hence the relatively high surface roughness. An increment in surface roughness was also observed by Martinez et al. [18]. In order to negate effect of the patches affecting the determination of the surface roughness, the scan length of the Dektak surface profiler was reduced to 1 mm resulting in average surface roughness variation for the films from 0.62 μm to 0.8 μm. However, since the inclusion of the Si-C interlayer did not have a significant contribution on surface roughness minimal effects from surface roughness on the film properties and characteristics should be expected.
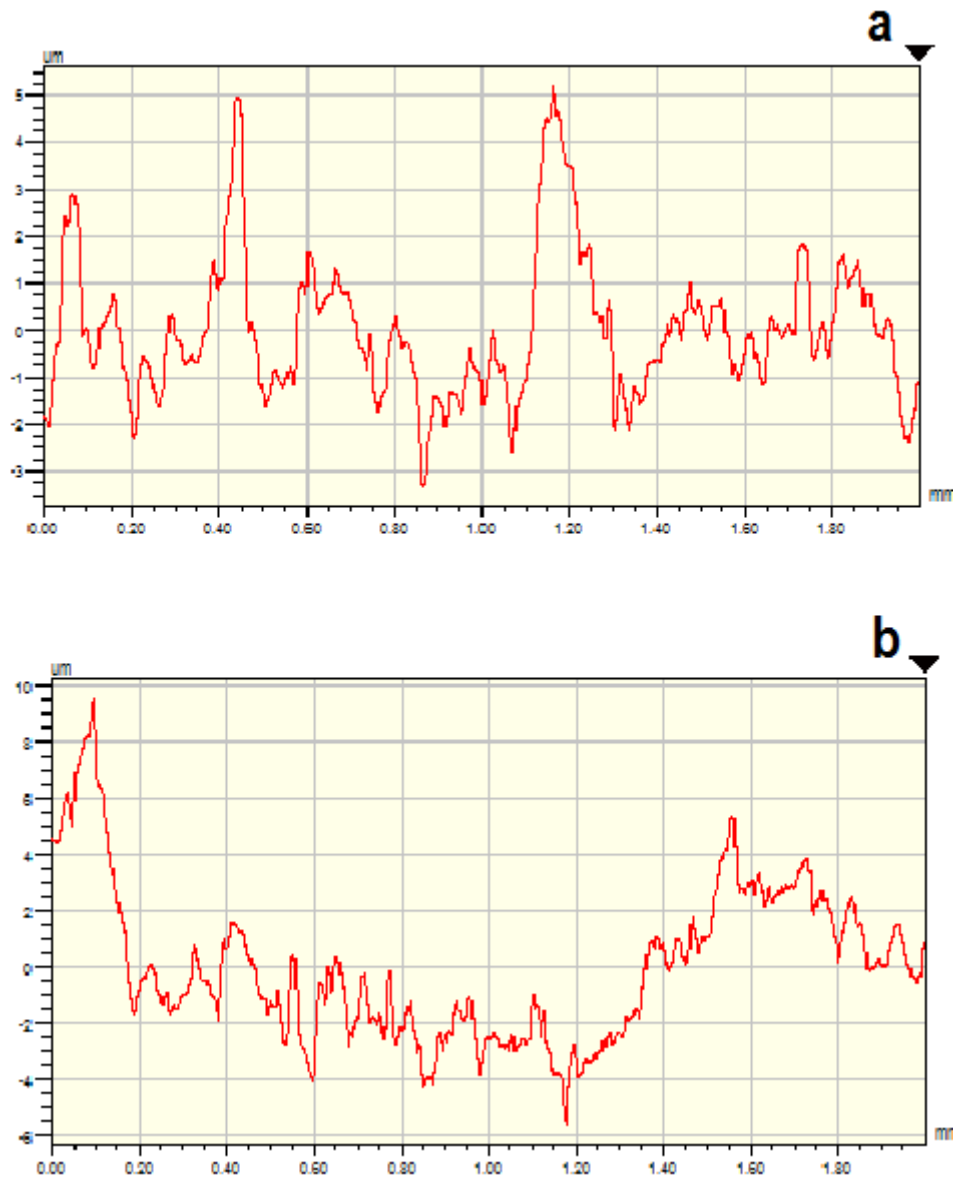
Figure 4.12. Surface profile for uncoated nitrile rubber sample (a) and DLC coated sample (b). The average roughness values were 1.1 μm and 2.1 μm respectively for uncoated nitrile and DLC coated sample

Figure 4.13 shows the digital microscopy profiles for the films an optical profile of DLC film deposited on nitrile rubber for a scan area of 0.3 mm by 0.25 mm. These images were used to observe how the morphology of the films evolves along the coating surface. The height profiles for most of the films were observed to vary differently for all of the films. This variation in the height profiles is expected again as a result of the patches on the coating surfaces for each of the films. These results are generally consistent with the results presented in Figure 4.8.
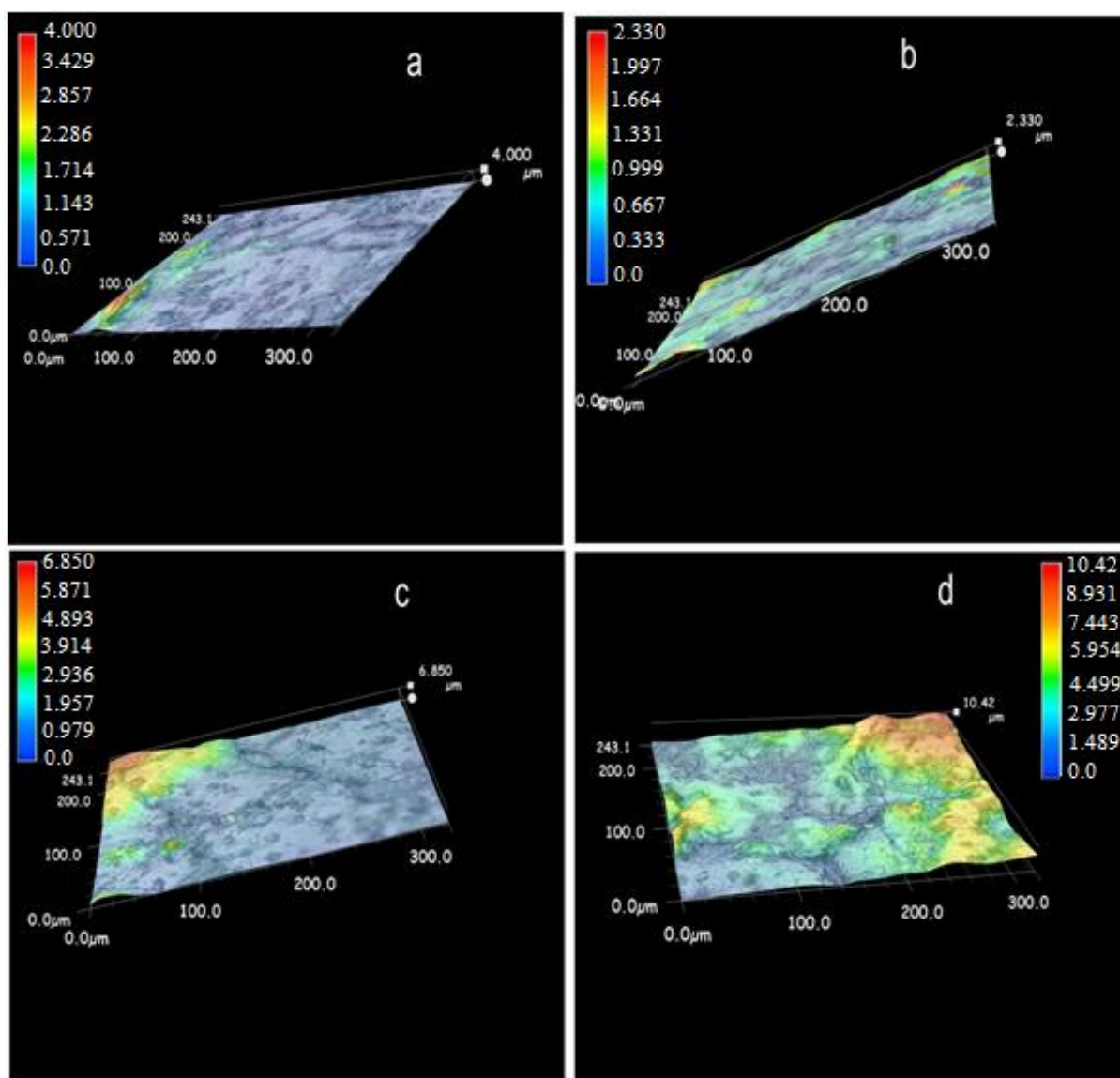
Figure 4.13. 3D surface profiles for the coated samples on nitrile rubber: (a) DLC; (b) Si-DLC; (c) DLC with Si-C interlayer; and, (d) Si-DLC with Si-C interlayer. Scale units are μm.

The roughness values for the films deposited on nitrile rubber were affected by the initial surface roughness of the nitrile rubber substrate which was relatively high at 1.1 μm (see Figure 4.12). This further enhanced the surface roughness as the impinging species were inclined at oblique angles due to interface shadowing instead of falling normally on the nitrile rubber substrates [22, 65, 167]. In the deposition process used the deposition temperature was low (approximately < 120°C) and as such the nucleation barrier was large and the super-saturation was low. Therefore large, but few nuclei were formed as a result of which coarse grained rough films were obtained [167].

4.4. Raman Spectroscopy analysis

4.4.1. G peak position, I_D/I_G, FWHM(G)

The chemical bonding of DLC and Si-DLC films has been studied by means of Raman spectroscopy using a 488 nm excitation wavelength. Figure 4.14 represents typical full Raman spectra (488 nm) for samples of DLC and Si-DLC coatings showing the prominent G peak (centred approximately at 1580 cm^{-1}) and a smaller underlying D peak (centred approximately at 1350 cm^{-1}). The G peak is due to the bond stretching of all pairs of hybridised carbon sp^2 atoms in both rings and chains. The G peak is mainly sensitive to the configuration of sp^2 sites because of their higher cross-section. In this study the G peak positions were close to the graphite vibrational density of states [95]. The D peak is correlated to the breathing modes of rings. The intensity of the D peak is proportional to the number and clustering of graphite like aromatic rings [91, 93, 95, 169].
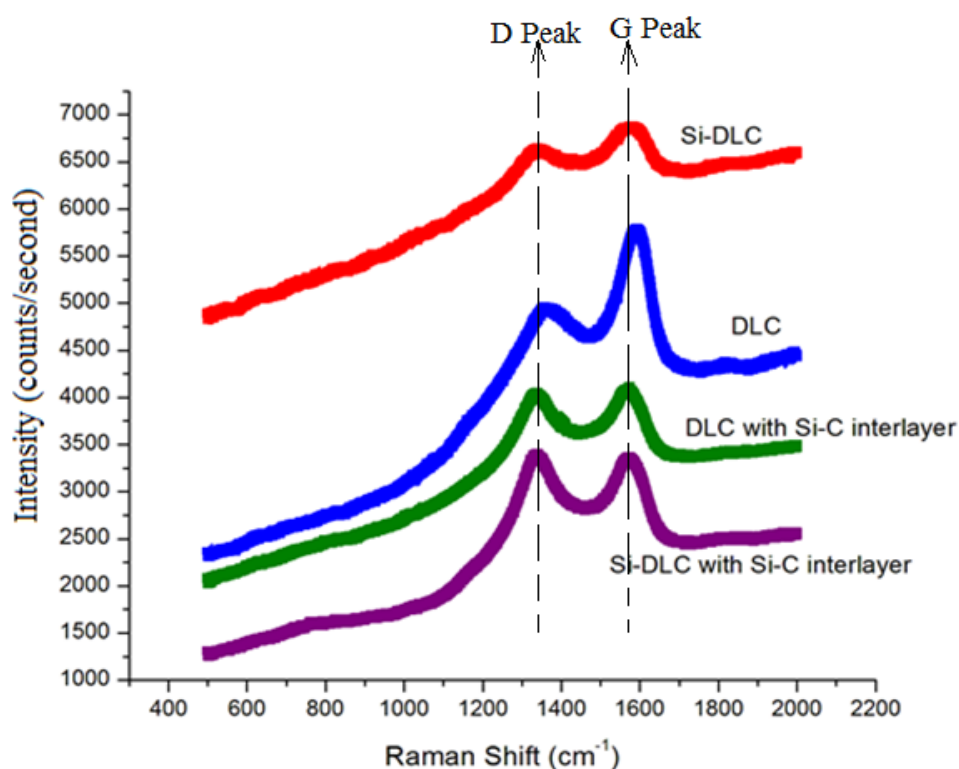
Figure 4.14. Raman spectra of DLC and Si-DLC films

Yoshida et al. [89] reported G peak position (Pos(G)) of 1530 cm^{-1} for DLC films deposited on silicone rubber by pulsed laser ablation. Martinez-Martinez et al. [68] reported Pos(G) between 1528 cm^{-1} and 1539 cm^{-1} for DLC films deposited by PECVD onto ACM rubber. In their study the bias voltages applied onto the rubber substrates were -300V, -400V and -600V [68]. Takikawa et al. [20] reported a hybrid Pos(G) of 1580 cm^{-1} for DLC films deposited onto EPDM rubber using a combination of PVD and CVD deposition techniques. In their deposition technology zero (0) bias voltage was applied onto the substrate and no external heating [20].

In this study the nitrile rubber substrates were biased by -30V. This is almost comparable to zero bias applied by Takikawa et al. [20] with similar results for Pos(G). In both studies the deposition of the films was done by a combination of PVD and CVD deposition processes. The combination of CFUBMSIP and PECVD during DLC and Si-DLC film deposition onto the nitrile rubber substrates enhances ion bombardment of the substrates and the unbalanced magnetic field allows a much more intensive stimulation of the plasma with a much higher content of ionized hydrocarbon species. These films are therefore characterised by an enhanced visible photoluminescence which is controlled by the hydrogen content in the films. [170]. Lackner et al. produced films with 40 at. % H using this approach after measuring the slope of the PL background and correctly categorised them as PLCH films [170]. The bonded hydrogen content for DLCH films is 20% < H at.% < 40% [42]. It has been shown that a substrate bias of -30 V is sufficient to obtain maximum ionisation efficiency in the plasma, which in turn results in much higher ion currents for CFUBMS systems due to improved magnetron design and the use of rare earth magnets employed by Teer Coatings UK [71].

The ratio of the intensities of the D peak, I_D, and G peak, I_G (I_D/I_G), is a measure of the sp^2 phase organized in rings [166]. Therefore, I_D/I_G can be used as a parameter for qualitatively evaluating the sp^3 fraction [95]. A plot of the ratio of the intensities of the D peak, I_D, and G peak, I_G, to the FWHM(G) is shown in Figure 4.15. The data points are more clustered for DLC and Si-DLC, than they are for DLC and Si-DLC with Si-C interlayer. A plot of I_D/I_G vs. G peak width (FWHM(G)) should give a straight line as the G peak width is partially determined by the graphitic cluster size [171]. However, Filik et al. [141] observed that a linear relationship between FWHM(G) and the I_D/I_G held for films deposited at DC bias values greater than approximately 150 V, while, for films deposited at DC bias values lower than 150 V, data points were more clustered, similar to the results shown in Figure 4.15. The

clustering of the DLC and Si-DLC films might be due to the presence of H-terminated aromatic groups, rather than extended networks of graphitic sheets, which suggests that at these lower ion impact energies the graphitic clusters have much less influence upon the G-peak width [141].
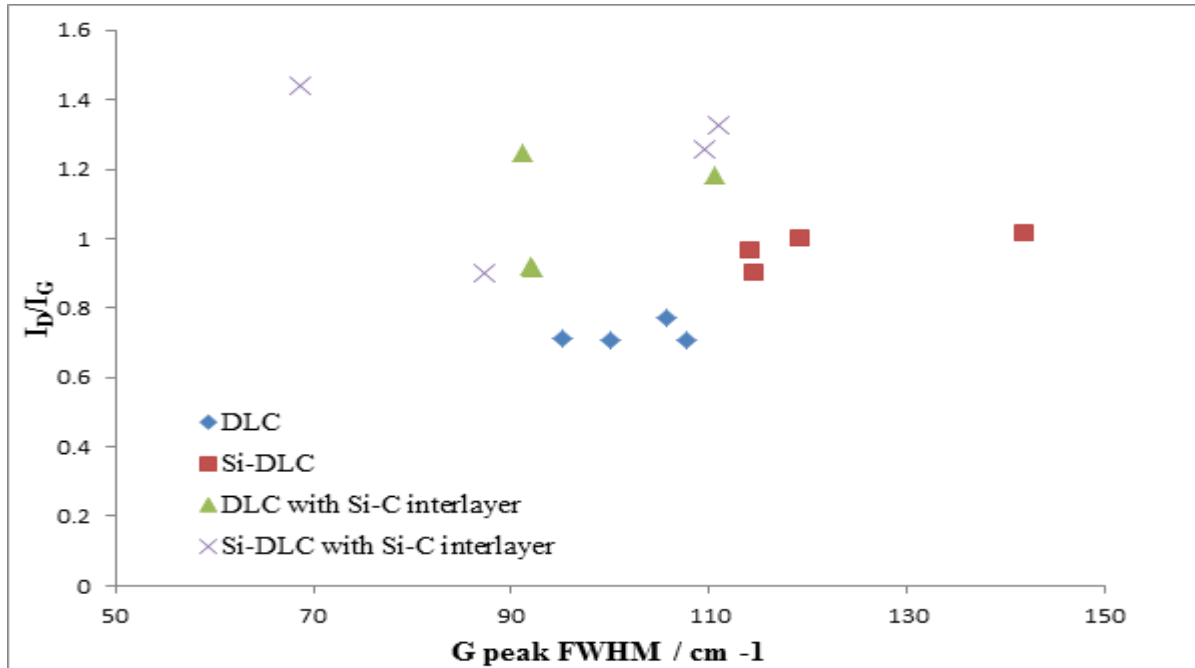
Figure 4.15. The intensity ratio, I_D/I_G plotted against FWHM(G)

Figure 4.16 shows a clearer comparison of the trends of the FWHM(G) and the I_D/I_G ratio for the DLC and Si-DLC films. The I_D/I_G ratio generally tended to increase for both DLC and Si-DLC films with the inclusion of Si-C interlayer compared to the films without Si-C interlayer. Average values of I_D/I_G showed DLC film with an intensity ratio of approximately 0.7 and DLC film with a Si-C interlayer with an intensity ratio of approximately 1.1. For Si-DLC film and intensity ratio of approximately 1.0 was observed and this ratio increased to approximately 1.2 for Si-DLC film with a Si-C interlayer. From this result, it can be inferred that the sp^3 content is decreasing as a result of the inclusion of the Si-C interlayer [172]. With increasing sp^3 content, sp^2 clusters within sp^3 network become smaller and more strained, causing increases in bond length and bond angle disorder [42]. Therefore, with decreasing sp^3 content the inverse can be implied. This discussion is supported by the implications of eq. (4.2). The graphitic size clusters for the films with the Si-C interlayers would be larger as these films had correspondingly higher intensity ratios.

It was observed that the FWHM(G) is lower for DLC and Si-DLC films with Si-C interlayer, which suggests that the graphitic clusters were unstrained [166]. The FWHM(G) is mainly sensitive to structural disorder, which arises from bond angle and bond length distortions. FWHM(G) would be small if the clusters were defect free, unstrained or molecular [166]. FWHM(G) measures the bond length and bond angle disorder in sp^2 clusters, which have close relations with the stress felt by the clusters. With increasing sp^3 content, sp^2 clusters within sp^3 networks become smaller and more strained, causing increases in bond length and bond angle disorder [42, 95]. Table 4.2 gives a summary of the G and D peak positions, I_D/I_G, and FWHM(G) for the films deposited on nitrile rubber. The variation of the G peak position is attributed to the surface roughness of the underlying rubber substrate which affects the depth of Raman spectroscopy measurements.
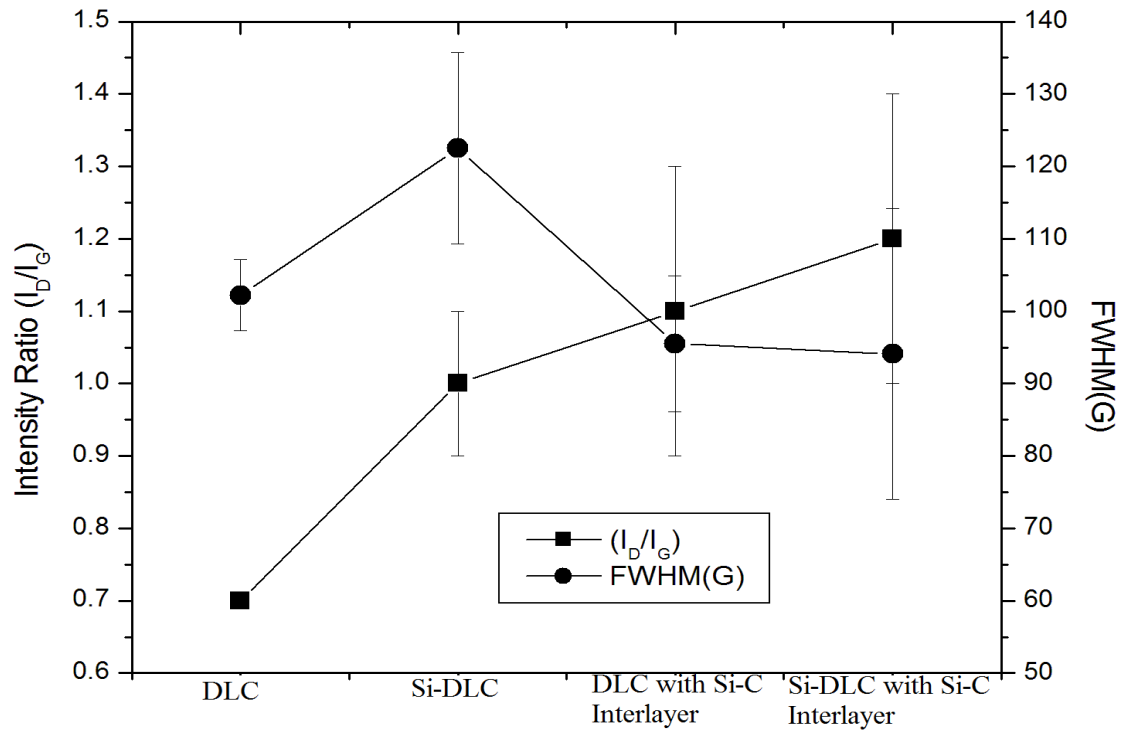
Figure 4.16. Comparison of FWHM(G) and I_D/I_G for the films

Table 4.2. Summative overview of the peak positions, I_D/I_G and FWHM(G) for the coatings

Coating	Pos(D)	Pos(G)	I_D/I_G	FWHM(G)
DLC	1357.7±0.1	1585.6±3.4	0.7±0.0	102.2±4.9
Si-DLC	1338.4±5.3	1573.9±8.6	1.0±0.1	122.5±13.3
DLC with Si-C Interlayer	1341.1±6.5	1579.6±8.7	1.1±0.2	96.5±9.4
Si-DLC with Si-C Interlayer	1339.2±6.8	1582.2±13.8	1.2±0.2	94.1±20.1

During some of the Raman spectroscopy measurements of the DLC and Si-DLC films, a sharply peaked band at around 1060 cm^{-1} was observed for Si-DLC, DLC with Si-C interlayer and Si-DLC with Si-C interlayer deposited on the nitrile rubber substrate as depicted in Figure 4.17. This peak signifies an increase in Raman scattering contributions from sp^3 sites due to vibration in C-C bonds [94]. The presence of this peak may be attributed to the Si dopant and Si in the interlayer. Such an explanation is supported by Paik [172] who observed a sharp Si-related peak at a similar position for DLC films (20 nm thick) deposited on Si wafer by magnetron sputter-type negative ion source method. Takikawa et al. attributed this shoulder to the existence of C-C bonds in the film [20]. However, the origin of this shoulder is still inconclusive in the literature with some arguments for assignment of these peaks to nano-crystalline diamond or other sp^3- bonded phases or as an indicator of C-C bonds in the films [96-98] and other arguments for assignment to transpolyacetylene segments at grain boundaries and surfaces [41, 99].
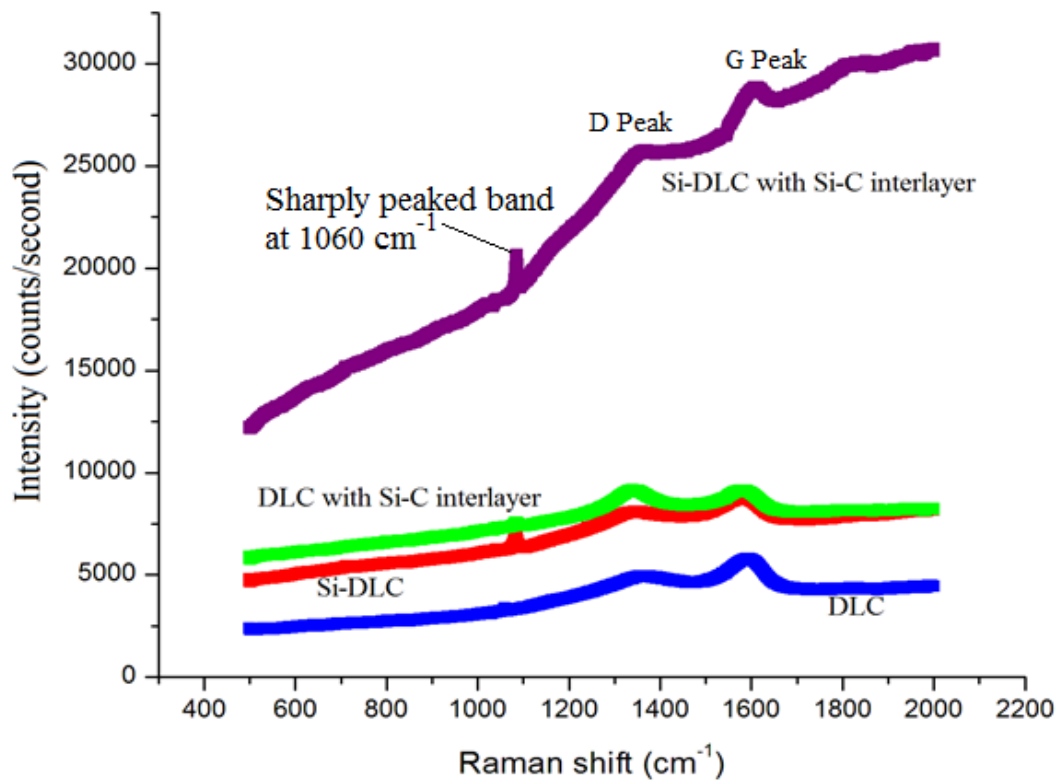
Figure 4.17. A sharp peak at around 1060 cm observed for Si-DLC, DLC with Si-C interlayer and Si-DLC with Si-C interlayer

4.4.2. Multi-wavelength Raman analysis

The chemical bonding of DLC and Si-DLC films was also studied by means of a multi-wavelength Raman analysis using a 325 nm (UV) and 488 nm (visible) excitation wavelengths. Few multi-wavelength Raman spectroscopy analyses have been carried out for DLC and DLC based films deposited on rubber substrates [20, 21]. UV Raman is particularly useful for hydrogenated amorphous carbons as it gives clear measurements in the D and G spectral regions for highly hydrogenated samples, for which the visible Raman spectra are overshadowed by photoluminescence [42, 173]. Casiraghi et al. [42] noted that a two-wavelength analysis was more than sufficient to achieve a multi-wavelength analysis

Figure 4.18 shows typical Raman spectra for UV and visible excitation. The absence of the photoluminescence peak is typical for UV Raman spectra [42, 174]. The photoluminescence peak features prominently for visible Raman spectra as shown in Figure 4.18b. It has been suggested that the photoluminescence peak is related to the bonded hydrogen in the film [21, 42, 95]. The main effect of hydrogen in hydrogenated DLC films is to modify the C-C network [41, 42]. Hydrogen is important for obtaining a wide optical gap and high electrical resistivity, removing mid-gap defect states, stabilizing the random network and preventing its collapse into a graphitic phase [54].
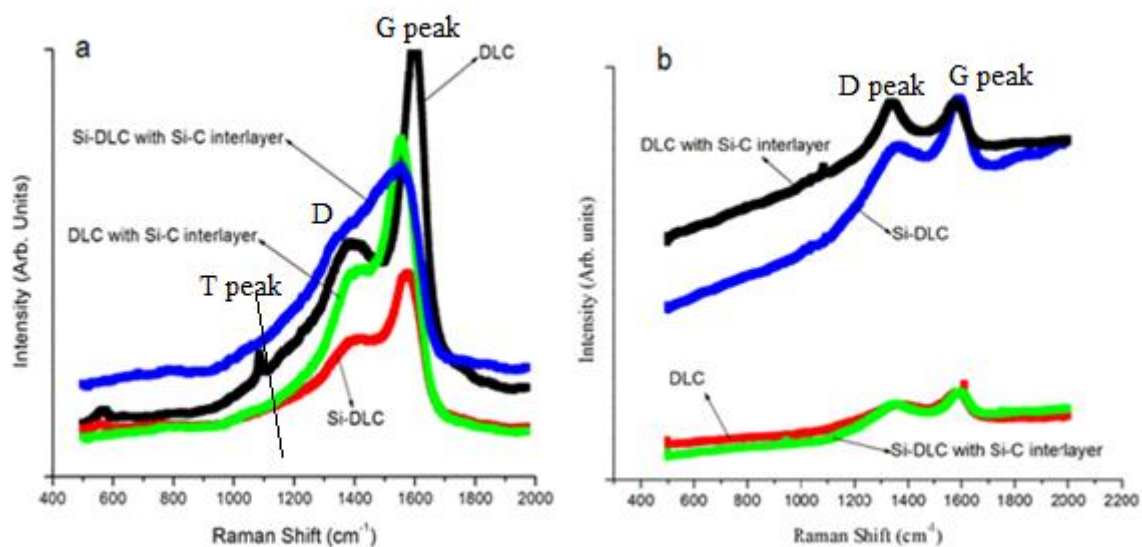
Figure 4.18. Multi-wavelength Raman spectra of typical DLC and Si-DLC films deposited on nitrile rubber; a) 325 nm and; b) 488 nm excitation wavelengths

Figure 4.19 shows the deconvolution of the UV Raman spectra using a multiple Gaussian approximation to determine the D, G and T peak positions ($R^2 = 0.9996$). The T peak position is represented by a weak shoulder at approximately $1150 - 1200$ cm^{-1} and is only observed for UV Raman spectra. The T peak is due to the C-C sp^3 vibrational modes [93, 94, 175]. Quantitative determination of sp^3 hybridisation content using the T peak has only been shown for hydrogen free DLC films. In hydrogenated DLC films the presence of the D peak limits the determination of sp^3 content [94, 175]. A 'D' like peak was observed around 1400 cm^{-1}. This D like peak survives in UV Raman spectra if the sp^2 sites are in disordered rings. As such this effect should be accounted for, in principle, by introducing an extra 'D' peak in fitting as shown in Figure 4.19 [91] Table 4.3 summarises the results of the Raman parameters for UV Raman spectroscopy analysis.
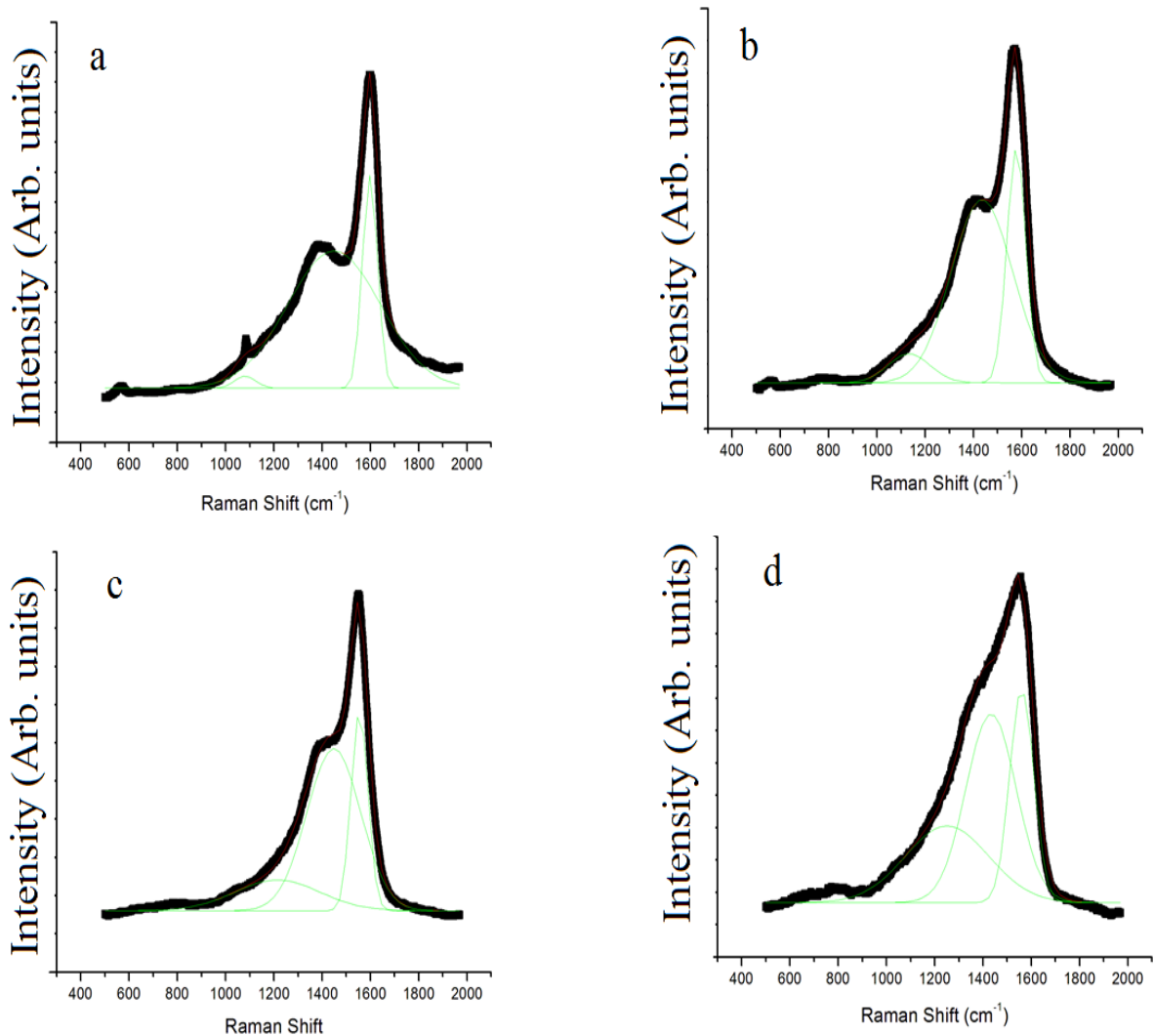
Figure 4.19. UV Raman spectra analysis: (a) DLC; (b) Si-DLC; (c) DLC with Si-C interlayer; and, (d) Si-DLC with Si-C interlayer

Table 4.3. UV Raman parameter for the coatings on nitrile rubbers

Coating	Pos(T)	Pos('D')	Pos(G)	FWHM(G)
DLC	1079.9	1449.1	1597.8	61.9
Si-DLC	1126.0	1433.8	1582.1	76.3
DLC with Si-C Interlayer	1174.9	1441.7	1558.7	74.4
Si-DLC with Si-C Interlayer	1234.3	1448.7	1569.3	92.0

4.4.3. G-peak dispersion (Disp(G))

Figure 4.20 shows a schematic representation of the dispersion of the G peak for Raman spectra obtained at excitation wavelength of 325nm and 488 nm for DLC and Si-DLC films deposited on nitrile rubber. The Raman spectra are not identical in Figure 4.20, despite the deposition process being reproducible due to influence of the Si-C interlayer and the relatively high surface roughness of the underlying nitrile rubber substrate. The estimated penetration depth of Raman spectra in this study was below 500 nm, but when the top film DLC and Si-DLC film is being deposited on the Si-C interlayer some ion exchange during magnetron sputtering deposition should be expected.
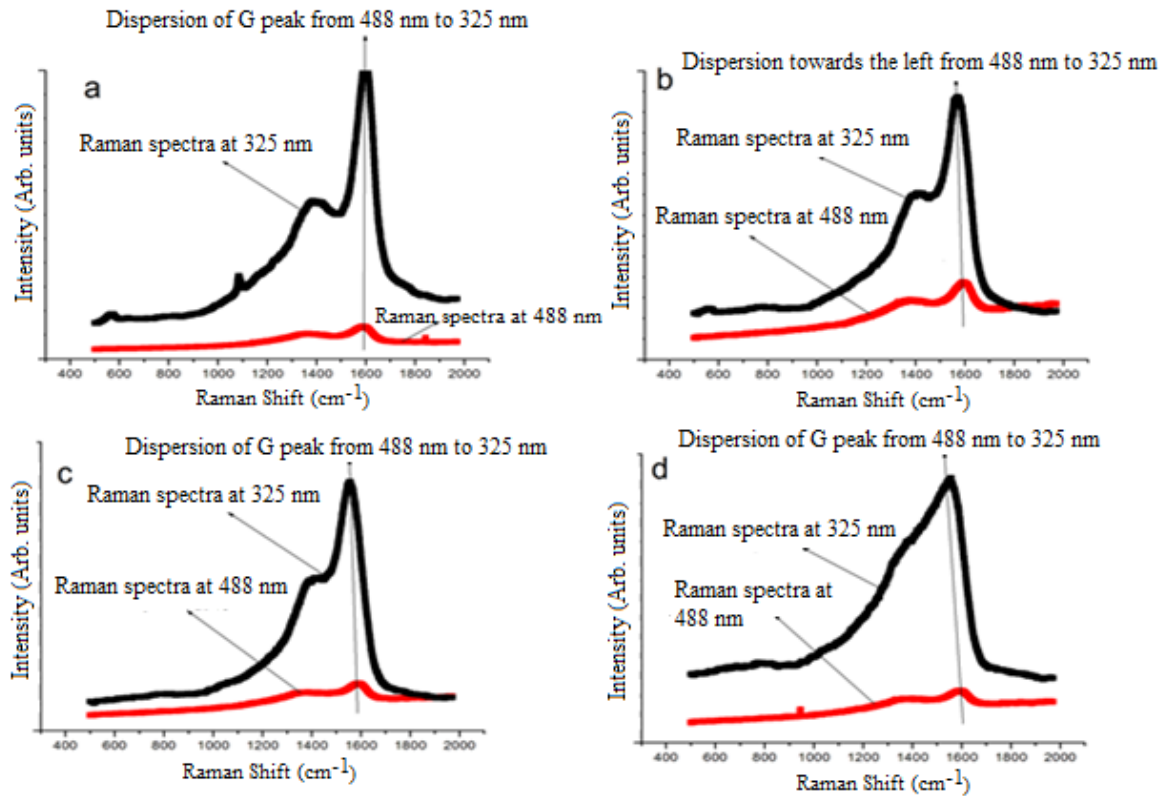
Figure 4.20. Disp(G) from 488 nm to 325 nm for: a) DLC; b) Si-DLC; c) DLC with Si-C; d) Si-DLC with Si-C films deposited on nitrile rubber

From eq. (3.4), Table 4.2, Table 4.3 and Figure 4.20, Disp(G) for DLC, Si-DLC, DLC with Si-C interlayer and Si-DLC with Si-C interlayer was calculated as 0.07, 0.05, 0.13 and 0.08, respectively. These low values for Disp(G) can be attributed to the deposition technology used in this study. The combination of a CFUBMSIP system and reactive magnetron sputtering in an Ar/C_4H_{10} plasma may explain these results. This deposition method allows DLC and Si-DLC films to be deposited onto nitrile rubber resulting in G peaks at approximately 1580 cm^{-1}, which is close to the graphite vibrational density of states [95]. Cui et al. also reported Disp(G) values below 0.20 for hydrogenated DLC films deposited on Si wafers using an arc ion plating system [143]. Casiraghi et al. reported Disp(G) results of 0.16 for DLCH films deposited by magnetron sputtering and 0.12 for GLCH films deposited by plasma enhanced chemical vapour deposition [42]. These values for Disp(G) are lower than Disp(G) results reported for ta-C:H and PLCH, which have Disp(G) values of 0.25 to 0.30 and 0.30 to 0.40, respectively [42]. Also in previous studies the Disp(G) was determined using positions of the G peak at 514 nm and 244 nm excitation wavelengths [42, 143].

Disp(G) is proportional to the degree of topological disorder. The dispersion arises from a resonant selection of sp^2 configurations or clusters with wider π band gaps and corresponding higher vibrational frequencies [91]. For UV Raman excitation the G peak position decreases with increasing sp^2 clustering [42, 91, 143, 173]. Therefore, if two samples have similar G peak positions in visible Raman but different ones in UV Raman, the sample with lower G peak position in UV has higher sp^2 clustering [42]. Therefore, DLC film with Si-C interlayer has more sp^2 clustering.

4.4.4. Hydrogen estimation

In this study bonded hydrogen in the films was determined using two approaches: the PL background method and Tauc gap method. The presence of a PL background for the visible spectra (488 nm) for DLC and Si-DLC films deposited on nitrile rubber is an indicator of bonded hydrogen in the films [41, 42, 173]. From eq. (3.5) and Figure 3.14, the bonded hydrogen content in the films was determined. Calculated hydrogen values for all of the films were between 24 and 31% as shown in Table 4.4. This implies that the DLC and Si-DLC films deposited on nitrile rubber can be classed as diamond-like a-C:H (DLCH) which has 20

– 40 at. % H [17, 42, 173]. The presence of hydrogen in hydrogenated DLC films modifies the C-C network [41, 42]. The introduction of hydrogen into an amorphous carbon links the amount and configuration of the sp^2 phase with the overall sp^3 hybridisation (C–C + C–H sp^3). However, for increments of hydrogen over 25% at.%, the overall sp^3 hybridisation can still increase, but not the C-C sp^3 hybridisation [42, 91, 95].

Table 4.4. PL slope (m), G peak intensity (I(G), and resulting bonded hydrogen estimation

Coating	Sample no.	m	I(G)	H (at. %)
DLC	1	0.2936	1118	28.6
	2	0.1569	804	26.5
	3	0.2028	1360	24.6
	4	1.5	5786	28.6
	5	0.45	2133	27.1
	6	2.352	6315	31.2
	7	0.27	1075	28.3
Si-DLC	1	0.605	1883	30.1
	2	0.4869	1640	29.5
	3	0.2748	1306	27.1
	4	0.819	2322	30.8
	5	2.773	9258	29.6
	6	2.202	8787	28.3
	7	1.0599	4306	28.2
DLC with Si-C Interlayer	1	0.4854	1818	28.8
	2	1.0415	3123	30.4
	3	0.49	1556	30.0
	4	1.338	9157	24.4
	5	0.565	2361	28.0
	6	0.823	4108	26.7
	7	0.373	2062	26.0
Si-DLC with Si-C Interlayer	1	0.667	2898	27.7
	2	0.299	1372	27.3
	3	0.375	1362	29.0
	4	1.925	6208	29.8
	5	0.864	2142	31.7
	6	0.823	3358	28.2

Figure 4.21a shows the Tauc plot for the coatings derived from UV-VIS measurements and Figure 4.21b shows the absorption coefficient, α, vs. photon energy. The Tauc gap was observed to decrease slightly for DLC from 1.63 eV to 1.57 eV for DLC with Si-C interlayer. For Si-DLC the Tauc gap was 1.45 eV, and this increased to 1.52 for Si-DLC with Si-C interlayer. The E_{04} gaps for the films was 2.06 eV for DLC, 1.99 eV for Si-DLC, 2.12 eV for DLC with Si-C interlayer, and 2.02 eV for Si-DLC with Si-C interlayer. Casiraghi et al. reported similar results [42]. These results were consistently reproduced on measurements

made on a series of different samples deposited under the same conditions. These results further characterise the DLC and Si-DLC films deposited as diamond-like a-C:H (DLCH) which have an optical gap between 1 and 2 eV [42].
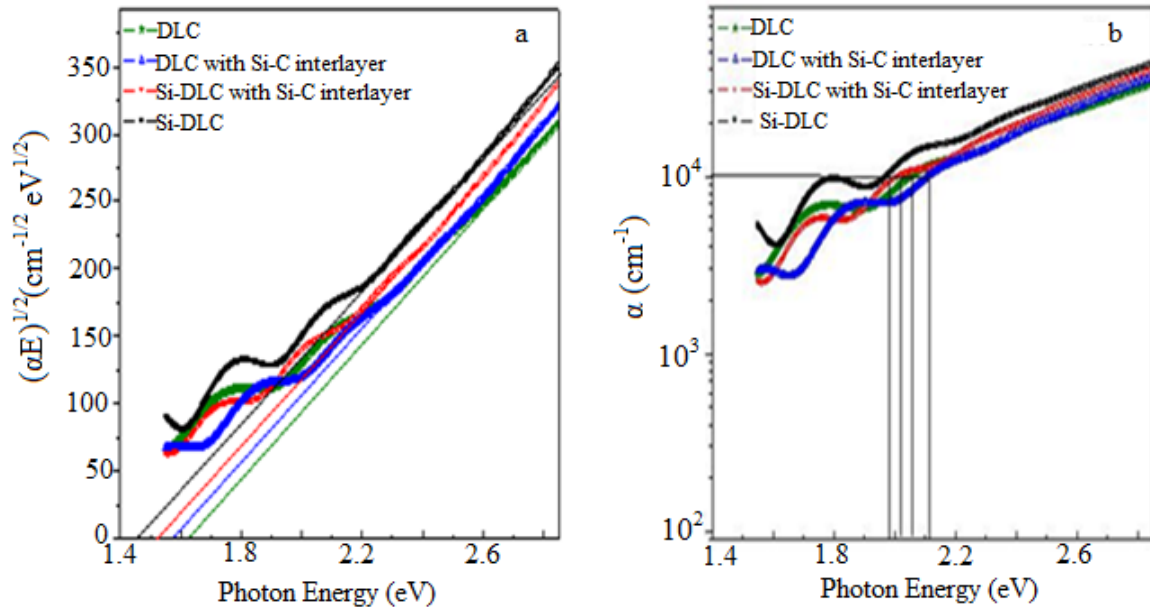
Figure 4.21. Tauc plot for films derived from UV-Vis measurements (a) and, absorption coefficient, α, vs. photon energy (b).

The Tauc gap is mainly determined by the status of sp^2 bonded clusters embedded in the amorphous carbon medium [139]. The increase in the Tauc gap can be explained by the cluster model theory proposed by Robertson [176]. The increase in the Tauc gap for the Si-DLC film with Si-C interlayer compared with the Si-DLC film implies that the sp^3 content increases which promotes the disordering in the films and lowers the sp^2 cluster size [147, 176]. The decrease in Tauc gap for the DLC film with Si-C interlayer compared to the DLC film may be due to an increase in the size of sp^2 bonded graphitic clusters in these films [177, 178]. This result is consistent with the previous discussion on I_D/I_G and Disp(G) where the DLC with Si-C interlayer film was noted to have more sp^2 clustering.

Using the measured values of the Tauc gap and eq. (3.8) the bonded hydrogen in the films was determined. The bonded hydrogen (at. %) was determined as 28.1% for DLC, 26.1% for Si-DLC, 27.4% for DLC with Si-C interlayer, and 26.9% for Si-DLC with Si-C interlayer. These results are shown in Figure 4.22.
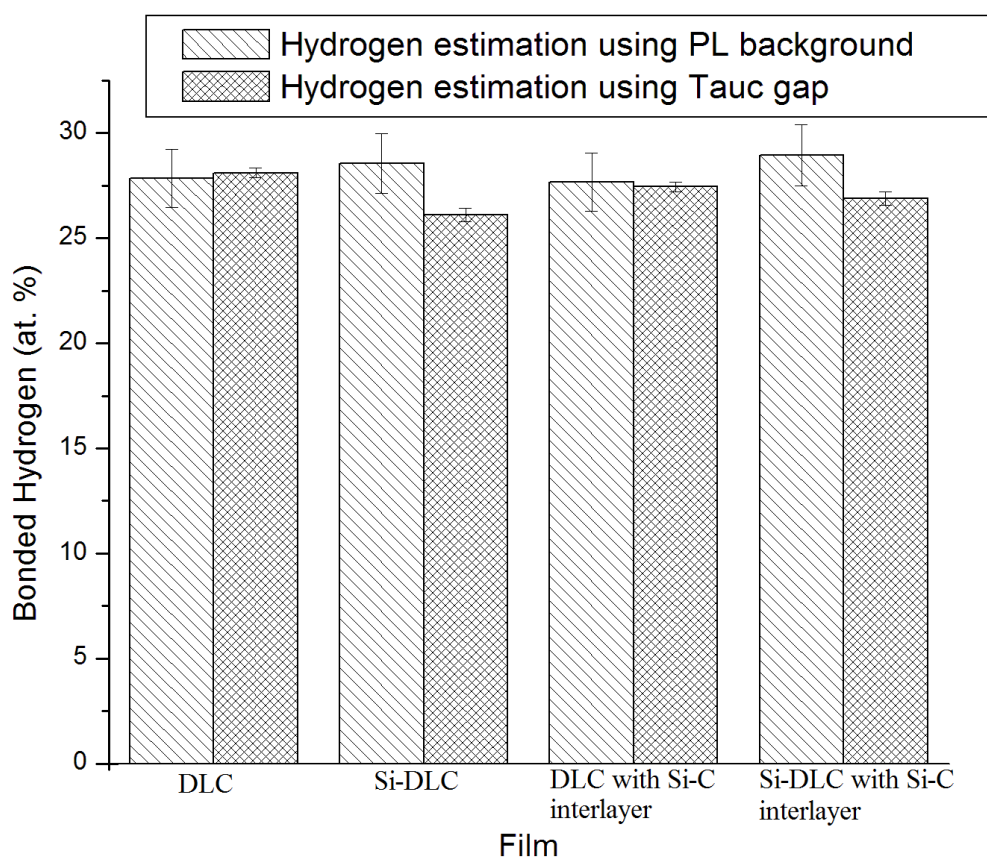
Figure 4.22. Bonded hydrogen estimation using PL background and Tauc gap

For hydrogen estimation using the PL background method, the results indicate that the hydrogen content in the samples is independent of doping with Si and the Si-C interlayer. Comparison of hydrogen content is particularly good using both methods for DLC and DLC with Si-C interlayer films. This implies that bonded hydrogen in the films is determined more by the reactive mechanisms that proceed between Ar gas and C_4H_{10} gas during the deposition stage of these films.

4.4.5. Internal compressive stress reduction

From Table 4.2 the G peak positions for all of the films are centred at approximately 1580 cm^{-1}. In order to determine the reduction in internal compressive stress the higher limit of the G peak positions for the films given in Table 4.2 was used. Takikawa et al. reported a G peak position of 1580 cm^{-1} for DLC films deposited on rubber substrates using a combination of PVD and CVD deposition technologies [20]. This value of G peak position was considered as

a reference value as in this study the films were deposited using a combination of CFUBMSIP and PECVD techniques. As such the reduction of internal compressive stress for the films was determined using eq. (3.6) as follows: 1.5 GPa for DLC, 0.4 GPa for Si-DLC, 1.4 GPa for DLC with Si-C interlayer and 2.6 GPa for Si-DLC with Si-C interlayer. G peak position shift upwards are indicative of lower amounts of internal compressive stress compared to the reference [144].

In this work the G peak position of DLC film deposited by Takikawa et al. [20] was taken as a reference value in the calculation of reduction of internal compressive stress using eq. (3.6). This may not indicate sufficiently the extent of the lower amounts of residual stress in the films as they were all deposited using the a deposition technology incorporating PVD and CVD techniques, which was similar to the deposition technology used in this study. Therefore the variation of G peak positions may be within the measurement error. However, once comparisons are made to results reported elsewhere for DLC films deposited on rubber where G peak position values were between 1528 -1539 cm^{-1} [68, 89], then the magnitude of internal compressive stress reduction in the films in this study becomes clear. The reduction in the internal compressive stress is attributed to the deposition technology used. The combination of CFUBMSIP and PECVD allowed the coatings to be deposited at substrate bias voltages of -30V. This implied that the films were deposited at low temperatures which further implies that the build-up in thermal stresses is inhibited for these films [167, 179]

The residual stress arises as a result of the correlation between the interatomic force constant and interatomic separation. The interatomic force constant is associated with the atomic vibrational frequency. If the tensile load on the material increases, bond lengths increase, force constants decrease, and vibrational frequencies decrease. On the other hand, if a material is subjected to mechanical compression, bond lengths decrease, force constants increase, and vibrational frequencies increase [144]. The lowest reduction to internal compressive stress was observed for Si-DLC films. Silicon cannot significantly contribute to internal stress reduction in diamond-like carbon–silicon composite films, since silicon atoms tetrahedrally bond to carbon and other silicon atoms [144]. Si doping reduces the average size of the sp^2 bonded clusters and promotes the formation of sp^3 bonding in the Si-DLC film. This is due to the Si valence structure which is well known to form only four–fold co-ordinated networks [165]

4.5. XPS Analysis

4.5.1. XPS survey scans

Figure 4.23 shows the XPS survey scans for the films. The contributions from C 1s (~285 eV), O 1s (~531 eV), Si 2p (~100 eV) and Si 2s (~151 eV) were clearly identified.
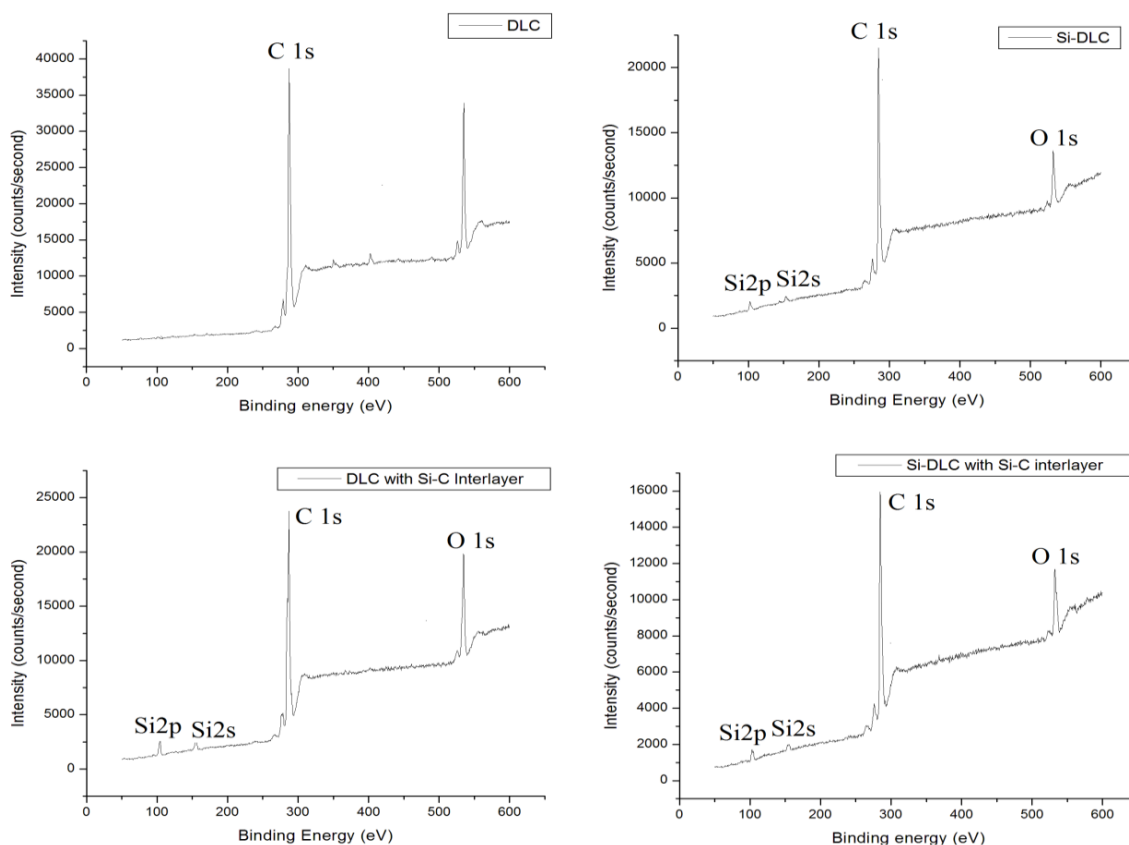
Figure 4.23. Survey scan for XPS spectra of the films showing C 1s, O 1s, Si2p and Si2s positions

The symmetrical O 1s peak at 531 eV is mainly attributed to adsorbed oxygen in the film surface [180]. The contributions from Si 2p and Si 2s were observed for the Si-DLC films and the DLC with Si-C interlayer film. The binding energy of the Si 2p peak may arise due to the presence of some Si-H or Si-O bonds. The Si 2s peak could be caused by Si atoms bonded to the carbon atoms in different hybridization states of sp^2 or sp^3 [155]. Srisang et al. suggests that the C-Si (C 1s) and Si-C (Si 2p) configurations correspond to the bonding between carbon and silicon in SiC [181]. Compared to XPS data obtained for a graphite surface and a diamond surface which had full width at half maximum (FWHM) values of 0.6 eV and 1.0 eV, respectively, [152], the C 1s peaks obtained in this study are broad as shown

120

in Table 4.5. This implies that possible contributions from directly bonded carbons to the C 1s peak can be determined.

4.5.2. Deconvolution of the C 1s peak

The deconvolution of the XPS spectra was done using the Origin-6 (professional) software with a Gaussian distribution function with R^2=0.9996 for all of the curve fittings. Figure 4.24 shows the deconvolution of the XPS spectra in the C 1s peaks for the films. The deconvolution of the spectra showed that the broad C 1s peak was composed of at most five peak positions depending on the film.
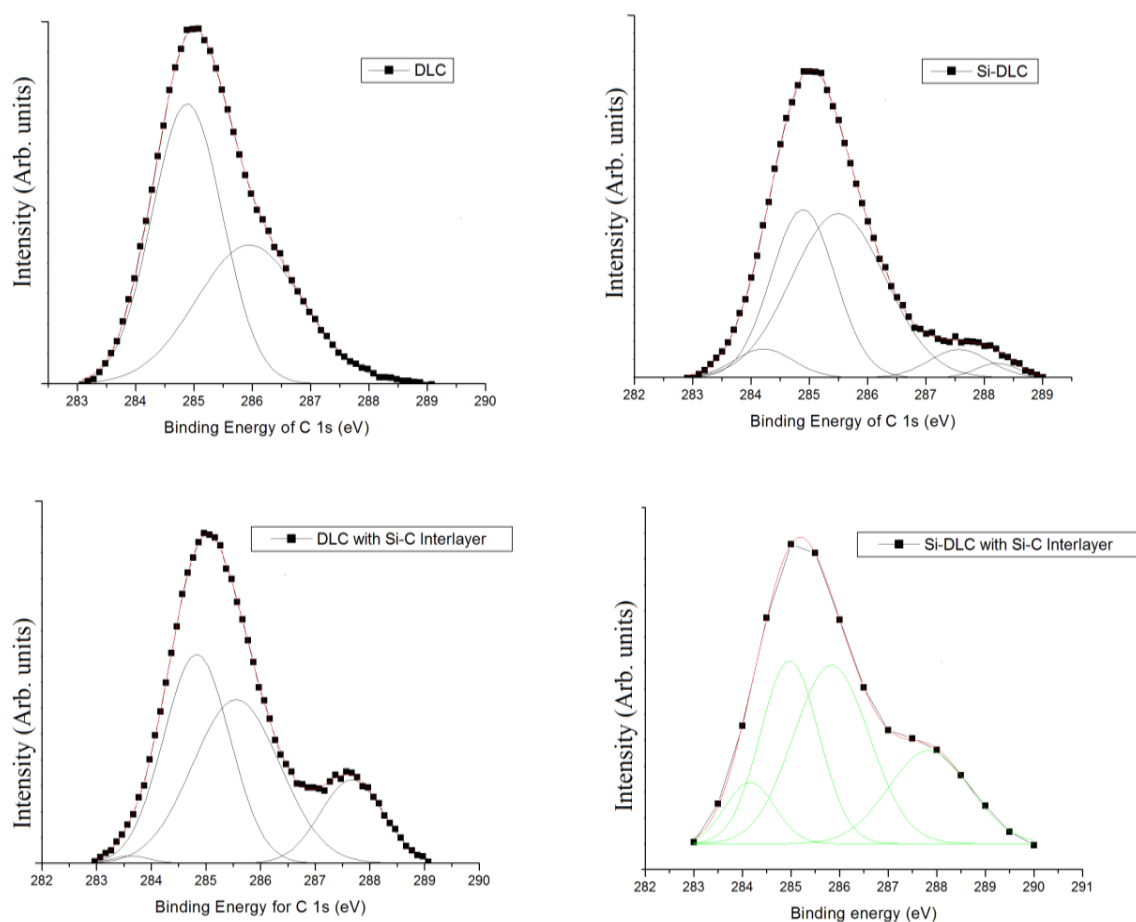
Figure 4.24. Deconvolution of the XPS spectra of C 1s peak of the films

The five peaks were positioned at 284.1 eV (C-Si), 284.8 eV (C=C), 285.7 eV (C-C), 287.0 eV (C-O) and 288.9 eV (C=O or O-C=O bond) [147, 149, 152, 155, 181]. When Si is co-

deposited into DLC films the contribution from silicon bonded carbon to the C 1s peak appears at ~ 284.1 eV and increases with Si [155]. This peak should not be seen in DLC films only. The low intensity peaks at ~ 287.0 and 288.9 eV come from contamination due to air exposure [147, 154, 155], or from co-sputtering during the deposition of the Si-C interlayer or the Si-DLC film. For each of the films multiple Gaussian fits were used at the peak positions so that a best fit of the C 1s peak was obtained. Table 4.5 details the binding energy and FWHM from XPS spectral deconvolution of the C 1s peak.

Table 4.5. The binding energy (eV) and FWHM (eV) for the films obtained from XPS spectral deconvolution of the C 1s peak

		C-Si	C=C	C-C	C-O	C=O/O-C=O
DLC	Binding energy	-	284.8±0.01	285.7±0.1	-	-
	FWHM	-	1.2±0.02	1.8±0.1	-	-
Si-DLC	Binding energy	284.2±0.3	284.8±0.4	285.5±0.3	287.5±0.4	288.5±0.4
	FWHM	1.0±0.7	1.1±0.8	1.6±0.8	1.0±0.5	0.7±0.7
DLC with Si-C interlayer	Binding energy	283.6±0.2	284.8±0.1	285.5±0.5	287.6±0.4	-
	FWHM	0.6±0.4	1.2±0.3	1.6±0.3	1.1±0.04	-
Si-DLC with Si-C interlayer	Binding energy	284±0.9	284.9±0.9	285.8±0.9	287.8±0.6	-
	FWHM	1.0±0.3	1.2±0.1	1.5±0.5	1.6±0.5	-

4.5.3. Determination of sp^3/sp^2 ratio

The structure of DLC films is extremely complex as carbon atoms can form bonds with three different types of hybridizations. Therefore, the properties of DLC films are largely determined by the relative proportion of the sp^2 and sp^3 components in the films [155]. The sp^2 and sp^3 fraction in the films were assigned following the method of Zhao et al. [155] and Ahmed et al. [147]. The carbon double bond (C=C) appearing at ~284.8 eV was assigned to the sp^2 bonding configuration in the films. The sp^3 component was positioned at the lower binding energy ~284.1 eV for the C-Si bonds or at the higher binding energy around ~285.5 eV for the C-C and C-H bonds [147, 155, 181]. By evaluating the integrated areas at these bands, the corresponding sp^2 and sp^3 fractions were obtained from which the sp^3/sp^2 ratio was determined as shown in Table 4.6.

Table 4.6. sp^2 and sp^3 fractions and sp^3/sp^2 ratio for the coatings

Coating	sp^2	sp^3	sp^3/sp^2
DLC	0.57	0.43	0.75
Si-DLC	0.36	0.57	1.60
DLC with Si-C interlayer	0.41	0.43	1.05
Si-DLC with Si-C Interlayer	0.31	0.48	1.55

The results in Table 4.6 confirm that the films deposited were hydrogenated DLC films [17, 42, 173]. From the results in Table 4.6 it was observed that the Si-DLC and Si-DLC with Si-C interlayer had the highest sp^3 fraction and sp^3/sp^2 ratio. These results confirm the assertion in Section 4.3.1 that more areas for potential delamination were observed for the Si-DLC and Si-DLC film with Si-C interlayer due to more C-C sp^3 content. The results in Table 5.6 also confirm our previous discussions in Section 4.4.1 on Raman parameters as sp^3 content decreases with the inclusion of the Si-C interlayer. In the discussion on Disp(G) of the DLC with Si-C interlayer film (see Section 4.4.3) it was stated that this film had more sp^2 clustering. From Table 4.6, DLC with Si-C interlayer has more sp^2 fractions than Si-DLC and Si-DLC with Si-C interlayer film. The discussion on internal compressive stress in Section 4.4.5 is also validated as from Table 4.6 it can be seen that Si doping reduces the average size of the sp^2 bonded clusters and promotes the formation of sp^3 bonding in the Si-DLC film.

The estimation of the sp^3/sp^2 ratio is helpful in understanding the effects of Si incorporation and the Si-C interlayer on the mechanical properties and tribological behaviour of the films. Since butane gas was used as a precursor gas the films are hydrogenated. Si incorporation also results in hydrogenated films [155]. A low DC bias is unlikely to cause disruption of H from the film by sputtering [141]. The deposition technology used in this study combines PECVD and CFUBMSIP at low temperatures. This implies that hydrogen atoms are bonded to both carbon and silicon. Since C-H bonds are more stable than Si-H bonds, carbon atoms are expected to be more hydrogenated than silicon atoms [155]. This explains the higher sp^3 fractions observed for the Si-DLC films. However, all of the films (DLC and Si-DLC with and without Si-C interlayer) will be relatively soft due to the development of polymer like chains [141, 155].

4.6. Hydrophobicity studies and surface free energy calculation

4.6.1. Water contact angle

Figure 4.25 shows a water droplet on DLC film coated on nitrile rubber. From the contact angle (θ) it was determined that films deposited on nitrile rubber were hydrophobic. The water contact angle for all the films varied between 101° and 106° as shown in Figure 4.26.
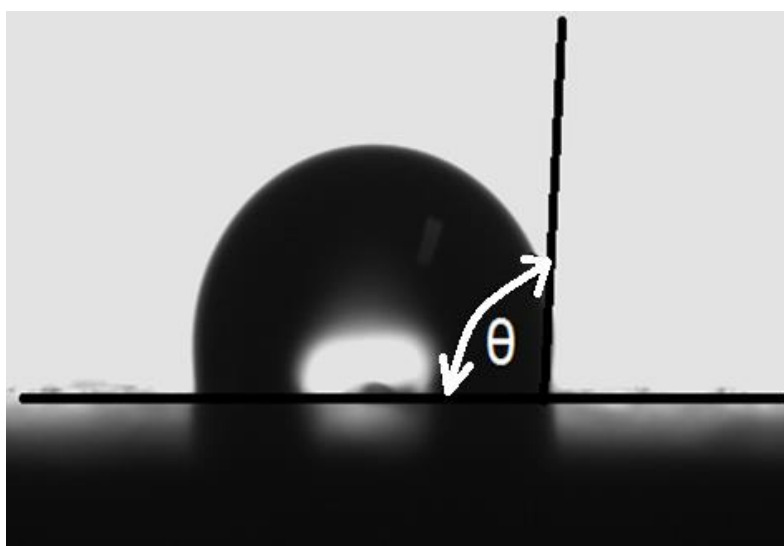
Figure 4.25. Water droplet on DLC film deposited on nitrile rubber showing water contact angle
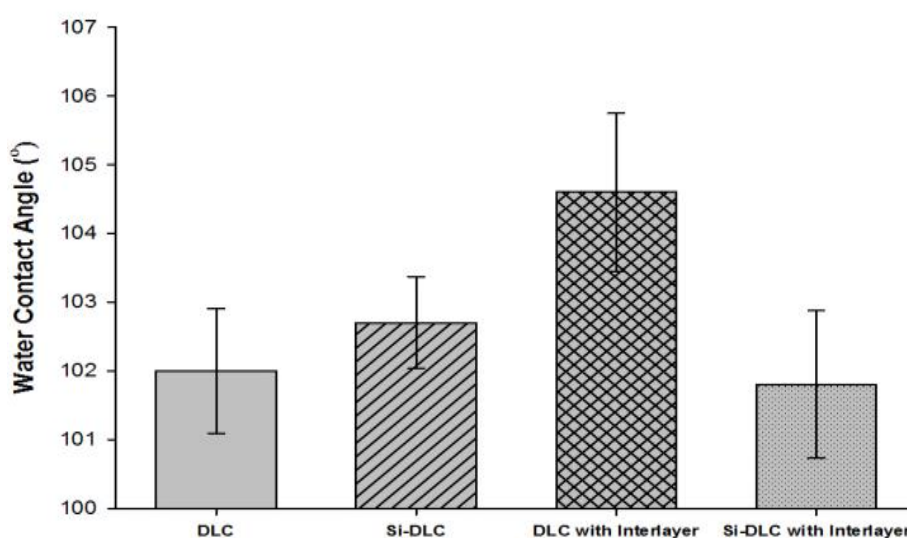
Figure 4.26. Water contact angle for DLC and Si-DLC films with and without Si-C interlayer

Hydrophobic surfaces were reported for DLC films deposited on rubber substrates [18-20]. An increase in the hydrophobic properties of DLC coated elastomers was explained by the presence of a mixture of sp^2 and sp^3 hybridized carbon bonds in the DLC coatings, which is also related to a lower reactivity of the DLC coated surface [103]. A hydrophobic surface implies that the water repellent property of the films was enhanced [19]. For various nitrile rubber substrates, Martinez et al. reported contact angles less than 95° [18]. This implies that all of the coatings applied onto nitrile rubber in this study have a greater water repellent property. This is particularly important when the potential application of the films is taken into consideration. For DLC and Si-DLC films deposited onto nitrile rubber piston seals the ability of the film to repel the water medium where these seals operate is essential to enhanced functionality of the seals.

The increase in the roughness of hydrophobic surfaces has been reported as being responsible for drastic decreasing of water contact angle [18]. As shown in Figure 4.8 and discussed in Section 4.3.4, the surface pattern of the coatings is characterized by a network of micro-cracks, with varying patch sizes. The average surface roughness for DLC coatings and Si-DLC coatings, with and without the inclusion of the Si-C interlayer were equivalent with measured values ranging from 1.5 μm to 2.2 μm. These results indicated an increase in the surface roughness of the coatings when compared to an uncoated substrate which had a measured average roughness of about 1 μm. An increment in surface roughness was also observed in the study by Martinez et al. [18]. However, since the inclusion of the Si-C interlayer did not have a significant contribution on surface roughness minimal effects on the contact angle measurements as a result of the surface roughness should be expected.

Dependence of the water contact angle (CA) and hence hydrophobicity on the I_D/I_G ratios of the films as obtained from the Raman studies is depicted in Figure 4.27. It was observed that the inclusion of the Si-C in the DLC coatings resulted in an increase in CA for DLC film with Si-C interlayer when compared to DLC film. This result implies that the DLC with Si-C interlayer has a greater water repellent potential compared to the other films which may affect its tribological behaviour as will be discussed later (see Section 4.11.1). As was discussed in the Raman studies and XPS studies the DLC film with Si-C interlayer has more sp^2 clustering which results in decreases in bond length and bond angle disorder.
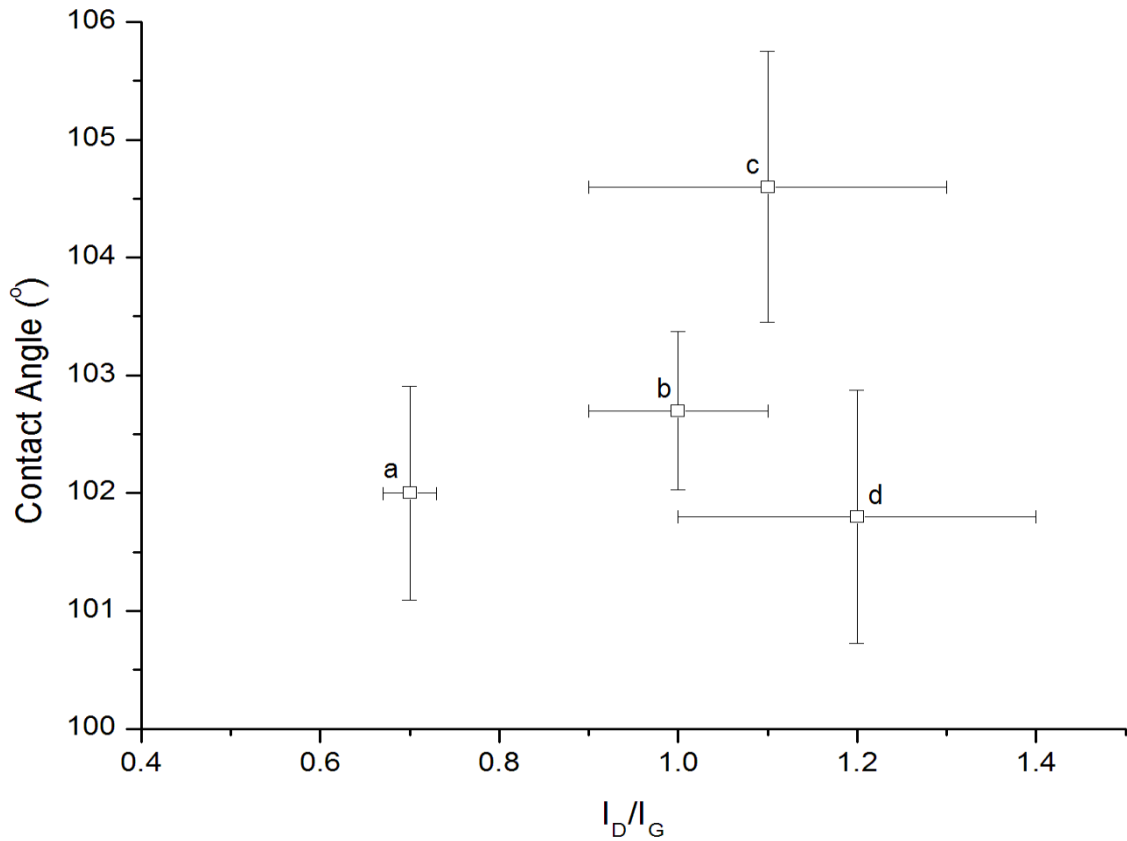
Figure 4.27. Relation between contact angle and intensity ratio for DLC – a, Si-DLC – b; DLC with Si-C Interlayer – c; and Si-DLC with Si-C Interlayer – d

4.6.2. Surface free energy

Table 4.7 shows the surface free energy (mJ/m2) of the studied samples determined by the Owens-Wendt-Rabel and Keable method. The inclusion of the Si-C interlayer increases the surface free energy of the films. A higher surface free energy is observed for Si-DLC with the Si-C interlayer (with lower water CA) compared to a lower surface energy for DLC with Si-C interlayer (with higher water CA). For Si-DLC with Si-C interlayer the sp^2 fraction is much lower than for DLC with Si-C interlayer. However, the inclusion of the Si-C interlayer suppressed the polar component of the surface free energy. This is contrary to the observations by Martinez et al. [18]. However, in the modification of elastomers by metal based layers the reduction in surface energy was attributed to the reduction in the polar part of the surface energy [60]. The higher atomic percentages of silicon and lower atomic percentages of oxygen observed for films with Si-C interlayers in Table 5.1 may be responsible for this result.

Table 4.7. Surface free energy (mJ/m^2) of the studied samples determined by the Owens-Wendt-Rabel and Keable method. The surface free energy is compared to results for DLC on NBR 7201, NBR 9003 and NBR 8002 from the work of Martinez et al. [18].

Sample	Surface free energy	Dispersive component	Polar component
DLC	30.3	30.0	0.3
Si-DLC	31.6	31.3	0.3
DLC with Si-C interlayer	33.4	33.4	0.0
Si-DLC with Si-C interlayer	35.6	35.6	0.0
DLC on NBR 7201	42.8	42.4	0.4
DLC on NBR 9003	34.1	33.6	0.5
DLC on NBR 8002	33.3	32.6	0.7

4.7. Adhesion

The adhesion levels for the DLC and Si-DLC films deposited on nitrile rubber were determined following the X-cut Peel Test method described in Section 3.6.3.1. Figure 4.28 shows optical microscopy images of X- cut locations after peel tests for the films. Table 3.4 was used to attribute adhesion levels for the DLC and Si-DLC films.
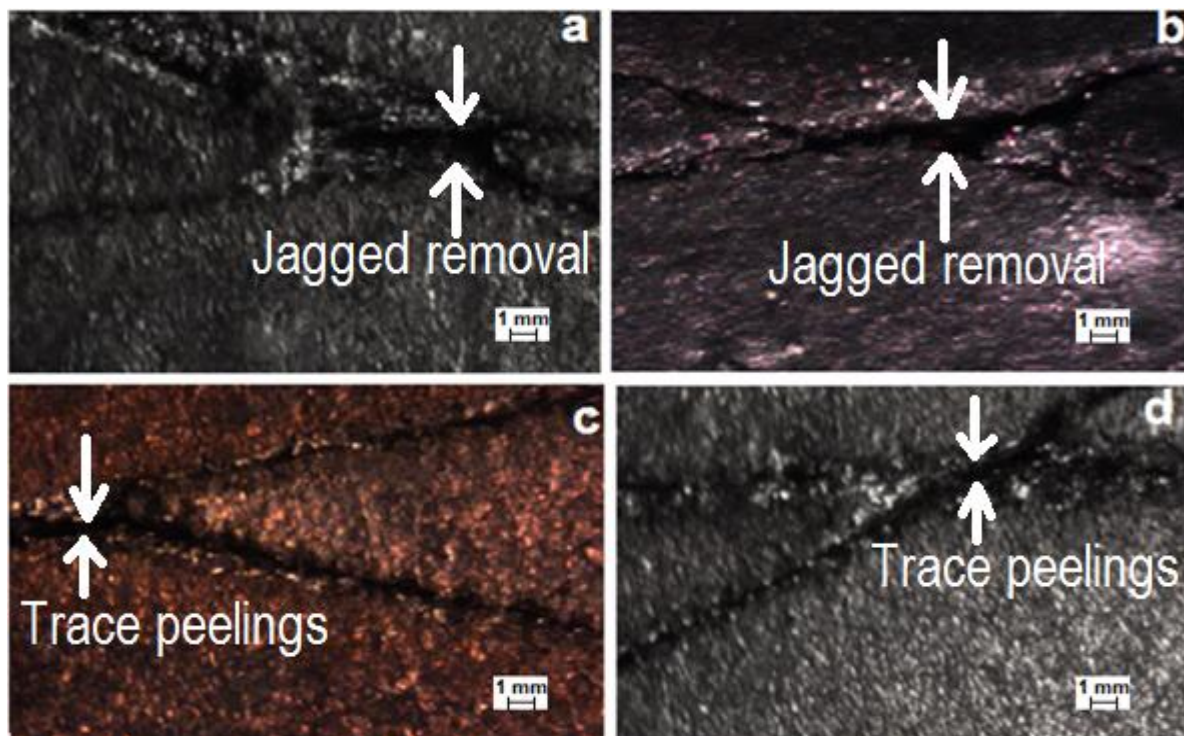
Figure 4.28. Optical Microscopy images of X-cut locations after peel tests for Si-DLC (a), DLC (b), DLC with Si-C interlayer (c) and Si-DLC with Si-C interlayer (d)

From Figure 4.28 it was observed that the DLC and Si-DLC films with Si-C interlayer had higher adhesion levels than the DLC and Si-DLC films without Si-C interlayer. For the DLC and Si-DLC films, jagged removal along incisions were observed up to 1.6 mm on either side of the X-cut resulting in an adhesion level of 3A. An adhesion level of 4A was determined for the films with Si-C interlayer due to trace peelings occurring along incisions with little peeling observed at the X-cut [105].

The relatively good adhesion levels for all of the films may be attributed to the deposition technology used in this study. The combination of CFUBMSIP and PECVD at low DC substrate bias values implies that the H in the films is not disrupted resulting in films consisting of relatively soft hydrocarbon or polymer-like chains. The presence of hydrogen is usually associated with the development of polymer-like chains [141, 155]. This phenomenon arises from the carbon atoms in the films being able to form three different types of hybridizations which affect the film properties based on the relative proportion of sp^2 and sp^3 contributions [155]. This development of polymer-like chains during film deposition is advantageous as elastomers, including nitrile rubbers from which handpump piston seals are made, are comprised of flexible polymer chains explaining the good adhesion ratings for these films [170].

The CFUBMSIP system enables plasma to be present in the deposition chamber between the target and the nitrile rubber substrate allowing energetic particles to bombard the substrate and enhance ionization of vapour species at even low energies. Particle bombardment of growing film surfaces causes densification of material and modified film properties [168]. A reduction of residual stresses can result from energetic ion bombardment of DLC films which improves on the film adhesion [182]. From the Raman spectroscopy results discussed in Section 4.4.1 it was determined that the inclusion of Si-C interlayer onto the DLC and Si-DLC films deposited on nitrile rubber substrates resulted in sp^2 clusters becoming larger and less strained, leading to decreased bond length and bond angle disorder. This results in a decrease in the magnitude of compressive residual stresses, and hence improving film adhesion [182]. A reduction in the magnitude of compressive residual stresses was shown and discussed in Section 4.4.5 of this thesis.

4.8. Flexibility

Figure 4.29 shows digital microscopy images of the DLC and Si-DLC films deposited on nitrile rubber at the location of flexibility testing. The surface morphology of DLC and Si-DLC films with and without Si-C interlayer is characterised by a dendritic crack-like structure as shown in Figure 4.29. A discussion on the surface morphology was given in Section 4.3.1. However, it is worth mentioning that the presence of these cracks has been attributed to the promotion of film flexibility without interfacial delamination [23, 24].
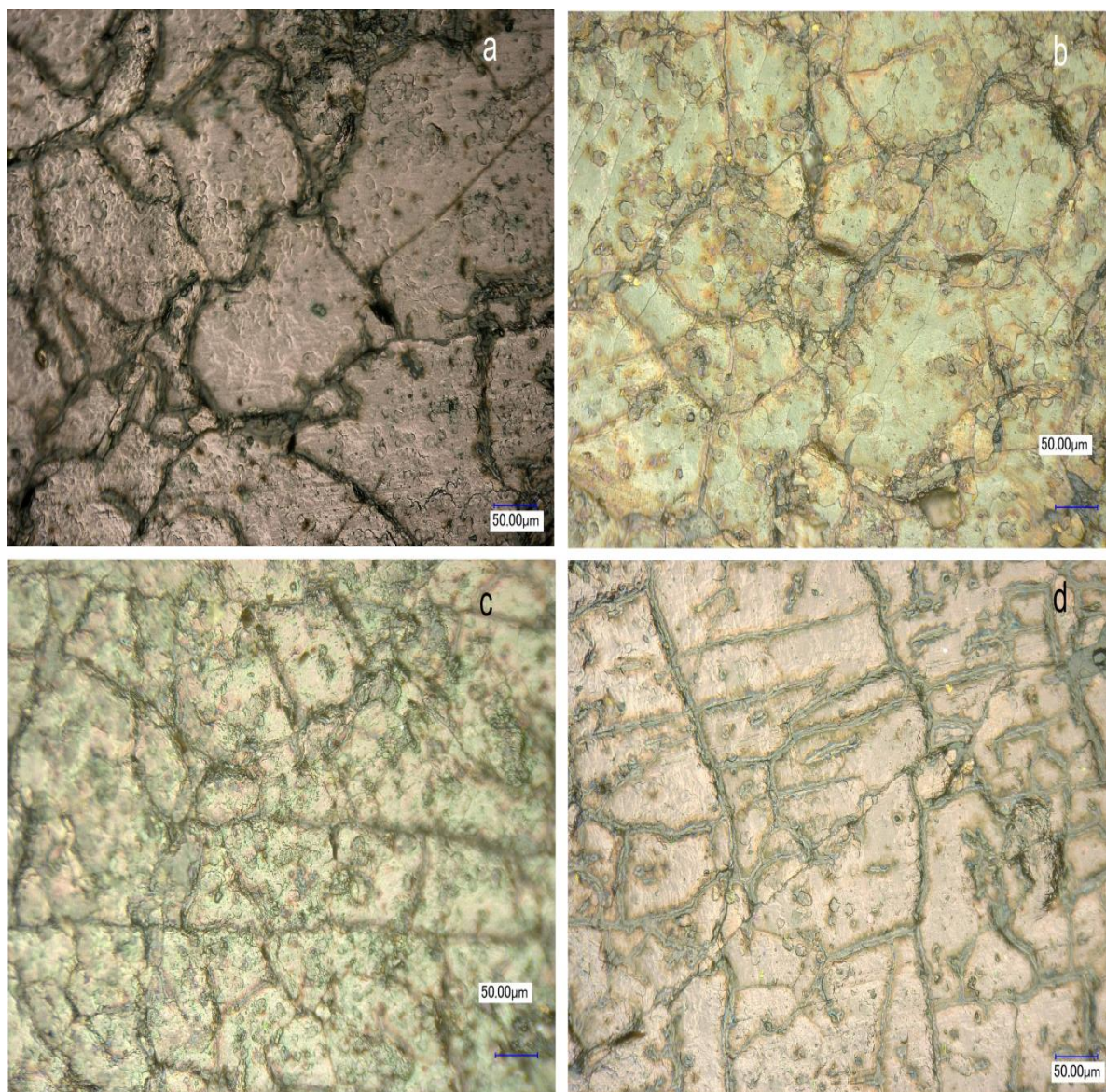
Figure 4.29. Digital microscopy images: (a) DLC; (b) Si-DLC; (c) DLC with Si-C interlayer; and, (d) Si-DLC with Si-C interlayer, deposited on nitrile rubber before flexibility testing

Figure 4.30 shows the film flexibility results for the films on the exterior as explained in Figure 3.18 at the same location as shown in Figure 4.29, but after performing the flexibility tests. For all of the films lateral cracks were seen to propagate across the patch crack boundary creating an island textured structure. However, some lateral cracks were initially present in the Si-DLC film before flexibility testing (see the top left corner of Figure 4.29b). This island textured structure allows the flexibility of the coating to follow the stretch of the rubber [20]. The generation of these lateral cracks (high crack density) is the only mechanism for the film to release stress and is an indicator of good adhesion between the film and the substrate [24, 110]. For Si-DLC films (Figure 4.30b) the lateral cracks open and de-bonding between the Si-DLC film and the nitrile rubber substrate occurs which implies that for Si-DLC films the adhesion rating is lower due to stress relaxation of the nitrile rubber substrate. This is due to more C-C sp^3 bonds in the Si-DLC film as discussed in the XPS studies in Section 4.5.3. This result is in-line with our previous discussion internal compressive stress (see Section 4.4.5) in the films and the film adhesion (see Section 4.7) for the results of the Si-DLC films deposited on nitrile rubber.
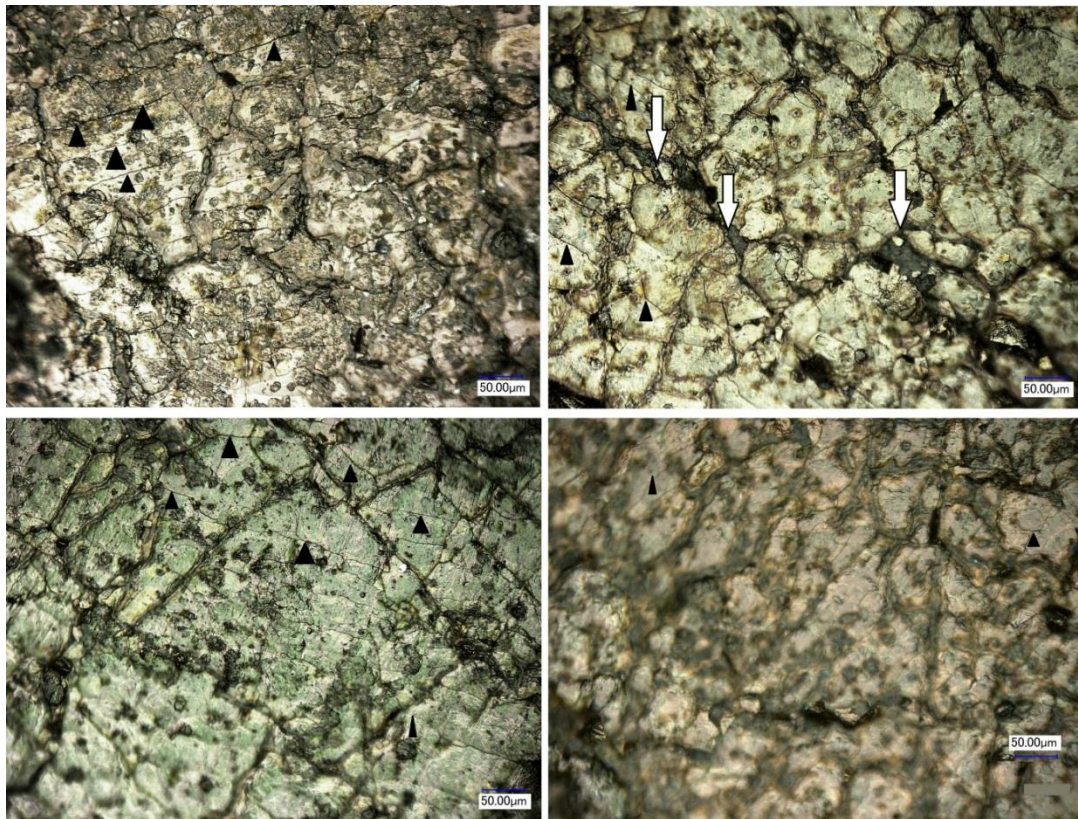
Figure 4.30. Flexibility testing results: (a) DLC; (b) Si-DLC; (c) DLC with Si-C interlayer; and, (d) Si-DLC with Si-C interlayer, deposited on nitrile rubber with the film on the exterior. Black solid filled triangles indicate lateral cracking. White solid filled arrows indicate de-bonding.

The results for film flexibility for the film on the interior are shown in Figure 4.31. The film on the interior would be under much higher stress at the point of observation than for the film on the exterior when compared to before flexibility testing at the same location as shown in Figure 4.29 for each respective film. Lateral crack development is evident for DLC film with and without Si-C interlayer. These lateral cracks promoted the film flexibility of these films [21, 110]. De-bonding was observed in the Si-DLC film. Some de-bonding was also observed in the Si-DLC film with the Si-C interlayer. This de-bonding is attributed to C-C sp^3 hybridizations in the Si-DLC film which reduces on the adhesive property of the film and increases on the film internal stress [182].
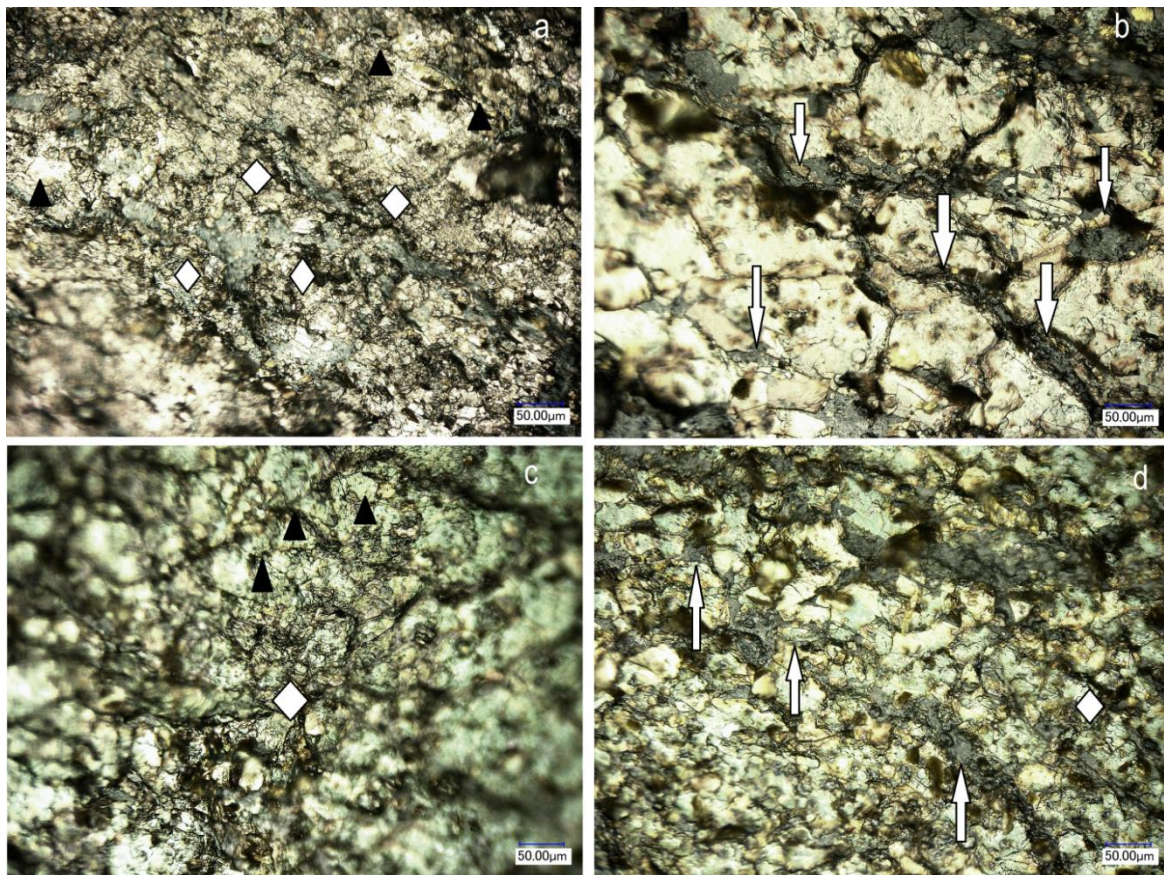
Figure 4.31. Flexibility testing results: (a) DLC; (b) Si-DLC; (c) DLC with Si-C interlayer; and, (d) Si-DLC films with Si-C interlayer, deposited on nitrile rubber for film on the interior. Black solid filled triangles indicate lateral cracking. White filled arrows indicate de-bonding. White filled diamond shapes indicate micro-cracking.

The improved flexibility of the DLC film, DLC with Si-C interlayer film and, to a smaller extent, the Si-DLC with Si-C interlayer film, was due to the generation and propagation of

131

micro- and nano- cracks as the film was continuously loaded and unloaded. This can be explained by the more C-H bonds and carbon sp^2 hybridization in DLC and DLC with Si-C interlayer film as discussed in Section 4.5.3 on XPS studies. The increase in the number of cracks (higher crack density) allowed the films to relax the stress applied onto them [21, 24, 110]. This results implies that better tribological and coated piston seal performance should be expected for the nitrile rubber substrate and handpump piston seal coated with DLC with Si-C interlayer.

4.9. Composite Micro-hardness

Based on the geometry of the Vickers indenter, theoretical contact depth was calculated from the size of the diagonals in order to determine the relative influence of the substrate on the micro-hardness measurements. For indentations in coated systems these measurements reflect the properties of the coating only if the depth of indentation is less than one-tenth of the coating thickness [183]. Table 4.8 provides a summary of Vickers micro-hardness results for applied indentation loads of 147.1 mN, 490.3 mN and 981 mN, with calculated theoretical depth for DLC and Si-DLC films deposited on Si wafer.

Table 4.8. Summary of Vickers micro-hardness (GPa) results for applied indentation loads of 147.1 mN, 490.3 mN, and 981 mN, with theoretical contact depth

Coating	Applied Force (mN)	d (µm)	Hv (average ± s.d)
DLC	147.1	0.6	15.5 ± 0.8
	490.3	1.3	10.5 ± 0.7
	981	1.9	9.4 ± 0.3
Si-DLC	147.1	0.7	11.1 ± 0.7
	490.3	1.4	9.7 ± 0.7
	981	2.0	8.6 ± 0.3
DLC with Si-C interlayer	147.1	0.8	9.1 ± 0.7
	490.3	1.4	9.6 ± 0.8
	981	2.1	8.4 ± 0.3
Si-DLC with Si-C interlayer	147.1	0.7	12.1 ± 1.2
	490.3	1.3	10.2 ± 0.3
	981	1.9	9.6 ± 0.4

For applied loads of 147.1 mN, the theoretical depth of the indentations did not exceed the film thickness for DLC and Si-DLC films without Si-C interlayer. However, as the depth was greater than one-tenth of the film thickness, the micro-hardness measurements were a function of both the coating and the substrate, thus, resulting in a composite micro-hardness

132

measurement. At higher applied indentation loads of 490.3 mN and 981 mN, there is no statistical significance of the micro-hardness measurements. This is due to the fact that the penetration depth at these loads was much greater than the film thicknesses.

In this study composite hardness results for applied load of 147.1 were considered from composite hardness results. From Table 4.8 it was observed that the inclusion of the Si-C interlayer had distinct impacts on the hardness of the DLC and Si-DLC films. For the DLC film with Si-C interlayer the hardness was 9.1 GPa compared to 15.5 GPa for the DLC film only. This reduction in hardness is attributed to an increase in sp^2 clustering in the DLC film with Si-C interlayer which relieves the compressive stresses in the films. For the Si-DLC film with Si-C interlayer an average micro-hardness value of 12.1 GPa compared to 11.1 GPa for Si-DLC films was obtained.

Figure 4.32 shows the composite hardness of the films vs. the intensity ratio, I_D/I_G. A reduction in the film hardness corresponded to an increase in the intensity ratio for DLC, Si-DLC and DLC with Si-C interlayer films. This has earlier been explained qualitatively as resulting from an increase in sp^2 content and a reduction in sp^3 content [42, 172]. However, for Si-DLC films contributions from sp^3 sites due to vibrations of C-C sp^3 bonds may be significant.
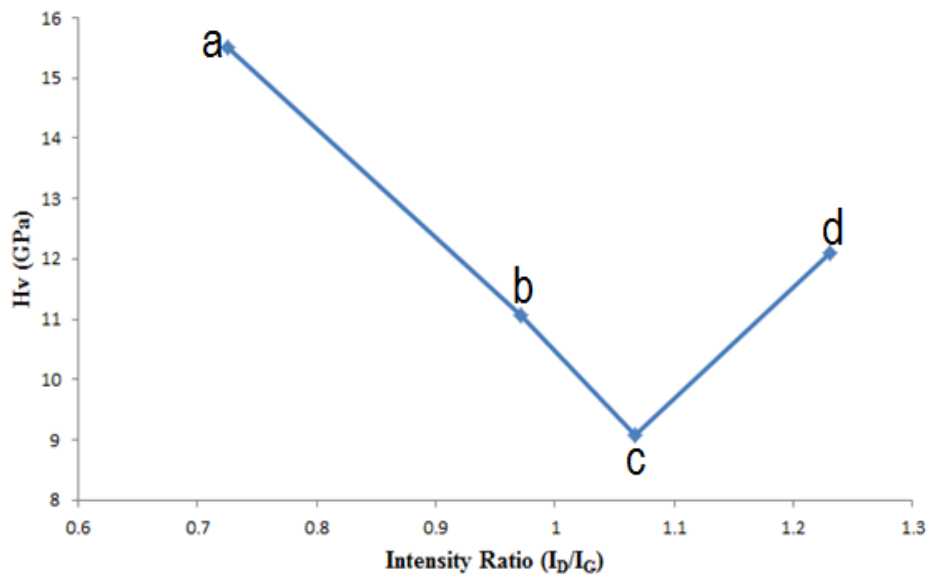
Figure 4.32. The micro-hardness (at 147.1 mN indentation load) of DLC (a), Si-DLC (b), DLC with Si-C interlayer (c) and Si-DLC with Si-C interlayer (d) films vs. intensity ratio, I_D/I_G

133

4.10. Nano-mechanical properties

For indentations in coated systems these measurements reflect the properties of the coating only if the depth of indentation is less than one-tenth of the coating thickness [183]. As such the nano-mechanical properties for DLC, Si-DLC and DLC with Si-C interlayer film were determined. Figure 4.33 shows the load versus the penetration depth for the films used in this study. All of the results were obtained using the Oliver and Pharr method described by eq. (3.9) to eq. (3.15) with a sample Poisson's ratio of 0.3 [17, 160].
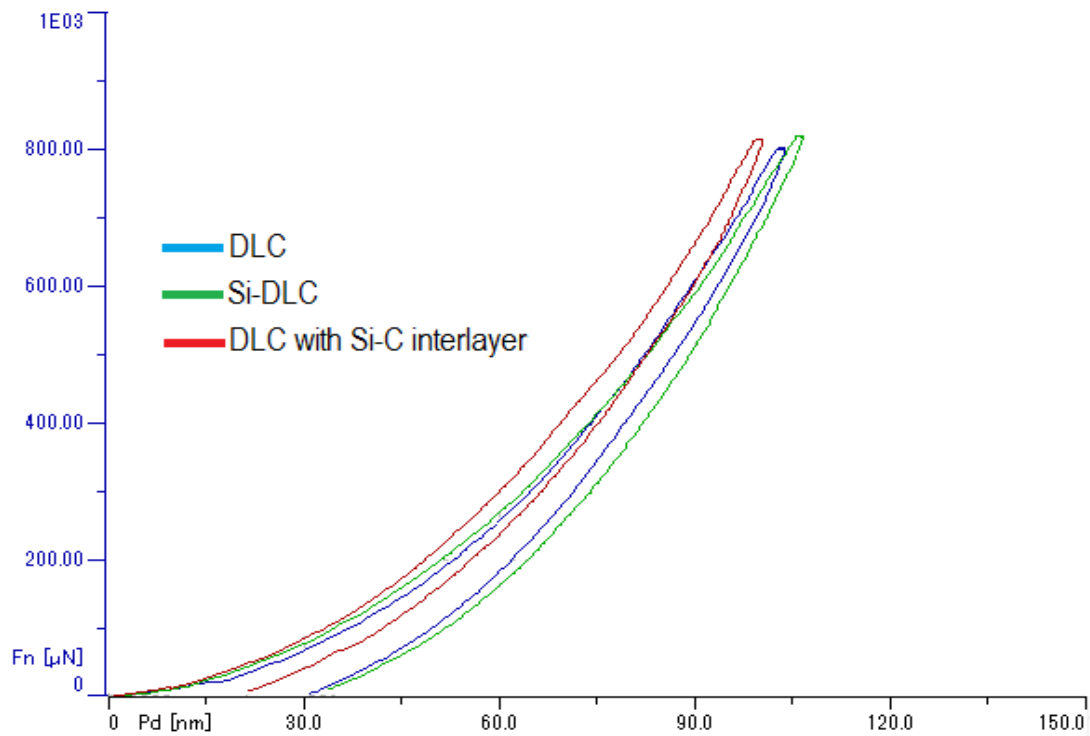
Figure 4.33. Load vs. penetration depth for DLC, Si-DLC and DLC with Si-C interlayer

The corresponding nano-indentation hardness and elastic modulus results are shown in Figure 4.34. The results show that for all of the films the hardness and elastic modulus results were of the same order with hardness around 3.6 GPa and elastic modulus around 35 GPa. There was no significant difference in indentation creep for all of the films.

An increase in the sp^3/sp^2 ratio as shown in Table 4.6 is typically associated with improved mechanical properties of amorphous carbons [30, 155]. However in this study a combination of PECVD and CFUBMSIP deposition technology used is responsible for the low hardness and elastic modulus values for the films.
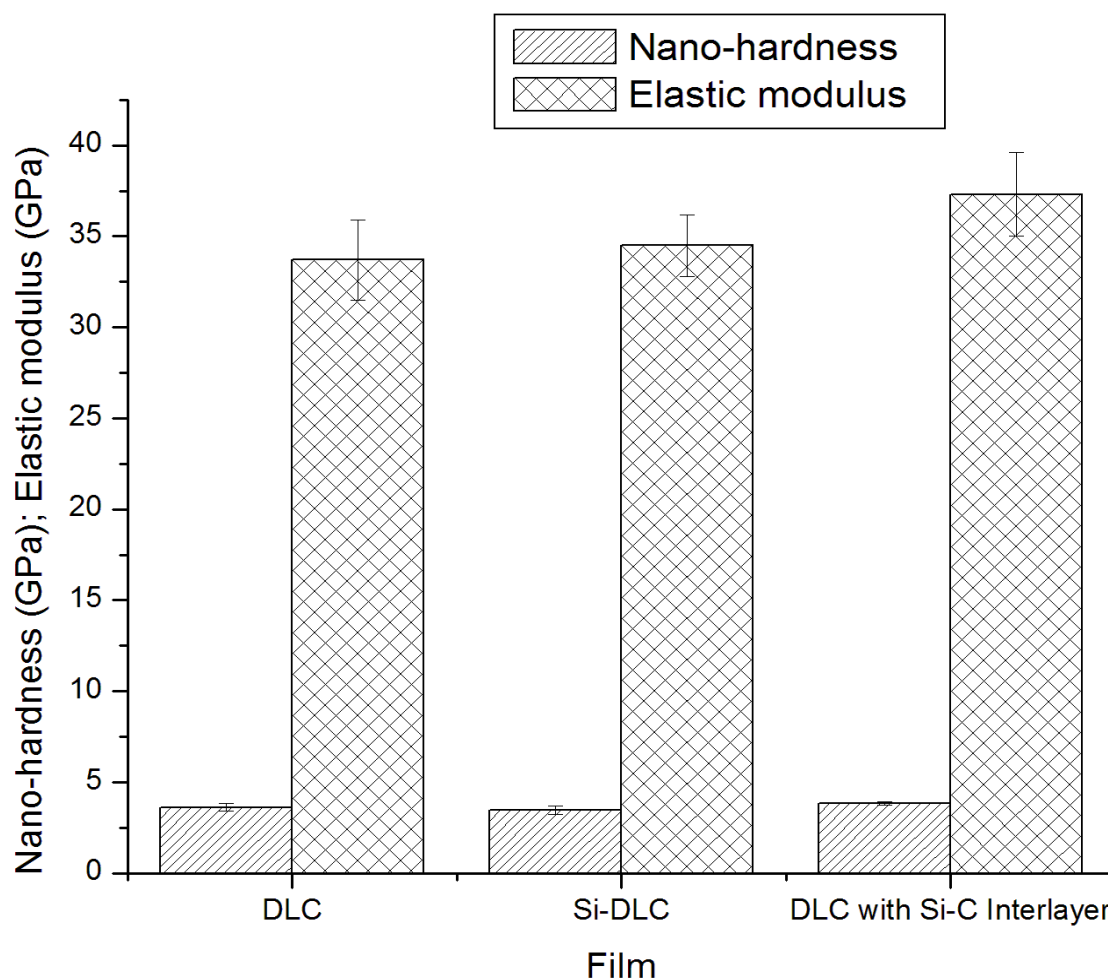
Figure 4.34. Comparative analysis of the indentation hardness and Elastic modulus for the films

For carbon-based coatings the mechanical properties are very dependent on the chemical binding of the carbon (sp^2 or sp^3 hybridization and H content) [42, 91, 95, 173]. C-C sp^3 type bonding leads to a three-dimensional network of high stiffness and hardness, while bonded H atoms loosen the network [170]. The low levels of elastic modulus as well as hardness strongly refer to hydrogen containing a-C:H film compositions [184]. Such films have been shown to have low residual stress and polymer like chains which enhances the adhesion and flexibility of these films onto nitrile rubber substrates and handpump piston seals.

During the film deposition process the ionization of the hydrocarbon species lead to the dissociation of highly reactive C_xH_y fragments. By comparing the binding energies at 298K of C-H (416 kJ mol^{-1}) to C-C (345 kJ mol^{-1}), C=C (615 kJ mol^{-1}) and C≡C (811 kJ mol^{-1}) the

135

tendencies for dissociation can be deduced. For acetylene (C_2H_2), consisting of C≡C and C-H bonds, the ionization by losing hydrogen atoms is easier than by breaking the triple bonds [185]. Thus structures with mixed double and single bonds as well as with cross-linking between chains can form more easily in the growing films resulting in higher hardness values. For butane (C_4H_{10}) hydrocarbon precursor such double bonds are missing and more difficult to form in the growing film resulting in lower hardness values for films [170].

Films prepared using a PECVD technique at low temperatures are likely to be saturated with hydrogen atoms [155]. The CFUBMSIP system at low substrate bias (-30V) is highly unlikely to remove H from the film by sputtering. This results in films probably consisting of relatively short hydrocarbon and polymer-like chains [141, 170, 184]. The deposition technology used in this study further implies that hydrogen atoms are likely to be bonded not only to carbon, but also to silicon in the case for Si-DLC films. Since C-H bonds are more stable than Si-H (298.74 kJ mol^{-1}), carbon atoms are expected to be more hydrogenated than silicon [155]. Upon silicon incorporation these polymeric structures could develop and weaken the structural and nano-mechanical properties of the films explaining the nano-mechanical values reported in this study [17, 155].

4.11. Tribological analysis

4.11.1. Coefficient of friction

The results of the frictional behaviour for tribo-tests for normal load of 1 N and 5 N under both dry and wet sliding using stainless steel and WC-Co counterparts are shown in Figure 4.35, Figure 4.36, Figure 4.37 and Figure 4.38. For all of the results the coefficient of friction is lower than the value reported by Nakahigashi et al. [19], of approximately 0.7 for tribo-tests conducted at a normal load of 0.1 N under dry sliding as shown in Table 2.1. Average coefficients of friction for the films sliding against WC-Co counterpart, have been compared with average coefficients of friction for the same films in this study sliding against stainless steel counterpart in Table 4.9. This study presents for the first time in this field the results of wet sliding tribo-tests for DLC films deposited on rubber substrates. Such an analysis has never been discussed before.
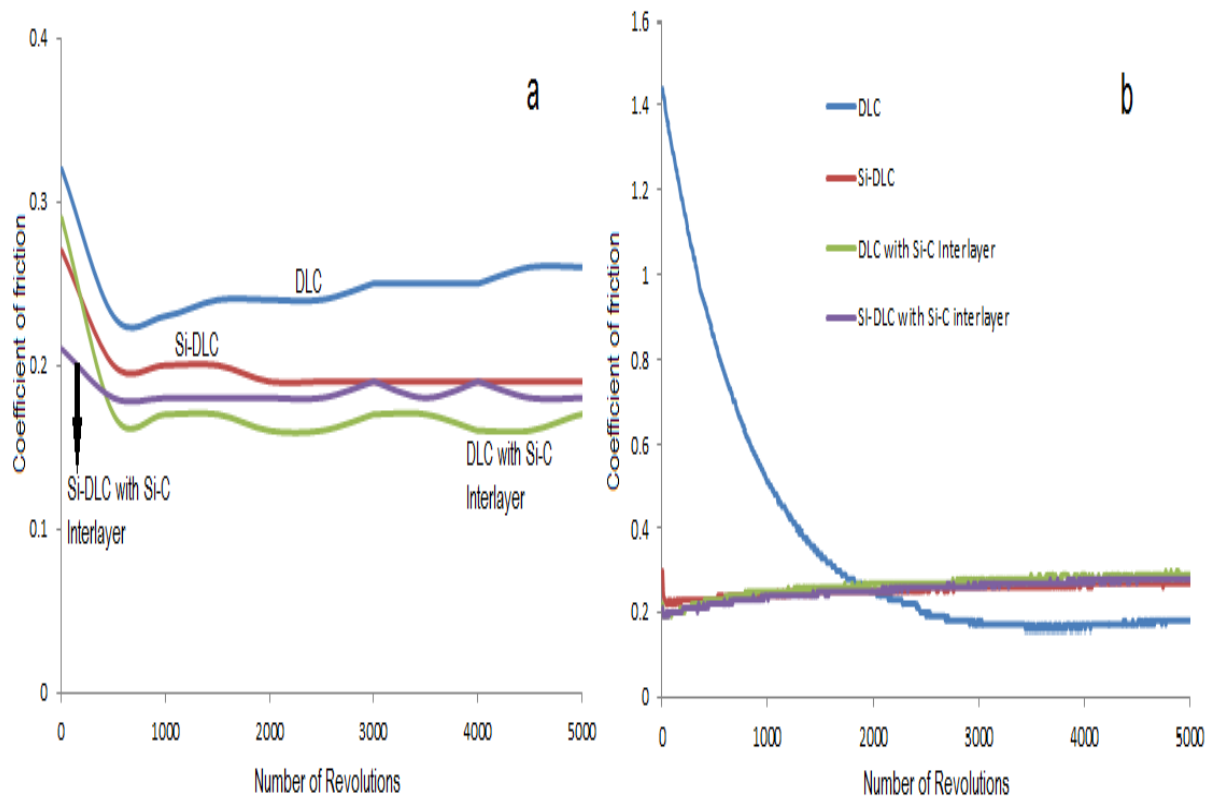
Figure 4.35. Coefficient of friction vs. number of revolutions for films deposited on nitrile rubber under normal load of 1N with stainless steel counterpart: (a) dry sliding; and, (b) wet sliding.
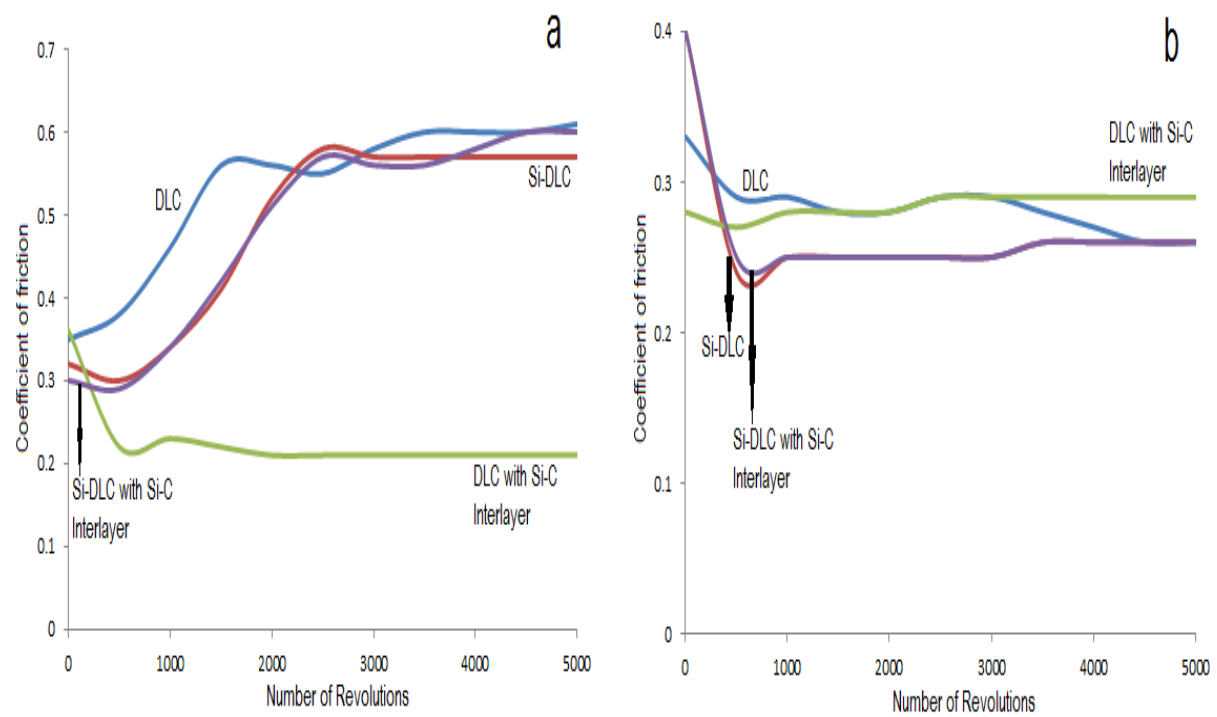
Figure 4.36. Coefficient of friction vs. number of revolutions for films deposited on nitrile rubber under normal load of 5N with stainless steel counterpart: (a) dry sliding; and, (b) wet sliding.

137
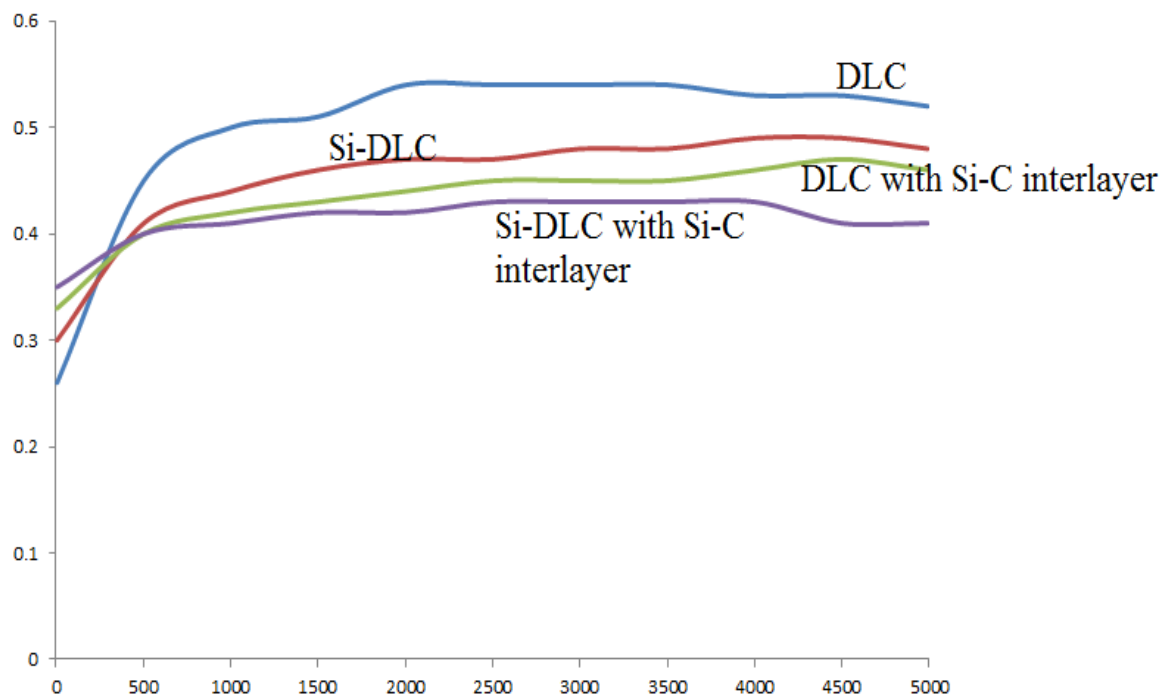
Figure 4.37. Coefficient of friction vs. number of revolutions for films deposited on nitrile rubber under normal load of 1 N with WC-Co counterpart for wet sliding
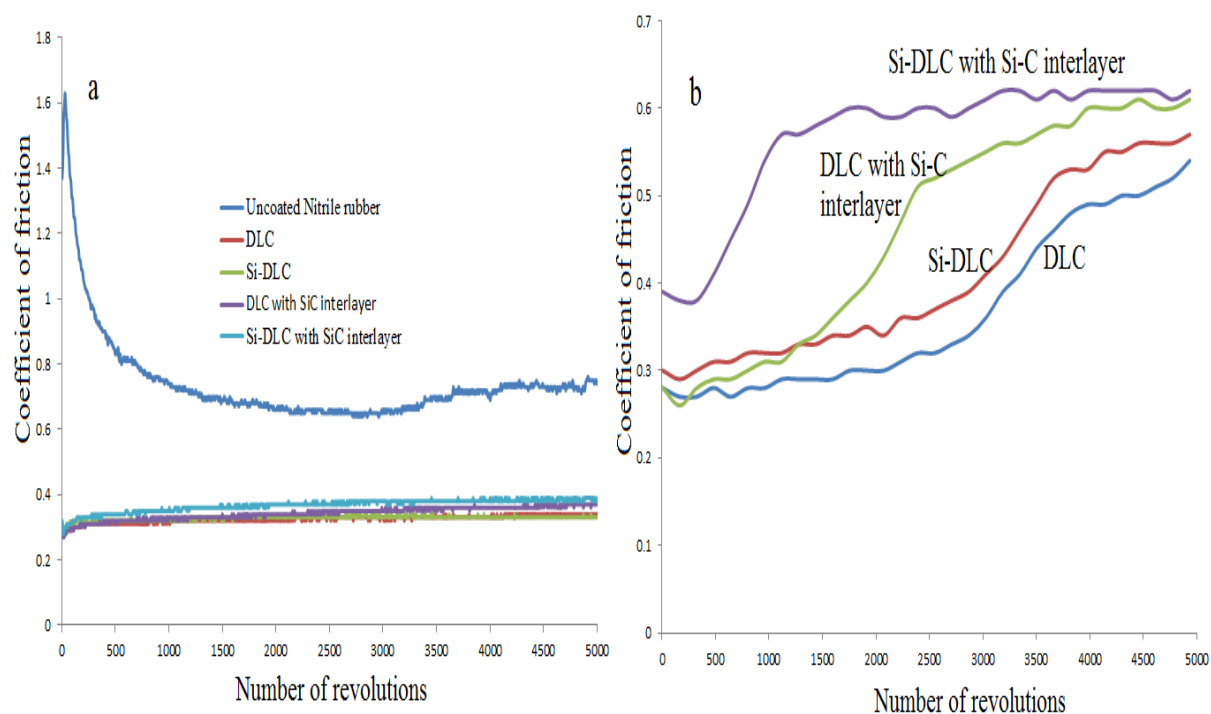
Figure 4.38. Coefficient of friction vs. number of revolutions for films deposited on nitrile rubber under normal load of 1 N (a) and 5 N (b) under dry sliding with WC-Co counterpart

138

Table 4.9. Average coefficients of friction for the films at normal load of 1 N for dry and wet sliding and normal load of 5 N for dry sliding. The total number of revolutions was 5000 revolutions

| | Stainless steel counterpart | | | | WC-Co counterpart | | |
| | Dry | | Wet | | Dry | | Wet |
	1N	5N	1N	5N	1N	5N	1N
DLC	0.25±0.02	0.53±0.09	0.29±0.22	0.28±0.02	0.34±0.01	0.37±0.09	0.51±0.06
Si-DLC	0.20±0.02	0.48±0.12	0.27±0.02	0.27±0.04	0.34±0.01	0.41±0.10	0.46±0.04
DLC with Si-C interlayer	0.18±0.03	0.23±0.04	0.28±0.03	0.28±0.01	0.36±0.03	0.46±0.12	0.44±0.03
Si-DLC with Si-C interlayer	0.19±0.01	0.48±0.12	0.27±0.02	0.27±0.04	0.38±0.02	0.57±0.08	0.41±0.02

From the Raman studies it was determined that the G peak position for all the films was centred approximately around 1580 cm^{-1}. This is very close to the graphite density of states implying that size of sp^2 bonded graphitic clusters is increased, hence the generally low coefficients of friction.

The results of frictional behaviour using stainless steel counterparts are shown in Figure 4.35 and Figure 4.36. From Figure 4.35a it was observed that films that had lower coefficients of friction also had higher Si (at. %) incorporation (see Table 4.1). This result is consistent with previous discussions above on Raman analysis and XPS analysis. Si doping in the films was associated with increases in sp^3 content in the films and a lowering in the sp^2 fractions (see Table 4.6). The therefore enhances the resistance of the film to penetration by the pin resulting in lower friction coefficients. In addition the increased sp^2 clustering for DLC with Si-C interlayer compared to the Si-DLC and Si-DLC with Si-C interlayer film is responsible for its better performance compared to the rest of the films. The coefficient of friction results under wet sliding shown in Figure 4.35b can be explained by a lowering of surface energy of the films due to water absorption. The films were already shown to have low surface energy in hydrophobicity studies discussed in Section 4.6 of this thesis. The low surface energy passivizes rapidly the dangling bonds on the wear scars, much in the same way as an increase in relative humidity reduces wear rate [186]. Generally at 1 N normal load for tribo-tests with stainless steel counterparts lower average values for coefficient of friction were observed for tribo-tests in dry conditions than in wet conditions irrespective of the counterpart material used. Several works have also reported frictional increase in humid conditions as a result of an increase of dipole-like interactions between the hydrogen terminated DLC surface and the water molecules [187-189].

The frictional performance under a normal load of 5 N and dry sliding was expected to result in higher coefficients of friction according to Archard's wear law [119]. This was indeed the case for most of the films studied, except DLC with Si-C interlayer as shown in Figure 4.36a. From Figure 4.34 it can be noted that the DLC with Si-C interlayer had a slightly higher nano-mechanical hardness which could be interpreted to mean better mechanical behaviour. But the difference in nano-mechanical hardness for DLC with Si-C interlayer is very small and within the error margin compared to the other films. Therefore this reasoning was discredited. The excellent performance of DLC with Si-C interlayer was therefore attributed to the higher sp^2 clustering in these films which allowed increased bonding with graphitic clusters. The frictional performance under normal load of 5 N and wet sliding suggests that when high loads are applied doping the film with Si had an effect of reducing frictional coefficients due to the formation of hydroxyl groups ($SiO_x(OH)_y$) [25].

In this study frictional performance was also determined using WC-Co counterpart materials. The results of this study are shown in Figure 4.37 and Figure 4.38. WC-Co ball was used as counterpart material because it has a higher hardness value compared to stainless steel [190, 191]. The different hardness values of the stainless steel and WC-Co counterpart materials were expected to influence the frictional characteristics during the tribo-testing. The hardness of the counterpart material affects the transferability of amorphous carbon onto the film as sliding progresses [192]. From Figure 4.37 it was observed that the trend of the frictional performance under normal load of 1 N was similar to that shown in Figure 4.35a at normal load of 1 N. The films that had lower coefficients of friction also had higher Si (at. %) incorporation (see Table 4.1). As such a similar discussion ensues. An increase in Si content in DLC reduces the coefficient of friction due to acceleration of tribo-chemical reactions with water to form hydroxyl groups ($SiO_x(OH)_y$) [25]. However, the higher values of the hardness of the WC-Co ball result in higher values of coefficient of friction due to reduced transferability of amorphous carbon onto the film [192].

Figure 4.38 shows the frictional performance of the films under dry sliding under normal loads of 1 N and 5 N with WC-Co counterpart. From Figure 4.38a it was observed that all of the coatings showed excellent tribological results with an over 50% reduction in the coefficient of friction compared to uncoated nitrile rubber. When low loads of 1 N were applied the frictional performance was similar to the results shown for stainless steel counterparts in Figure 4.35a. This may indicate that when low loads are applied the

differences in hardness of the counterpart material have little effect on the coefficient of friction results. From Figure 4.38b it was observed that all of the samples showed a friction increase between 0.25 – 0.4 at 200 to 400 revolutions to between 0.45 and 0.6 at 4,000 to 5,000 revolutions indicating a clear transition region. This transition region was also observed for normal load of 5 N under dry sliding with stainless steel counterparts, except for the DLC film with Si-C interlayer.

An analysis was carried out to study the slope of the increase of the coefficient of friction as a function of number of revolutions (first derivative) for tribo-tests under normal load of 5 N with WC-Co counterpart for dry sliding as shown in Figure 4.39. The frictional behaviour from initial friction and the friction performance vs. number of revolutions was explained by the differences in composite micro-hardness between the coatings as a result of the inclusion of the Si-C interlayer.
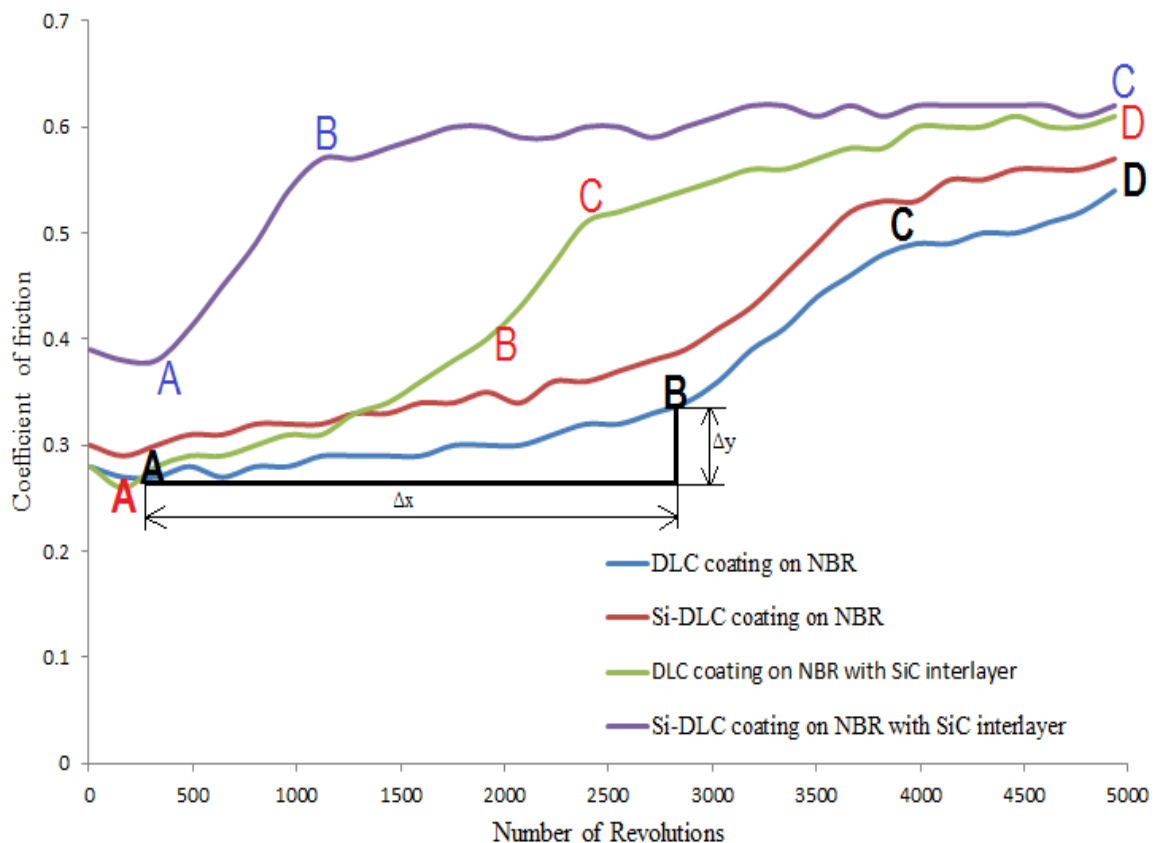
Figure 4.39. Coefficient of friction vs. number of revolutions for DLC and Si-DLC with and without Si-C interlayer. Points A, B, C and D are indicated for estimation of slopes of the increase of the coefficient of friction

The frictional behaviour over the testing duration of 5,000 revolutions was segmented into different regions for each coating: region AB, region BC and region CD. For each of these regions the slope was determined as $\Delta y/\Delta x$ (change in coefficient of friction/change in number of revolutions) as shown in Figure 4.39. The aim of determining this first derivative was so that an estimation of the film failure rate could be determined. Table 4.10 shows the results of the slope determinations for regions AB, BC and CD.

Table 4.10. Slopes of coefficient of friction as a function of number of revolutions for DLC and Si-DLC films corresponding to regions AB, BC and CD for tribo-test under normal load of 5 N

	Region AB (x 10^{-5})	Region BC (x 10^{-5})	Region CD (x 10^{-5})
DLC	2.3	11.4	4.6
Si-DLC	5.0	12.5	3.9
DLC with Si-C Interlayer	8.6	25.0	3.8
Si-DLC with Si-C Interlayer	22.5	1.3	-

In the region AB, the highest slope was obtained for Si-DLC and DLC with Si-C interlayers, at 22.5×10^{-5} and 8.6×10^{-5}. The high slopes for DLC and Si-DLC films with Si-C interlayers in region AB can be related to the comparatively lower composite micro-hardness of these films at 9.1 GPa and 12.1 GPa, respectively. Si-DLC had a lower composite micro-hardness value of 11.1 GPa than Si-DLC with Si-C interlayer, but had a slope of 5×10^{-5}. This difference is explained by the inclusion of the Si-C interlayer that resulted in an increase in sp^2 clusters that were unstrained and reduced compressive stress within the films. The lowest slope of 2.3×10^{-5} was obtained for DLC films. This is a direct result of the high composite micro-hardness values for these films at 15.5 GPa. Therefore, in region AB film failure classification from highest to lowest would be Si-DLC with Si-C interlayer, DLC with Si-C interlayer, Si-DLC and DLC films.

In region BC the lowest slope was obtained for Si-DLC with Si-C interlayer at 1.3×10^{-5}. This very low slope is an indicator that the film had stabilized at steady state conditions for the remainder of the tribo-test. However, for DLC, Si-DLC and DLC with Si-C interlayer the penetration of the pin deeper into the film/interlayer/substrate samples is related to the composite micro-hardness with higher slopes being observed for samples with lower composite hardness values. Therefore, low composite micro-hardness of films enhanced film failure in this region. In region CD, the slopes tend towards steady state conditions which

142

may indicate that there was a transfer of the film onto the pin so that no more transitions are observed.

From the results of the field visit to Makondo parish (see Figure 4.5) it was determined that the failure of handpump components could result in a scenario where the piston seals remain in water for a number of days before the handpump is repaired. As such nitrile rubber substrates were placed in water for 4 days. From Figure 4.40 it was observed that there was no significant variation in the percentage increase in mass between the coatings after immersion in water for 4 days. These samples were tribo-tested to determine their frictional behaviour.
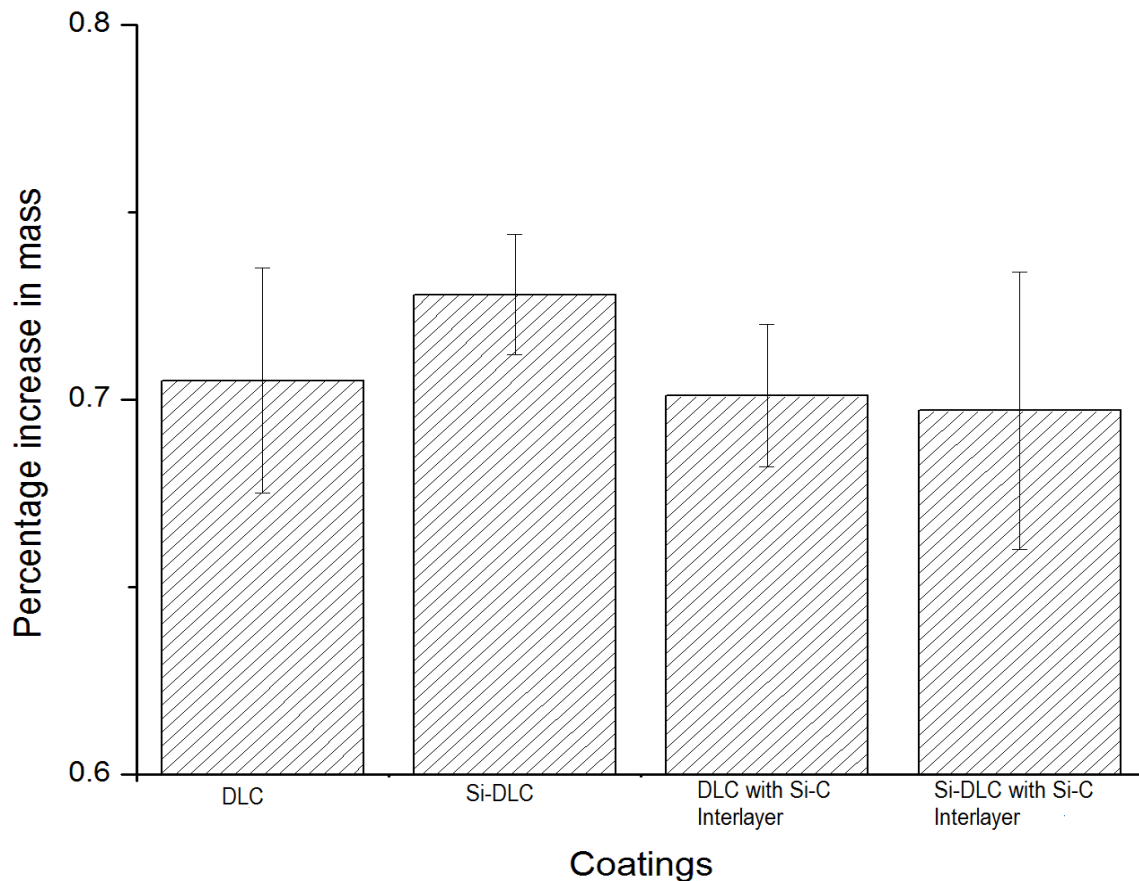
Figure 4.40. Percentage increase in mass of the various coating categories after immersion in water for 4 days

Table 4.11 shows the frictional results after tribo-tests after immersing in water for 4 days. Lower frictional coefficients were observed for all of the coatings tested at normal load of 1 N after immersing in water for four days. This may be a result of low surface energy due to

water absorption which passivizes rapidly the dangling bonds on the wear scars, much in the same way as an increase in relative humidity reduces wear rate [186]. The performance under a load of 5 N was expected to indicate a higher coefficient of friction. The performance of the DLC coating under this testing condition showed a lower coefficient of friction than the Si-DLC film and the DLC and Si-DLC films with Si-C interlayers. This result indicates that at higher loads there may be a detrimental effect due to the inclusion of Si. A similar observation can be made for tests carried out under dry sliding for normal load of 5 N [165].

Table 4.11. Coefficient of friction for tribo-tests after immersing in water for 4 days. The number of revolutions for each test was 10,000.

	Sliding after water immersion for 4 days	
	1 N	5 N
DLC	0.26±0.02	0.30±0.01
Si-DLC	0.30±0.01	0.48±0.10
DLC with Si-C Interlayer	0.28±0.01	0.49±0.11
Si-DLC with Si-C Interlayer	0.36±0.06	0.49±0.11

4.11.2. Frictional heating

It has been proposed that the sliding induced heat accumulation on local contact areas between two counterfaces can probably cause a gradual de-stabilization of the sp^3 C-H bonds. The de-stabilization promotes the transformation of the sp^3 bonded structure to the graphite-like sp^2 structure [161]. It is expected that the temperature at the contact asperities may be raised further by heat accumulation through repeated friction in the subsequent sliding [31, 161].

Sufficient temperature rise can promote the transformation of the thermodynamically meta-stable bonding structure (sp^3) into the more stable graphite-like structure (sp^2). The transition temperatures for hydrogenated DLC coatings were generally in the range of 400-500°C. This graphitization process is accompanied by desorption of hydrogen incorporated in the DLC matrix. The critical temperature of hydrogen desorption corresponds to sp^3-sp^2 transition temperature [193]. Le Huu et al. [193] showed that the critical phase transition could be reduced to a lower value (127-167°C) depending on the initial hydrogen content in the coatings as well as the sliding parameters resulting in graphitization at lower temperatures. For hydrogenated DLC coatings the transition temperature was determined between 130-240°C [31].

Table 4.12 shows the average surface temperatures for the films at normal load of 1 N for dry and wet sliding; and, for normal load of 5 N for dry sliding determined from eq. (3.17) and eq. (3.18). The results indicate that the influence of frictional heating is significant only for tribo-tests conduction under dry condition and normal load of 5 N. Tribo-testing under dry sliding at normal load of 5 N more than likely increases the possibility of graphitization. However, graphitization processes occurring on the wear surfaces cannot be simply explained by frictional heating [31]. During wet sliding tribo-tests the temperature at the contact asperities is suppressed resulting in a decreased graphitization rate [189].

Table 4.12. Average surface temperatures for the films at normal load of 1 N for dry and wet sliding and normal load of 5 N for dry sliding.

	Stainless steel counterpart			WC-Co counterpart		
	Dry		Wet	Dry		Wet
	1N	5N	1N	1N	5N	1N
DLC	33.2	157.7	38.6	9.0	21.9	13.5
Si-DLC	26.6	142.9	35.9	9.0	24.3	12.2
DLC with Si-C interlayer	23.9	68.5	37.2	9.5	27.2	11.6
Si-DLC with Si-C interlayer	25.3	142.9	35.9	10.1	33.8	10.9

4.11.3. Wear Analysis

Figure 4.41, Figure 4.42, Figure 4.43 and Figure 4.44 show the wear tracks for DLC, Si-DLC, DLC with Si-C interlayer and Si-DLC with Si-C interlayer films deposited on nitrile rubber after tribo-tests at under normal loads of 1 N and 5 N for both dry and wet sliding with a stainless steel counterpart, respectively. Generally, the wear results correlate very well with the results on the frictional characteristics of these films. It was also observed that there was no penetration of the coating for all of the films during both dry and wet sliding for tribo-tests performed under a normal load of 1 N. The wear track diameter for all of the films was similar and related to the applied load. For applied normal loads of 1 N the wear track diameter was observed to be smaller compared to the wear track diameters for normal loads of 5 N.
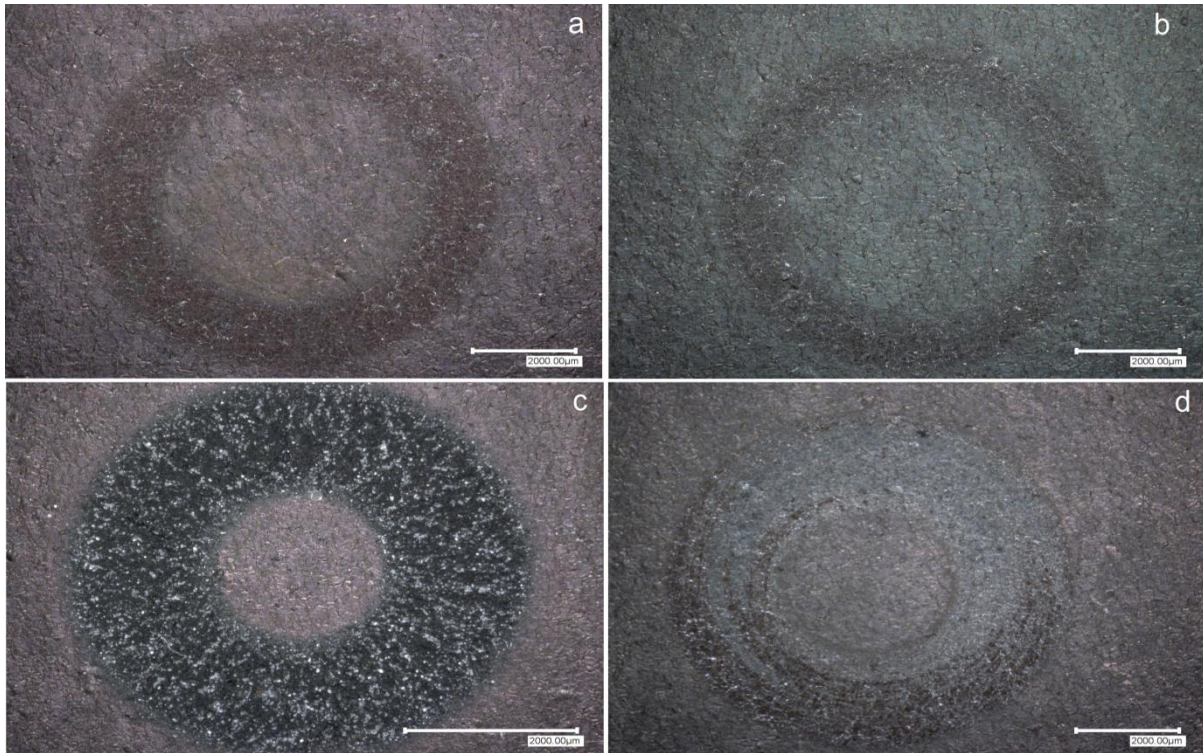
Figure 4.41. Wear tracks for DLC after tribo-testing under: (a) 1 N dry sliding; (b) 1 N wet sliding; (c) 5 N dry sliding; and, (d) 5 N wet sliding; with stainless steel counterpart
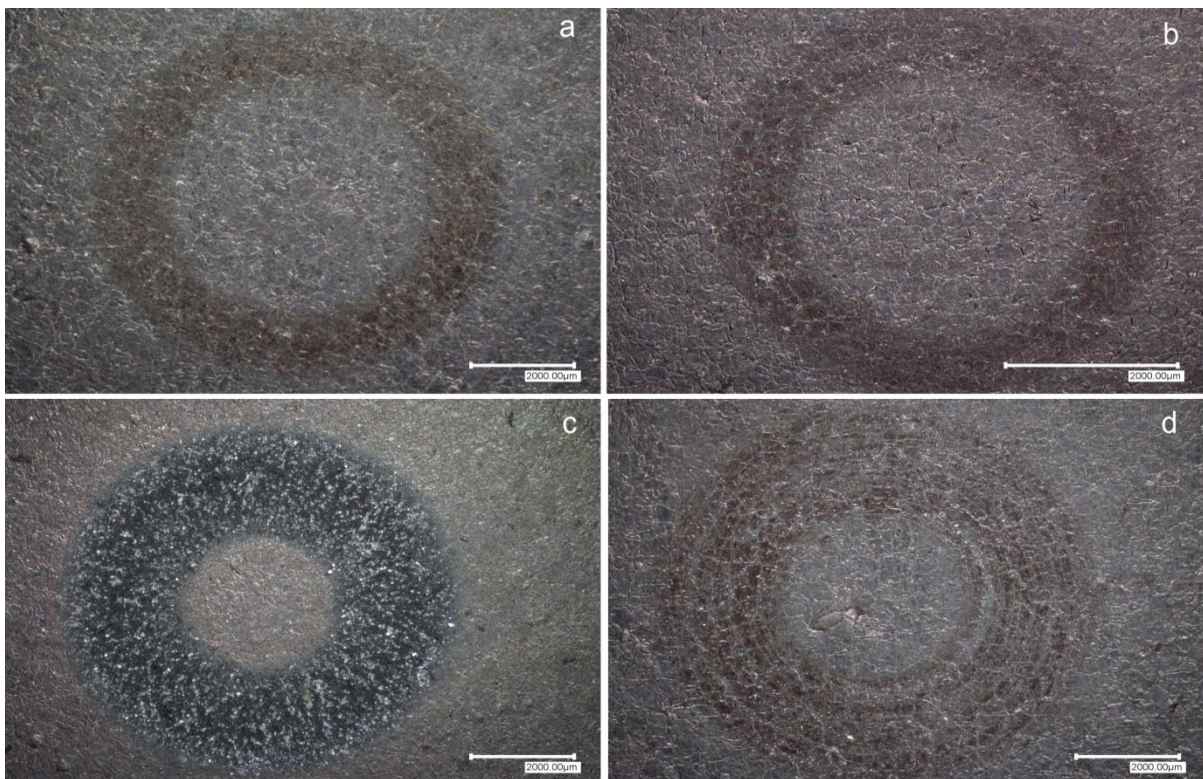
Figure 4.42. Wear tracks for Si-DLC after tribo-testing under: (a) 1 N dry sliding; (b) 1 N wet sliding; (c) 5 N dry sliding; and, (d) 5 N wet sliding; with stainless steel counterpart

146
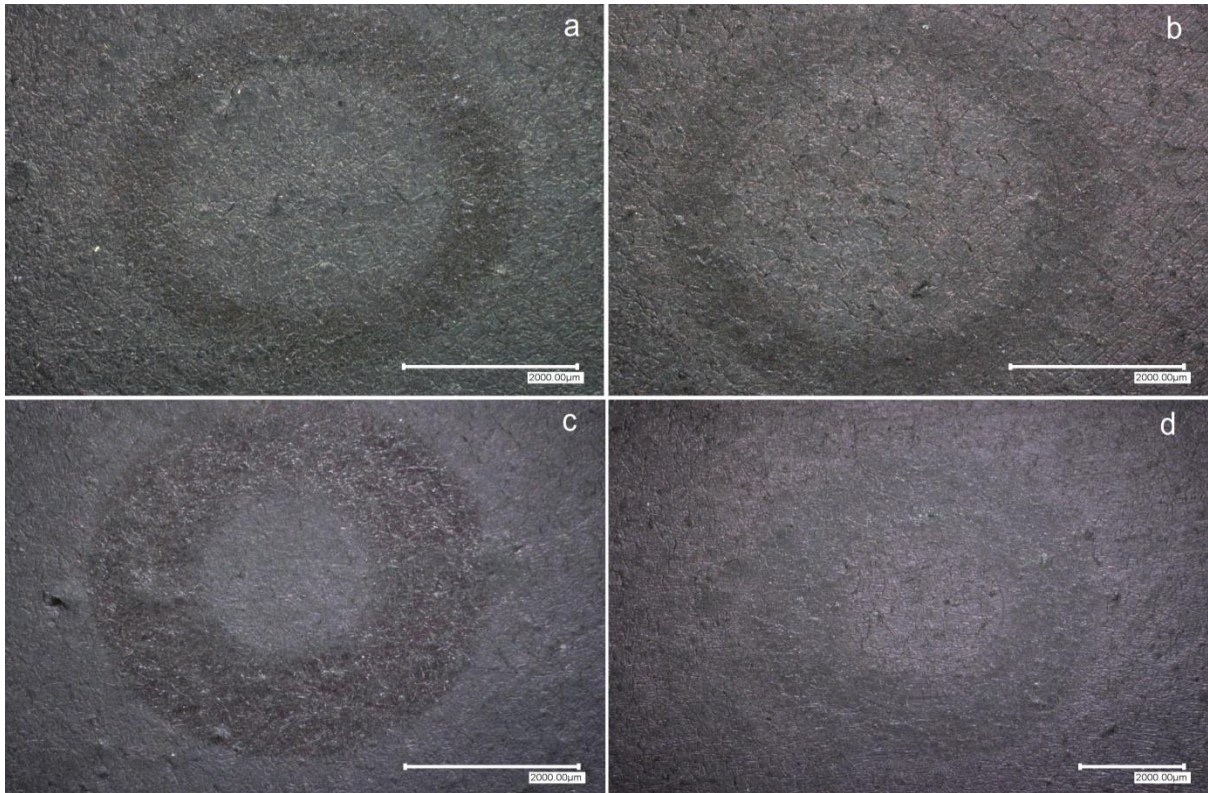
Figure 4.43. Wear tracks for DLC with Si-C interlayer after tribo-testing under: (a) 1 N dry sliding; (b) 1 N wet sliding; (c) 5 N dry sliding; (d) 5 N wet sliding; with stainless steel counterpart.
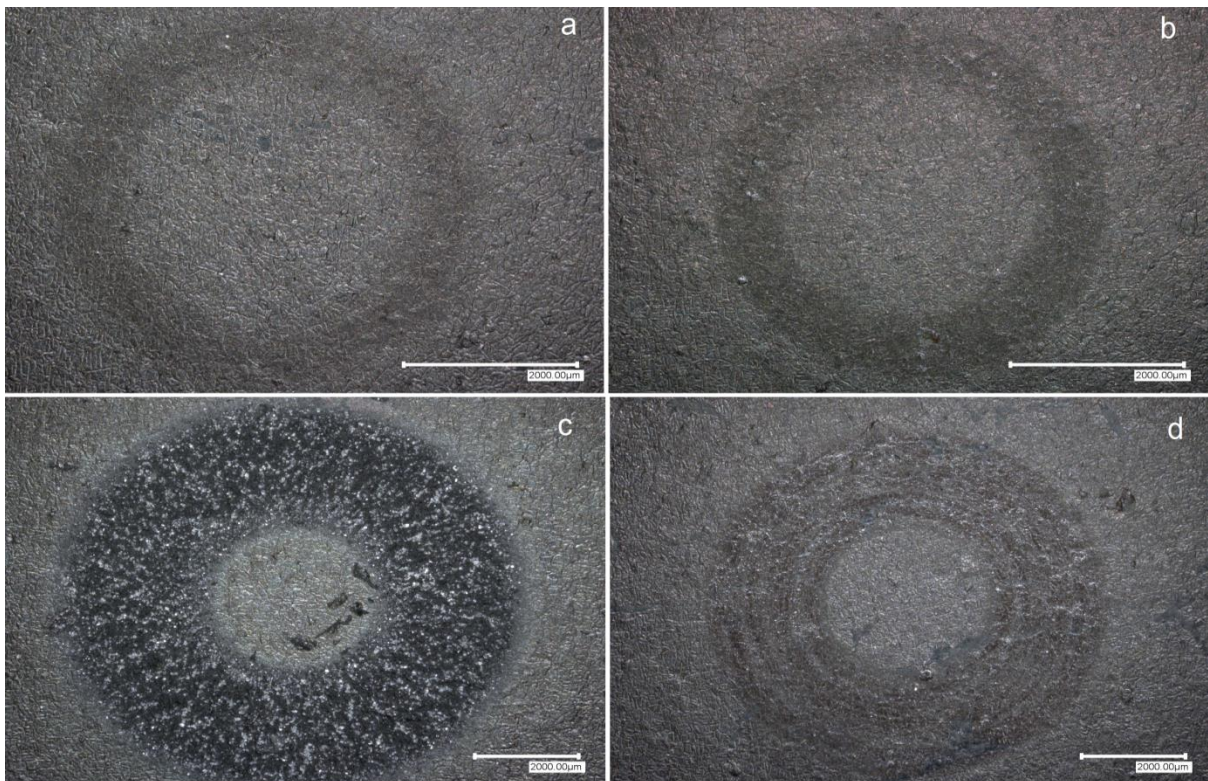
Figure 4.44. Wear tracks for Si-DLC with Si-C interlayer after tribo-testing under: (a) 1 N dry sliding; (b) 1 N wet sliding; (c) 5 N dry sliding; (d) 5 N wet sliding; with stainless steel counterpart

147

The wear mechanism taking place on the coatings during the tribo-tests is based on the generation and removal of wear debris [194, 195]. For tribo-tests conducted under normal load of 1 N for both dry and wet sliding the generation of wear debris was explained by the transfer from the coatings to the steel balls of an adherent transfer layer as the surface of the films became more and more graphitized. The material transfer from the coatings to the balls is associated with the adhesive wear mechanism. The formation of these graphitized tribo-layers on the wear surfaces of both coatings and steel ball provides good wear protection of the rubbing surfaces and a self-lubricating effect on the sliding friction resulting in long endurance life of the coatings [196]. The formation of this transfer layer is supported by previous results in Raman studies (see Table 4.2) which showed the films having a G peak position at about 1580 cm^{-1} which is close to the graphite vibrational density of states. Also from the XPS studies (see Table 4.6) it was ascertained that the coatings contain a significant fraction of sp^2 content which is significant for generation of graphite like sp^2 structures on the surface during tribo-testing. Under dry sliding the performance of the DLC with Si-C interlayer and Si-DLC with Si-C interlayer the wear resistance is higher (see Figure 4.43a and Figure 4.44a) compared to DLC and Si-DLC films as seen from the fainter shade of the wear track. This is due to the presence of the interlayer which improves the adhesion to the rubber substrate as well as absorbs the impact when the load is applied onto the film/interlayer system. This also explains the excellent frictional coefficient results discussed previously (see Figure 4.35a).

At normal loads of 5 N the wear behaviour of the coatings was different for both dry and wet sliding. For all of the films, apart from DLC with Si-C interlayer quite a number of wear debris particles were produced via fatigue processes [194, 195]. From Figure 4.41c, Figure 4.42c and Figure 4.44c micro-pitting on the wear surfaces was observed signifying the possibility of fatigue wear occurring. Micro-pitting originates from the surface initiated fatigue crack growth under repeated contact loading at the asperity tips [197]. The Raman studies indicated that the DLC with Si-C interlayer coating has more sp^2 clustering. As a result, DLC with Si-C interlayer easily formed a tribo-layer that enhanced its wear performance. For wet sliding under normal load of 5 N the improved wear performance was attributed to the water molecules saturating on the film surfaces and decreasing the amount of dangling bonds between the films and counterpart [188]. Figure 4.45 and Figure 4.46 provide a more detailed view (at higher magnification) of the wear track after tribo-tests at an applied load of 5 N with a stainless steel counterpart

148
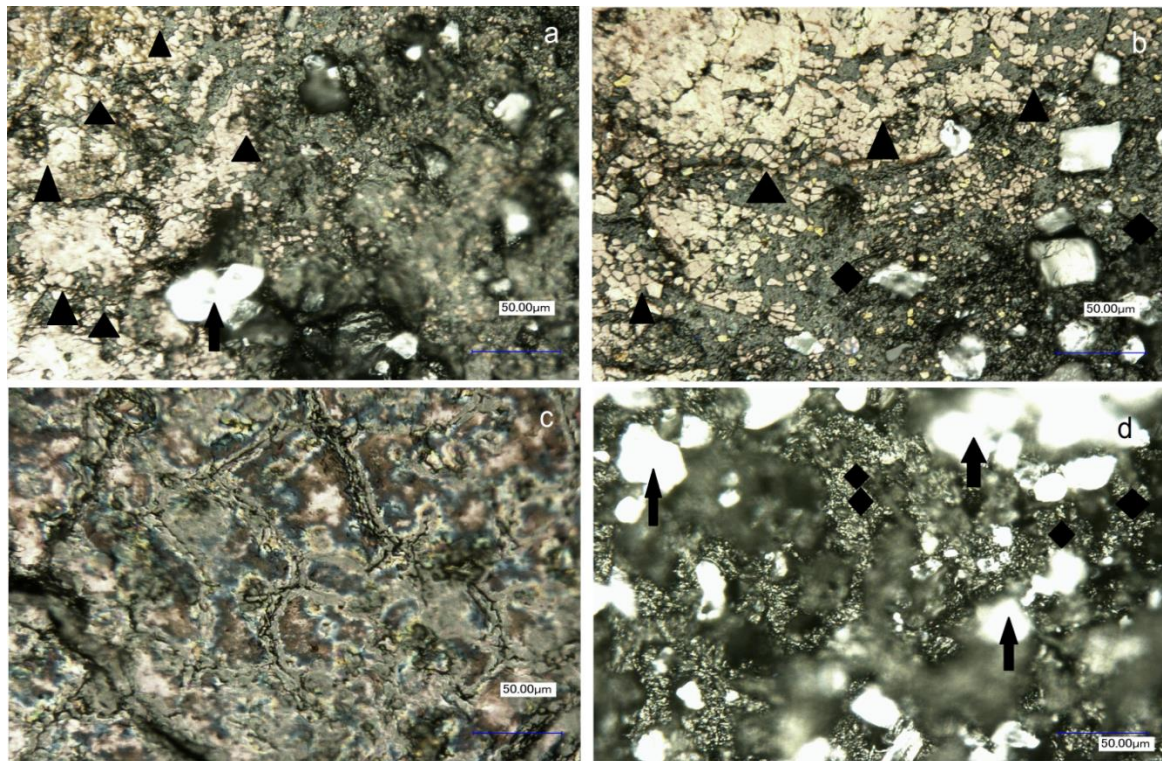
Figure 4.45. Digital microscopy examination of wear track after pin on disc experiments for dry sliding under normal load of 5N with stainless steel counterpart: (a) DLC; (b) Si-DLC; (c) DLC with Si-C Interlayer; and, (d) Si-DLC with Si-C Interlayer. The solid triangles show the micro-cracked film. The solid diamonds show the exposed nitrile rubber. The solid arrows show solid particles in the nitrile rubber
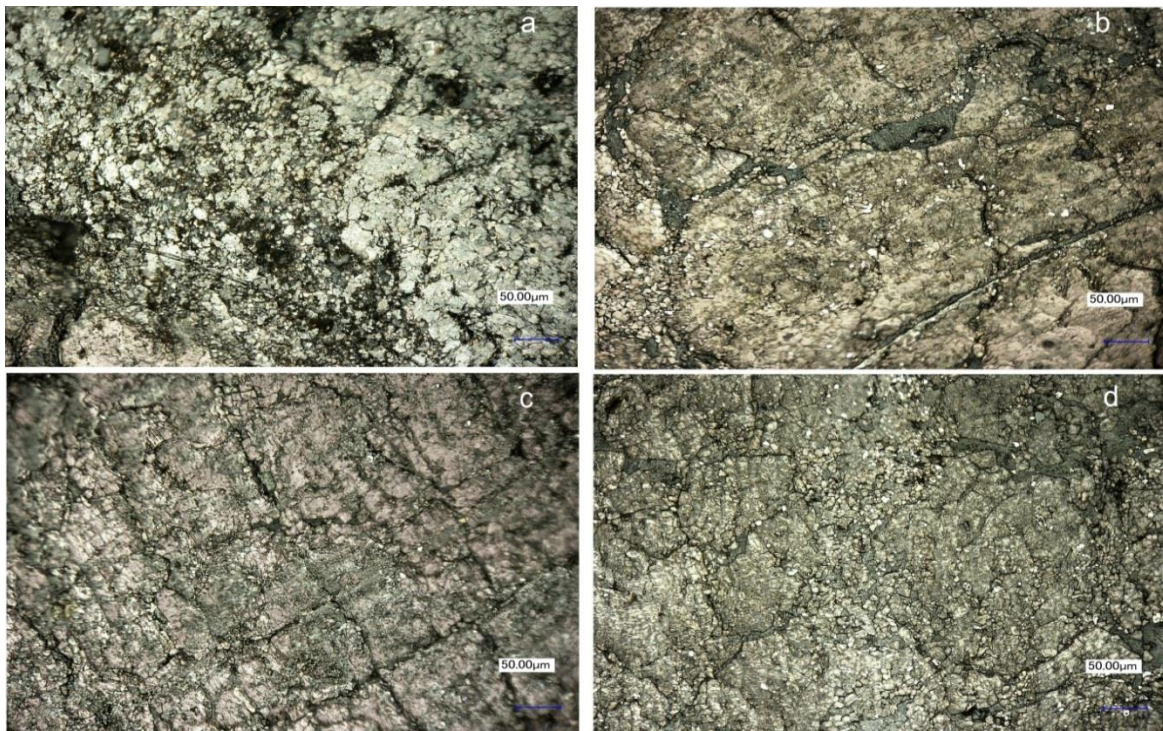
Figure 4.46. Digital microscopy examination of wear track after wet sliding tests at 5 N normal load: (a)DLC; (b)Si-DLC; (c)DLC with Si-C Interlayer; and, (d) Si-DLC with Si-C Interlayer; deposited on nitrile rubber with stainless steel counterpart

149

Under dry sliding tribo-tests the underlying rubber substrate was observed indicating that the pin penetrated the coating apart from the DLC with Si-C interlayer. The explanation given for the behaviour of DLC film with Si-C interlayer is related to its film flexibility. During each pass of the stainless steel ball on the film at a normal load of 5 N, the DLC film with Si-C interlayer generates lateral micro- and nano- cracks and as such may require greater stress intensity to reach the critical stress for de-bonding to occur [110]. Also, the Si-C interlayer promotes the excellent adhesion of the film to the rubber substrate. From Figure 4.45c it was observed that the DLC with Si-C interlayer film maintained the typical dendritic structure for such films. Micro-cracks were also observed for wet sliding tribo-tests as shown in Figure 4.46. The presence of these micro-cracks was related to improved film flexibility in Section 4.8.

For dry sliding the wear track becomes a complex system involving the micro-cracked coating and the nitrile rubber substrate. The presence of the DLC based coating resists the increment of frictional coefficient imposed by the nitrile rubber substrate. This result is very important because it implies that as long as the penetrated coating still contains micro-cracked DLC films the frictional coefficient will be reduced. Figure 4.46 explains the reason for the good wear performance of all of the coatings under wet sliding at applied normal loads of 5 N. The micro-cracking in the films which improved film flexibility is evident. This implies that during the tribo-test the coatings form micro- and nano- cracks increasing the crack density and stress absorbing capability of these films.

However, from Figure 4.45 and Figure 4.46, the micro-cracked coatings observed at higher loads are also wear debris particles that most probably arise from fatigue processes at the tips of the asperities. These particles may embed into the wear surface and abrade the surface during sliding from coarse abrasion grooves along the wear track due to micro-cutting. This means that three-body abrasion may also be taking place during the tribo-test [198]. These point-like abraded particles at the sliding interfaces induce high contact stresses that can probably exceed the fatigue limit of the coating and steel counterpart [31].

Figure 4.47 shows optical microscopy images of the stainless steel ball before and after tribo tests. The presence of light scratches was observed on the steel ball possibly indicating wear of the stainless steel ball by the DLC based coating. The scratches on the ball were few due to

the fact that the DLC based films studied had low nano-hardness values of approximately 3.6 GPa.
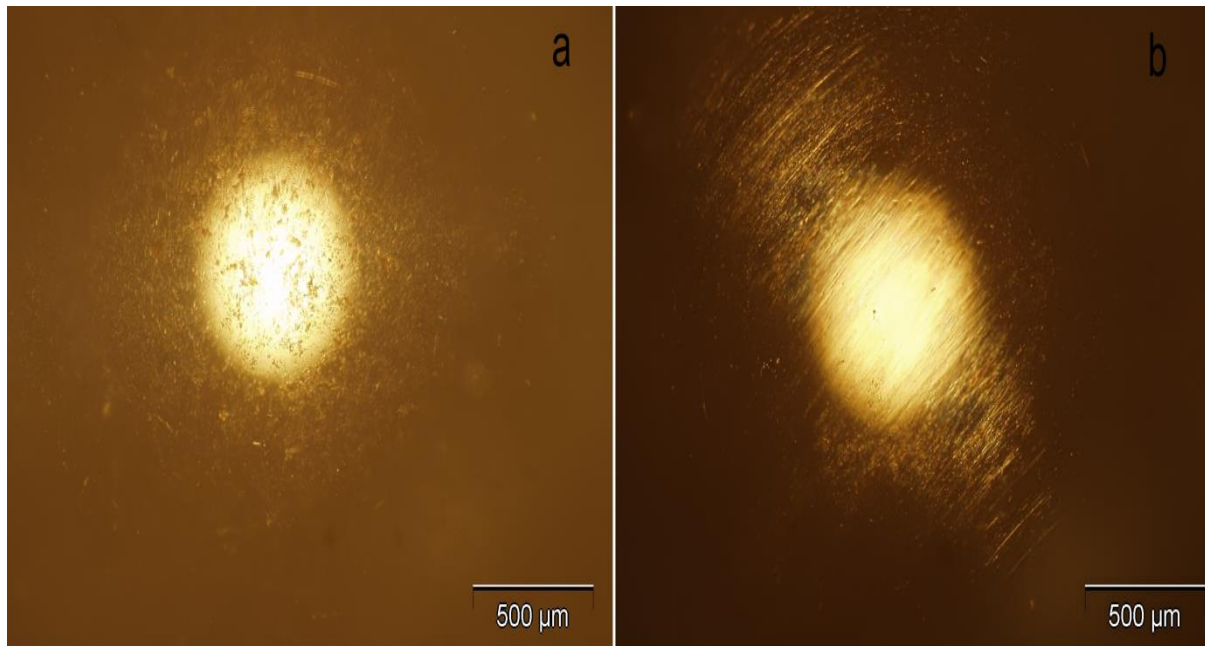
Figure 4.47. Optical microscopy images of the stainless steel ball: (a) before; and. (b) after pin of disc experiments

Figure 4.48 shows the wear profile of the wear tracks formed on the films obtained after tribo-testing for dry sliding under load of 5 N with a WC-Co counterpart, which indicate non-uniformity of the wear track. The wear depth for each film was calculated by taking the average of two depths, W_1, and W_2, associated with the maximum locations below the datum line (0.00) for each trace along the diameter from the outermost circumference of the wear track. The non-uniformity of the wear track can be explained by the high deformation and elasticity of the rubber substrate.

Table 4.13 shows the average wear depth for the films after testing with WC-Co counterpart at normal load of 5 N under dry sliding and after immersing in water. The results of the wear depth show less material loss for the DLC films. These results correlate well with the results for the frictional characteristics of the films. However, in comparison to coating thickness wear depth is about three orders of magnitude larger for tribo-tests at normal load of 5 N. The DLC films that have the lowest material loss as measured by the lowest wear depth also had the lowest coefficient of friction for these conditions.
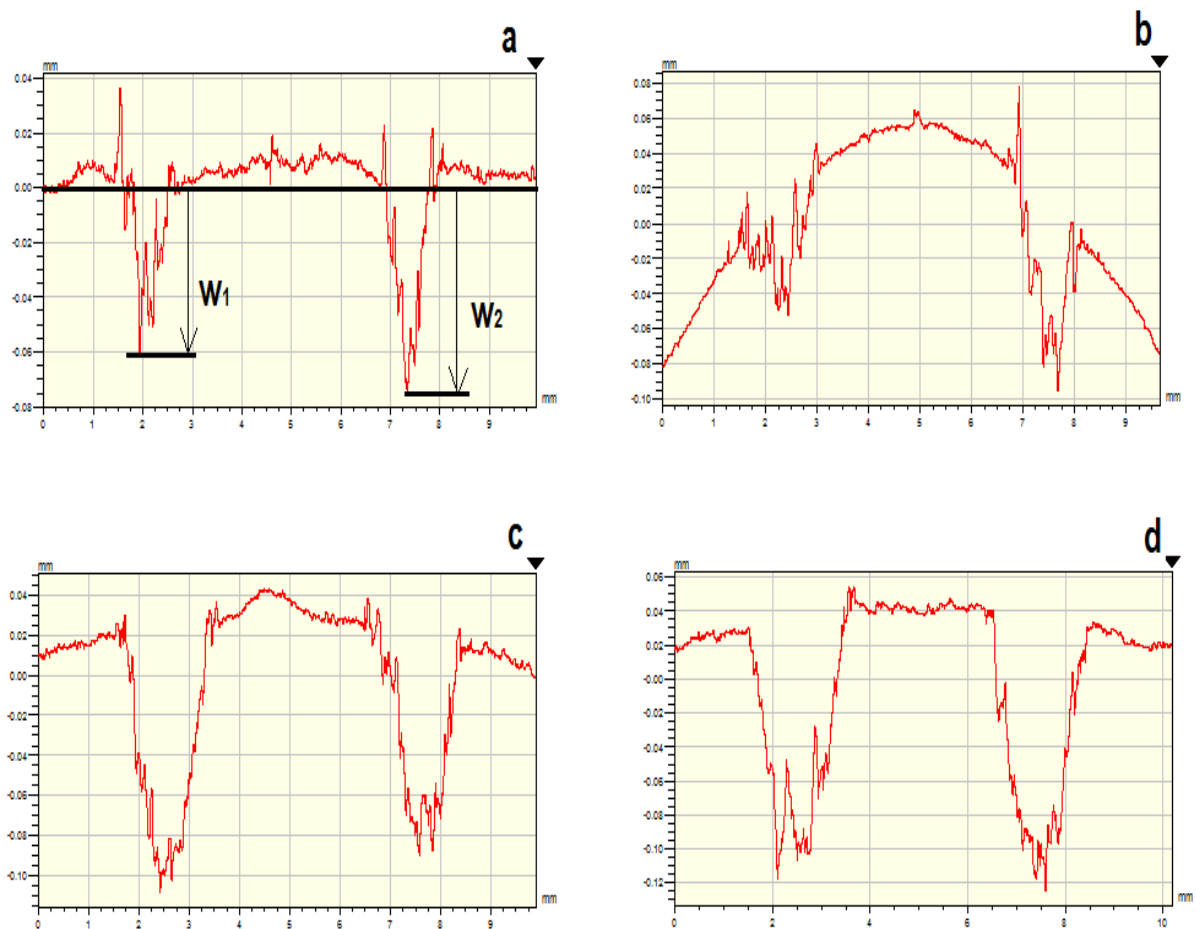
Figure 4.48. Wear profile of the wear tracks for the films under a load of 5 N. DLC – a; Si-DLC – b; DLC with Si-C interlayer – c; Si-DLC with Si-C interlayer – d

Table 4.13. Wear depth after tribo-tests with WC-Co counterpart at normal loads of 5 N after dry sliding and sliding after water immersion are shown. The number of revolutions for each test was 10,000.

	Wear Depth wet sliding (mm)	Wear Depth after sliding water immersion (mm)
	5 N	5 N
DLC	0.068	0.008
Si-DLC	0.073	0.130
DLC with Si-C Interlayer	0.100	0.163
Si-DLC with Si-C Interlayer	0.123	0.115

The results shown in Table 4.13 can be explained by the higher composite micro-hardness value (15.5 GPa) for the DLC films. The higher wear depth of Si-DLC films is attributed to doping with Si which results in a decrease in hardness [165]. According to Archard's wear law [119], wear rate or volume is inversely proportional to hardness. Therefore as wear depth increases the film composite micro-hardness is expected to reduce as the pin transits from contact between the DLC/Si-DLC top layer, to the Si-C interlayer to the nitrile rubber substrate or between DLC/Si-DLC top to the nitrile rubber substrate. Due to the influence of

the nitrile rubber substrate viscoelasticity, the wear depth increases slowly on each pass of the ball over the film. However, once film failure occurs, overall wear depth increases rapidly before reaching steady state [199].

4.11.3.1. Raman analysis of wear track

The visible Raman spectra (488 nm) for the wear tracks of the coatings after tribo-testing using stainless steel counterpart are shown in Figure 4.49 and Figure 4.50.
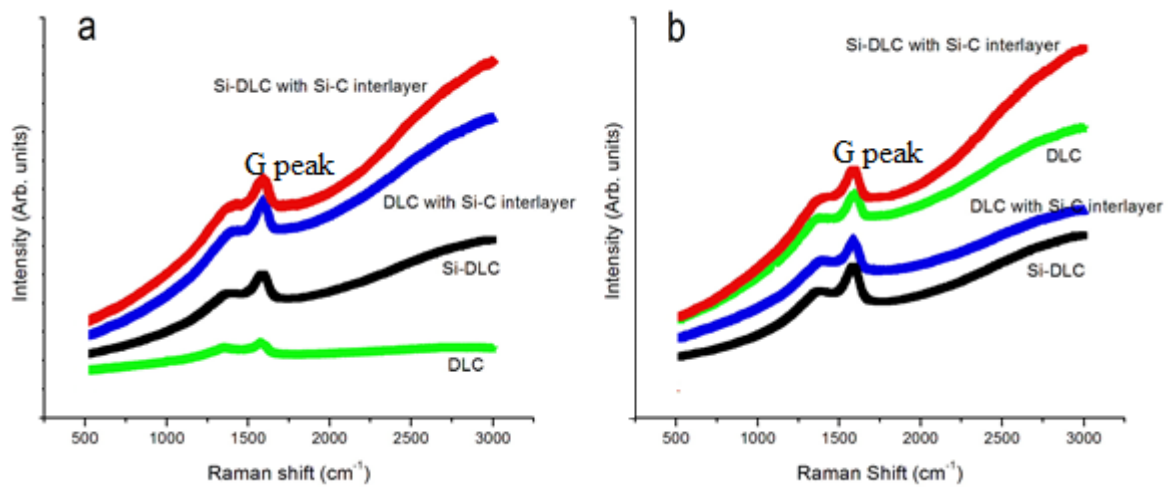
Figure 4.49. Raman spectra (488 nm) of the wear tracks after pin-on-disc tests under normal load of 1 N under: a) dry sliding, and, b) wet sliding
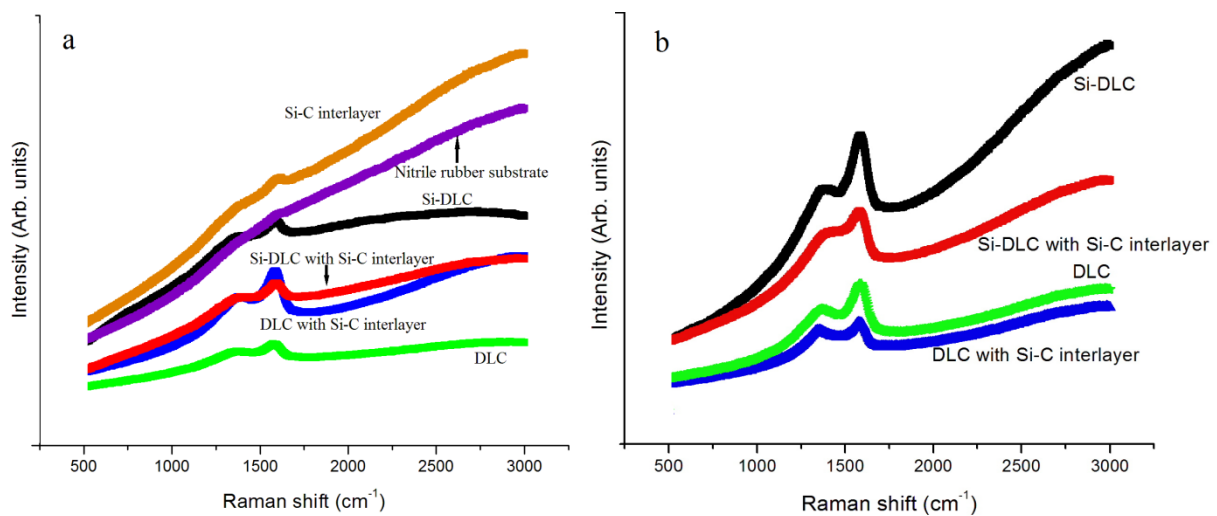
Figure 4.50. Raman spectra (488 nm) of wear tracks after pin-on-disc tribo tests under a normal load of 5 N: a) dry sliding, and, b) wet sliding.

153

Generally, the Raman spectra for all of the wear tracks were characterised by a broad C-H stretching band around 2800 cm^{-1} to 2900 cm^{-1}, further supporting the classification of these films as hydrogenated amorphous carbons [21]. For dry sliding under normal load of 1 N and 5 N, the increased PL background for the Si-DLC, DLC with Si-C and Si-DLC with Si-C interlayer films compared to DLC film is attributed to Si (at. %) present in these films [147]. Si incorporation results in a hydrogenated DLC film since hydrogen atoms are bonded not only to carbon but also to silicon to form Si-H bonds [155]. After wet sliding the PL background increases for all of the films under normal load of 1 N and 5 N. The increase in PL background is attributed most probably to a tribo-chemical reaction between the films and the water to form various hydroxyl groups [25]. Also, the low surface energy of the films passivizes rapidly the dangling bonds [186].

In discussing the wear mechanisms involved in the coatings during the tribo-tests it was suggested that an adhesive wear mechanism through the formation of a lubricious tribo-layer was responsible for the behaviour of wear tracks observed for both dry and wet sliding under normal load of 1 N. The Raman spectra of the coatings after tribo-tests at normal load of 1 N under both dry and wet sliding showed a corresponding increase in the G-peak value for all of the coatings. Table 4.14 shows the G peak positions for all of the films after tribo-testing. These results indicate a progressive transformation from sp^3 structure towards a more graphite-like sp^2 structure at the wear track [31, 32, 51].

Table 4.14. G peak position for the film after tribo-testing under normal load of 1 N and 5 N for both dry and wet sliding

Coating	Before	Dry (1 N)	Dry (5 N)	Wet (1 N)	Wet (5 N)
DLC	1585.6±3.4	1584.4±0.8	1585.9±0.8	1592.9±1.5	1585.5±0.7
Si-DLC	1573.9±8.6	1585.4±1.5	1587.2±1.2	1584.4±1.6	1586.2±0.7
DLC with Si-C interlayer	1579.6±8.7	1587.8±1.6	1585.8±0.8	1584.9±1.2	1581.1±1.1
Si-DLC with Si-C interlayer	1582.2±13.8	1585.7±1.5	1597.0±10.2	1585.6±1.7	1580.9±1.3

The results in Table 4.14 correspond well with the frictional behaviour observed in Figure 4.35a and Figure 4.35b for tribo-tests conducted under a normal load of 1 N under both dry and wet sliding. The higher G peak positions were indicative of the coatings that displayed better frictional behaviour. From Raman studies it was determined that the DLC with Si-C interlayer had more sp^2 clustering. This enhances its frictional performance under dry sliding conditions. From XPS studies (see Table 4.6) it was determined that DLC film had the

highest sp^2 fraction. This implies a film that is already stable with more sp^2 structures. Generally, G peak shift upwards is attributed to a progressive reduction of defects (bond angle and bond-bending disorder) in the sp^2 amorphous carbon network. These changes can be explained by an increment in number, size, and order of sp^2 aromatic clusters from an initial amorphous sp^2 bonded carbon network [196].

For dry sliding under normal load of 5 N, there was penetration of all of the films after tribo-testing, except for DLC with Si-C interlayer. The performance of the DLC with Si-C interlayer film is attributed to increase in the size of sp^2 bonded graphitic clusters in these films. For wet sliding under normal load of 5 N, there was no penetration of all of the films after tribo-testing. This is due to the water molecules saturating on the film surfaces and decreasing the amount of dangling bonds between the films and counterpart [188].

Figure 4.51 shows I_D/I_G, and FWHM(G) for the wear tracks of the films deposited on nitrile rubber. For the DLC and DLC film with Si-C interlayer I_D/I_G ratio were higher than before wear testing for both dry and wet sliding at normal loads of 1 N (see Table 4.2). This generally implies that DLC and DLC with Si-C interlayer have a higher sp^2 fraction compared to Si-DLC and Si-DLC with Si-C interlayer films [95]. This is consistent with XPS analysis results shown in Table 4.6.
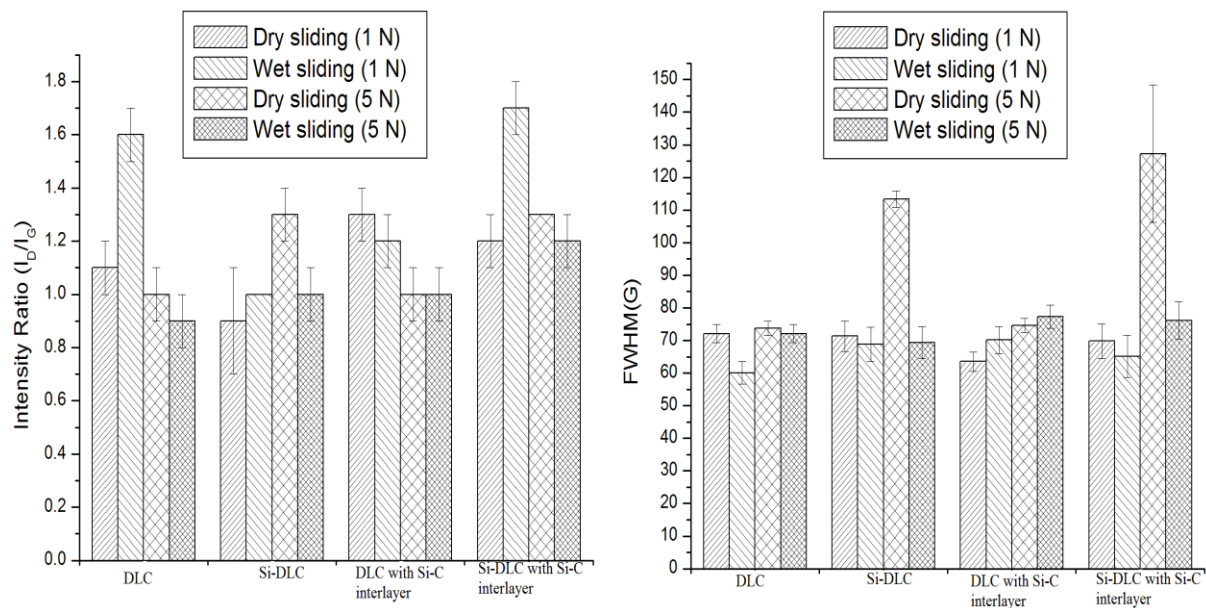
Figure 4.51. Raman parameters for the wear tracks: a) Intensity ratio, I_D/I_G, and, b) full width at half maximum of the G peak, FWHM(G)

The FWHM(G) for all of the films is below the values before tribo-testing which suggests that the graphitic clusters within the films were unstrained [166]. FWHM(G) is mainly sensitive to structural disorder, which arises from bond angle and bond length distortions. Therefore, the low values of FWHM(G) are attributed to reduction of defects in the sp^2 amorphous carbon networks indicating a more graphitic organization and a decrease of sp^3 C-C hybridisation percentage [42, 95, 100].

4.12. Piston seal wear mechanisms

Figure 4.52 compares the surface morphology for DLC, Si-DLC and DLC with Si-C interlayer coatings deposited onto nitrile rubber piston seals. From Figure 4.52 the formation of the crack-like dendritic structure typical for DLC films was observed as discussed in Section 4.3.1. These cracks are known to improve film flexibility. This is advantageous since the coated piston seals will be able to deform and perform their sealing function without interfacial delamination [23, 24]. However, the surface morphology was different at the base and the side of the piston seal. This is attributed to the known difficulty of using sputtering for depositing films on three-dimensional objects [64]. Therefore, the coating deposited on the rubber substrates very much depended on the orientation of the coated piston seal to the target surface.

Figure 4.53, Figure 4.54 and Figure 4.55 show the evolution of the surface morphology of the coated piston seals after over 100,000 strokes of operation in the piston seal wear test rig with water with sand particles for both the top and bottom seal in the piston assembly of a reciprocating handpump. The surface evolution was analysed at the base (Figure 4.53), side (Figure 4.54) and lip (Figure 4.55) so that the wear mechanisms involved could be determined.
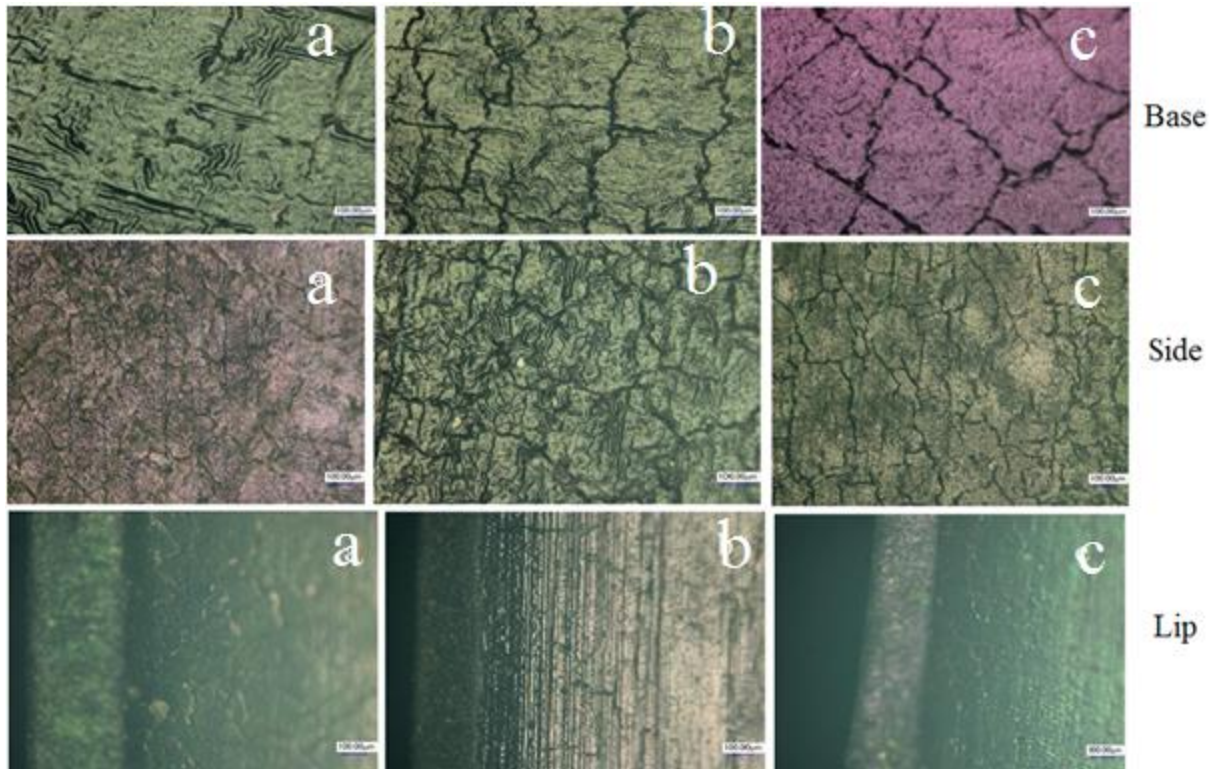
Figure 4.52. Comparison of the surface morphology of: a) DLC; b) Si-DLC; and, c) DLC with Si-C coatings deposited on nitrile rubber piston seals.
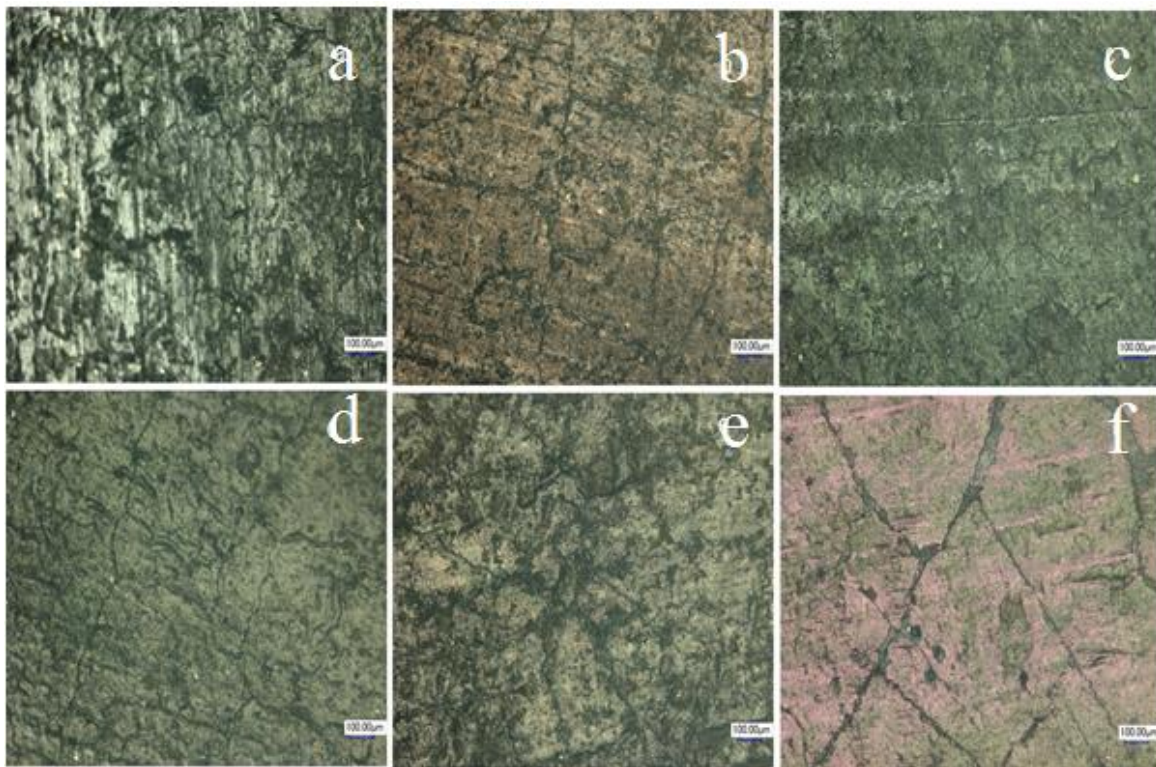
Figure 4.53. Coated piston seal base comparisons after 100,000 strokes of testing in wear rig for wet sliding with solid particles: a) DLC; b) Si-DLC; c) DLC with Si-C interlayer; for top seal, and d) DLC; e) Si-DLC; and, f) DLC with Si-C interlayer for bottom seal

157
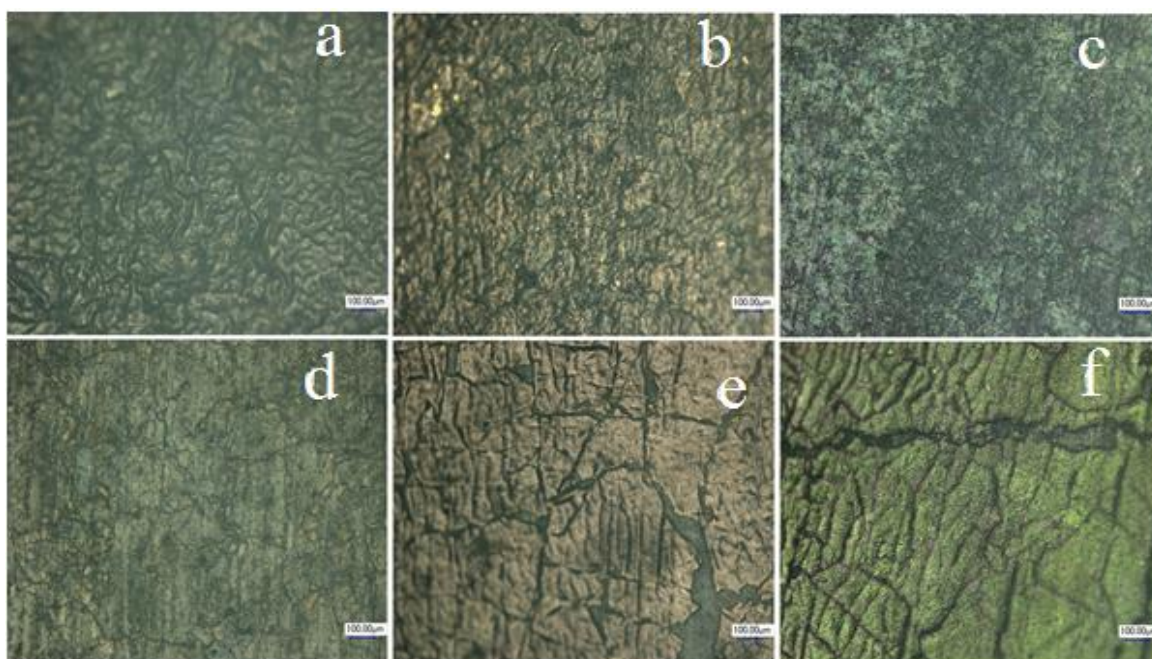
Figure 4.54. Coated piston seal side comparisons after 100,000 strokes testing in wear rig for wet sliding with solid particles: a) DLC; b) Si-DLC; c) DLC with Si-C interlayer; for top seal, and d) DLC; e) Si-DLC; and, f) DLC with Si-C interlayer for bottom seal
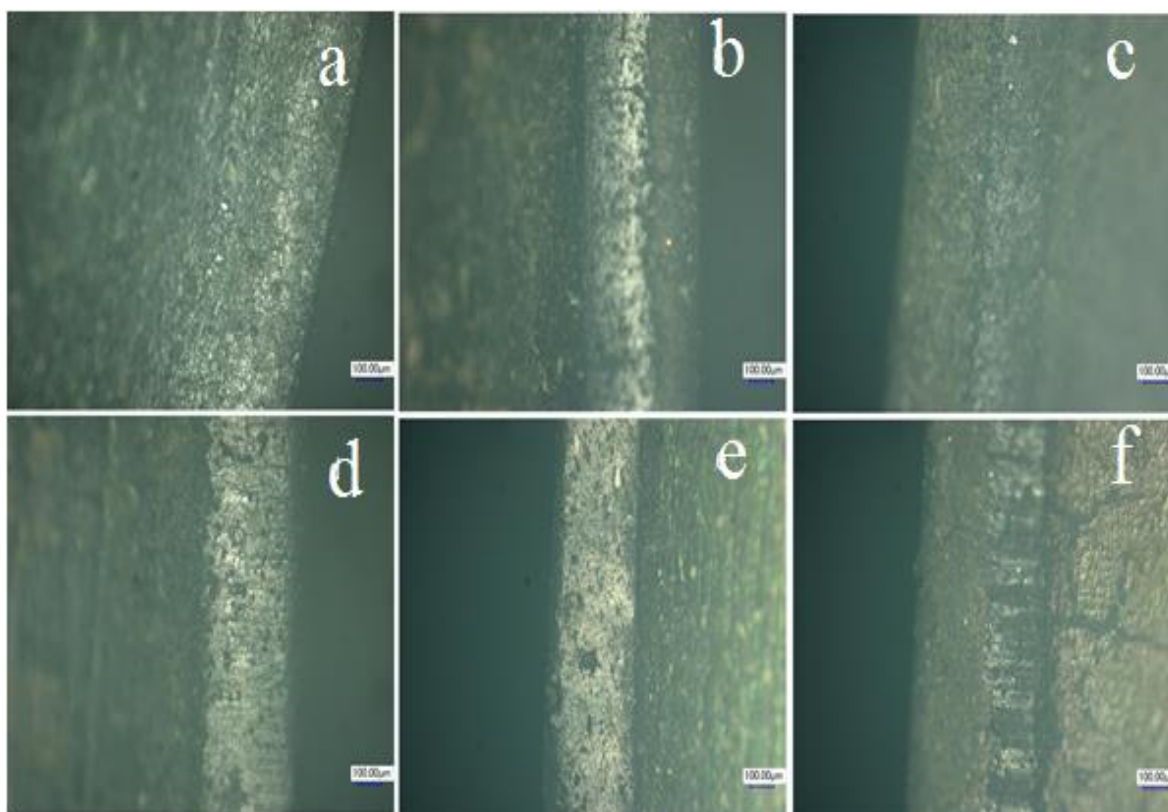
Figure 4.55. Coated piston seal lip edge comparisons after 100,000 strokes testing in wear rig for wet sliding with solid particles: a) DLC; b) Si-DLC; c) DLC with Si-C interlayer; for top seal, and d) DLC; e) Si-DLC; and, f) DLC with Si-C interlayer for bottom seal

The wear mechanisms involved at the base of the coated piston seals (see Figure 4.53) was characterised by the presence of scuff marks and micro-pitting marks. More scuff marks were observed for the top seals of coated DLC and DLC with Si-C interlayer compared to the bottom seals. For the Si-DLC coating more scuff marks were identified in the bottom seal compared to the top seal. The wear mechanisms in the top and bottom coated Si-DLC piston seals did not appear to differ significantly. The scuff marks are attributed to abrasive wear between the base of the coated piston seal and the brass piston seal housing [198]. The micro-pitting marks are an indicator of fatigue wear [31].

The sides and lip of the coated piston seals are always in contact with the cylinder of the piston seal assembly. Figure 4.54 shows the evolution of the sides of the coated piston seals after 100,000 strokes of operation of the piston seal wear test rig. The top seals of all of the coated piston seals indicate micro-cracking taking place. The presence of these micro-cracks was explained in flexibility studies (see Section 4.8). The micro-cracks allow the coated piston seals to deform and perform their sealing function by being able to accommodate higher stress intensities applied onto them without interfacial delamination occurring [110].

For the bottom coated seals in Figure 4.54, more interfacial delamination was observed for Si-DLC and DLC with Si-C interlayer coated seal. The DLC coated piston seal showed more scuff marks but did not show any interfacial delamination. However for the coated DLC piston seal solid particles were observed to have embedded into the coating suggesting that three-body abrasion was evident. Figure 4.56 shows a solid particle embedded in the side of a coated piston seal. The wear mechanism involved was attributed to both abrasion (from the scuff marks) and three-body abrasion [198]. The coated DLC piston seal performance was probably due to the enhanced graphitization process at the surface of the coating resulting in the formation of a tribo-layer in an adhesive wear mechanism [31]. For the Si-DLC and DLC with Si-C interlayer three-body abrasion ensues due to repeated contact with the cylinder in the presence of solid particles. Also, the wear debris from the coated piston seals contributes to three body abrasion. The lip edge of all of the coated piston seals was observed not to be affected significantly after wear testing experiments.
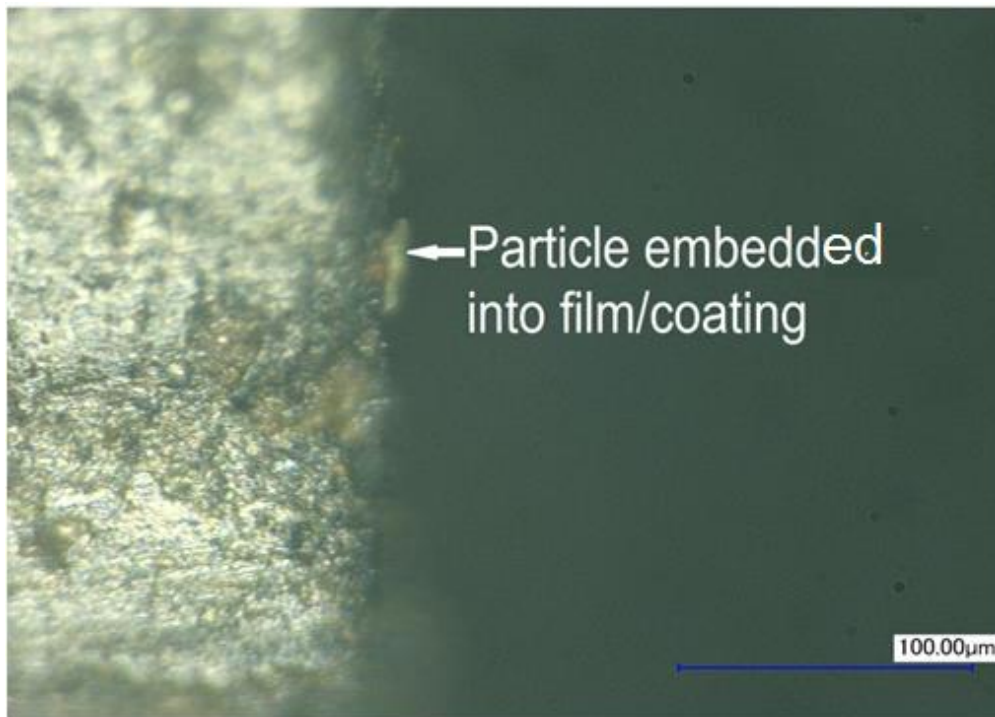
Figure 4.56. Particle embedment into film/substrate interface of piston seal

Table 4.15 shows a comparison of the masses of the coated piston seals before and after 100,000 strokes of operation of the piston seal wear testing rig. This analysis was carried out so that the potential of applying these coatings onto piston seals could be ascertained.

Table 4.15. Comparison of the masses of the coated seals before and after 100,000 strokes of operation of the piston seal wear testing rig.

Testing condition	Coating	Mass of top seals (g)			Mass of bottom seals		
		Initial	Final	Difference	Initial	Final	Difference
Water and solid particles	DLC	18.8752	18.8720	0.0032	17.6020	17.5991	0.0029
	Si-DLC	18.8618	18.8582	0.0036	17.5762	17.5749	0.0013
	DLC with Si-C interlayer	18.7995	18.7945	0.0050	17.1003	17.0968	0.0035
Water	DLC	17.4696	17.4561	0.0135	17.0816	17.0769	0.0047
	Si-DLC	16.9763	16.9625	0.0138	17.4953	17.4784	0.0169
	DLC with Si-C interlayer	17.3635	17.3623	0.0012	18.3161	18.3132	0.0029

For the top seal tested in water with solid particles it was determined that the DLC coated piston seal experienced less mass loss compared to the Si-DLC and DLC with Si-C interlayer coated seals. This result is due to the enhanced graphitization of the DLC surface to form a

lubricious tribo-layer. For the bottom seal tested in water with solid particles the seal coated with Si-DLC experienced the least mass difference at the end of testing. The very low mass differences were attributed to the presence of the coating which negated the onset of wear taking place compared to uncoated piston seals. The piston seal coated with DLC with Si-C interlayer had the least mass difference for both the top and bottom seals for piston seal wear testing in water (without solid particles). This low mass difference is in line with discussions made on DLC with Si-C interlayer in Raman and XPS studies. The mass difference of DLC and Si-DLC coated top seals was much higher than expected.

In Section 4.2.3 it was determined that the wear of uncoated nitrile rubber piston seals was due to a complex interaction involving adhesion, abrasion and fatigue wear. From the surface analysis of the coated piston seals it was determined that abrasive wear and fatigue wear are the dominant wear mechanisms. The coated seals have less adhesive wear compared to the uncoated piston seal determined by the absence of features typical for identification of adhesive wear as described in Section 4.2.3. The adhesive wear mechanism on the coated piston seals is described in terms of generation and transfer of a lubricious tribo-layer which reduces the frictional coefficients and hence reduces wear.

4.13. Cost Analysis

The investment cost for a CFUBMSIP rig ranges from 80,000 to 200,000 United States Dollars (USD). Handpumps range from between 1,000 to 2,500 USD. If 30 handpumps are installed in Makondo at a cost 1,000USD, then the total cost becomes 30,000 USD. Therefore, the total cost of investment is 110,000 USD if a magnetron sputtering rig of 80,000 USD is installed. The average maintenance cost for handpumps in is 300 USD per pump per year [200]. This implies a total maintenance cost of 9,000 USD for the 30 handpumps installed in Makondo. This means that in about 12.2 years total maintenance cost will surpass total investment cost.

However, since the piston seals are responsible for 24% of all maintenance interventions, the possible extension of the life of the piston seals by application of the coatings described in this thesis may provide a significant increase in the time it takes for the maintenance cost to catch up with the investment costs. Figure 4.38a showed that an over 50% reduction in

coefficient of friction was realised for the DLC and Si-DLC films compared to uncoated nitrile rubber. The coefficient of friction results are directly related to the wear results (see Section 4.11.3). This implies that as a result of the coatings applied onto handpump nitrile rubber piston seals increase in the wear resistance is expected. If a corresponding 50% increase in wear resistance is achieved, then this would mean that an additional 1.5 years would be required for the maintenance costs to overtake the initial investment costs as a result of the reduction assuming that the 24% contribution from wear of piston seals is completely solved. This is significant considering the fact that the life of a typical handpump ranges from 7-15 years.

The cost analysis presented here is very simplistic. It shows that since the wear resistance of the coated piston seal is increased compared to the uncoated piston seal, a corresponding reduction in the maintenance cost should be expected. The number of maintenance interventions will also be reduced and the availability of the handpump will be increased. The prospect of increasing on the availability of the handpump is very important because the human cost of its unavailability as a result of worn piston reals is very difficult to account for in terms of health spending and time lost walking to functioning handpumps located more than 1km from peoples' homes.

4.14. Summary

In this chapter the results of field visits to Makondo Parish were reported and discussed. Some of the problems faced by the handpump users were related to the wear of the nitrile rubber piston seal. The possible wear mechanisms involved in the wear of nitrile rubber piston seals were discussed. The results of the experimental and characterization techniques that were used in this study were reported and discussed extensively. The DLC, Si-DLC, DLC with Si-C interlayer and Si-DLC with Si-C interlayer morphology, chemical and microstructural composition were presented and discussed. A detailed Raman spectroscopy analysis was performed. Such an analysis has never been performed before for DLC based films deposited on rubber substrates (See Table 4.3, Table 4.2 and Table 4.14). XPS analysis was presented and the sp^2 and sp^3 bonding structure in the films were determined and explained (See Table 4.5 and Table 4.6). Using the results of morphological, chemical, Raman and XPS analysis the chapter then proceeded to discuss the hydrophobicity, surface

free energy, adhesion, flexibility, composite micro-hardness, nano-mechanical properties and tribological behaviour of the coatings. Tribological performances of the coatings are highlighted in Table 4.9, Table 4.10, Table 4.11 and Table 4.12. A summative overview of other characterisation results is given in Table 4.16. Preliminary results of wear testing of DLC, Si-DLC and DLC with Si-C interlayer coated piston seals were discussed. The lowest mass loss of the coated piston seals after 100,000 strokes of operation in piston seal wear test rig with water only was recorded for DLC with Si-C interlayer. However, for testing conditions involving water and sand particles DLC with Si-C interlayer recorded the highest mass loss after 100,000 strokes of operation (See Table 4.15). This implies that the coating application may be specific to the testing regime involved. The wear mechanisms taking place in the coated piston seals were identified as mainly abrasive wear and fatigue wear.

Table 4.16. Summative overview of some characterisation results

	Nitrile Rubber	DLC	Si-DLC	DLC with Si-C interlayer	Si-DLC with Si-C interlayer
Surface Morphology	Powdery [23]	Dendritic crack-like surface with patches on a micro-scale			
Film Thickness [μm]	-	1.2	1.2	0.5 – 0.6	0.5 – 0.6
Surface Roughness [μm]	1.1	1.5 – 2.2			
Contact Angle [°]	<95 [18]	102.0±1.0	102.6±0.5	104.5±1.0	101.6±1.0
Adhesion	-	3A	3A	4A	4A
Flexibility (Film on interior)	-	Lateral cracks	De-bonding	Lateral cracks	De-bonding
Flexibility (Film on Exterior)	-	Lateral cracks	Lateral cracks and de-bonding	Lateral cracks	Lateral cracks and de-bonding
Composite Hardness [GPa]	-	15.5±0.8	11.1±0.7	9.1±0.7	12.1±1.2
Nano-hardness [GPa]	-	3.6±0.2	3.5±0.2	3.9±0.1	-
Tauc gap [eV]	-	1.63	1.45	1.57	1.52
E_{04} gap [eV]	-	2.06	1.99	2.12	2.02
Disp(G) [cm^{-1}/nm]	-	0.07	0.05	0.13	0.08
Compressive stress reduction [GPa]	-	1.5	0.4	1.4	2.6
H [at.%] PL method	-	27.8±1.4	28.6±1.4	27.7±1.4	29.0±1.4
H [at.%] Tauc gap method	-	28.1±0.2	26.3±0.3	27.4±0.4	26.9±0.3

Chapter Five

Conclusions, thesis contributions and recommendations for future work

5.1. Conclusions

This study presented a novel approach to solving the problem of unreliable handpumps. By specifically being embedded in a rural community for a given period of time it was determined that the functional sustainability of most handpumps was essentially determined by the wear of the nitrile rubber piston seals. Some of the problems that the handpump users identified with the handpump were shown to be related to wearing of the piston seal. Using the first level of surface analysis it was further determined that the wear of the nitrile rubber piston seal involved a complex interaction between adhesive, abrasive and fatigue wear. Therefore, any intervention focussing on increasing wear resistance of the nitrile rubber piston seals would be a positive contribution towards improving the functional sustainability of piston seals. This led to the novel idea of applying DLC and Si-DLC films onto nitrile rubber substrates and onto actual piston seals.

In this study DLC and Si-DLC films with and without Si-C interlayers were deposited onto nitrile rubber substrates using a combination of CFUBMSIP and PECVD. The deposition was done in Ar/C_4H_{10} plasma at a substrate bias voltage of -30V which was maintained the same. The coatings were characterised using visible (488 nm) and UV (325 nm) Raman spectroscopy , X-ray Photoelectron Spectroscopy (XPS), Energy Dispersive X-ray (EDX) analysis, Scanning electron microscopy (SEM), surface profilometry, hardness measurements, hydrophobicity and surface energy analysis, adhesion and flexibility analysis, and tribological investigations under dry and wet conditions for normal loads of 1N and 5N. A piston seal wear test rig was used to test the wear resistance of the coated piston seals. The piston seal wear test rig was based on the India Mark II model of handpump.

The surface morphology of the DLC and Si-DLC coatings was characterised by a dendritic crack-like network. These cracks originate at the first atomic layer of DLC on rubber due to thermal stress mismatch and continuously grow upwards together with the film itself

164

resulting in a patch size of the DLC films. The presence of a dendritic micro-crack like network was attributed to enhancing film flexibility by allowing the coatings to deform without interfacial delamination. However, the surface morphology of Si-DLC and Si-DLC coating with a Si-C interlayer showed more areas for potential delamination. These were attributed to the effect of Si dopant in the Si-DLC film, which causes an increase in contributions from sp^3 sites due to vibration in C-C bonds in sp^3 hybridisations of the Si-DLC films. The enhancement of sp^3 fraction is related to the Si valence structure which forms four-fold co-ordinated networks.

The DLC and Si-DLC films had a thickness of approximately 1.2 μm. When an interlayer was included the DLC and Si-DLC films had a thickness of approximately 500 nm and the interlayer had a thickness of approximately 500 nm. Fracture cross-sections of the coatings deposited on nitrile rubber did not show the typical columnar structures. This was attributed to the substrate bias voltage of -30V applied in this study. In this study, a closed field unbalanced magnetron sputtering ion plating system was used where the coating deposition is carried out using a high density of low energy bombarding ions (- 30V) bias voltage in this case), resulting in very dense, non-columnar coating structures. In this deposition configuration, the plasma that is present in vacuum chamber between the source and the nitrile rubber substrate is ideal for ion plating since the plasma allows energetic ion bombardment of the substrate which enhances ionization of vapour species at low energies.

The visible Raman spectroscopy for the DLC and Si-DLC coatings showed the prominent G peak (centred approximately 1580 cm^{-1}) and a smaller underlying D peak (centred approximately 1350 cm^{-1}). These films were also characterised by an enhanced visible photoluminescence which is controlled by the hydrogen content in the films. The I_D/I_G ratio generally tended to increases for both DLC and Si-DLC films with the inclusion of Si-C interlayer compared to the films without Si-C interlayer. This implied that the graphitic size clusters for the films with the Si-C interlayers would be larger as these films had correspondingly higher intensity ratios. The Raman results showed that the FWHM(G) is lower for DLC and Si-DLC films with Si-C interlayer, which suggests that the graphitic clusters were unstrained.

The chemical bonding of DLC and Si-DLC films was also studied by means of a multi-wavelength Raman analysis using a 325 nm (UV) and 488 nm (visible) excitation

wavelengths. The T peak position represented by a weak shoulder at approximately $1150 - 1200$ cm^{-1} was observed for Si-DLC, DLC with Si-C and Si-DLC with Si-C coatings. The T peak is due to the C-C sp3 vibrational modes and was observed for only UV excitation. Generally low values for Disp(G) were determined. This was attributed to the combination of a CFUBMSIP system and reactive magnetron sputtering in an Ar/C$_4$H$_{10}$ plasma that result in G peak positions at approximately 1580 cm^{-1}, which is close to the graphite vibrational density of states. DLC with Si-C interlayer had more sp^2 clustering.

Bonded hydrogen in the films was determined using both the PL and Tauc gap method. Calculated hydrogen values for all of the films were between 24% and 31%. For hydrogen estimation using the PL background method the results indicate that the hydrogen content in the samples is independent of doping with Si and the Si-C interlayer. Comparison of hydrogen content is particularly good using both methods for DLC and DLC with Si-C interlayer films. This implies that bonded hydrogen in the films is determined more by the reactive mechanisms that proceed between Ar gas and C$_4$H$_{10}$ gas during the deposition stage of these films.

In all of the coatings a general reduction in internal compressive stress was determined. The combination of CFUBMSIP and PECVD allowed the coatings to be deposited at substrate bias voltages of -30V. This implied that the films were deposited at low temperatures which further imply that the build-up in thermal stresses is inhibited for these films. The lowest reduction to internal compressive stress was observed for Si-DLC films. This was attributed to the chemical structure of silicon. Silicon cannot significantly contribute to internal stress reduction in diamond-like carbon–silicon composite films, since silicon atoms tetrahedrally bond to carbon and other silicon atoms. Si doping reduces the average size of the sp^2 bonded clusters and promotes the formation of sp^3 bonding in the Si-DLC film.

XPS survey scans showed the contributions from C 1s (~285 eV), O 1s (~531 eV), Si 2p (~100 eV) and Si 2s (~151 eV). C-Si (C 1s) and Si-C (Si 2p) configurations corresponding to bonding between carbon and silicon atoms in SiC were observed. Deconvolution of the C 1s peak resulted in the determination of the sp^2 and sp^3 hybridisations in the coatings. Si-DLC and Si-DLC with Si-C interlayer had the highest sp^3 fraction and sp^3/sp^2 ratio. These results confirmed the discussions on surface morphology, Raman analysis and internal compressive stress reduction.

All of the coatings deposited on nitrile rubber were hydrophobic. An increase in the hydrophobic properties of DLC coated elastomers was explained by the presence of a mixture of sp^2 and sp^3 hybridized carbon bonds in the DLC coatings, which is also related to a lower reactivity of the DLC coated surface. The inclusion of the Si-C interlayer increases the surface free energy of the films as a result of supressing the polar component of surface free energy. For Si-DLC with Si-C interlayer the sp^2 fraction is much lower than for DLC with Si-C interlayer.

The deposited coatings showed excellent adherence with an adhesion rating of 4A for films with a Si-C interlayer. The combination of CFUBMSIP and PECVD at low DC substrate bias values implies that the H in the films is not disrupted resulting in films consisting of relatively soft hydrocarbon or polymer-like chains. The presence of hydrogen is usually associated with the development of polymer-like chains. This development of polymer-like chains during film deposition is advantageous as elastomers, including nitrile rubbers, are comprised of flexible polymer chains explaining the good adhesion ratings for these films. Particle bombardment of growing film surfaces causes densification of material and increased adhesion to the substrate. After performing flexibility tests lateral cracks were seen to propagate across the patch crack boundary for all of the coatings creating an island textured structure. The generation of these lateral cracks (high crack density) was credited with enhancing the films to release stress and is an indicator of good adhesion between the film and the substrate. The de-bonding observed in the Si-DLC coatings was attributed to the higher fraction of C-C sp^3 hybridisations.

The composite micro-hardness was highest for DLC coatings at 15.5 GPa for indentation load of 147.1 mN using a Vickers micro-hardness tester. Nano-indentation results show that all of the coatings tested had the same order of nano-mechanical properties with hardness values of approximately 3.6GPa and Elastic modulus values of 35GPa. The determination of the sp^3/sp^2 ratio was helpful in understanding the effects of Si incorporation and the Si-C interlayer on the mechanical properties of the coatings. The low nano-hardness values were attributed to the use of butane gas as a precursor resulting in hydrogenated films with polymer like chains.

All of the coatings showed excellent tribological results with an over 50% reduction in the coefficient of friction compared to uncoated nitrile rubber. There was no penetration of the

coatings for normal loads of 1N and 5N under wet sliding and 1 N normal load under dry sliding, which is important for potential application onto piston seals. These results were attributed to reduction of defects in the sp^2 amorphous carbon networks indicating a more graphitic organization and a decrease of sp^3 C-C hybridisation percentage. Raman analysis of the wear tracks indicated a possibility of increased graphitization during pin-on-disc experiments. After over 100,000 strokes of operation of the piston seal wear test rig, extremely small changes in weight for the coated piston seals were observed with increased crack density of the coatings. The wear mechanisms taking place on the coated and uncoated piston seals were identified as a combination of fatigue and abrasive wear. The results and discussion indicate the potential of applying DLC and Si-DLC with and without Si-C interlayers onto nitrile rubber piston seals.

5.2. Thesis contribution

This thesis has contributed significantly to both academia in the surface engineering field and developmental studies in the following ways:

- Synergies between development work and academia: This study originated from the problem of safe drinking water in Makondo parish as part of Irish Aid developmental initiatives. A surface engineering approach was used to attempt to solve the problem of the wear of the piston seal singly responsible for most handpump interventions. The application of DLC and Si-DLC coatings on nitrile rubber for piston seals used in handpumps has never been carried out before.

- Review of DLC films deposited on nitrile rubber: Chapter Three of this thesis presents a thorough review on the literature on DLC films deposited on rubber substrates. This state of the art review has never been presented before in literature on DLC and DLC based films deposited on nitrile rubber.

- The deposition technology: The combination of CFUBMSIP and PECVD at low substrate bias (-30V) in Ar/C_4H_{10} has never been attempted before for the deposition of DLC and DLC based films deposited on nitrile rubber. This deposition process resulted in the production of unique DLC and Si-DLC films with G peak positions at approximately 1580 cm^{-1} close to the graphite density of states. The 'soft' DLC and Si-DLC films had polymer like chains which enhanced their adhesion to the rubber

substrates. The process design of this thesis involved the production of DLC films and Si-DLC films deposited on nitrile rubber. This categorisation of films deposited on nitrile rubber has never been presented before in the literature for DLC and DLC based films deposited on rubber substrates.

- Characterization and tribological behaviour of DLC and Si-DLC films deposited on nitrile rubber: This thesis presents for the first time efforts to characterize DLC and Si-DLC films with and without Si-C interlayers deposited on nitrile rubber. The role of the Si-C interlayer in enhancing film properties was discussed. Typical characterization techniques were used. However, as a result of the novel deposition technology that was used in this study for nitrile rubber substrates, the film properties presented were very interesting. This thesis also presents for the first time a thorough Raman spectroscopy analysis of DLC based films deposited on rubber substrates. Raman analysis was also performed on the wear track. This study presented for the first time tribological performance for DLC and Si-DLC films deposited on rubber substrates under wet sliding. This had never been presented before in the literature.

- Application of DLC and Si-DLC films onto actual piston seals: This thesis presents the results of DLC, Si-DLC and DLC with Si-C interlayer deposited on actual piston seals. The real application of these coating has never been presented before. In the literature the presentation of results ends with the film properties of DLC and DLC based films deposited on rubber substrates. Translation and transfer onto real applications has not been presented before.

5.3. Recommendations for future work

The following are the recommendations for future work:

- Influence of the variation of substrate bias voltage from 0 to -100 V on DLC and Si-DLC films deposited on nitrile rubber deposited using a combination of CFUBMSIP and PECVD in Ar/C_4H_{10} plasma. Most of the work on DLC deposited on rubber substrate was done at substrate bias voltages ranging from -100 V to -600 V. This implies that the evolution of the film properties when the substrate is biased between 0 to -100 V is not known.

169

- Influence of Si doping on the properties of Si-DLC films deposited on nitrile rubber substrates. The Si (at. %) in this study varied between 2% and 6%. In order to understand completely the influence of doping with Si a comprehensive analysis involving variations of Si (at. %) from 0% to 20% is required. Such a study has not been attempted for Si-DLC films deposited on nitrile rubber.

- Influence of different interlayers deposited under the same deposition technologies. Cr and Ti interlayers have been discussed in the literature as interlayers between DLC films and substrates with mixed film property results. The role of an interlayer particularly for DLC films deposited on rubber substrates continues to be a grey area.

- Tribological testing at different speeds: The tribo-tests in this study were carried out under varying loads (1 N and 5 N) and conditions (dry and wet sliding). The tests were also done using different counterparts (stainless steel and WC-Co). However, the sliding speed was kept constant at 10 cm/s. The influence of sliding speed on the tribological behaviour under the same condition used in this study would be worth considering in the future as sliding speed is known to affect tribological behaviour.

- Longer term testing in the piston seal wear test rig: In order to understand clearly the wear mechanism involved in coated DLC and Si-DLC film, longer term testing is ultimately required. Ideally testing to complete failure would be recommended so that adequate comparisons can be made with uncoated piston seals.

- Water analysis: The coated piston seal are envisaged to operate in handpumps for drinking water supply. As such it is recommended future work investigates the impact of the coated piston seals on the drinking water quality. Such an investigation has never been carried out.

References

[1] WHO and UNICEF, (2010), *JMP Progress on Sanitation and Drinking Water 2010 Update,* , WHO, UNICEF, Geneva & New York.

[2] UNDP, (2009), *Water in a Changing World, World Water Assessment Programme,* (Report No. 3 ed.), Earthscan, Paris & London.

[3] MacDonald, A.M., et al. (2012), "Quantitative maps of groundwater resources in Africa", *Environ. Res. Let.,* Vol.7 pp. 024009.

[4] Vorosmarty, C.J., et al. (2010), "Global threats to human water security and river biodiversity", *Nature,* Vol.467 (7315), pp. 555-561.

[5] Arlosoroff, S., et al., (1987), *Community Water Supply: The Handpump Option,* , The World Bank, Washington D.C.

[6] Reynolds, J., (1992), *Handpumps: Towards a sustainable Technology,* (Report No. 11467 ed.), UNDP-World Bank, Washington D.C.

[7] Erpf, K., (2004), *Technology selection and Buyer's guide for public domain handpumps for drinking water,* Skat-foundation, Resource Centre for Development, At. Gallan, Switzerland.

[8] UNDP and World Bank (1984), *Laboratory tests for handpump use in developing countries,* World Bank, Washington D.C.

[9] Esposto, S. (2009), "The sustainability of applied technologies for water supply in developing countries.", *Technol. Soc.,* Vol.31 pp. 257-262.

[10] Harvey, P.A., (2003), *Sustainable handpump projects in Africa,* Loughborough University, UK.

[11] Black, M., (1998), *Learning what works: A 20 year retrospective view on International Water and Sanitation Cooperation,* World Bank, Washington D.C.

[12] Gleitsmann, B.A.G., Kroma, M.M.and Steenhuis, T., (2007), "Analysis of rural water supply projects in three communities in Mali: Participation and sustainability", *Natural Res. Forum,* Vol.31 pp. 142-150.

[13] Aspegren, H., Hahn, R.and Johansson, P., (1987), *Piston seals for handpumps,* Department of Environmental Engineering, Lund Institute of Technology, University of Lund.

[14] Yau, G.S., (1985), *Laboratory and field testing of handpumps,* , IDRC, Ottawa, Canada.

[15] Nikas, G.K. (2009), "Eighty years of research on hydraulic reciprocating seals: review of tribological studies and related topics since the 1930s", *Proc. IMechE Part J: J. Eng. Tribol.,* Vol.224 pp. 1-23.

[16] van Beers, P. H. 2011, "Reliable low-cost maintenance handpumps are the key for sustainable rural water supply", *R. Shaw, ed., The future of water, sanitation and hygiene: Innovation, adaptation and engagement in a changing world. Proceedings of the 35th WEDC International Conference,*Vol.35, *6-8 July, 2011,*: Loughborough University Loughborough, UK,.

[17] Robertson, J. (2002), "Diamond like amorphous carbon", *Materials Science and Engineering:* Vol.R 37 pp. 129-281.

[18] Martinez, L., et al. (2009), "Application of diamond-like coatings to elastomer frictional surfaces", *Tribology International,* Vol.42 pp. 584-590.

[19] Nakahigashi, T., et al. (2004), "Properties of flexible DLC film deposited by amplitude-modulated RF P-CVD", *Tribology International,* Vol.37 pp. 907-912.

[20] Takikawa, H., et al. (2004), "Fabrication of diamond-like carbon film on rubber by T-shape filtered-arc-deposition under the influence of various ambient gases", *Thin Solid Films,* Vol.457 pp. 143-150.

[21] Miyakawa, N., et al. (2004), "Physical-chemical hybrid deposition of DLC film onto rubber by T-shape filtered-arc deposition", *Vacuum,* Vol.73 pp. 611-617.

[22] Bui, X.L., Pei, Y.T.and De Hosson, J.T.M., (2008), "Magnetron reactively sputtered Ti-DLC coatings on HNBR: The influence of substrate bias", *Surf. Coat. Technol.,* Vol.202 pp. 4939-4944.

[23] Pei, Y.T., et al. (2008), "Tribological behaviour of W-DLC coated rubber seals", *Surf. Coat. Technol.,* Vol.202 pp. 1869-1875.

[24] Pei, Y.T., Bui, X.L.and De Hosson, J.T.M., (2010), "Deposition and characterization of hydrogenated diamond-like carbon films on rubber seals", *Thin Sol. Films,* Vol.518 pp. S42-S45.

[25] Wu, X., et al. (2008), "Characteristics and tribological properties in water of Si-DLC", *Diamond Relat. Mater.,* Vol.17 pp. 7-12.

[26] Ronkainen, H., Varjus, S.and Holmberg, K., (2001), "Tribological performance of different DLC coatings in water lubricated conditions", *Wear,* Vol.249 pp. 267-271.

[27] Masami, I., et al. (2011), "Low temperature Si-DLC coatings on fluoro rubber by a bipolar pulse type PBII system", *Surf. Coat. Technol.,* Vol.206 pp. 999-1002.

[28] Ikeyama, M., et al. (2005), "Effects of Si content in DLC films on their friction and wear properties", *Surf. Coat. Technol.,* Vol.191 pp. 38-42.

[29] Drees, D., et al. (1996), "The electrochemical and wear behaviour of amorphous diamond-like carbon coating and multilayered coatings in aqueous environments", *Surf. Coat. Technol.,* Vol.86-87 pp. 575-580.

[30] Bonelli, M., et al. (2000), "Structural and mechanical properties of diamond-like carbon films prepared by pulsed laser deposition with varying laser intensity", *Mat. Res. Soc. Symp. Proc.,* Vol.593 pp. 359-364.

[31] Zhou, Z.F., et al. (2005), "Study of tribological performance of ECR-CVD diamond-like carbon coatings on steel substrates; Part 2. The analysis of wear mechanism", *Wear,* Vol.258 pp. 1589-1599.

[32] Choi, W.S., Park, M.and Hong, B., (2007), "An examination of trace surface on diamond-like carbon film after ball-on disk measurement", *Thin Sol. Films,* Vol.515 pp. 7560-7565.

[33] Bui, X.L., et al. (2009), "Adhesion improvement of hydrogenated diamond-like carbon thin films by pre-deposition plasma treatment of rubber substrate", *Surf. Coat. Technol.,* Vol.203 pp. 1964-1970.

[34] Martinez-Matrinez, D., et al. (2011), "Microstructural and frictional control of diamond-like carbon films deposited on acrylic rubber by plasma assisted chemical vapour deposition", *Thin Sol. Films,* Vol.519 pp. 2213-2217.

[35] Irish Aid., (2007)*, Programme of Strategic Cooperation between Irish Aid and Higher Education and Research Institutes 2007 - 2011, ,* Department of Foreign Affairs, Ireland, Dublin, Ireland.

[36] Irish Aid., (2010)*, Uganda Country Strategy Paper 2010-2014, ,* Department of Foreign Affairs, Ireland, Dublin, Ireland.

[37] Macri, G., et al. A socio-spatial survey of water issues in Makondo Parish, Uganda. 2013;ISBN: 978-1-873769-30-0:1-47.

[38] Aisenberg, S.and Chabot, R., (1971), "Ion-beam deposition of thin films of diamond-like carbon", *J. Appl. Phys.,* Vol.42 pp. 2953-2958.

[39] Grill, A. (1999), "Diamond-like carbon: state of the art", *Diamond & Rel. Mater.,* Vol.8 pp. 428-434.

[40] Grill, A. (1997), "Tribology of diamond-like carbon and related materials: an updated review", *Surf. Coat. Technol.,* Vol.94-95 pp. 507-513.

[41] Singha, A., et al. (2006), "Quantitative analysis of hydrogenated diamondlike carbon films by visible Raman spectroscopy", *J. Appl. Phys.,* Vol.100 pp. 044910.

[42] Casiraghi, C., Ferrari, A.C.and Robertson, J., (2005), "Raman spectroscopy of hydrogenated amorphous carbons", *Phys. Rev. B,* Vol.72 pp. 085401.

[43] Robertson, J. (1986), "Amorphous carbon", *Adv. Phys.,* Vol.35 pp. 317-374.

[44] Donnet, C. andErdemir, A.(2008), "Diamond-like Carbon Films: A Historical Overview", *in C. Donnet andA. Erdemir, eds., Tribology of Diamond-Like Carbon Films,* Springer Science + Business Media, LLC, 233 Spring Street, New York, NY 10013, USA, pp. 1-10.

[45] Persson, B.N.J. (2006), "Rubber friction: role of the flash temperature", *J. Phys. Condens. Matter.,* Vol.18 pp. 7789-7823.

[46] Myshkin, N.K., Petrokovets, M.I.and Kovalev, A.V., (2005), "Tribology of polymers: Adhesion, friction, wear and mass transfer", *Tribol. Int.,* Vol.38 pp. 910-921.

[47] Schallamach, A. (1968), "Abrasion, fatigue and smearing of rubber", *J. Appl. Polym. Sci.,* Vol.12 pp. 281-293.

[48] Grosch, K.A.and Schallamach, A., (1965), "Relation between abrasion and strength of rubber", *Trans.Inst. Rubber Ind,* Vol.41 pp. 80-82.

[49] Karger-Kocsis, J. andFelhos, D.(2008), "Friction and sliding wear of "nanomodified" rubbers and their coatings: Some new developments", *in K. Friedrich andA.K. Schlarb, eds., Tribology of Polymeric Nanocomposites: Friction and wear of bulk materials and coatings,* Elsevier, Oxford, UK, pp. 304-324.

[50] Matthews, A.and Eskildsen, S.S., (1994), "Engineering applications for diamond-like carbons", *Diamond & Rel. Mater.,* Vol.3 pp. 902-911.

[51] Liu, Y., Erdemir, A.and Meletis, E.I., (1996), "An investigation of the relationship between graphitization and frictional behavior of DLC coatings", *Surf. Coat. Technol.,* Vol.86-87 pp. 564-568.

[52] Erdemir, A. (2001), "The role of hydrogen in tribological properties of diamond-like carbon films", *Surf. Coat. Technol.,* Vol.146-147 pp. 292-297.

[53] Fukui, H., et al. (2001), "An investigation of the wear track of DLC (a-C:H) film by time-of-flight secondary ion mass spectroscopy", *Surf. Coat. Technol.,* Vol.146-147 pp. 378-383.

[54] Donnet, C. (1998), "Recent progress on the tribology of doped diamond-like and carbon alloy coatings: a review", *Surf. Coat. Technol.,* Vol.100-101 pp. 180-186.

[55] Oguri, K.and Arai, T., (1990), "Low friction coatings of diamond-like carbon with silicon prepared by plasma-assisted chemical vapour deposition", *J. Mater. Res.,* Vol.5 pp. 2567-2571.

[56] Hauert, R.and Muller, U., (2003), "An overview of tailored tribological and biological behaviour of diamond-like carbon", *Diamond & Rel. Mater.,* Vol.12 pp. 171-177.

[57] Holmberg, K. and Matthews, A., (2009), *Coatings tribology-properties, mechanisms, techniques and applications in surface engineering,* (2nd ed.), Elsevier, Amsterdam, The Netherlands.

[58] Pei, Y.T., et al. (2008), "Microstructure and tribological behavior of tungsten-containing diamondlike carbon coated rubbers", *J.Vac. Sci. Technol. A,* Vol.26 pp. 1085-1092.

[59] Tashlykov, I.S., et al. (1999), "Elastomer treatment by arc metal deposition assisted with self-ion irradiation", *Surf. Coat. Technol.,* Vol.116-119 pp. 848-852.

[60] Tashlykov, I.S., Kasperovich, A.V.and Wolf, G.K., (2002), "Elastomer surface modification by means of SIAD of metal-based layers", *Surf. Coat. Technol.,* Vol.158-159 pp. 498-502.

[61] Gilmore, R.and Hauert, R., (2001), "Control of the tribological moisture sensitivity of diamond-like carbon films by alloying with F, Ti, or Si", *Thin Sol. Films,* Vol.398-399 pp. 199-204.

[62] Gangopadhyay, A.K., et al. (1997), "Amorphous hydrogenated carbon films for tribological application I. Development of moisture insensitive films having reduced compressive stress", *Tribol. Int.,* Vol.30 pp. 9-18.

[63] Michler, T., et al. (1999), "Continuously deposited duplex coatings consisting of plasma nitriding and a-C:H:Si deposition", *Surf. Coat. Technol.,* Vol.111 pp. 41-45.

[64] Bunshah, R.F.and Deshpandey, C.V., (1985), "Plasma assisted physical vapour deposition precesses: A review", *J. Vac. Sci. Tech. A,* Vol.3 pp. 553-560.

[65] Martin, P.M. editor. (2009), *Handbook of Deposition Technologies for Films and Coatings,* Third ed., Elsevier, UK.

[66] Verheyde, B., et al. (2009), "Influence of surface treatment of elastomers on their frictional behaviour in sliding contact", *Wear,* Vol.266 pp. 468-475.

[67] Martinez, L., et al. (2007), "Surface analysis of NBR and HNBR elastomers modified with different plasma treatments", *Vacuum,* Vol.81 pp. 1489-1492.

[68] Martinez-Matrinez, D., et al. (2011), "Microstructure and chemical bonding of DLC films deposited on ACM rubber by PACVD", *Surf. Coat. Technol.,* Vol.205 pp. S75-S78.

[69] Schenkel, M., et al. (2011), "Tribological performance of DLC films deposited on ACM by PACVD", *Surf. Coat. Technol.,* Vol.205 pp. 4838-4843.

[70] Pei, Y.T., Bui, X.L.and De Hosson, J.T.M., (2010), "Flexible protective diamond-like carbon film on rubber", *Scr. Mater.,* Vol.63 pp. 649-652.

[71] Kelly, P.J.and Arnell, R.D., (2000), "Magnetron sputtering: a review of recent developments and applications", *Vacuum,* Vol.56 pp. 159-172.

[72] Grove, W.R. (1852), "On the electro-chemical polarity of gases", *Phil. Trans. R. Soc. Lond.,* Vol.142 pp. 87-101.

[73] Depla, D., Mahieu, S.and Green, J.E.(2009), "Sputter Deposition Process", *in P.M. Martin, ed., Handbook of deposition technologies for films and coatings,* (Third ed.), Elsevier, UK, pp. 253-296.

[74] Fox, V., Hampshire, J.and Teer, D.G., (1999), "MoS2 metal composite coatings deposited by closed-field unbalanced magnetron sputtering: tribological properties and industrial uses", *Surf. Coat. Technol.,* Vol.112 pp. 118-122.

[75] Rossnagel, S.M.and Cuomo, J.J., (1988), "Ion beam bombardment effects during films deposition", *Vacuum,* Vol.38 pp. 73-81.

[76] Savvides, N.and Window, B., (1986), "Unbalanced magnetron ion-assisted deposition and property modification of thin films", *J. Vac. Sci. Technol. A,* Vol.4 pp. 504-508.

[77] Window, B.and Savvides, N.J., (1986), "Unbalanced DC magnetrons as sources of high ion fluxes", *J. Vac. Sci. Technol. A,* Vol.4 pp. 453-456.

[78] Monaghan, D.P., et al. (1993), "Deposition of wear resistant coatings based on diamond like carbon by unbalanced magnetron sputtering", *Surf. Coat. Technol.,* Vol.60 pp. 525-530.

[79] Munz, W.D., et al. (1991), "A new concept for physical vapour deposition coating combining the methods of arc evaporation and unbalanced-magnetron sputtering", *Surf. Coat. Technol.,* Vol.49 pp. 161-167.

[80] Sproul, W.D., et al. (1990), "High rate reactive sputtering in an opposed cathode closed-field unbalanced magnetron sputtering system", *Surf. Coat. Technol.,* Vol.43-44 pp. 270-278.

[81] Safi, I. (2000), "Recent aspects concerning DC reactive magnetron sputtering of thin films: a review", *Surf. Coat. Technol.,* Vol.127 pp. 203-219.

[82] Sproul, W.D., Christie, D.J.and Carter, D.C., (2005), "Control of reactive sputtering processes", *Thin Sol. Films,* Vol.491 pp. 1-17.

[83] Fouad, O.A., Rumaiz, A.K.and Shah, I., (2009), "Reactive sputtering of titanium in Ar/CH4 gas mixture: Target poisoning and film characteristics", *Thin Sol. Films,* Vol.517 pp. 5689-5694.

[84] Berg, S.and Nyberg, T., (2005), "Fundamental understanding and modeling of reactive sputtering processes", *Thin Sol. Films,* Vol.476 pp. 215-230.

[85] Thornton, J.A. (1974), "Influence of apparatus geometry and deposition conditions on the structure and topography of thick sputtered coatings", *J.Vac. Sci. Technol.,* Vol.11 pp. 666-670.

[86] Messier, R., Giri, A.P.and Roy, R.A., (1984), "Revised structure zone model for thin film physical structure", *J. Vac. Sci. Technol. A,* Vol.2 pp. 500-503.

[87] Kelly, P.J.and Arnell, R.D., (1998), "Development of a novel structure zone model relating to the closed-field unbalanced magnetron sputtering system", *J. Vac. Sci. Technol. A,* Vol.16 pp. 2858-2869.

[88] Aoki, Y.and Ohtake, N., (2004), "Tribological properties of segment-structured diamond-like carbon films", *Tribol. Int.,* Vol.37 pp. 941-947.

[89] Yoshida, S., Okoshi, M.and Inoue, N., (2007), "Femtosecond-pulsed laser deposition of diamond-like carbon films onto silicone rubber", *J. Phys.: Conf. Ser.,* Vol.59 pp. 368-371.

[90] Mattox, D.M., (2010), "Non-elemental characterization of films and coatings", *in P.M. Martin, ed., Handbook of deposition technologies in films and coatings,* (Third ed.), Elsevier, UK, pp. 716-748.

[91] Ferrari, A.C.and Robertson, J., (2001), "Resonant Raman spectroscopy of disordered, amorphous, and diamondlike carbon", *Phys. Rev. B,* Vol.64 pp. 075414.

[92] Ferrari, A.C.and Robertson, J., (2004), "Raman Spectroscopy in Carbons: From Nanotubes to Diamond", *Philos. Trans. R. Soc. London A,* Vol.362 pp. 2269-2270.

[93] Piscanec, S., et al. (2005), "Ab initio resonant Raman spectra of diamond-like carbons", *Diamond & Rel. Mater.,* Vol.14 pp. 1078-1083.

[94] Gilkes, K.W.R., et al. (2000), "Direct quantitative detection of the sp3 bonding in diamond-like carbon films using ultraviolet and visible Raman spectroscopy", *J. Appl. Phys.,* Vol.87 pp. 7283-7289.

[95] Ferrari, A.C.and Robertson, J., (2000), "Interpretation of Raman spectra of disordered and amorphous carbon", *Phys. Rev. B,* Vol.61 pp. 14095-14107.

[96] Nishitani-Gamo, M., et al. (1997), "A nondiamond phase at the interface between oriented diamond and Si (100) observed by confocal Raman spectroscopy", *Appl. Phys. Lett.,* Vol.70 pp. 1530-1532.

[97] Nistor, L.C., et al. (1997), "Nanocrystalline diamond films: transmission electron microscopy and Raman spectroscopy characterization", *Diamond & Rel. Mater.,* Vol.6 pp. 159-168.

[98] Shroder, R.E.and Nemanich, R.J., (1990), "Analysis of the composite structures in diamond thin films by Raman spectroscopy", *Phys. Rev. B,* Vol.41 pp. 3738-3745.

[99] Ferrari, A.C.and Robertson, J., (2001), "Origin of the 1150-cm-1 Raman mode in nanocrystalline diamond", *Phys. Rev. B,* Vol.63 pp. 121405.

[100] Jaoul, C., et al. (2009), "Raman analysis of DLC coated engine components with complex shape: Understanding wear mechanisms", *Thin Sol. Films,* Vol.518 pp. 1475-1479.

[101] Pei, Y.T., et al. (2008), "Microstructural control of TiC/a-C nanocomposite coatings with pulsed magnetron sputtering", *Acta Mater.,* Vol.56 pp. 696-709.

[102] Kiuru, M.and Alakoski, E., (2004), "Low sliding angles in hydrophobic and oleophobic coatings prepared with plasma discharge method", *Mater. Lett.,* Vol.58 pp. 2213-2216.

[103] Alisoy, H.Z., Baysar, A.and Alisoy, G.T., (2005), "Physicomathematical analysis of surface modification of polymers by glow discharge in SF6+N2 medium", *Physica A,* Vol.351 pp. 347-357.

[104] Tiainen, V.M. (2001), "Amorphous carbon as a bio-mechanical coating - mechanical properties and biological applications", *Diamond & Rel. Mater.,* Vol.10 pp. 153-160.

[105] American Society for Testing and Materials. Standard test methods for measuring adhesion by tape test. ASTM D: 3359-97 1998:368.

[106] Trakhtenberg, I.S., et al. (2000), "Substrate surface temperature as a decisive parameter for diamond-like carbon film adhesion to polyethylene substrates", *Diamond & Rel. Mater.,* Vol.9 pp. 711-714.

[107] Guo, Y.-.and Hong, C.-., (2003), "Adhesion improvement of diamond-like carbon films on polycarbonate and polymethylmethacrylate substrates by ion plating with inductively coupled plasma", *Diamond & Rel. Mater.,* Vol.12 pp. 946-952.

[108] Pei, Y.T., et al. (2012), "Flexible diamond-like carbon films on rubber: On the origin of self acting segmentation and film flexibility", *Acta Mater.,* Vol.60 pp. 5526-5335.

[109] Pei, Y.T., et al. (2012), "Flexible diamond-like carbon films on rubber: Friction and the effect of viscoelastic deformation of rubber substrates", *Acta Mater.,* Vol.60 pp. 7216-7225.

[110] Tsubone, D., et al. (2007), "Fracture mechanics of diamond-like carbon (DLC) films coated on flexible polymer substrates", *Surf. Coat. Technol.,* Vol.201 pp. 6423-6430.

[111] Zhang, S., Bui, X.L.and Fu, Q., (2003), "Magnetron sputtered hard a-C coatings of very high toughness", *Surf. Coat. Technol.,* Vol.167 pp. 137-142.

[112] Hutchings, I.M., (1992)*, Tribology, ,* Arnold, London.

[113] Rabinowicz, E., (1965)*, Friction and wear of materials, ,* Wiley, New York.

[114] Voevodin, A.A., et al. (1996), "Friction induced phased transformation of pulsed laser deposited diamond-like carbon", *Diamond & Rel. Mater.,* Vol.5 pp. 1264-1269.

[115] Stallard, J., et al. (2004), "A study of the tribological behaviour of three carbon-based coatings tested in air, water and oil environments at high loads", *Surf. Coat. Technol.,* Vol.177-178 pp. 545-551.

[116] Donnet, C., et al. (1998), "The respective role of oxygen and water vapour on the tribology of hydrogenated diamond-like carbon coatings", *Tribol. Lett.,* Vol.4 pp. 259-265.

[117] Erdemir, A., et al. (2000), "Effect of source gas chemistry on tribological performance of diamond-like carbon films", *Diamond & Rel. Mater.,* Vol.9 pp. 632-637.

[118] Kato, K., (2005), "Classification of wear mechanisms/models", *in G.W. Stachowiak, ed., Wear: Materials, Mechanisms and Practice,* John Wiley and Sons, England, UK, pp. 9-20.

[119] Archard, J.F. (1953), "Contact and rubbing of flat surfaces", *J. Appl. Phys.,* Vol.24 pp. 981-988.

[120] Hwang, W.-., Wei, K.-.and Wu, C.-., (2004), "Preparation and mechanical properties of nitrile butadiene rubber/silicate nanocomposites", *Polymer,* Vol.45 pp. 5729-5734.

[121] Hertz Jr, D.L., (2001), "Introduction", *in A.N. Gent, ed., Engineering with rubber: How to design rubber components,* (Second ed.), Hanser Gardner Inc., Cincinnati, USA, pp. 1-9.

[122] Garbarczyk, M., et al. (2002), "Characterization of aged nitrile rubber elastomers by NMR spectroscopy and microimaging", *Polymer,* Vol.43 pp. 3169-3172.

[123] Katritzky, A.R.and Weiss, D.E., (1974), "Nuclear Magnetic Resonance spectroscopy of polymers. Part II. Determination of monomer sequence distribution in butadiene - acrylonitrile copolymer", *J. Chem. Soc. Perkin Trans. II,* pp. 1542-1547.

[124] Willoughby, B.G. (1989), "A structural analysis of nitrile rubbers - the 13C resonance technique", *Polym. Test.,* Vol.8 pp. 45-70.

[125] Hamed, G.R., (2001), "Materials and compounds", *in A.N. Gent, ed., Engineering with rubber: How to design rubber components,* (Second ed.), Hanser Gardner Inc., Cincinnati, USA, pp. 13-34.

[126] Hayashi, S., et al. (1991), "Low-temperature properties of hydrogenated nitrile rubber (HNBR)", *Rubber Chem. Technol.,* Vol.64 pp. 534-544.

[127] Ludema, K.C., (1996)*, Friction, wear,lubrication: a textbook in tribology,* , CRC Press, Boca Raton, Florida.

[128] Abu Bakar, T.A. , (2012), "Tribological investigation of nickel titanium shape memory alloy (NITI SMA) coatings", PhD, Dublin City University, Dublin, Ireland.

[129] DataPhysics Instruments GmbH., (2002)*, Operating manual DataPhysics OCA,* , DaraPhysics Instruments GmbH, Filderstadt, Gemany.

[130] Okuji, S., et al. (2009), "Characteristics of poly(vinylidene difluoride) modified by plasma-based ion implantation", *Nucl. Instrum. Meth. B,* Vol.267 pp. 1557-1560.

[131] Dilsiz, N.and Wightman, J.P., (2000), "Effect of acid-base properties of unsized and sized carbon fibres on fiber/epoxy matrix adhesion", *Colloids Surf. A,* Vol.164 pp. 325-336.

[132] Chu, P.K.and Li, L., (2006), "Characterization of amorphous and nanocrystalline carbon films", *Mater. Chem. Phys,* Vol.96 pp. 253-277.

[133] Friel, J.J., (2003)*, X-ray and image analysis in electron microscopy,* (2nd ed.), Princeton Gamma-Tech. Inc., Princeton, New Jersey.

[134] Irmer, G.and Reisel, A.D., (2005), "Micro Raman studies on DLC coatings", *Adv. Eng. Mater.,* Vol.7 pp. 694-705.

[135] Yoshikawa, M., et al. (1988), "Raman spectra of diamond like amorphous carbon films.", *J. Appl. Phys.,* Vol.64 pp. 6464-6468.

[136] Wagner, J., et al. (1989), "Resonant Raman scattering of amorphous carbon and polycrystalline diamond films", *Phys. Rev. B,* Vol.40 pp. 1817-1824.

[137] Chalker, P.R., (1991), "Characterization of diamond and diamond-like films", *in R.E. Clausing, ed., Diamond and Diamond-like Films and Coatings,* Plenum Press, New York, pp. 127-150.

[138] Nathan, M.I., Smith Jr, J.E.and Tu, K.M., (1974), "Raman-spectra of glassy carbon", *J. Appl. Phys.,* Vol.45 pp. 2370.

[139] Robertson, J. (1992), "Properties of diamond-like carbon", *Surf. Coat. Technol.,* Vol.50 pp. 185-203.

[140] Tamor, M.A.and Vassell, W.C., (1994), "Raman "fingerprinting" of amorphous carbon films", *J.Appl. Phys.,* Vol.76 pp. 3823.

[141] Filik, J., et al. (2003), "XPS and laser Raman analysis of hydrogenated amorphous carbon films", *Diamond Relat. Mater.,* Vol.12 pp. 974-978.

[142] Matthews, M.J., et al. (1999), "Origin of dispersive effects of the Raman D band in carbon materials", *Phys. Rev. B,* Vol.59 pp. R6585-R6588.

[143] Cui, W.G., et al. (2010), "Quantitative measurements of sp3 content in DLC films with Raman spectroscopy", *Surf. Coat. Technol.,* Vol.205 pp. 1995-1999.

[144] Narayan, R.J. (2005), "Laser processing of diamond-like carbon-metal composites", *Appl. Surf. Sci,* Vol.245 pp. 420-430.

[145] Nakamatsu, K., et al. (2005), "Mechanical characteristics and its annealing effect of diamondlike-carbon nanosprings fabricated by focused-ion-beam chemical vapor deposition", *J. Vac. Sci. Technol. B,* Vol.23 pp. 2801-2805.

[146] De Wolf, I. (1996), "Micro-Raman spectroscopy to study local mechanical stress in silicon integrated circuits", *Semicond. Sci. Technol,* Vol.11 pp. 139-154.

[147] Ahmed, S.F., et al. (2011), "Visible photoluminescence from silicon incorporated diamond-like carbon films synthesized via direct current PECVD technique", *J. Lumin.,* Vol.131 pp. 2352-2358.

[148] Teo, K.B.K., et al. (2002), "Highest optical gap tetrahedral amorphous carbon", *Diamond Relat. Mater.,* Vol.11 pp. 1086-1090.

[149] Diaz, J., et al. (1996), "Separation of the sp3 and sp2 components in the c1s photoemission spectra of amorphous carbon films", *Phys. Rev. B,* Vol.54 pp. 8064-8069.

[150] Li, L.H., et al. (2002), "Structural analysis of arc deposited diamond-like carbon films by Raman and X-ray photoelectron spectroscopy", *Mater. Sci. Eng. B,* Vol.94 pp. 95-101.

[151] Haerle, R., et al. (2002), "sp2/sp3 hydridization ratio in amorphous carbon from C 1s core-level shifts: C-ray photoelectron spectroscopy and first principles calculation", *Phys. Rev. B,* Vol.65 pp. 045101-045110.

[152] Merel, P., et al. (1998), "Direct evaluation of the sp3 content in diamond-like-carbon films", *Appl. Surf. Sci.,* Vol.136 pp. 105-110.

[153] Chen, D.and Jing, G.Y., (2002), "The determination of sp3 fraction in tetrahedral amorphous carbon films by Raman and X-ray photoelectron spectroscopy", *Int. J. Mod. Phys. B,* Vol.16 pp. 4413-4417.

[154] Yan, X.B., et al. (2004), "Characterization of hydrogenated diamond-like carbon films electrochemically deposited on a silicon substrate", *J. Phys. D. Appl. Phys.,* Vol.37 pp. 2416-2424.

[155] Zhao, J.F., et al. (2000), "The effects of Si incorporation on the microstructure and nanomechanical properties of DLC thin films", *J. Phys. Condens. Matter.,* Vol.12 pp. 9201-9213.

[156] Baglin, J.E.E., (1995), "Interface structure, adhesion and ion beam processing", *in Y. Pauleau, ed., Materials and processes for surface and interface engineering,* 290, Kluwer Academic, Dordrecht, The Netherlands, pp. 111.

[157] Ollivier, B.and Matthews, A., (1994), "Adhesion of diamond-like carbon films on polymers: an assessment of the validity of the scratch test technique applied to flexible substrates", *J. Adhes. Sci. Technol.,* Vol.8 pp. 651-662.

[158] Vaughn, G.D., Frushour, B.G.and Dale, W.C., (1994), "Scratch indentation, a simple adhesion test method for films on polymeric supports", *J. Adhes. Sci. Technol.,* Vol.8 pp. 635-650.

[159] Freeman, M.J.and Harding, D.R., (1994), "Plasma enhanced deposition of diamond-like carbon films on high temperature tolerant polymers", *J. Polym. Sci. B,* Vol.32 pp. 1377-1388.

[160] Oliver, W.C.and Pharr, G.M., (1992), "An improved technique for determining hardness and elastic modulus using load and displacement sensing indentation experiments", *J. Mater. Res.,* Vol.7 pp. 1564-1583.

[161] Liu, Y., Erdemir, A.and Meletis, E.I., (1996), "A study of the wear mechanism of diamond-like carbon films", *Surf. Coat. Technol.,* Vol.82 pp. 48-56.

[162] Bonny, K., et al. (2009), "EDM machinability and dry sliding friction of WC-Co cemented carbides", *Int. J. Manufacturing Research,* Vol.4 pp. 375-394.

[163] Mofidi, M. , (2009), "Tribology of elastomeric seal materials", PhD, Lulea University of Technology, Lulea, Sweden.

[164] Moore, D.F. (1980), "Friction and wear in rubbers and tyres", *Wear,* Vol.61 pp. 273-282.

[165] Papakonstanitinou, P., et al. (2002), "The effects of Si incorporation on the electrochemical and nanomechanical properties of DLC thin films", *Diamond Relat. Mater.,* Vol.11 pp. 1074-1080.

[166] Paul, R., et al. (2008), "Synthesis of DLC films with different sp2/sp3 ratio and their hydrophobic behaviour", *J. Phys. D. Appl. Phys.,* Vol.41 pp. 055309.

[167] Wasa, K. and Hayakawa, S. eds. (1992), *Handbook of sputter deposition technology: Principles, Technology and Application,* Noyes Publications, New Jersey, USA.

[168] Helmersson, U., et al. (2006), "Ionized physical vapour deposition (IPVD): A review of technology and applications", *Thin Sol. Films,* Vol.513 pp. 1-24.

[169] Tuinstra, F.and Koenig, J.L., (1970), "Raman spectrum of graphite", *J. Chem. Phys.,* Vol.53 pp. 1126-1130.

[170] Lackner, J.M., et al. (2009), "RF deposition of soft hydrogenated amorphous carbon coatings for adhesive interfaces on highly elastic polymer materials", *Surf. Coat. Technol.,* Vol.2003 pp. 2243-2248.

[171] Schwan, J., et al. (1996), "Raman spectroscopy on amorphous carbon films", *J. Appl. Phys.,* Vol.80 pp. 440-447.

[172] Paik, N. (2005), "Raman and XPS studies of DLC films prepared by a magnetron sputter-type negative ion source", *Surf. Coat. Technol.,* Vol.200 pp. 2170-2174.

[173] Casiraghi, C., et al. (2005), "Bonding in hydrogenated diamond-like carbon by Raman spectroscopy", *Diamond Relat. Mater.,* Vol.14 pp. 1098-1102.

[174] Casiraghi, C. (2011), "Effect of hydrogen on the UV Raman intensities of diamond-like carbon", *Diamond & Rel. Mater.,* Vol.20 pp. 120-122.

[175] Gilkes, K.W.R., et al. (1997), "Direct observation of sp3 bonding in tetrahedral amorphous carbon using ultraviolet Raman spectroscopy", *Appl. Phys. Lett.,* Vol.70 pp. 1980-1982.

[176] Robertson, J. (1988), "Clustering and gap states in amorphous carbon", *Phil. Mag. Lett.,* Vol.57 pp. 143-148.

[177] Robertson, J.and O'Reilly, E., (1987), "Electronic and atomic structure of amorphous carbon", *Phys. Rev. B,* Vol.35 pp. 2946-2957.

[178] Silva, S.R.P., et al. (1996), "Structure and luminescence properties of an amorphous hydrogenated carbon", *Philos. Mag. B,* Vol.74 pp. 369-386.

[179] Peng, X.L.and Clyne, T.W., (1998), "Residual stress and debonding of DLC films on metallic substrates", *Diamond Relat. Mater.,* Vol.7 pp. 944-950.

[180] Benndorf, C., et al. (1996), "Photoelectron spectroscopic investigations and exoelectron emission of CVD diamond surfaces modified with oxygen and potassium", *Diamond Relat. Mater.,* Vol.5 pp. 784-789.

[181] Srisang, C., et al. (2012), "Characterization of SiC in DLC/a-Si films prepared by pulsed filtered cathodic arc using Raman spectroscopy and XPS", *Appl. Surf. Sci.,* Vol.258 pp. 5605-5609.

[182] Pauleau, Y., (2008), "Residual stresses in DLC films and adhesion to various substrates", *in C. Donnet andA. Erdemir, eds., Tribology of diamond-like carbon films,* Springer, New York, pp. 102-136.

[183] Hainsworth, S.V.and Page, T.F., (1997), "Mechanical property data for coated systems-The prospects for measuring coating only properties using nanoindentation", *Mater. Res. Soc. Symp. Proc.,* Vol.436 pp. 171-176.

[184] Capote, G.and Freire Jr, F.L., (2004), "Production and characterization of hydrogenated amorphous carbon thin films deposited in methane plasmas diluted by noble gases", *Mat. Sci. Eng. B,* Vol.112 pp. 101-105.

[185] Jemmer, P. (1999), "Mathematical modelling and interpretation of reactive plasma chemistry", *Math. Comput. Model.,* Vol.30 pp. 61-76.

[186] Jiang, J., Zhang, S.and Arnell, R.D., (2003), "The effect of relative humidity on wear of diamond-like carbon coating", *Surf. Coat. Technol.,* Vol.167 pp. 221-225.

[187] Tillman, W., Vogli, E.and Hoffmann, F., (2009), "Wear-resistant and low-friction diamond-like carbon (DLC) layers for industrial tribological applications under humid conditions", *Surf. Coat. Technol.,* Vol.204 pp. 1040-1045.

[188] Ozmen, Y., Tanaka, A.and Sumiya, T., (2000), "The effect of humidity on the tribological behaviour of diamond like carbon (DLC) film coated on WC-Co by physical vapouur deposition method", *Surf. Coat. Technol.,* Vol.133-134 pp. 455-459.

[189] Liu, Y., Erdemir, A.and Meletis, E.I., (1997), "Influence of environmental parameters on the frictional behaviour of DLC coatings", *Surf. Coat. Technol.,* Vol.94-95 pp. 463-468.

[190] Sen, U., Sen, S.and Yilmaz, F., (2005), "Effects of process time on the tribological properties of boronized GGG-80 ductile cast iron", *Ind. Lubr. Trib.,* Vol.57 pp. 243-248.

[191] Kurzenhauser, S., et al. (2008), "Tribological characterization and numerical wear simulation of microcomponents under sliding and rolling conditions", *Microsyst. Technol.,* Vol.14 pp. 1839-1846.

[192] Liu, H., Tanaka, A.and Kumagai, T., (1999), "Influence of sliding materials on the tribological behaviour of diamond-like carbon films", *Thin Sol. Films,* Vol.352 pp. 145-150.

[193] Le Huu, T., et al. (1996), "Transformation of sp3 to sp2 sites of diamond like carbon coatings during friction in vacuum and under water vapour environment", *Thin Sol. Films,* Vol.290-291 pp. 126-130.

[194] Jiang, J.and Arnell, R.D., (1998), "The effect of sliding speed on wear of diamond-like carbon coatings", *Wear,* Vol.218 pp. 223-231.

[195] Jiang, J., Arnell, R.D.and Tong, J., (1998), "An investigation into the tribological behaviour of DLC coatings deposited on sintered ferrous alloy substrate", *Wear,* Vol.214 pp. 14-22.

[196] Sanchez-Lopez, J.C., et al. (2003), "Friction-induced structural transformations of diamondlike carbon coatings under various atmospheres", *Surf. Coat. Technol.,* Vol.163-164 pp. 444-450.

[197] Flasker, J., et al. (2001), "Numberical simulation of surface pitting due to contact loading", *Int. J. Fatigue,* Vol.23 pp. 599-605.

[198] Hutchings, I.M. (2002), "Abrasion processes in wear and manufacturing", *Proc. IMechE Part J: J. Eng. Tribol.,* Vol.216 pp. 55-62.

[199] Martinez-Martinez, D., et al. (2011), "Performance of diamond-like carbon protected rubber under cyclic friction. I. Influence of substrate viscoelasticity on the depth evolution", *J. Appl. Phys.,* Vol.110 pp. 124906.

[200] Pezon, C. and Bassono, R., (2013)*, The cost of handpump water supply services in the Sahel (In French),* IRC, International Water and Sanitation Service, The Hague, The Netherlands.

Appendices

Appendix A: Field visit questionnaires

Dear Facilitator/Researcher,

OBJECTIVES OF THE SUSTAINABLE HANDPUMP TECHNOLOGIES PROJECT AND HOW IT IS BEING IMPLEMENTED

Thank you for your interest in this project. The overall aim of this project is to improve the sustainability, availability and reliability of handpumps used in your community. In order to achieve this aim, the implementation of this project has been divided into three stages:

Stage 1 aims to ground the handpump in Makondo Parish. Structured interviews will be held with women, men and children in Makondo Parish, as well as handpump mechanics in Makondo. Issues pertaining to handpump water supply, maintenance, technical, financial and social issues will be discussed with handpump users. The main aim of this stage of the project will be to quantify user responses to the wear of piston seals.

Stage 2 of the project will involve friction and wear investigation of particular surface coatings applied on nitrile rubber in order to determine the possibility of using these coatings on piston seals for use in handpumps. The final stage of the project will be the deposition of coatings with the most promising results onto actual piston seals. These will be tested in a piston seal wear test rig developed in Dublin City University.

Therefore, administering these questionnaires and/or conducting interviews with the community as a means of finding out what the handpump users actually think about the handpumps in their communities is a crucial requirement for stage 1 of this project. As such, anything that you the facilitator can do to help the users communicate their actual thought and intentions will be greatly appreciated.

HANDPUMP USERS/COMMUNITY QUESTIONNAIRE

Due to ethical considerations, it would be desirable for this questionnaire to be administered in the presence of a facilitator who is known to the community/users. The interviews will be carried out by the researcher who will be accompanied by the facilitator.

The main aim of the questionnaire is to determine the perception of users towards the handpumps installed in their communities. It will be critical to understand how the users cope with the failures of the handpumps.

The questionnaire is divided into four sections. Section 1 includes introductory questions related to the community. In section 2, cards with pictures of different handpumps will be used to obtain user preferences. Using these pictures, users will be able to communicate the problems of the different pumps located in their communities. Section 3 covers issues pertaining to handpump maintenance. It covers breakdowns, repairs and care for the handpumps. Finally, in section 4, the institutional arrangements within the community will be covered.

COMPLETING THE QUESTIONNAIRE: NOTES TO THE FACILITATOR

The handpump users' evaluation of their own situation is important for the success of the interview. It is important that women and children are the main respondents in the interviews and are allowed to dominate the interview without any bias whatsoever from the interviewer. The questionnaire structure is straight forward, except in section 2 where picture cards will be used to garner users' perceptions of the pumps in their communities.

The purpose of the cards with pictures of different handpumps is to primarily guide the users in recognizing the different types of handpumps found in their areas. Through display of the cards discussion should be generated about the problems the users have concerning the particular handpumps in their areas, and any mitigation measures towards these problems. The display of the cards should be random. This will be achieved by shuffling the cards each time they are displayed.

In order to facilitate this section, the users will play two games with the cards. In the first game, the cards will be shuffled, after which, each of the respondents will be asked how many of each type of handpump they have in their area. In the second game, the cards will be shuffled again and this time the users will be asked what problems they face when using handpumps. As a result of this interaction with the users the interviewer will be building capacity amongst the users concerning the handpumps in their communities.

The rest of the questionnaire is generally structured in a straight forward manner and do not require any special instructions. However, should further clarification be required, please contact any of the following:

Michael Lubwama

Makerere University
Faculty of Technology
P.O. Box 7062
Kampala, Uganda
michael.lubwama2@mail.dcu.ie

Arleen Folan
Project Manager
Water is Life Project
arleen.folan@dkit.ie

SUSTAINABLE HANDPUMP TECHNOLOGIES
AN IRISHAID/HEA – FUNDED PROJECT UNDER THE WATER IS LIFE PROJECT
A JOINT PROJECT BETWEEN IRISH HIGHER INSTITUTIONS AND MAKERERE UNIVERSITY

HANDPUMP USERS' QUESTIONNAIRE

This questionnaire forms part of the Sustainable Handpump Technologies project. Thank you for taking time out and answering this questionnaire. Your contribution to the project is highly appreciated.

Section 1: Introductory questions about the community
Today's date (dd/mm/yy)

Village GPS co-ordinates

1.1 Community information

Name		Parish	
Name of nearest town			
Number of people (Approx.)			

1.2 Description of person(s) being interviewed:

Number of men			
Number of Women			
Number of children			
Number of pump users			
Number of pump caretakers	Women		Men	

Section 2: Background information, basic preferences and problems
Please refer to interviewer's notes for the recommended method of conducting this section of the interview
2.1 People's overall preference for types of handpumps *(Use extra sheet of paper for game 2 if necessary)*

Handpump type	Game 1		Game 2
	Yes	Number Seen	
No. 6			
Malda			
Nira AF-85			
Tara			
Jibon			

Vergnet			
Rope Pump			
Walimi			
India Mark II			
India mark III			
U3M			
Afridev			
Volanta			

2.2 From the list below, what are the particular aspects that users dislike most about the identified handpumps in the community? What are the problems? Also, rank the answers with a scale of 1-5 in terms of most disliked/greatest problem ranked lowest together with the users during this part of the interview.

General Comments made:			
Important points	Responses	Unsolicited	Canvassed
We were not consulted before the pumps were installed			
The pumps are difficult to operate			
The pumps don't pump enough water			
Sometimes there are long queues at the pump			
The pumps are far away from where we live			
The pumped water tastes bad			
The pumped water makes us sick			
The pumped water colour is bad			
The pumps are always breaking down; they are unreliable			
When the pumps breakdown, they don't get fixed for a long time			
We wish we knew how to fix the pumps			
The pump fees are too high			
Other			
Other			
Other			

2.3 How many handpumps are there in this community? *(Play Game 3 where respondents draw a community map displaying key community features and the handpump locations)*

2.4 Who actually uses the handpumps in the community?

2.5 Who owns the handpumps? *(Use cards for identification if necessary)*

Private		Community	
Government		NGOs	
Please specify, if another			

2.6 What is the water from the handpumps used for?

Domestic Water		Water for cattle, goats, etc.	
Water for user's gardens		Other	
If other please specify			

2.7 What do you like most about the best pump in your community?

2.8 What do you dislike most about the worst handpump in your area?

2.9 Does the community only depend on handpumps for their water?

Yes		No	

2.10 Do you use water from these other sources when the handpumps breakdown

Yes		No	

2.11 On average how far do people walk to use each handpump? How long does it take to get to the handpump? How long does it take to walk home with the water that has been collected?

km	minutes	minutes

2.12 At busy times, is there a queue of people waiting for water at the handpumps? How long do you take waiting to get water?

Yes		No		
				minutes

Section 3: Maintenance issues

3.1 How many handpumps are now working and how many are now broken?

Number working		Number broken	

3.2 Are breakdowns of the handpumps frequent?

Yes		No	

3.3 How long does it take before the handpump is repaired?

Days	Hours

3.4 Are there specific people in the community who care for the handpumps?

Yes		No	

3.5 Does the handpump give water all year round?

Yes		No	
If no, when does the handpump not give water?			

3.6 How many handpump caretakers are there in the community?

Number	

3.7 Can you describe how the handpump caretakers care for the handpumps?

3.8 Do the handpump caretakers have any tools to do maintenance work?

Yes		No	

3.9 Where do the handpump caretakers get spare parts for the handpumps when they need them?

3.10 Does anybody from outside the community come to check how the handpumps are working and to do maintenance before the pumps break down?

Yes		No	

3.11 Is the community charged any fee for handpump maintenance?

Yes		No	

3.13 In the event that a handpump break down, is the breakdown reported to somebody?

Yes		No	
If yes, is that person a pump caretaker or community leader?			

3.14 Do the users ever repair the handpump themselves after a breakdown?

Yes		No	
If yes, what sort of repairs and who carries the repairs out?			

3.15 When a handpump breaks down and the community cannot fix it, who is responsible for getting outside help?

3.16 Who usually does repairs on the handpumps?

Government		Pump supplier	
Private pump mechanic		If pump mechanic, does he stay in the community	
Yes		No	

3.17 Who usually pays for the repair work of the handpump?

3.18 Why do you think handpumps usually break down?

There is no water in the borehole	
Some part of the pump in the borehole breaks	
Some part of the pump outside (use cards) breaks	
Because of rough use or vandalism	
Other reasons given by community	

Section 4: Community Institutional structures
4.1 Is there a water committee in the community?

Yes		No	

4.2 Do members of the community participate in the committee meetings?

Yes		No	

4.3 What can be done so that the handpumps can be more reliable?

4.4 Does everyone in the community have access to the handpumps?

Yes		No	

4.5 During installation of the handpumps were the users involved?

Yes		No	
If yes, to what extent?			

4.6 Does the community know how much it costs to maintain the pump?

Yes		No	

4.4 Are the users interested in the learning more about the following?

How to maintain handpumps	Yes		No	
Owning their own handpumps	Yes		No	
Paying more handpump fees	Yes		No	
Other	Yes		No	

Thank you for your time and valuable contribution.
Michael Lubwama
Water is life Project
Sustainable Pump Technologies
Emails: michael.lubwama2@mail.dkit.ie mlubwama@tech.mak.ac.ug
Tel.: +256 712 025970 /+353 857 822733

HANDPUMP MECHANICS' QUESTIONNAIRE

Dear Respondent,

Thank you for the time that you spend on this questionnaire. The information gathered will be of great benefit to us.

OBJECTIVES OF THE HANDPUMP MECHANICS' QUESTIONNAIRE

The main objectives of this questionnaire are to:

- Determine the reason for most failures of handpumps
- Evaluate the maintenance interventions for the handpump failures
- Ascertain the involvement of handpump mechanics with regard to the handpump in its social context.

The information garnered from this questionnaire will increase the understanding of the specific context of each of the handpumps used in each particular community. Comparison of the information obtained from this questionnaire will be made with literature surveys, local pump manufacturers and suppliers and the handpump user questionnaire.

At the end of the above survey, it is hoped that coated piston seals will be tested in a piston seal wear test rig developed in Dublin City University. The questionnaire has five sections. Section 1 seeks to obtain details of the respondent. In section 2 technical specifications of the handpumps is sought. Handpump repairs and break downs are handled in section 3. Section 4 seeks to find out more about the maintenance strategies. The questionnaire ends with a general remark in section 5 that seeks the opinion of the handpump mechanic on interventions that may help increase the sustainability of the handpumps.

If further clarification on any of the questions or on the study itself, please feel free to contact any of the following:

Michael Lubwama
Makerere University
Dept. of Mechanical Engineering
P.O. BOX 7062
Kampala, Uganda
michael.lubwama2@mail.dkit.ie
Tel.: +256 712 025970/+353 857 822733

Stephen Katende
MMM Health Centre
Makondo

Arleen Folan
Project Manager
Water is Life
arleen.folan@dkit.ie

SUSTAINABLE HANDPUMP TECHNOLOGIES
AN IRISHAID/HEA – FUNDED PROJECT UNDER THE WATER IS LIFE
PROJECT
A JOINT PROJECT BETWEEN IRISH HIGHER INSTITUTIONS AND
MAKERERE UNIVERSITY

HANDPUMP MECHANICS' QUESTIONNAIRE

Section 1: Details of Respondent

Today's date (dd/mm/yy)

Type of Company

Government		NGO		Consultant		Private		Other	
If other, please specify									

Name (Optional Response)

Name of company that you represent (Optional question)

Address where you can be contacted: (Optional question)

Telephone number	

Are you a member of the community's water committee?

Yes		No	

How long have you been working as a pump mechanic?

Section 2: Technical Data

2.1 Please specify each of the type of handpumps under your care

Item	Specification
Type of pump	
Model	
Country of origin	
Pumping lift	
Type of well	
Installation depth	

Depth to cylinder	
Cylinder material	
Rising main material	
Piston seal material	
Pump rod material	
Piston material	
Cylinder diameter	
Pump rod diameter	
Rising main diameter	
Approximate yield (strokes/litre; litres/second)	
Number of strokes to arrival of water	
General condition upon arrival	

Section 3: Handpump break down and failure

3.1 How often do the handpumps fail in any given month and/or year?

Month		Year	

3.2 How many handpumps are now working and how many are now broken in this community?

Number working		Number broken	

3.3 Which type of handpumps fail the most and why?

3.4 Which part of the handpump breaks down the most? Why?

3.5 Do you think the breakdown of this part in 3.4 could be triggered by the failure of another part of the handpump?

3.6 What tools do you use to carry out the repairs?

3.7 Briefly describe the process involved in repairing a handpump to solve the repairs mentioned in 3.4 above.

3.8 During repairs, what modifications and improvements do you occasionally make on the handpump as a result of lack of spares?

3.8 Are there any particular repairs where external help is required?

Yes		No	
If yes, explain that repair and how long it takes before help arrives			

3.9 Are any members of the community involved in carrying out any repairs?

Yes		No	
If yes, please explain their exact contribution:			

4. Maintenance strategy

4.1 Do you carry out preventive maintenance of the handpumps under your care?

Yes		No	

4.2 At what interval is the preventive maintenance carried out?

4.3 Describe briefly the steps taken in carrying out preventive maintenance on the pump:

4.4 Which spare parts do you mainly stock up and why?

4.5 Are the supplies of the main spare parts readily accessible?

Yes		No	
In no, please explain			

4.6 Are the community involved in carrying out any maintenance on the handpumps?

Yes		No	

4.7 Are you paid by the community for the handpump repairs and maintenance work?

Yes		No	
Please explain:			

5. Finally, in your opinion what measures can be taken to ensure both the availability and reliability of the handpump.

Thank you for your time and valuable contribution.
Michael Lubwama
Water is life Project
Sustainable Pump Technologies
Emails: michael.lubwama2@mail.dkit.ie mlubwama@tech.mak.ac.ug
Tel.: +256 712 025970 / +353 857 822733